

1-1-1998

Equilibrium studies of ion sorption on zeolitized tuff from Rainier Mesa, Nye County, Nevada

Derek Alan Sloop
University of Nevada, Las Vegas

Follow this and additional works at: <https://digitalscholarship.unlv.edu/rtds>

Repository Citation

Sloop, Derek Alan, "Equilibrium studies of ion sorption on zeolitized tuff from Rainier Mesa, Nye County, Nevada" (1998). *UNLV Retrospective Theses & Dissertations*. 855.
<http://dx.doi.org/10.25669/djlk-1a1y>

This Thesis is protected by copyright and/or related rights. It has been brought to you by Digital Scholarship@UNLV with permission from the rights-holder(s). You are free to use this Thesis in any way that is permitted by the copyright and related rights legislation that applies to your use. For other uses you need to obtain permission from the rights-holder(s) directly, unless additional rights are indicated by a Creative Commons license in the record and/or on the work itself.

This Thesis has been accepted for inclusion in UNLV Retrospective Theses & Dissertations by an authorized administrator of Digital Scholarship@UNLV. For more information, please contact digitalscholarship@unlv.edu.

INFORMATION TO USERS

This manuscript has been reproduced from the microfilm master. UMI films the text directly from the original or copy submitted. Thus, some thesis and dissertation copies are in typewriter face, while others may be from any type of computer printer.

The quality of this reproduction is dependent upon the quality of the copy submitted. Broken or indistinct print, colored or poor quality illustrations and photographs, print bleedthrough, substandard margins, and improper alignment can adversely affect reproduction.

In the unlikely event that the author did not send UMI a complete manuscript and there are missing pages, these will be noted. Also, if unauthorized copyright material had to be removed, a note will indicate the deletion.

Oversize materials (e.g., maps, drawings, charts) are reproduced by sectioning the original, beginning at the upper left-hand corner and continuing from left to right in equal sections with small overlaps. Each original is also photographed in one exposure and is included in reduced form at the back of the book.

Photographs included in the original manuscript have been reproduced xerographically in this copy. Higher quality 6" x 9" black and white photographic prints are available for any photographs or illustrations appearing in this copy for an additional charge. Contact UMI directly to order.

UMI

A Bell & Howell Information Company
300 North Zeeb Road, Ann Arbor MI 48106-1346 USA
313/761-4700 800/521-0600

NOTE TO USERS

**The original manuscript received by UMI contains indistinct, slanted and or light print. All efforts were made to acquire the highest quality manuscript from the author or school.
Microfilmed as received.**

This reproduction is the best copy available

UMI

**EQUILIBRIUM STUDIES OF ION SORPTION ON ZEOLITIZED TUFF
FROM RAINIER MESA, NYE COUNTY, NEVADA**

by

Derek Alan Sloop

**Bachelor of Science
University of New Mexico
1993**

**A thesis submitted in partial fulfillment
of the requirements for the degree of**

Master of Science

in

Water Resources Management

**Department of Geoscience
University of Nevada, Las Vegas
May 1998**

UMI Number: 1390658

UMI Microform 1390658
Copyright 1998, by UMI Company. All rights reserved.

**This microform edition is protected against unauthorized
copying under Title 17, United States Code.**

UMI
300 North Zeeb Road
Ann Arbor, MI 48103



Thesis Approval
The Graduate College
University of Nevada, Las Vegas

April 27, 1998

The Thesis prepared by

Derek Alan Sloop

Entitled

Equilibrium Studies of Ion Sorption on Zeolitized Tuff from Rainier
Mesa, Nye County, Nevada

is approved in partial fulfillment of the requirements for the degree of

Master of Science in Water Resources Management

Examination Committee Chair

Dean of the Graduate College

Examination Committee Member

Examination Committee Member

Graduate College Faculty Representative

ABSTRACT

Equilibrium Studies of Ion Sorption on Zeolitized Tuff from Rainier Mesa, Nye County, Nevada

by

Derek Alan Sloop

Dr. Charalambos Papelis, Examination Committee Chair
Assistant Research Professor
Desert Research Institute
University of Nevada, Las Vegas

The partitioning of solutes between the solid mineral and aqueous phase frequently controls the fate and transport of contaminants in the subsurface environment. Consequently, parametric studies were performed to investigate the equilibrium sorption of Pb(II), Sr(II), CrO_4^{2-} , and SeO_3^{2-} ions on zeolitized tuff from Rainier Mesa, Nevada, and on clinoptilolite from Jordan Valley, Oregon. The fractional uptake of the ions on the zeolitized tuff was investigated so that sorption isotherms and partitioning coefficients describing the affinity of the ions for the zeolitized tuff could be calculated. The fractional uptake of the ions on the clinoptilolite was investigated so that a comparison between the natural zeolitized tuff and the most common zeolite present in the tuffs could be made. Along with the geochemical parameters calculated, an interpretation of the qualitative differences in the partitioning behavior of these ions was made. This study

indicates a markedly different behavior between the two cations, between the two anions, and between the cations and anions. Batch equilibrium sorption studies were performed as a function of pH, ionic strength, total solid adsorbent concentration, and total ion concentration in order to evaluate the importance of these geochemical parameters, and to investigate any similarities and differences in the partitioning behavior between these four ions.

TABLE OF CONTENTS

ABSTRACT.....	iii
LIST OF TABLES.....	vii
LIST OF ILLUSTRATIONS.....	ix
ACKNOWLEDGEMENTS.....	xiii
CHAPTER 1. INTRODUCTION.....	1
Background	2
The Ions of Interest.....	4
Research Objectives & Hypotheses.....	7
Thesis Organization.....	9
CHAPTER 2. BACKGROUND INFORMATION.....	10
General Geologic Settings.....	10
The Nevada Test Site.....	10
Rainier Mesa.....	12
Zeolites.....	14
Formation.....	15
Occurrence at the Nevada Test Site.....	17
CHAPTER 3. MATERIALS & METHODS.....	18
Adsorbent Characterization.....	18
Particle Size Distribution.....	19
Particle Morphology.....	22
Adsorbent Mineralogy.....	25
Major and Trace Element Analyses.....	27
Surface Area and Pore Size Distribution.....	29
Porosity and Density.....	37
Cation Exchange Capacity.....	38
Methods.....	41
Batch Equilibrium Sorption Experiments.....	41
Sorption Parameter Estimation Techniques.....	43

CHAPTER 4. SORPTION OF Pb(II) AND Sr(II) ON ZEOLITIZED TUFF AND CLINOPTILOLITE: EQUILIBRIUM EXPERIMENTS, SORPTION PARAMETER ESTIMATION, AND SPECIATION.....	47
Sorption of Pb(II) and Sr(II) on Zeolitized Tuff	48
Sorption of Pb(II) and Sr(II) on Clinoptilolite.....	91
Comparison of Pb(II) and Sr(II) Sorption as a Function of Adsorbent Type.....	104
CHAPTER 5. SORPTION OF CrO ₄ ²⁻ AND SeO ₃ ²⁻ ON ZEOLITIZED TUFF AND CLINOPTILOLITE: EQUILIBRIUM EXPERIMENTS, SORPTION PARAMETER ESTIMATION, AND SPECIATION.....	112
Sorption of CrO ₄ ²⁻ and SeO ₃ ²⁻ on Zeolitized Tuff.....	113
Sorption of CrO ₄ ²⁻ and SeO ₃ ²⁻ on Clinoptilolite.....	139
Comparison of CrO ₄ ²⁻ and SeO ₃ ²⁻ Sorption as a Function of Adsorbent Type.....	148
CHAPTER 6. CONCLUSIONS AND RECOMMENDATIONS FOR FUTURE RESEARCH.....	155
Conclusions.....	156
Recommendations for future research.....	160
APPENDIX I CALCULATED BEST-FIT DISTRIBUTION COEFFICIENTS.....	163
APPENDIX II CALCULATED RETARDATION FACTORS BASED ON THE DISTRIBUTION COEFFICIENTS.....	165
REFERENCES.....	169
VITA.....	174

LIST OF TABLES

Table 1. Particle size distributions for zeolitized tuff and clinoptilolite.....	20
Table 2. Major element analyses for the zeolitized tuff and clinoptilolite.....	28
Table 3. Trace element analyses for the zeolitized tuff and clinoptilolite.....	28
Table 4. Surface area and pore size measurements for the zeolitized tuff and clinoptilolite.	31
Table 5. Specific surface area of the zeolitized tuff as a function of particle size.	36
Table 6. Density and porosity measurements for the zeolitized tuff and clinoptilolite....	38
Table 7. Calculated exchange capacity of the zeolitized tuff and clinoptilolite for divalent cations.....	41
Table 8. Freundlich isotherm parameters for Pb(II) equilibrium sorption isotherms in 1.0 M NaNO ₃	60
Table 9. Distribution coefficients (K _d) for Pb(II) in 1.0 M NaNO ₃ at different pH values.	62
Table 10. Chemical analysis of the groundwater from well U-20 on the NTS.	65
Table 11. Freundlich isotherm parameters for Sr(II) equilibrium sorption isotherms in 0.1 M NaNO ₃	77
Table 12. Distribution coefficients (K _d) for Sr(II) in 0.1 M NaNO ₃ at different pH values.	79
Table 13. Freundlich isotherm equation parameters for Sr(II) in 0.01 M NaNO ₃	80
Table 14. Distribution coefficients (K _d) for Sr(II) sorption isotherms 0.01 M NaNO ₃ at different pH values.	81
Table 15. Distribution coefficients (K _d) for CrO ₄ ²⁻ in 1.0, 0.1, and 0.01 M NaNO ₃ for different pH values.	119
Table 16. Freundlich isotherm parameters for SeO ₃ ²⁻ in 1.0 and 0.1 M NaNO ₃ for different pH values.	130
Table 17. Distribution coefficients (K _d) for SeO ₃ ²⁻ in 1.0 and 0.1 M NaNO ₃ for different pH values.....	133
Table I- 1. Best-fit calculated slopes and intercepts for Pb(II) in 1.0 M NaNO ₃ at different pH values.....	163
Table I- 2. Best-fit calculated slopes and intercepts for Sr(II) in 0.1 and 0.01 M NaNO ₃ at different pH values.....	164
Table I- 3. Best-fit calculated slopes and intercepts for SeO ₃ ²⁻ in 1.0 and 0.1 M NaNO ₃ at different pH values.....	164

Table II- 1. Retardation factors for the Pb(II) cation in 1.0 M NaNO ₃ at different pH values.....	166
Table II- 2. Retardation factors for the Sr(II) cation in 0.1 and 0.01 M NaNO ₃	167
Table II- 3. Retardation factors for the CrO ₄ ²⁻ anion in 1.0, 0.1, and 0.01 M NaNO ₃ at different pH values.	168
Table II- 4. Retardation factors for the SeO ₃ ²⁻ anion in 1.0 and 0.1 M NaNO ₃ at different pH values.....	168

LIST OF ILLUSTRATIONS

Figure 1. Map of the Nevada Test Site and surrounding areas showing the location of Rainier Mesa.	11
Figure 2. Mass population (%) vs. particle size diameter for the ground zeolitized tuff and clinoptilolite.	21
Figure 3. Photomicrograph of the zeolitized tuff at a 950-fold magnification.	23
Figure 4. Photomicrograph of the zeolitized tuff at a 1700-fold magnification.	23
Figure 5. X-ray diffraction spectrum of the zeolitized tuff.	26
Figure 6. Isotherm of nitrogen adsorption on the zeolitized tuff.	32
Figure 7. Isotherm of nitrogen adsorption on the clinoptilolite.	32
Figure 8. Pore volume distribution of the zeolitized tuff derived from nitrogen adsorption isotherm.	35
Figure 9. Pore volume distribution of the clinoptilolite derived from nitrogen adsorption isotherm.	35
Figure 10. Sorption of 1.0×10^{-4} M Pb(II) on 2.5 g/L zeolitized tuff as a function of ionic strength.	49
Figure 11. Sorption of 1.0×10^{-5} M Pb(II) on 3.0 g/L zeolitized tuff in 2.0 and 1.0 M NaNO ₃	51
Figure 12. Sorption of 1.0×10^{-5} M Pb(II) on 3.0 g/L zeolitized tuff as a function of ionic strength.	52
Figure 13. Sorption of 1.0×10^{-5} M Pb(II) in 1.0 M NaNO ₃ as a function of zeolitized tuff concentration.	55
Figure 14. Sorption of 1.0×10^{-4} M Pb(II) in 0.1 M NaNO ₃ as a function of zeolitized tuff concentration.	56
Figure 15. Sorption of Pb(II) on 20 g/L zeolitized tuff in 1.0 M NaNO ₃ as a function of Pb(II) concentration.	57
Figure 16. Freundlich isotherms of Pb(II) sorption on zeolitized tuff in 1.0 M NaNO ₃ at pH values of 7, 8, and 9.	61
Figure 17. Linear isotherms of Pb(II) sorption on zeolitized tuff in 1.0 M NaNO ₃ at pH values of 7, 8, and 9.	63
Figure 18. Speciation modeling of 1.0×10^{-4} M Pb(II) in groundwater from well U-20 at the NTS.	66
Figure 19. Speciation modeling of 1.0×10^{-6} M Pb(II) in groundwater from well U-20 at the NTS.	67

Figure 20. Speciation modeling of 1.0×10^{-4} M Pb(II) in 0.01 M NaNO ₃ closed to the atmosphere.....	69
Figure 21. Speciation modeling of 1.0×10^{-6} M Pb(II) in 0.01 M NaNO ₃ closed to the atmosphere.....	69
Figure 22. Sorption of 1.0×10^{-4} M Sr(II) on 2.5 g/L zeolitized tuff as a function of ionic strength.	71
Figure 23. Sorption 1.0×10^{-6} M Sr(II) on 2.5 g/L zeolitized tuff as a function of ionic strength.	73
Figure 24. Sorption of 1.0×10^{-4} M Sr(II) in 0.1 M NaNO ₃ as a function of zeolitized tuff concentration.....	74
Figure 25. Sorption of Sr(II) on 2.5 g/L zeolitized tuff in 0.01 M NaNO ₃ as a function of Sr(II) concentration.	75
Figure 26. Freundlich isotherm of Sr(II) sorption on zeolitized tuff in 0.1 M NaNO ₃	78
Figure 27. Linear isotherm of Sr(II) sorption on zeolitized tuff in 0.1 M NaNO ₃	79
Figure 28. Freundlich isotherm of Sr(II) sorption on zeolitized tuff in 0.01 M NaNO ₃ . .	80
Figure 29. Linear isotherm of Sr(II) sorption on zeolitized tuff in 0.01 M NaNO ₃	82
Figure 30. Speciation modeling of 1.0×10^{-4} M Sr(II) in groundwater from well U-20 at the NTS.....	83
Figure 31. Speciation modeling of 1.0×10^{-6} M Sr(II) in groundwater from well U-20 at the NTS.....	84
Figure 32. Speciation modeling of 1.0×10^{-4} M Sr(II) in 0.01 M NaNO ₃ closed to the atmosphere.....	86
Figure 33. Comparison of the sorption behavior of 1.0×10^{-4} M Pb(II) and Sr(II) on 2.5 g/L zeolitized tuff in 0.1 M NaNO ₃	88
Figure 34. Comparison of the sorption behavior of 1.0×10^{-4} M Pb(II) and Sr(II) on 20 g/L zeolitized tuff in 0.1 M NaNO ₃	88
Figure 35. Comparison of the sorption behavior of 1.0×10^{-6} M Pb(II) and Sr(II) on 2.5 g/L zeolitized tuff in 1.0 M NaNO ₃	89
Figure 36. Sorption of 1.0×10^{-5} M Pb(II) on 1.0 g/L clinoptilolite as a function of ionic strength.	93
Figure 37. Sorption of 1.0×10^{-6} M Pb(II) on 1.0 g/L clinoptilolite as a function of ionic strength.	93
Figure 38. Sorption of 1.0×10^{-5} M Pb(II) in 0.01 M NaNO ₃ as a function of clinoptilolite concentration.....	94
Figure 39. Sorption of 1.0×10^{-4} M Pb(II) in 0.1 M NaNO ₃ as a function of clinoptilolite concentration.....	95
Figure 40. Sorption of Pb(II) on 20 g/L clinoptilolite in 1.0 M NaNO ₃ as a function of Pb(II) concentration.	97
Figure 41. Sorption of Pb(II) on 1.0 g/L clinoptilolite in 0.1 M NaNO ₃ as a function of Pb(II) concentration.	97
Figure 42. Sorption of 1.0×10^{-4} M and 1.0×10^{-5} M Sr(II) on 1.0 g/L clinoptilolite as a function of ionic strength.....	99
Figure 43. Sorption of 1.0×10^{-4} M Sr(II) in 0.1 M NaNO ₃ as a function of solid concentration.....	100

Figure 44. Sorption of Sr(II) on 1.0 g/L clinoptilolite in 0.1 M NaNO ₃ as a function of Sr(II) concentration.....	101
Figure 45. Comparison of the sorption behavior of 1.0x10 ⁻⁴ M Pb(II) and Sr(II) on 1.0 g/L clinoptilolite in 0.1 M NaNO ₃	103
Figure 46. Sorption of 1.0x10 ⁻⁶ M Pb(II) in 1.0 M NaNO ₃ as a function of adsorbent type.....	105
Figure 47. Sorption of 1.0x10 ⁻⁴ M Pb(II) in 0.1 M NaNO ₃ as a function of adsorbent type.....	106
Figure 48. Sorption of 1.0x10 ⁻⁴ M Sr(II) in 0.1 and 0.01 M NaNO ₃ as a function of adsorbent type.....	109
Figure 49. Sorption of 5.0x10 ⁻⁷ M CrO ₄ ²⁻ on 100 g/L zeolitized tuff as a function of ionic strength.....	115
Figure 50. Sorption of CrO ₄ ²⁻ on 100 g/L zeolitized tuff in 1.0 M NaNO ₃ as a function of CrO ₄ ²⁻ concentration.....	117
Figure 51. Speciation modeling of 1.0x10 ⁻⁴ M CrO ₄ ²⁻ in groundwater from well U-20 at the NTS.....	121
Figure 52. Speciation modeling of 1.0x10 ⁻⁴ M CrO ₄ ²⁻ in 0.01 M NaNO ₃ closed to the atmosphere.....	122
Figure 53. Sorption of 1.0x10 ⁻⁵ M SeO ₃ ²⁻ on 100 g/L zeolitized tuff as a function of ionic strength.....	125
Figure 54. Sorption of 1.0x10 ⁻⁶ M SeO ₃ ²⁻ on 100 g/L zeolitized tuff as a function of ionic strength.....	126
Figure 55. Sorption of SeO ₃ ²⁻ on 100 g/L zeolitized tuff in 0.1 M NaNO ₃ as a function of SeO ₃ ²⁻ concentration.....	128
Figure 56. Freundlich isotherms of SeO ₃ ²⁻ sorption on zeolitized tuff in 1.0 M NaNO ₃ at pH values of 4, 5, and 6.....	130
Figure 57. Freundlich isotherms of SeO ₃ ²⁻ sorption on zeolitized tuff in 0.1 M NaNO ₃ at pH values of 4, 5, and 6.....	131
Figure 58. Linear isotherms of SeO ₃ ²⁻ sorption on zeolitized tuff in 1.0 M NaNO ₃ at pH values of 4, 5, and 6.....	133
Figure 59. Linear isotherms of SeO ₃ ²⁻ sorption on zeolitized tuff in 0.1 M NaNO ₃ at pH values of 4, 5, and 6.....	134
Figure 60. Speciation modeling of 1.0x10 ⁻⁴ M SeO ₃ ²⁻ in the groundwater from well U-20 at the NTS and in the batch equilibrium reactors.....	135
Figure 61. Comparison of the sorption behavior of 1.0x10 ⁻⁵ M CrO ₄ ²⁻ and SeO ₃ ²⁻ on 100 g/L zeolitized tuff in 1.0 M NaNO ₃	138
Figure 62. Comparison of the sorption behavior of 1.0x10 ⁻⁶ M CrO ₄ ²⁻ and SeO ₃ ²⁻ on 100 g/L zeolitized tuff in 1.0 M NaNO ₃	138
Figure 63. Sorption of 1.0x10 ⁻⁷ M CrO ₄ ²⁻ on 33 g/L clinoptilolite as a function of ionic strength.....	140
Figure 64. Sorption of CrO ₄ ²⁻ on 33 g/L clinoptilolite in 0.1 M NaNO ₃ as a function of CrO ₄ ²⁻ concentration.....	142
Figure 65. Sorption of 1.0x10 ⁻⁵ M SeO ₃ ²⁻ on 33 g/L clinoptilolite as a function of ionic strength.....	144

Figure 66. Sorption of SeO_3^{2-} on 33 g/L clinoptilolite in 1.0 M NaNO_3 as a function of SeO_3^{2-} concentration.	145
Figure 67. Comparison of the sorption behavior of CrO_4^{2-} and SeO_3^{2-} on 33 g/L clinoptilolite in 1.0 M NaNO_3	147
Figure 68. Comparison of the sorption behavior of 1.0×10^{-6} M CrO_4^{2-} and SeO_4^{2-} on 33 g/L clinoptilolite in 0.1 M NaNO_3	147
Figure 69. Comparison of the sorption behavior of 1.0×10^{-6} M CrO_4^{2-} in 0.1 M NaNO_3 as a function of adsorbent type.	150
Figure 70. Comparison of the sorption behavior of 1.0×10^{-5} M SeO_3^{2-} in 1.0 M NaNO_3 as a function of adsorbent type.	152
Figure 71. Comparison of the sorption behavior of 1.0×10^{-6} M SeO_3^{2-} in 0.1 M NaNO_3 as a function of adsorbent type.	153

ACKNOWLEDGEMENTS

The successful completion of this research project was made possible by a number of people and places, and I would like to briefly acknowledge the help and support that I received throughout the course of my studies at the University of Nevada, Las Vegas.

Financial support for this project was provided by the Department of Energy / Nevada Operations Office for which I am very grateful.

I would like to especially thank my committee chair Dr. Charalambos Pangelis. I don't think that I would have ever graduated if he had not been willing to take me on as his student. I learned more from him in two years than I ever thought was possible. I would like to thank him for the many helpful comments, suggestions, and discussions we had throughout the course of the project, and the fact that he is an extremely patient man. I must have asked him repeatedly the same types of questions a couple of dozen times, and every time he made the time to talk to me, even when he was extremely busy (which is always). I would also like to thank him for taking me to the American Chemical Society conference in San Francisco, which in itself was an extremely enjoyable and educational experience. Lastly, I would like to thank him for making this research project so interesting and enjoyable.

I am also grateful for the help and support that I received from my other

committee members including Dr. Hodge, Dr. Steinberg, and Dr. Johnson. Their comments and suggestions throughout the course of the project, and the many meetings I had them attend also made the completion of this project possible. I would like specifically to thank Dr. Steinberg for allowing me the use of his equipment and for showing me how to calculate both the cation-exchange capacities, and the surface areas of both adsorbents.

I am also grateful for help that I received from various people at the Desert Research Institute (DRI). Marg Herdon, Amy Dudenake, Eva Stowers, and Heather Nelson all helped me out at one time or another, and they made working at the DRI that much more enjoyable.

A number of people in the Geoscience Department at the University of Nevada, Las Vegas also deserve recognition. I would like to thank Dr. Clay Crow for performing the XRD analysis of the clinoptilolite, and for the many times he discussed the theory behind XRD with me. I would like to also thank Alex Sanchez for performing the XRF analyses on both adsorbents that were used in this study. Finally, I would like to thank Dr. David Kreamer for providing me the opportunity during my second semester at UNLV to make some additional money working with him on a project dealing with hydrocarbons.

Last, but not least, I would also like to acknowledge the support (financial or otherwise) and understanding that was provided by my parents. They had to endlessly listen to my complaints, comments, and concerns about the whole graduate school experience over the whole 3 years, and for that I am extremely grateful.

CHAPTER 1

INTRODUCTION

Sorption is the general term for any number of processes where solutes in natural waters are taken up by the solids they contact. Sorption processes can include adsorption, absorption, or surface precipitation. Adsorption is the accumulation of solutes at the interface between an aqueous solution phase and a solid adsorbent without the development of a three-dimensional molecular arrangement. This definition implies the formation of a two-dimensional molecular arrangement on the surface, and the terms specific sorption and non-specific sorption are sometimes used to denote chemisorption and physisorption, respectively. Absorption is the incorporation of an aqueous chemical species into a solid phase by diffusion or some other means, such as dissolution of the solid followed by reprecipitation of the solid with the formerly aqueous chemical species included as part of a solid inclusion. Surface precipitation is the formation of a solid phase of a different composition and structure than the solid substrate that exhibits a three-dimensional structure (Brown, 1990).

The partitioning of solutes between the solid mineral and aqueous phase by one of these three processes is of particular importance to environmental scientists and engineers for several reasons. For example, solid-liquid interactions play a critical role in the

quality of the world's fresh water, the development of soils, and the geochemical cycling of elements (Hochella and White, 1990). More important, however, the sorption of solutes at the solid-liquid interface can effect the fate and transport of potentially hazardous elements throughout the hydrogeosphere. In fact, it has been said that the distribution of solutes at the mineral-water interface is often the paramount process controlling the migration of contaminants in the subsurface environment (Piwoni and Keeley, 1991). For this reason, the partitioning of solutes between the solid mineral and aqueous phase must be known during any attempt to characterize the fate and transport of contaminants in the subsurface. The failure to consider sorption processes can result in an overestimation of the amount of a contaminant at a point some distance from the source, as well as the time required for travel. It has been noted by various researchers that by gaining an understanding of the chemical and physical characteristics of the contaminant, the composition of the surface of the solid, and the fluid medium encompassing both, the impact of sorption on the movement and distribution of contaminants in the subsurface can often be explained (Bedient et al., 1994).

Background

Since the start of the United States' nuclear weapons testing program at the Nevada Test Site (NTS) on January 27, 1951, over 100 atmospheric nuclear tests and 804 underground nuclear tests have been conducted at the NTS (U.S. Department of Energy, 1994). Underground testing of nuclear devices was carried out in a variety of geologic and hydrogeologic environments, and was begun in order to prevent the atmospheric fallout of radioactive debris from aerial detonations at the NTS. These underground

nuclear detonations have released large quantities of radionuclides and other hazardous materials into the subsurface aqueous environment, and any migration of these materials within and off of the NTS in the groundwater poses both a potential human and ecological health hazard.

In an attempt to assess whether the movement of radionuclides at the NTS might be retarded due to sorption process, samples of zeolitized tuff from Rainier Mesa, Nye County, Nevada were collected. These particular samples were collected because their matrix controls the recharge rate of groundwater to the underlying and more permeable Paleozoic aquifers at the NTS, and because of the intense interest by environmental scientists and engineers in zeolites as potential natural barriers to the spread of aqueous contamination. Specifically, this study tested the potential of the widely distributed zeolitized tuff to retard the transport of lead (Pb(II)), strontium (Sr(II)), chromate (Cr(VI)), and selenite (Se(IV)) ions. These particular ions were selected for study because of their potentially hazardous effects to plant and animal life, and because all of the ions except SeO_3^{2-} can occur in the subsurface environment at the NTS as either fission products of past nuclear detonations (e.g. ^{90}Sr), or as by-products of the materials that were used for the construction of the devices (e.g. Pb was used for shielding of the devices, and Cr was used in the stainless steel of the devices). The SeO_3^{2-} anion is not expected to occur in the subsurface environment at the NTS as a result of the detonations, but it was selected for study for comparative purposes because it is known to be a strongly binding anion on hydrous oxide surfaces.

The Ions of Interest

Lead is a Group IVB metallic element that occurs naturally in the Earth's surface usually in the +2 oxidation state. Lead has an average concentration of 13 parts per million (ppm) in the Earth's crust. The chief ore of Pb is galena (PbS), however, it is also commonly found in nature as cotunnite (PbCl₂), anglesite (PbSO₄), cerrusite (PbCO₃), and crocoite (PbCrO₄). The two major commercial uses of Pb are in storage batteries, and, in the past, in gasoline as the antiknocking agent tetraethyllead, (C₂H₅)₄Pb (Chang, 1988). In addition, for a number of years white lead, Pb₃(OH)₂(CO₃)₂, was used as a pigment, but, because of its toxicity to humans, its use in the United States has been banned. Another interesting use for Pb is that since the metal is relatively impenetrable to low-energy photon radiation, it is also used in protective shields for nuclear chemists, X-ray operators, and radiologists.

Lead has no known beneficial function in human metabolism, and its toxicity to humans has been known for over 2000 years (Chang, 1988). In addition to lead's extreme toxicity, its effects on humans are cumulative. It can enter the body either as the inorganic lead cation (Pb²⁺) or as tetraethyllead (Chang, 1988). Inhaled or ingested Pb concentrates in the blood, tissues, and bones in mammals. A Pb content in human blood exceeding 0.40 ppm is considered dangerous. Lead poisoning is known to cause anemia, brain damage, affect the central nervous system, and impair kidney functions (Chang, 1988).

Strontium is a naturally occurring alkaline earth metal that is also found in nature in the +2 oxidation state. Strontium has an average concentration of 384 ppm in the Earth's crust. It occurs in nature primarily as the carbonate strontianite (SrCO₃), or as the

sulfate celestite (SrSO_4). There are no large-scale uses of Sr, but Sr salts such as $\text{Sr}(\text{NO}_3)_2$ and SrCO_3 are used in red fireworks as well as in the red warning flares on highways (Chang, 1988).

Being chemically similar to calcium, strontium only poses a health risk to humans when it is radioactive. The radioactive isotope ^{90}Sr , which has been released into the subsurface environment at the NTS, can potentially reach humans via a relatively short food chain. For example, ^{90}Sr can be passed along to humans in milk from cows that have consumed either contaminated grass or water. Because Ca and Sr are chemically similar, $^{90}\text{Sr}^{2+}$ cations can replace Ca^{2+} cations in our bodies (Chang, 1988). Radioactive $^{90}\text{Sr}^{2+}$ that has replaced Ca^{2+} in human bones would constantly expose the body to β -radiation which can lead to anemia, leukemia, and other chronic illnesses (Chang, 1988).

Chromium occurs naturally at the Earth's surface at average concentrations of 10 to 100 ppm. Chromium is a Group VI transition element that occurs in the environment primarily as Cr(III). It is the 21st most abundant element in the Earth's crust, but it occurs in much greater concentrations in the Earth's core and mantle (Squibb and Snow, 1993). There are over 30 known chromium-containing minerals, including oxides, hydroxides, carbonates, sulfides, nitrides, silicates, and chromates. The most economically important chromium ore, however, is chromite (FeCr_2O_4) (Squibb and Snow, 1993). Chromium ores are widely used in the production of steel and other metal alloys. The high resistance of chromium metals to corrosion and their intense hardness and strength make them ideally suited for the manufacture of vehicles, industrial equipment, and specialized machinery. In fact, 75% of the chromium used in steel production in the United States goes to the production of stainless steel (Squibb and Snow, 1993).

Unlike Pb, which has no known beneficial function in human metabolism. Cr is a natural constituent of living matter and an essential trace element for both plants and animals. Chromium is required in living systems for normal glucose tolerance. At higher concentrations and particularly in the +6 oxidation state (CrO_4^{2-}), Cr may be lethal or produce severe systemic toxicity to living systems. (Squibb and Snow, 1993). As a soluble anion, Cr(VI) can easily cross cell membranes and can be reduced and trapped intra-cellularly. The cation Cr(III), however, is normally soluble only when bound to organic complexes and thus does not readily penetrate into cells (Squibb and Snow, 1993). Numerous reports have shown a strong correlation between exposure to insoluble Cr(III) and weakly soluble Cr(VI) and human cancer. Because of the carcinogenicity and toxicity of Cr, regulations and advisories exist regarding acceptable concentrations of Cr compounds in air and water. For example, drinking water standards and guidance values for Cr range between 0.05 and 1.1 mg/L, and air quality standards for Cr range from 0.05 to 50 mg/m^3 (Squibb and Snow, 1993).

Selenium is the 68th most abundant element in the earth's crust with average concentrations ranging from 0.08 to 2 ppm. It is widely found in rocks and soils that are enriched with copper, silver, sulfur, and iron. It is mostly associated, however, with the sulfur ores of heavy metals, in small quantities in pyrite, and in the minerals clausthalite (PbSe), naumannite (Ag_2Se), tiemannite (HgSe), and cadmoselite ($\beta\text{-CdSe}$) (Papelis, 1992). Selenium is mainly used in photography as a pigment, in electronics, and in semiconductor fusion mixtures (Papelis, 1992).

Selenium has also been shown an essential trace element for a number of organisms. For example, deficiencies of selenium are associated with a number of

disorders including ovarian cysts, metritis, and a decreased conception rates in cattle (Hogan, 1993). It is known that deficiencies of Se affect the function of the thyroid gland, causing a depression of plasma levels. At higher doses, Se, like Cr, is clearly toxic. Even at less than lethal doses it can cause selenosis (Se poisoning). Unfortunately, at sublethal doses selenosis results in a broad range of adverse effects which makes the identification of selenium poisoning difficult (Hogan, 1993).

Research Objectives & Hypotheses

Due to the potential adverse health effects that ions like Pb(II), Sr(II), CrO_4^{2-} , and SeO_3^{2-} pose to humans, the fate and transport of these ions in the subsurface environment is the focus of substantial research efforts. These research efforts have shown that the sorption of inorganic ions on mineral phases is one of the major processes controlling the concentration of inorganic contaminants in aqueous environments (Papelis, 1992). Sorption studies must be conducted, therefore, before transport models can provide accurate estimates of the fate of aqueous contaminants. To further this effort at the NTS, several objectives were identified for this thesis. The first objective of this thesis was to determine the extent of the equilibrium partitioning of Pb(II), Sr(II), CrO_4^{2-} , and SeO_3^{2-} between the zeolitized tuff from Rainier Mesa and the aqueous phase. This was done in order to increase our understanding of the sorption behavior of these ions on the zeolitized tuff, and to provide sorption isotherms and partitioning coefficients of the ions for the zeolitized tuff. By doing this, this study helps to define the mobility of these metal ions at Rainier Mesa. In addition, preliminary studies of the zeolitized tuff indicated that the predominate zeolite mineral present in the volcanic tuff was clinoptilolite. The

second objective of this thesis, therefore, was to determine the equilibrium sorption behavior of the same ions with mineralogically pure clinoptilolite obtained from Jordan Valley, Oregon. By doing this, a detailed comparison could be made of the equilibrium sorption behavior of the ions between the natural, well-characterized zeolitized tuff from the NTS and the simple mineral clinoptilolite with well-known characteristics. This comparison of the simple case (pure clinoptilolite) versus the complex case (zeolitized tuff field samples) might provide a means to estimate the partitioning of these ions by other zeolitized rocks, assuming that they also contain a significant percentage of the zeolite mineral clinoptilolite. These types of extrapolations would allow for a more widespread use of the partitioning coefficients that were calculated for the Pb(II), Sr(II), CrO_4^{2-} , and SeO_3^{2-} ions. The last objective of this study was to obtain a detailed physical characterization of both adsorbents. This was necessary because an understanding of the composition of the surface of the solid is required in order to draw logical conclusions about the impact of sorption on the movement and distribution of contaminants in the subsurface environment.

These objectives were designed to test the following hypotheses. It was hypothesized that the movement of these potentially hazardous ions in the saturated zone would be retarded due to interactions of the inorganic ions with zeolitized tuff which is found within many of the stratigraphic units at the NTS. In addition, it was hypothesized that cationic contaminants would be retarded to a greater extent than anionic contaminants on the zeolitized tuff, and lastly, that the zeolite mineral clinoptilolite is the dominant mineral phase controlling the sorption behavior of the ions.

Thesis Organization

This thesis is divided into six Chapters. Following this introduction (Chapter 1), Chapter 2 provides background information on the general geologic and hydrogeologic setting of the study area, and on the physical and chemical properties of zeolites. The discussion on zeolites also provides background information on their possible formation mechanisms and occurrence at the NTS. This background chapter is only intended as an introduction to each topic covered and is not meant to be exhaustive. Additional information can be found in the references given. Chapter 3 presents the physiochemical characterization of the adsorbents, as well as the experimental methods that were employed. The results of this thesis are presented in Chapters 4 and 5. Chapter 4 discusses the batch equilibrium sorption experiments, the sorption parameter estimations, and the chemical speciation modeling of the cations, while Chapter 5 discusses the results with the anions. The conclusions and recommendations for future research are presented in Chapter 6.

CHAPTER 2

BACKGROUND INFORMATION

General Geologic Settings

The Nevada Test Site

The NTS is a 1350 square mile area in Nye County approximately 65 miles northwest of Las Vegas, Nevada (Figure 1). The region is within the southernmost part of the Great Basin section of the Basin and Range physiographic province, and consists of predominantly north-south trending mountain ranges separated by alluvial valleys. The area is an excellent example of Great Basin topography with the contrast in slope between the valley floors and flanking ridges striking, even when the relief between them is small (Winograd and Thordarson, 1975). The area also lies within one of the most arid regions of the United States. The average annual precipitation on the alluvial valleys ranges from 3 to 6 inches per year, and on most of the mountain ridges and mesas the average is less than 10 inches (Winograd and Thordarson, 1975).

Many studies on the geology and hydrogeology of the NTS and surrounding areas have been conducted including those by Blankennagel (1968), Ekren (1968), Winograd et al. (1971), Blankennagel and Weir (1973), and Winograd and Thordarson (1975). In general, the NTS and adjacent areas are within the miogeosynclinal belt of the Cordilleran

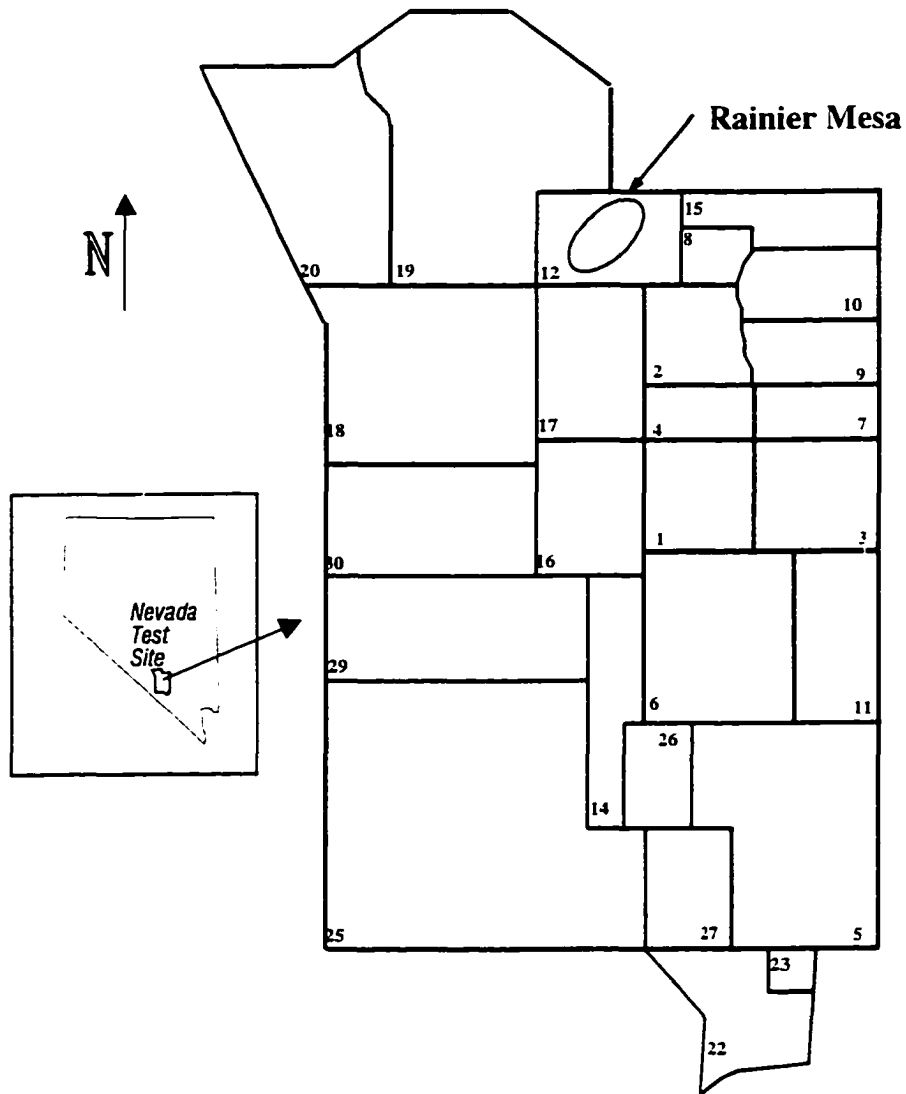


Figure 1. Map of the Nevada Test Site and surrounding areas showing the location of Rainier Mesa.

geosyncline, in which 37,000 feet of marine sediments accumulated during the Precambrian and Paleozoic Eras (Winograd and Thordarson, 1975). The region is also located within a Tertiary volcanic province in which extrusive rocks, locally more than 13,000 feet thick erupted largely from caldera centers. Quaternary detrital sequences, largely alluvium, fill most of the low-lying areas in the region.

The region underwent two major periods of deformation. The first orogeny occurred in the late Mesozoic and perhaps early Tertiary time, resulting in folding and thrust faulting of the Precambrian and Paleozoic rocks. During the mid-to-late Cenozoic, the region underwent normal block faulting, which produced the Basin and Range topography (Winograd et al., 1971). The intensely fractured Precambrian and Paleozoic carbonate and clastic rocks, and the block-faulted Cenozoic volcanic and sedimentary strata at the NTS are divided into 10 hydrogeologic units in order of decreasing age as follows: lower clastic aquitard; lower carbonate aquifer; upper clastic aquitard; upper carbonate aquifer; tuff aquitard; lava-flow aquitard; bedded-tuff aquifer; welded-tuff aquifer; lava-flow aquifer; and valley-fill aquifer (Winograd and Thordarson, 1975).

According to Winograd and Thordarson (1975), of the six aquifers in the region, the lower carbonate and the valley-fill aquifers have the widest areal distribution and are the principal aquifers within the region. The remaining four aquifers, however, have a limited occurrence in local areas, as in the case of Jackass Flats where the welded tuff aquifer is the sole source of water. The lower and upper carbonate aquifers and the welded-tuff aquifer store and transmit groundwater chiefly through secondary openings developed along fractures, but the bedded-tuff and the valley-fill aquifers store and transmit water chiefly through primary or interstitial openings (Winograd and Thordarson, 1975).

Rainier Mesa

Rainier Mesa is the highest of a group of ridges and mesas within the NTS, and it was the site for the first series of nuclear detonations. It is approximately 9.5 square miles in area and reaches a maximum altitude of 7,679 feet. The geology of Rainier Mesa

and its surrounding areas has been documented by Thordarson (1965), and by the authors cited in the previous section. For a detailed description of the area, one should consult the references cited. In general, rocks exposed in the Rainier Mesa area are of sedimentary and igneous origin and range in age from late Precambrian to the Holocene (Thordarson, 1965). The oldest rocks exposed are quartzite and argillite of Precambrian age and dolomite of Paleozoic age. These geologic units are, in turn, overlain by zeolitized tuff, friable-bedded tuff, and welded tuff of the Indian Trail Formation and the Piapi Canyon Group of Tertiary age. These three tuff units, which range from 2000 to 5000 feet in thickness, rest unconformably upon the thrust-faulted miogeosynclinal rocks of Paleozoic age (Thordarson, 1965).

An understanding of the sorption potential of the zeolitized tuff at the base of the tuff sequence is of critical importance for Rainier Mesa, because these widely distributed rocks control the recharge rate of groundwater to the underlying and more permeable Paleozoic aquifers (Thordarson, 1965). The zeolitized tuff found at Rainier Mesa, which is 600 to 800 feet in thickness, is a fractured aquitard with high interstitial porosity, but with very low interstitial permeability and fracture transmissibility. The interstitial porosity of the zeolitized tuff ranges from 25 to 38%, while the interstitial permeability is generally less than 0.005 gpd/ft^2 , and the fracture transmissibility ranges from 10 to 100 gpd/ft (Thordarson, 1965). The zeolitized tuff is generally fully saturated interstitially hundreds of feet above the regional water table, yet no appreciable volume of water moves through the interstices because of the very low permeability. The movement of groundwater is generally restricted to nearly vertical fractures and faults within the highly zeolitized tuff units (Thordarson, 1965).

Zeolites

Zeolites are best defined as crystalline, hydrated aluminosilicate minerals enclosing cavities occupied by large ions and water molecules, both of which have considerable freedom of movement permitting ion exchange and reversible dehydration (Deer et al., 1992). Zeolites, along with quartz and feldspar minerals, are tectosilicates, which means that they consist of three-dimensional frameworks of SiO_4^{4-} tetrahedra wherein all four corner oxygen ions of each tetrahedron are shared with adjacent tetrahedra (Mumpton, 1981). This arrangement of silicate tetrahedra reduces the overall Si:O ratio to 1:2, and if each tetrahedron in the framework contains silicon (Si) as the central cation, the structure is electrically neutral, as in quartz (SiO_2) (Mumpton, 1981). In zeolite structures, however, some of the Si^{4+} is replaced by trivalent aluminum (Al^{3+}), giving rise to a deficiency of positive charge in the three-dimensional framework. The net negative charge caused by the substitution of Al^{3+} for Si^{4+} in the framework structure is then balanced by cations, generally Ca^{2+} , Na^+ , or K^+ , contained elsewhere in the cavities of the framework (Mumpton, 1981). This substitution of Al^{3+} for Si^{4+} in the framework structure is responsible for the high cation-exchange capacities (CEC) of zeolite minerals with increasing substitutions increasing the CEC of a zeolite mineral. A general formula for natural zeolites is $(\text{Li}, \text{Na}, \text{K})_a(\text{Mg}, \text{Ca}, \text{Sr}, \text{Ba})_d[\text{Al}_{(a+2d)}\text{Si}_{n-(a+2d)}\text{O}_{2n}]^m\text{H}_2\text{O}$, where the part of the chemical formula in the square brackets represents the framework atoms and the part outside the square brackets represents the extraframework atoms, cations plus water molecules (Gottardi and Galli, 1985).

The three-dimensional framework structure of zeolites is characterized by channels and relatively large interconnecting cavities in which the cations and water

molecules are loosely bound, thus the cations and water molecules can be readily removed or replaced without disrupting the overall framework structure (Hay 1966). In practice, however, the cation-exchange behavior of a zeolite mineral also depends on a number of other factors including the framework topology (channel configuration and dimensions), size and shape (polarizability) of the ions, valence and charge density of the ions, and the electrolyte composition and concentration in the external solution (Ming and Mumpton, 1989). It has also been noted that, to some extent, zeolite surface chemistry resembles that of smectite clays. In contrast to clays, however, natural zeolites can occur as millimeter or greater sized particles, and are free of the shrinking and swelling behavior of clays (Haggerty and Bowman, 1994). Due to these unique properties, zeolites exhibit superior hydraulic characteristics, and may act as permeable barriers for controlling the spread of contaminated groundwater by cation exchange (Haggerty and Bowman, 1994). Since zeolites were discovered in 1756, about 50 natural species have been identified, and at least 150 species having no natural counterparts have been synthesized in the laboratory (Ming and Mumpton, 1989).

Formation

The formation of zeolites in a variety of different geologic environments has been extensively documented by numerous investigators including Gottardi and Galli (1985), Hay (1966), Hoover (1968), and Ming and Mumpton (1989). In general, zeolites are formed within a variety of rock types, both marine and non-marine, and are especially abundant in altered vitric tuffs. Zeolites found in vitric rocks are often formed by the reactions of the constituent minerals with pore water. Volcanic glass is a common reactant as are amorphous and poorly crystalline clay, montmorillonite, plagioclase,

nephelin, biogenic silica, and quartz (Hay, 1981). Both clay minerals and zeolites can form from a parent material, and whether a clay or zeolite mineral is formed depends on the physical environment and on the activities of dissolved species such as H^+ , alkali- and alkaline earth cations, or H_4SiO_4 (Hay, 1981). Chemical reactions that form zeolites can be caused by any number of processes, such as, hydrothermal alterations, burial metamorphism, reactions of glass and water in a saturated system, and leaching and deposition in an unsaturated system (Hoover, 1968). The species of zeolite that crystallizes will depend on the temperature, pressure, and activities of various ions and on the activity of the pore water (Hay, 1981).

According to Hoover (1968), zeolites found at the NTS formed from a volcanic material in an unsaturated environment in which vitric rocks were altered by leaching and deposition. Zeolites formed just above permeability barriers where the cation content of the groundwater and the saturation of vitric rocks were high enough to produce zeolites. The permeability barriers identified that could have caused zeolitization included impermeable welded tuffs, lava flows, Paleozoic clastic rocks, clay minerals formed by the leaching of vitric rocks just above permeable Paleozoic carbonate rocks, and zeolitized rocks formed by groundwater reactions just above one of the previously mentioned permeability barriers (Hoover, 1968). Moncure et al. (1981), however, proposed an alternative mechanism for zeolite diagenesis at the NTS. They stated that zeolites below Pahute Mesa at the NTS are a result of three factors: changing pore-water chemistry in an essentially closed hydrologic system, disequilibrium or kinetic precipitation of metastable phases, and a higher thermal gradient (Moncure et al., 1981).

Occurrence at the Nevada Test Site

Regardless of the particular mechanism for zeolite diagenesis at the NTS and surrounding areas, zeolitized rocks occur as outcrops, which cover an area of several thousand square miles. Zeolitized rocks also underlie most of the volcanic formations and alluvial basins in the area, from a few hundred to more than 6000 ft in thickness (Hoover, 1968). The zeolitized tuff found at Rainier Mesa, however, was deposited as volcanic ash consisting predominantly of pumice and glass shards, that was later massively altered, as discussed previously, to the zeolite minerals clinoptilolite, mordenite, and analcime (Thordarson, 1965). The zeolitized tuff at Rainier Mesa also contains minor amounts of clay, with some silica and hematite as cementing agents. Non-zeolitic constituents, which generally amount to 5 to 30 percent of the zeolitized tuff, are small crystals of quartz, feldspar, biotite, and dense lithic fragments. These unaltered constituents are nearly impermeable to water, and are surrounded by a slightly permeable zeolitic matrix (Thordarson, 1965).

The zeolitized tuff used in the batch equilibrium sorption experiments for this study was obtained from the Tunnel Beds, which are informal local units, of the Indian Trail Formation of Tertiary age. It was hoped that the partitioning parameters calculated using the zeolitized tuff from Rainier Mesa might be applied to other zeolitized rocks at the NTS, if it could be proven that the clinoptilolite present in the altered vitric tuffs is, mainly, responsible for the fractional uptake of the ions of interest, and if the other zeolitized rocks also contain a significant percentage of the zeolite mineral clinoptilolite.

CHAPTER 3

MATERIALS & METHODS

Adsorbent Characterization

A detailed physiochemical characterization of the zeolitized tuff from Rainier Mesa and the clinoptilolite from Jordan Valley, Oregon was necessary in order to draw logical conclusions about the possible impacts of sorption on the movement and distribution of Pb(II), Sr(II), CrO₄²⁻, and SeO₃²⁻ contaminants in the subsurface environment at the NTS. This physiochemical characterization included a particle size analysis after grinding, an investigation into the zeolitized tuff's morphology by scanning electron microscopy (SEM), an analysis of the zeolitized tuff's mineralogy by X-ray diffraction (XRD), a major and trace element analysis by X-ray fluorescence (XRF), an estimation of surface area and pore volume, an analysis of porosity and density, and a determination of the cation-exchange capacity. As pointed out earlier, the zeolitized tuff and clinoptilolite adsorbents selected for this research were chosen because of the intense interest by environmental scientists and engineers in zeolite minerals as potential natural barriers to the spread of aqueous contaminants in the subsurface environment, and because the zeolitized tuff controls the recharge rate of groundwater to the underlying and more permeable Paleozoic aquifers at the NTS.

Particle Size Distribution

A particle size distribution is the percentage by mass, number, or surface area of particles in a range of specific sizes. The particle size distribution is important because it is well known that fine particles are more “reactive”, through their higher surface areas and adsorption capacities, than coarse particles (Percival and Lindsay, 1997). For sorption studies, it is desirable that all adsorbents have similar particle sizes after grinding. Grinding of the field samples was accomplished using a Brinkmann ZM 1000 centrifugal grinder with a 0.25 mm stainless steel sieve and a six-tooth rotor.

Micromeritics Inc., a material analysis laboratory, determined the particle size distribution of the ground adsorbents by x-ray scattering and sedimentation analysis in a 60% glycerin, 0.3% Daxad23 solution using a Micromeritics SediGraph 5100. Particle size distributions for both adsorbents were calculated in terms of particle mass, number, and surface area. The particle size distributions for the ground zeolitized tuff from Rainier Mesa will be discussed first, followed by a discussion of the particle size distributions for the ground clinoptilolite from Jordan Valley, Oregon.

Table 1 summarizes the results of the particle size analyses that were carried out on both adsorbents. The table reveals that the ground zeolitized tuff had a median mass diameter of 11.84 μm with a modal mass diameter of 16.87 μm . The median of a frequency distribution is the value that divides the distribution into two equal areas, and the mode of the distribution is the value that occurs most frequently (Stockham, 1979). The table also reveals that the ground zeolitized tuff had a median number diameter of 0.53 μm with a modal number diameter of 0.38 μm . Lastly, inspection of the table reveals that the ground zeolitized tuff had a median surface area diameter of 1.22 μm with

Table 1. Particle size distributions for zeolitized tuff and clinoptilolite.

Particle Size Distribution	Zeolitized Tuff	Clinoptilolite
Mass		
Median Distribution	11.84 μm	12.34 μm
Modal Distribution	16.87 μm	22.21 μm
Number		
Median Distribution	0.53 μm	0.39 μm
Modal Distribution	0.38 μm	0.33 μm
Surface Area		
Median Distribution	1.22 μm	0.98 μm
Modal Distribution	0.55 μm	0.45 μm

a modal surface area diameter of 0.55 μm . These particle size diameters are consistent with the expected particle size distribution for particles that were ground and passed through a 0.25 mm stainless steel sieve. Figure 2 illustrates the mass fraction (percent of total mass) versus particle size diameter for both adsorbents. Most fine-particle systems have particle size distributions that obey the log-normal distribution function.

Consequently, when particle size is plotted as a function of the number of times each size occurs, a skewed particle size distribution is obtained (Stockham, 1979). Inspection of the figure clearly shows that for the ground zeolitized tuff, the equivalent spherical diameters do, in general, follow a log-normal distribution. In addition, there appears to be relatively little skew with the median value occurring at approximately 10 μm .

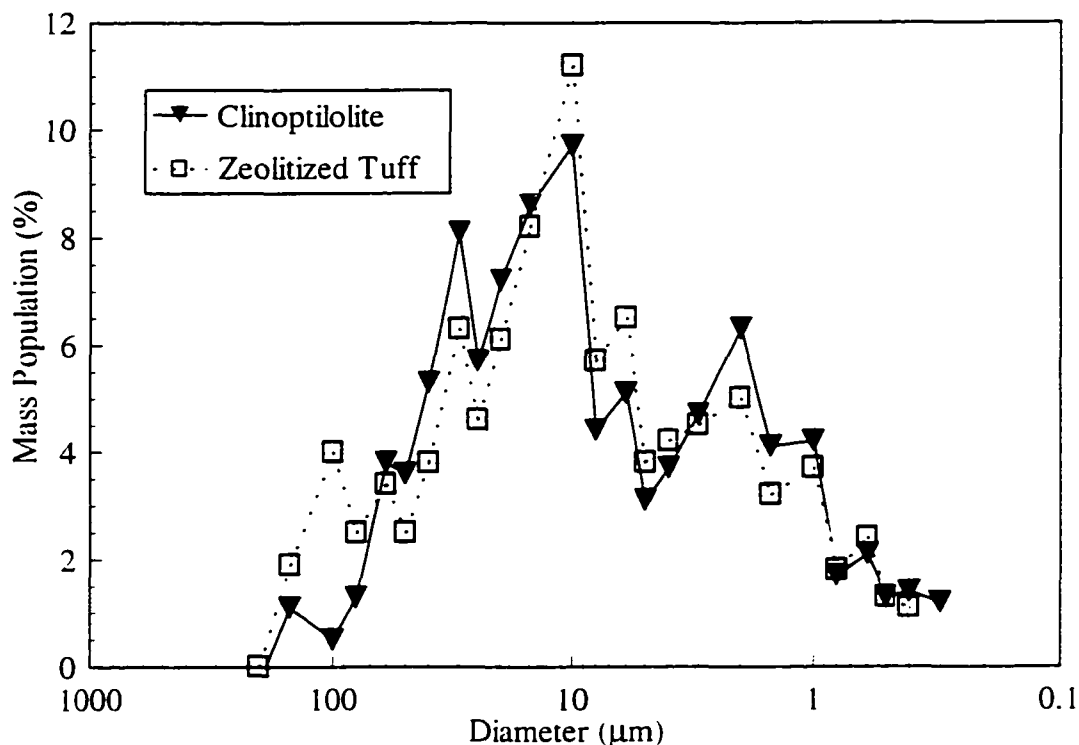


Figure 2. Mass population (%) vs. particle size diameter for the ground zeolitized tuff and clinoptilolite.

Table 1 also shows the particle size distributions for the ground clinoptilolite.

The ground clinoptilolite had a median mass diameter of 12.34 μm with a modal mass diameter of 22.21 μm . In addition, the ground clinoptilolite had a median number diameter of 0.39 μm with a modal number diameter of 0.33 μm . The surface area distribution was the last particle size distribution calculated, and an inspection of the table reveals that the ground clinoptilolite had a median surface area diameter of 0.98 μm with a modal surface area diameter was 0.45 μm . Inspection of Figure 2 also shows that the mass fraction of the ground clinoptilolite follows a log-normal distribution around the median diameter that occurs at approximately 10 μm . In addition, the particles size distributions for the ground clinoptilolite are also consistent with the expected particle

size distribution for particles that were ground and passed through a 0.25 mm stainless steel sieve.

In conclusion, the particle size distributions for both adsorbents agree extremely well with each other, which is to be expected because both adsorbents were ground using the same equipment and settings to achieve particle sizes of less than 250 μm . Overall, these particle size diameters indicate that there would be little, if any, variation in the magnitude of the “reactivity” of these particles based on size. These particle size distributions, however, also have a significant physical meaning. For instance, the distributions revealed that the mass of the ground samples is distributed among the larger sized particles, and that the surface area and number of the ground samples is distributed among the smaller sized particles. These particle size diameters are expected and in no way surprising because it is well known that larger sized particles weigh more than smaller sized particles, and that surface area increases with decreasing particle size.

Particle Morphology

The morphology of the zeolitized tuff was also investigated using SEM. Scanning electron micrographs of the zeolitized tuff from Rainier Mesa were obtained with a JEOL JSM-840A SEM / EDX spectrometer at 950- and 1700-fold magnifications (Figures 3 and 4). Scanning electron micrographs of the clinoptilolite were not obtained since those samples were assumed to be relatively pure. SEM is one of the most universal and useful techniques available for the study of the physical characteristics of solid surfaces because of its ease of use, imaging resolutions down to a few tens of angstroms, and its great depth of field (Hochella, 1990). A complete explanation of the SEM technique is beyond the scope of this thesis, however, comprehensive reviews on SEM and related techniques

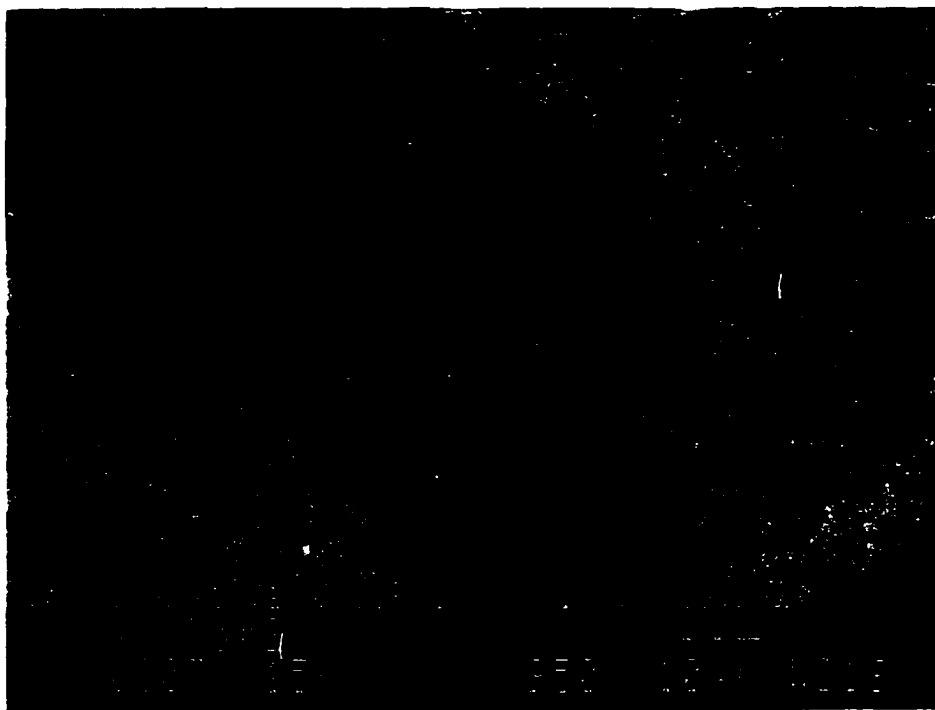


Figure 3. Photomicrograph of the zeolitized tuff at a 950-fold magnification.



Figure 4. Photomicrograph of the zeolitized tuff at a 1700-fold magnification.

can be found in books by Goldstein et al. (1981), and Newbury et al. (1985).

Zeolite minerals formed in sedimentary rocks are extremely photogenic, and the characteristic morphology of several members of the zeolite group may commonly be used for identification (Mumpton and Ormsby, 1976). For example, the zeolite mineral clinoptilolite can occur as laths and plates, many of which display the characteristic tabular morphology typical of basalt-vug heulandite (Ming and Mumpton, 1989). These laths of clinoptilolite are commonly 1 to 3 μm in thickness and 5 to 20 μm in length. Clinoptilolite also occurs, however, in almost anhedral masses with only rare crystal faces or edges. Even though euhedral grains are relatively easy to identify by their distinctive morphological features, much of the material in a zeolitized tuff, even one relatively rich in a single zeolite (i.e., >90%), can commonly occur as formless masses that lack any characteristic morphology (Ming and Mumpton, 1989). Reliable identification of zeolite minerals in rocks or soils, therefore, relies on SEM used in close conjunction with XRD (Ming and Mumpton, 1989).

Inspection of the zeolitized tuff micrograph in Figure 3 reveals one of the textbook situations described by Ming and Mumpton (1989). Most of the particles at the 950-fold magnification in this micrograph are present in the form of anhedral masses with few, if any, well defined crystal faces. The anhedral masses in the micrographs, however, were identified as the zeolite mineral clinoptilolite by XRD (see next section). In addition to the anhedral masses of clinoptilolite that were clearly seen in both micrographs, there appears to be another mineral phase present in the form of short, narrow fibers. The zeolite mordenite commonly coexists with clinoptilolite in the form of fine fibers (about 0.1 μm in diameter and 5 to 25 μm in length) spanning gaps and

crevices between clinoptilolite crystals (Ming and Mumpton, 1989). Mordenite can also occur as intertwined nests of fibers and as thin laths and needles about 0.5 to 1.5 μm in diameter and about 10 to 30 μm in length. Inspection of the zeolitized tuff micrographs in Figure 3 and Figure 4 clearly reveal that in addition to the dominant anhedral masses of clinoptilolite, mordenite also appears to be present in limited quantities in the field samples from the NTS in the form of fine fibers spanning the gaps and crevices between the clinoptilolite crystals. In addition to the two zeolite mineral phases present in the micrographs, a third mineral phase is present, with comparatively larger grains at both magnifications. These angular particles are probably either a dense lithic fragment or some type of accessory silicate mineral phase present in the volcanic tuff, possibly a feldspar or quartz phase.

Adsorbent Mineralogy

The mineralogy of the zeolitized tuff and clinoptilolite was determined by XRD using Cu $K_{\alpha 1}$ radiation ($\lambda=1.5405 \text{ \AA}$) to identify the specific minerals within each adsorbent, and to complement the SEM morphological investigation. XRD analysis is the best means of identifying individual members of the zeolite group because zeolite minerals for the most part yield characteristic XRD lines that allow for easy distinction among the several members of the group, and between zeolites and other common constituents of rock and soil systems (Ming and Mumpton, 1989). The XRD spectrum for the zeolitized tuff from Rainier Mesa is shown in Figure 5. The XRD spectrum for the clinoptilolite will not be shown because it revealed that the clinoptilolite was pure and free of impurities.

It can be seen in the figure that the zeolitized tuff contains a number of well

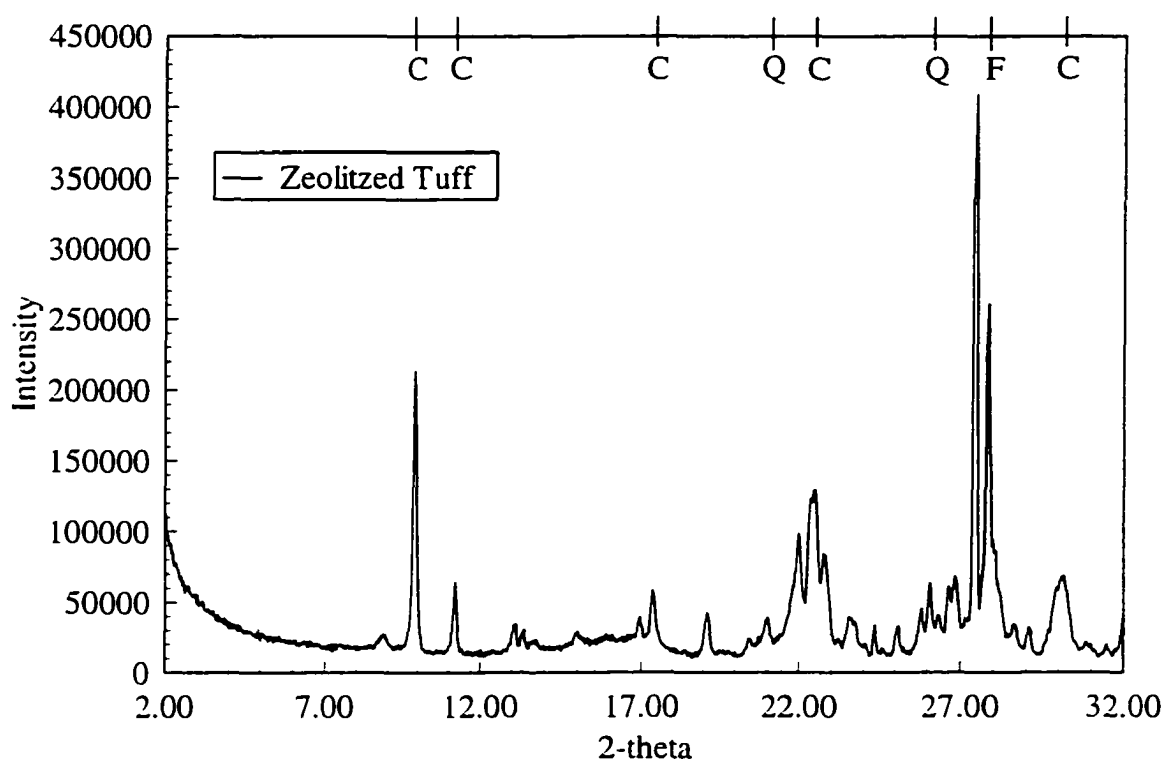


Figure 5. X-ray diffraction spectrum of the zeolitized tuff.

crystallized minerals. This can be concluded because of the intensity of the peaks, and because there is a relatively low background signal. Inspection of the figure also reveals that the zeolitized tuff spectrum contains a number of peaks that correspond to the zeolite mineral clinoptilolite. These peaks are labeled at the top of the figure with a C. The spectrum also reveals that at a 2-theta value of approximately 28° there are two peaks that do not correspond to the zeolite clinoptilolite. These two peaks were identified as belonging to the feldspar group of aluminosilicate minerals. These peaks most likely correspond to the K^{+} rich alkali-feldspar sanidine. In addition to the clinoptilolite and feldspar, the zeolitized tuff spectrum also contains peaks corresponding to quartz that are labeled at the top of the figure with a Q. The presence of these other two minerals in the zeolitized tuff is consistent with other studies. For example, Thordarson (1965) stated

that the zeolitized tuff from Rainier Mesa contained from 5-30% nonzeolitic constituents that included small crystals of quartz, feldspar, biotite, and dense lithic fragments.

Major and Trace Element Analyses

The major and trace element compositions of both adsorbents were also determined using XRF. The analysis of geologic materials by XRF provides data on the major oxide percentages of the whole rock sample, as well as on the trace element concentrations. The XRF data in Table 2 and Table 3 were collected at the University of Nevada, Las Vegas, using a Rigaku 3030 X-ray Spectrometer. This spectrometer uses a Rh target with a side window X-ray tube. Calibration of the spectrometer was based on the international rock standards from the United States Geologic Survey. Samples of both adsorbents were processed into fused glass disks for analysis by heating 1.7 g of the sample, 8.5 g lithium tetraborate ($\text{Li}_2\text{B}_4\text{O}_7$), and 0.27 g ammonium nitrate (NH_4NO_3) to 1100 degrees in a muffle furnace for 30 minutes in gold-platinum alloy crucibles and pouring the resulting melt into heated Au-Pt molds. All samples and reagents were weighed to 0.0005 g, and were stored in desiccators prior to analysis.

As shown in Table 2, both adsorbents have remarkably similar oxide percentages for each major element. It is interesting to note, however, that on a whole sample basis the clinoptilolite has an only 3% greater Al_2O_3 concentration than the zeolitized tuff, but on a relative scale the clinoptilolite has approximately 15% more Al_2O_3 compared to the zeolitized tuff. A greater Al_2O_3 composition suggests that the clinoptilolite has a greater degree of substitution of Al^{3+} for Si^{4+} within the framework structure of the zeolite compared to the zeolitized tuff, assuming that the Al_2O_3 concentration of the zeolitized tuff is related to the presence of a single zeolite. A greater substitution of Al^{3+} for Si^{4+}

Table 2. Major element analyses for the zeolitized tuff and clinoptilolite.

Weight %	Zeolitized Tuff	Clinoptilolite
SiO ₂	73.7	71.5
Al ₂ O ₃	13.8	16.3
TiO ₂	0.190	0.294
Fe ₂ O ₃ (T)	1.69	2.16
CaO	1.44	1.24
K ₂ O	5.43	5.05
MnO	0.079	0.009
P ₂ O ₅	0.005	0.061
Na ₂ O	3.44	4.21
MgO	0.364	0.263

Table 3. Trace element analyses for the zeolitized tuff and clinoptilolite.

Trace Element	Zeolitized Tuff (ppm)	Clinoptilolite (ppm)
Rb	176.1	174.5
Sr	188.7	211.8
Y	28.17	100.1
Zr	213.0	373.0
Nb	29.32	44.41
Cr	124.3	33.97

within the framework structure of the clinoptilolite would cause the clinoptilolite to have a higher CEC than the zeolitized tuff, because the cation-exchange capacity of a zeolite is primarily a function of the degree of substitution of Al^{3+} for Si^{4+} in its framework tetrahedra (Ming and Mumpton, 1989). Another explanation, however, for the greater Al_2O_3 concentration of the clinoptilolite is that the zeolitized tuff is not compositionally 100% pure clinoptilolite. Compositional differences could show up because the zeolitized tuff is a combination of different minerals, and XRF examines the whole rock sample.

Inspection of the data in Table 3 reveals that the adsorbents have dissimilar trace element analyses except for the trace element Rb. It is interesting to note from the trace element analyses, though, that both adsorbents have fairly high concentrations of Sr. In addition, the zeolitized tuff has approximately 124 ppm Cr, and the clinoptilolite has approximately 34 ppm Cr. Trace element analyses for Pb and Se were not obtained. These trace element data are interesting because they show that both adsorbents have minor amounts of two of the elements of interest to this study.

Surface Area and Pore Size Distribution

The sample characterization of both adsorbents also included an estimation of the total surface area and pore size distribution as determined by nitrogen adsorption at 77.4 K and the BET model (Brunauer et al., 1938). The specific surface area of a material is the amount of reactive surface area available for adsorbing solutes per unit weight of the material. The surface area of a material is important to be aware of because it enables normalization of solute adsorption data to surface area, and is required for applying electrical double layer models (Davis and Kent, 1990). In addition, it allows for an

estimation of the quantity of surface functional groups per unit mass of solids, if the group density per unit area is already known. Micromeritics measured the specific surface area and pore size distribution of both adsorbents with an ASAP 2405. This data was essential because it allowed for the solid concentration of the adsorbents to be normalized with respect to the surface area of the adsorbents. Normalizations of this type allowed for comparisons of the sorption behavior of the ions as a function of the adsorbent type to be made. Accurate surface area estimates for these types of comparisons are essential because the number of available binding sites for the ions of interest are directly proportional to the overall surface area of the adsorbent.

Due to the importance of surface area, additional estimates of the surface area of the zeolitized tuff were obtained in order to verify the results from Micromeritics. These additional surface area estimates included a second estimate of the surface area of the ground zeolitized tuff, as well as estimates of the surface area of the zeolitized tuff adsorbent at different particle sizes. Each of these separate analyses was obtained at the University of Nevada, Las Vegas with a Micromeritics Gemini 2370 surface area analyzer. The BET-surface area estimates for both adsorbents, and the surface area estimates for the verification samples were obtained from the slope of the linearized BET function, and the adsorption branches of the nitrogen isotherms were used for both adsorbents.

The results of the surface area and pore size distributions determined by Micromeritics are shown in Table 4. As can be seen from the table, the clinoptilolite has a surface area of $36.03 \text{ m}^2/\text{g}$. This surface area is roughly three times greater than the $12.27 \text{ m}^2/\text{g}$ surface area of the zeolitized tuff. These surface area estimates allow for the

Table 4. Surface area and pore size measurements for the zeolitized tuff and clinoptilolite.

	Zeolitized Tuff	Clinoptilolite
BET-Surface Area	12.27 m ² /g	36.03 m ² /g
BJH Adsorption Average Pore Diameter (4V/A)	193.0 Å	178.43 Å
BJH Desorption Average Pore Diameter (4V/A)	254.83 Å	207.04 Å
Average Pore Diameter (4V/A)	238.06 Å	212.18 Å

normalization of the solid concentration of both adsorbents. For example, the clinoptilolite would need roughly 1/3 the solid concentration of the zeolitized tuff to have roughly the same overall surface area. Figure 6 and Figure 7 illustrate the adsorption and desorption branches of the nitrogen isotherms for the zeolitized tuff and clinoptilolite adsorbents, respectively. Based on the overall shapes of the figures, the nitrogen isotherms can be classified using the International Union of Pure and Applied Chemistry's (IUPAC) naming scheme as Type IV nitrogen isotherms with type H3 hysteresis loops (Gregg and Sing, 1982). A Type IV nitrogen adsorption isotherm is often found with inorganic oxide xerogels and other porous solids that contain well-defined mesopores, and type H3 hysteresis loops are generally given by aggregates of platy particles of solids containing slit-shaped mesopores, which possess an assortment of interconnected pores of different size and shape (Gregg and Sing, 1982). A mesopore is a type of pore with a diameter (width) of 20 to 500 Å. Mesoporous materials exhibit enhanced adsorption above relative pressures of about 0.4 because of capillary condensation of liquid N₂ in the mesopores (Davis and Kent, 1990). These types of

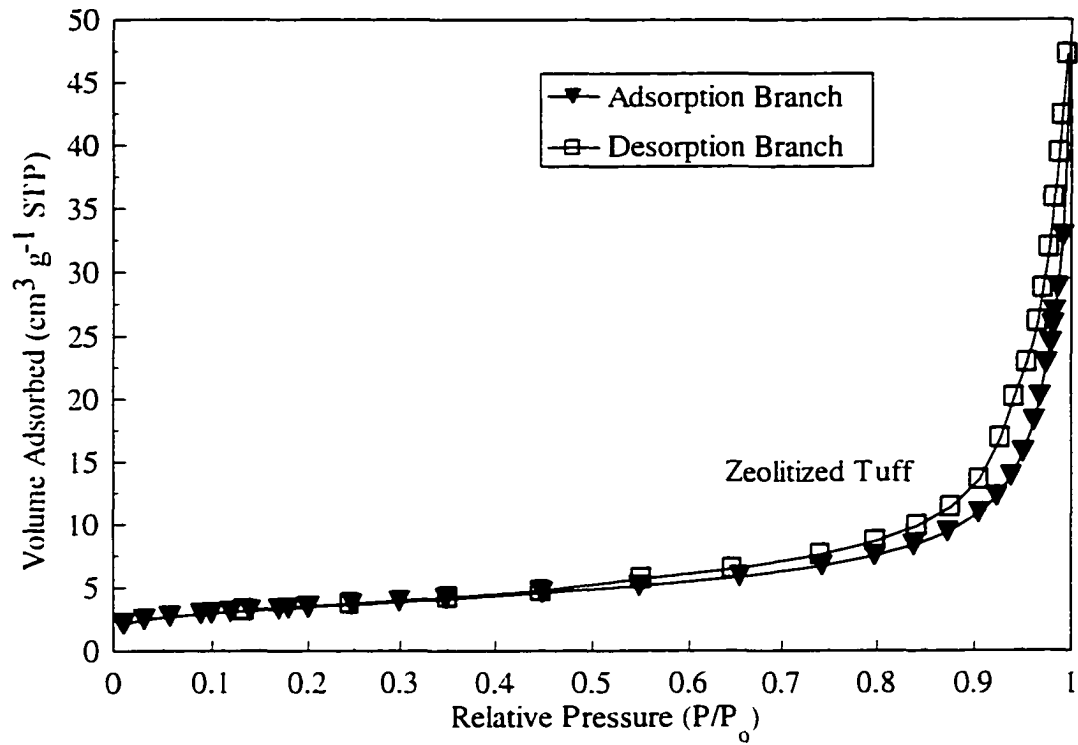


Figure 6. Isotherm of nitrogen adsorption on the zeolitized tuff.

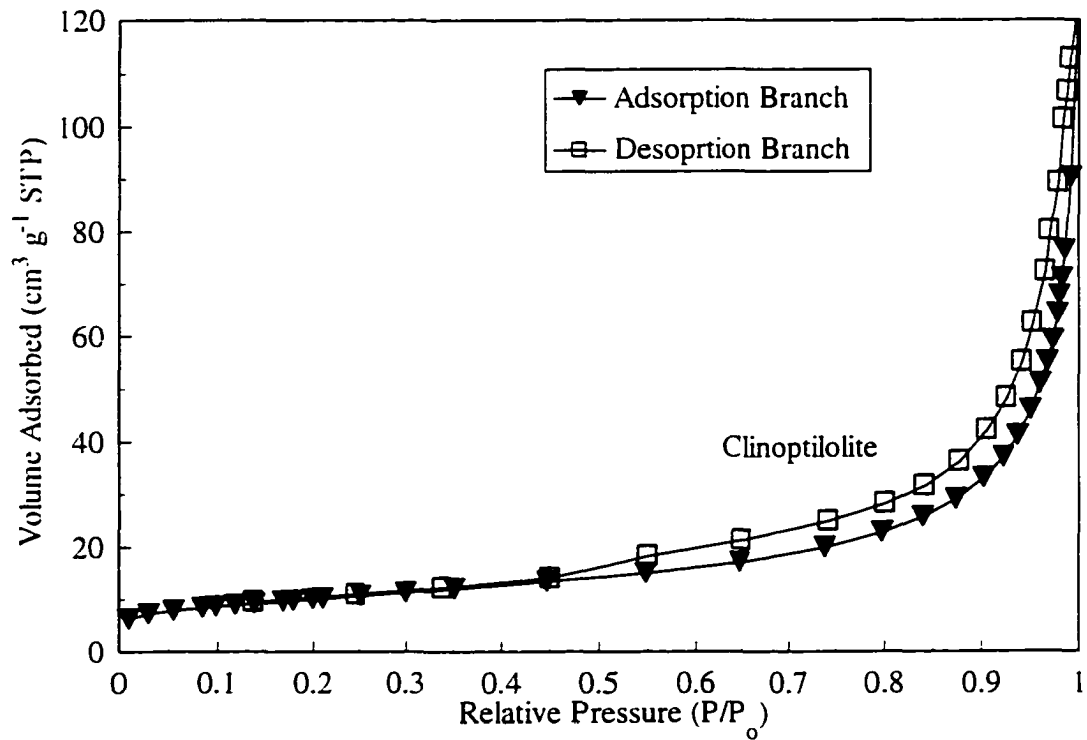


Figure 7. Isotherm of nitrogen adsorption on the clinoptilolite.

nitrogen adsorption isotherms indicate adsorbents with monolayer and multilayer adsorption.

Table 4 also shows the average pore diameters ($4V/A$) calculated from the adsorption and desorption branches of both adsorbents using the Barrett, Joyner, and Halenda (BJH) method (Barrett et al., 1951), and the average pore diameter ($4V/A$) calculated from the BET model. These pore size diameters were also obtained from the nitrogen isotherms and the assumption that the pores were cylindrical. Using this assumption, the average pore size diameters from either branch of the nitrogen isotherm can be calculated utilizing the Kelvin equation and the method described by BJH. The average pore diameter, however, is calculated by dividing the total volume adsorbed by the specific surface area determined by the BET model and by multiplying by four. It can be seen from the table that the zeolitized tuff has an average pore diameter from the adsorption branch of the nitrogen isotherm equal to 193.0 Å, and an average pore diameter from the desorption branch of the nitrogen isotherm equal to 254.83 Å. Pore size determinations are equally valid computationally using either branch of the nitrogen isotherm, however, discrepancies between the two are often seen when the pore system of the adsorbent forms a network, which is often the case with mesoporous solids (Gregg and Sing, 1982). The overall average pore diameter ($4V/A$), however, is equal to 238.06 Å. The clinoptilolite has an average pore diameter of 178.43 Å from the adsorption branch of the nitrogen isotherm, and an average pore diameter of 207.04 Å from the desorption branch of the nitrogen isotherm. The overall average pore diameter ($4V/A$) of the clinoptilolite, however, is equal to 212.18 Å. In conclusion, it can be seen from the table that the zeolitized tuff has a somewhat larger average pore diameter than the

clinoptilolite. The differential pore volume distributions of the zeolitized tuff and clinoptilolite as a function of mean pore radius are shown in Figure 8 and Figure 9, respectively. From the figures, it can be seen that the distributions obtained from the two branches are somewhat similar for both adsorbents. The peaks in the desorption branches of both distributions below 50 Å are likely to be artifacts of the nitrogen tensile strength effects (Gregg and Sing, 1982).

As stated previously, additional surface area measurements of the ground zeolitized tuff were conducted to verify the results from Micromeritics, and to investigate the relationship between surface area of the zeolitized tuff and particle size. By doing this, a determination can be made whether the overall surface area of the zeolitized tuff is controlled by the internal framework structure of the zeolite minerals contained in the zeolitized tuff. In order to do this, samples of the original zeolitized tuff were ground using a mortar and pestle with every precaution taken to prevent contamination of the zeolitized tuff. The ground adsorbent was then passed through several sieves and divided into 4 different size fractions. The different particle size fractions analyzed included fractions with particles greater than 500 µm, particles between 500 µm and 250 µm, particles between 250 µm and 125 µm, and particles smaller than 125 µm. These surface area measurements were conducted in order to investigate the relationship between particle size and the total surface area. For example, if the overall surface area of the zeolitized tuff is not dependent on the particle size, which is a distinct possibility with zeolites because most of the surface area of zeolites is due to the internal framework structure of the mineral, then these sorption experiments would be more widely applicable to the subsurface environment, and not just to the same material that had been

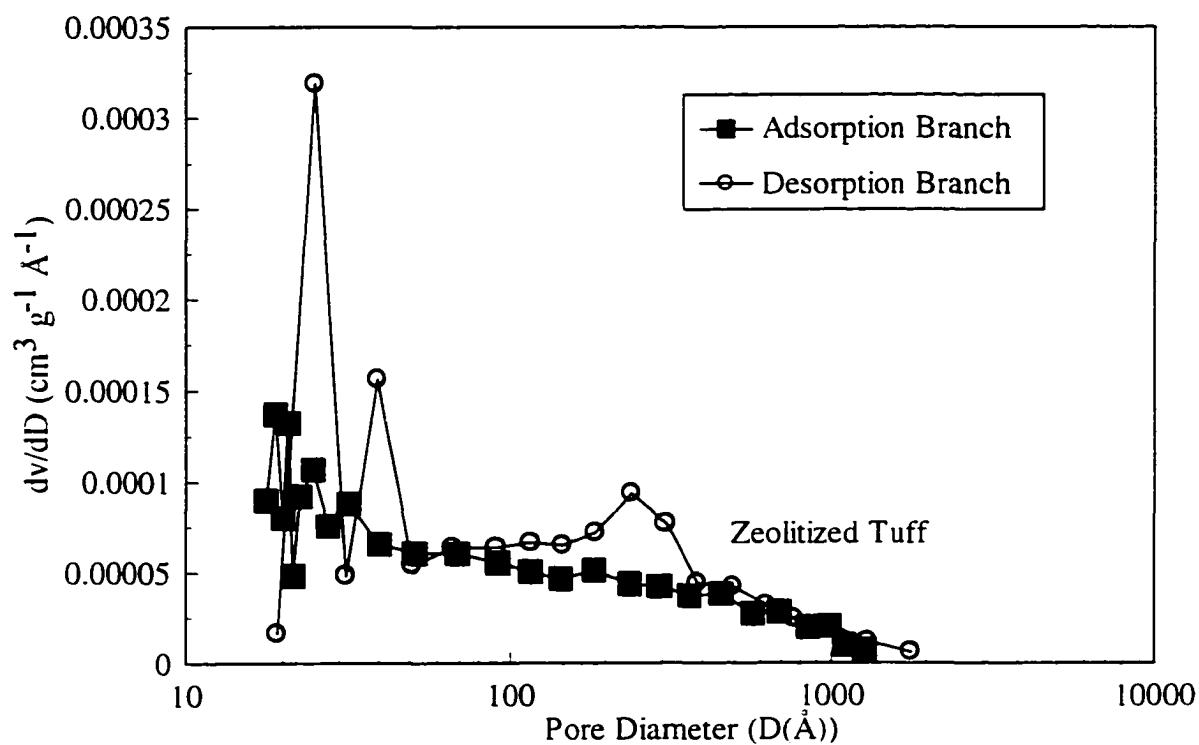


Figure 8. Pore volume distribution of the zeolitized tuff derived from nitrogen adsorption isotherm.

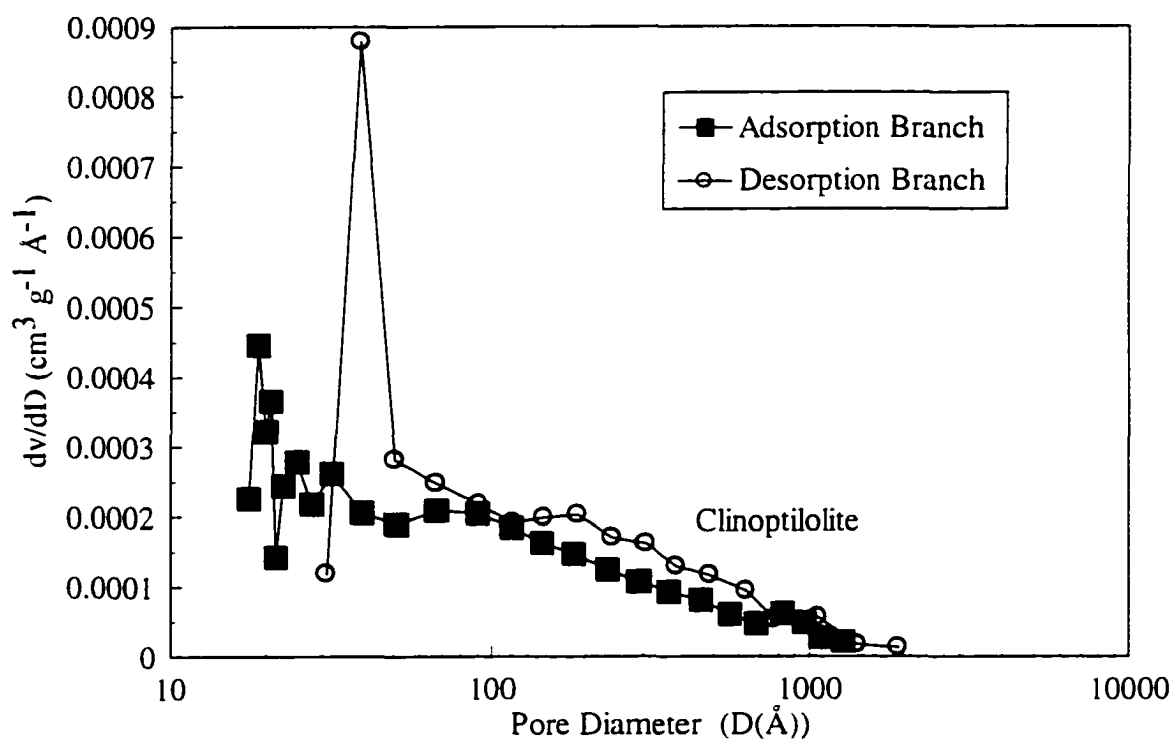


Figure 9. Pore volume distribution of the clinoptilolite derived from nitrogen adsorption isotherm.

crushed to less than 20 μm .

Table 5 reveals the results of the surface area estimates as a function of the particle size, as well as the verification of the surface area of the ground zeolitized tuff. As can be seen from the table, the second estimate of the surface area of the zeolitized tuff compares well to the original estimate of the surface area. The original estimate of the surface area of the zeolitized tuff was $12.27 \text{ m}^2/\text{g}$, and the duplicate surface area estimate returned a surface area of $13.63 \text{ m}^2/\text{g}$. These surface area estimates are in good agreement and clearly show that the zeolitized tuff has a surface area that is approximately 1/3 the surface area of the clinoptilolite.

In addition, the table clearly shows that there is not a large variation in the surface area of the zeolitized tuff as a function of the particle size. Although, it can be seen from the table that the largest particle size does result in the smallest surface area, as expected. Additionally, it can be seen from the table that as the overall particle size of the adsorbent

Table 5. Specific surface area of the zeolitized tuff as a function of particle size.

Size Fraction	Surface Area
Original Ground Sample	$13.63 \text{ m}^2/\text{g}$
Samples > 500 μm	$10.85 \text{ m}^2/\text{g}$
Samples between 500 and 250 μm	$12.12 \text{ m}^2/\text{g}$
Samples between 250 and 125 μm	$13.40 \text{ m}^2/\text{g}$
Samples < 125 μm	$14.05 \text{ m}^2/\text{g}$

decreases, the specific surface area increases slightly. The small variations in the specific surface area as a function of the particle size can most likely be attributed to the non-zeolitic mineral phases contained within the zeolitized tuff. The overall surface area of the ground zeolitized tuff would increase as the particle size of these types of minerals decreases. The small change in the overall surface area as a function of particle size, however, suggests that the internal framework structure of the clinoptilolite contained within the zeolitized tuff is, in fact, responsible for most of the surface area of the zeolitized tuff, and that the surface area is apparently accessible to nitrogen, and potentially the ions of interest. For example, the framework structure of clinoptilolite is composed of 3-dimensional channels with the smallest channel measuring $4.0 \times 5.5 \text{ \AA}$ (Ming and Mumpton, 1989). This channel size is large enough to permit the movement of N_2 (g) to any of the available surface area contained in the framework cavities because the radius of N_2 (g) is 2.27 \AA . These surface area estimates are important because they tend to support the assertion that the partitioning coefficients calculated from the batch equilibrium sorption experiments with the ground zeolitized tuff would be, in fact, relevant for the natural adsorbent located in the field.

Porosity and Density

The sample characterization also included a determination of the porosity and density of both adsorbents. Micromeritics determined the porosity of both adsorbents using an AccuPyc 1330 mercury porosimeter. As can be seen from Table 6, the porosity of the zeolitized tuff is approximately 20%, while the porosity of the pure clinoptilolite is approximately 16.8%. This calculated porosity of the zeolitized tuff compares well with previously reported results. For example, according to Thordarson (1965), the zeolitized

Table 6. Density and porosity measurements for the zeolitized tuff and clinoptilolite.

	Zeolitized Tuff	Clinoptilolite
Porosity	20.12%	16.80%
Average Density	2.32 g/cm ³	2.22 g/cm ³
Bulk Density	0.77 g/cm ³	0.68 g/cm ³

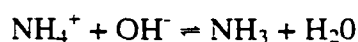
tuff found at Rainier Mesa has an average interstitial porosity of 25%.

Micromeritics also calculated the density of both adsorbents using the AccuPyc 1330 mercury porosimeter. As can again be seen in Table 6, the densities of both adsorbents are almost identical with the zeolitized tuff having an average density of 2.32 g/cm³, and the clinoptilolite having an average density of 2.22 g/cm³. These average densities compare well with each other, and agree well with a textbook reported value for pure clinoptilolite that varies between 2.1 to 2.29 g/cm³. The higher density of the zeolitized tuff can likely be attributed to the presence of quartz and alkali feldspars contained in the altered vitric tuff that have densities of 2.65 g/cm³ and 2.54 to 2.62 g/cm³, respectively. In addition to the average density, the bulk densities of both adsorbents also compare well. The zeolitized tuff had a bulk density of 0.77 g/cm³, and the clinoptilolite had a bulk density of 0.68 g/cm³.

Cation-Exchange Capacity

Cation-exchange capacity is a measure of the quantity of readily exchangeable cations in an adsorbent, and it is usually expressed in milliequivalents per kg of soil (meq/kg). The cation-exchange capacity of each adsorbent was determined at the

University of Nevada, Las Vegas using the method developed by Busenberg and Clemency (1973). In general, this procedure consists of the saturation of the cation-exchange sites of an adsorbent with ammonium ions. The method then utilizes an ammonia electrode to determine the amount of ammonia released by treatment of the ammonium saturated adsorbent by a strong base. Assuming that all of the cation-exchange sites were indeed saturated with ammonium ions, the addition of a strong base will release ammonia and be detectable by the ammonia electrode due to the following reaction:



This method of determining the cation-exchange capacity of an adsorbent has the advantage of simplicity, speed, and accuracy. In addition, this method has the ability to utilize small sample sizes (50 mg), and it is relatively free from interferences (Busenberg and Clemency, 1973).

The cation-exchange capacity measurements for each adsorbent were performed in duplicate, and the final value obtained was the average of the two individual experiments. The cation-exchange capacity of the zeolitized tuff from Rainier Mesa was 1,430 meq/kg, and the cation-exchange capacity of the clinoptilolite was 2,100 meq/kg. As can be seen from these results, the cation-exchange capacity of the clinoptilolite is almost 1.5 times as large as the cation-exchange capacity of the zeolitized tuff. This higher cation-exchange capacity indicates that the clinoptilolite would have a much greater capacity to bind cations than the zeolitized tuff. The large cation-exchange capacity of the clinoptilolite can be attributed to the substitution of Al^{3+} for Si^{4+} within the framework structure of the clinoptilolite that was verified with the XRF studies in this

chapter. This substitution of Al^{3+} for Si^{4+} gives rise to a higher negative charge that is countered by the presence of framework cations. The lower cation-exchange capacity of the zeolitized tuff could be attributed to the fact that it is not a pure zeolite. For example, if the zeolitized tuff is composed of 50% clinoptilolite and 50% accessory minerals, then one could assume that the cation-exchange capacity of the zeolitized tuff would be approximately half as large as that of the pure clinoptilolite. The exact proportion of zeolites to other mineral phases present in the zeolitized tuff, however, cannot be easily determined.

Based on the cation-exchange capacity measurements for each adsorbent, calculations were made to determine the molar amount of divalent metal cations that could be theoretically exchanged with the cations that are contained within the framework structure of either adsorbent. Calculations were performed at solid concentrations of 1.0, 2.5, 3.0, and 20 g/L because the experimental work with the cations was performed at these solid adsorbent concentrations. Inspection of the data in Table 7 reveals that both adsorbents have the capacity to readily accept divalent metal cation concentrations up to 1.0×10^{-4} M even at a relatively low solid adsorbent concentration of 2.5 g/L. It should be noted that a 1.0×10^{-4} M metal cation concentration was the highest concentration used during the batch equilibrium sorption experiments. The data in the table reveal, however, that even at this highest metal cation concentration, the entire molar concentration could be theoretically exchanged for the cations contained within the framework structure of either adsorbent at solid concentrations of 2.5, 3.0, and 20.0 g/L. These calculations do not take into account, however, the concentration of any background electrolyte which would also supply cations that could just as easily exchange with the cations of either

Table 7. Calculated exchange capacity of the zeolitized tuff and clinoptilolite for divalent cations.

Adsorbent Concentration	Zeolitized Tuff	Clinoptilolite
1.0 g/L	7.15×10^{-4} M	1.05×10^{-3} M
2.5 g/L	1.79×10^{-3} M	2.63×10^{-3} M
3.0 g/L	2.15×10^{-3} M	3.15×10^{-3} M
20 g/L	1.43×10^{-2} M	2.10×10^{-2} M

adsorbent. In such a scenario, there would be a competition between all of the aqueous cations for the available cation-exchange sites located within the framework structure of either adsorbent.

Methods

Batch Equilibrium Sorption Experiments

For all experiments in this study, reagent-grade chemicals were used, as received without further purification or modification. High purity water for all experiments was provided by a Nanopure water purification system, which produced water with at least 18.1 M Ω -cm of resistivity.

The batch equilibrium sorption experiments were conducted in individual polypropylene test tubes by mixing weighed quantities of the crushed zeolitized tuff or clinoptilolite with varying amounts of NaNO₃ to adjust the total ionic strength, HNO₃ and NaOH to adjust the pH, and either Pb(NO₃)₂, Sr(NO₃)₂, K₂CrO₄, or Na₂SeO₃ to vary the total ion concentration. The batch equilibrium sorption experiments comparing the

sorption behavior of the cations as a function of adsorbent type were conducted with 3.0 g/L zeolitized tuff and 1.0 g/L clinoptilolite to normalize the experiments with respect to the overall surface area of the adsorbents. The batch equilibrium sorption experiments comparing the sorption behavior of the anions, however, were performed with 100 g/L zeolitized tuff and 33 g/L clinoptilolite.

The samples were then equilibrated in the test tubes by an end-over-end rotation at 8 rpm at room temperature for approximately 24 hours. After equilibration, the final pH of the suspension was measured using an Orion model 720 pH meter with an Orion Ross glass combination electrode. The pH meter was calibrated daily using pH 4.0, 7.0, and 10.0 buffers. The equilibrated samples were then centrifuged at 9000 rpm for approximately 30 minutes with a Marathon 21 K/R refrigerated centrifuge to achieve solid-solution separation. After centrifugation, a 2 mL aliquot was removed from the supernatant and acidified with concentrated nitric acid (HNO₃) before analysis.

Ion concentrations of the aliquots were measured with a Perkin-Elmer 4110 ZL Atomic Absorption Spectrometer equipped with a graphite furnace and Zeeman background correction. The relative fractional uptake of the ions of interest was determined by comparing the ion concentrations in the supernatant to the concentration of a control sample, to which no solid had been added. The fractional uptake for each sample was calculated as:

$$\text{Percent Sorbed} = \frac{M_o - M_s}{M_o} \times 100 \quad (1)$$

where M_o is the total metal concentration added to the sample, and M_s is the concentration remaining in the supernatant.

Sorption Parameter Estimation Techniques

Once the batch equilibrium sorption experiments were completed, the fractional uptake data were used to obtain Freundlich and linear isotherm parameters. These parameters can be used in transport codes to model the movement of these potentially hazardous ions in the subsurface environment. For example, distribution coefficients based on linear isotherms can be used in conjunction with the retardation equation, which relates the average velocity of a contaminant, V_c , to the average groundwater velocity, V_{gw} :

$$V_c = \frac{V_{gw}}{\left(1 + \frac{\rho_b}{\theta} * K_d\right)} \quad (2)$$

where

ρ_b = bulk density of the aquifer material

θ = porosity of the aquifer material

K_d = distribution coefficient for the solute

Predictions concerning the mobility of contaminants in a groundwater flow system may be made employing this equation if the distribution coefficient for the solute and aquifer material of interest and the other hydrogeological parameters are known.

The Freundlich isotherm is the oldest of the nonlinear sorption isotherms, and it has been used widely to describe the sorption of solutes by soils (Travis and Etnier, 1981). This isotherm equation applies very well to solids with heterogeneous surface properties and generally for heterogeneous solid surfaces, and it is very convenient for plotting equilibrium sorption data empirically in a sorbed concentration versus an equilibrium concentration plot (Stumm and Morgan, 1996). A graphical plot of the

quantity adsorbed from solution (S) as a function of the equilibrium concentration (C) is known as the Freundlich isotherm equation (Stumm and Morgan 1996):

$$S = K_f * (C)^{1/n} \quad (3)$$

where

S = quantity of adsorbate associated with the adsorbent (g/g)

C = total concentration of adsorbate in solution (g/m³)

K_f = Freundlich constant (g/g)/(g/m³)^{1/n}

1/n = a measure of nonlinearity

It should be kept in mind that when applying the Freundlich isotherm equation the flexibility of the two constants allows for easy curve fitting, but it does not guarantee accuracy if the data are extrapolated beyond the experimental data points (Travis and Etnier, 1981). Equilibrium sorption data will plot on a straight line in a linear scale if the value of 1/n is equal to 1.0. In those situations, the Freundlich isotherm equation reduces to the linear isotherm equation, and the calculated distribution coefficients are mathematically valid. If the value of 1/n in the Freundlich isotherm equation is not equal to 1.0, the sorption data, however, can be plotted on a log-log scale, and for many trace solutes in contact with geologic media the data often plots on a straight line, with the resulting equilibrium sorption data then being described by the equation:

$$\log S = \frac{1}{n} * \log C + \log K_f \quad (4)$$

where

1/n = slope of the isotherm

log K_f = intercept of the isotherm with the y-axis

The linear isotherm is the simplest and most widely used of the equilibrium sorption isotherms. Equilibrium sorption data fitted by the linear isotherm can be used to calculate distribution coefficients of the solute for the solid adsorbent when the $1/n$ term of the Freundlich isotherm equation is equal to 1.0. Using the linear isotherm equation, it is assumed that the amount of solute sorbed on the solid adsorbent (S), and the concentration of the solute remaining in solution (C) are related by the linear relationship,

$$S = K_d C \quad (5)$$

where K_d is a measure of the retention of the solute known as the distribution coefficient. This linear isotherm represents the situation where the affinity of the sorbent for the sorbate remains the same for all levels of C (Stumm and Morgan, 1996).

In conclusion, partitioning coefficients describing the fractional uptake of the ions on the zeolitized tuff from Rainier Mesa were calculated utilizing the following methods. First, equilibrium data points that describe the total concentration of adsorbate in solution (C) to the quantity of adsorbate associated with the adsorbent (S) for each ion were obtained by hand-fitting a best fit curve to the fractional uptake data for various ion concentrations and solid concentrations. Next, Freundlich isotherms were constructed at specific pH values and for specific background electrolyte concentrations using the equilibrium data points. This was done in order to evaluate the validity of the linear isotherm under those specific geochemical conditions. Finally, linear isotherms were constructed using the equilibrium data points for those same pH values and specific background electrolyte concentrations. This was done even if the experimental data was best described by the Freundlich isotherm because the linear isotherm produces the parameters required by modelers to estimate the transport of these ions in the subsurface

environment. One limitation of the Freundlich and linear isotherms, however, is that they do not indicate a maximum quantity of adsorption, which is clearly not the case when dealing with the cation-exchange capacity of adsorbents.

CHAPTER 4

SORPTION OF Pb(II) AND Sr(II) ON ZEOLITIZED TUFF AND CLINOPTILOLITE: EQUILIBRIUM EXPERIMENTS, SORPTION PARAMETER ESTIMATION, AND SPECIATION

It has been documented by previous studies that in natural systems the fractional uptake of cations and anions by oxides and other minerals in the subsurface environment can be pH dependent, or influenced by ionic strength effects (Hayes and Leckie, 1987; Hayes et al., 1988). In addition, the total concentration of the ion of interest and the total solid concentration of the mineral phase in natural aqueous systems determine the ratio of sorbate ions to the total number of sorbent sites, thereby affecting the relative fractional uptake of the ions. Consequently, the geochemical parameters that were included in this thesis to help determine the equilibrium sorption behavior of the ions for both adsorbents were pH, ionic strength, total solid adsorbent concentration, and total ion concentration.

This chapter contains the results of the batch equilibrium sorption experiments, the sorption parameter estimations, and the speciation calculations for the Pb(II) and Sr(II) cations. The chapter is divided into three major sections. The first section contains the results of the batch equilibrium sorption experiments performed with the zeolitized tuff, the sorption parameter estimations, and the speciation calculations for each cation.

The second section of this chapter contains the results of the batch equilibrium sorption experiments performed with the clinoptilolite, and the final section of the chapter discusses the sorption behavior of each cation as a function of the adsorbent type in order to address any similarities and differences in the fractional uptake behavior of the cations by the adsorbents.

Sorption of Pb(II) and Sr(II) on Zeolitized Tuff

Sorption Behavior of Pb(II)

Batch equilibrium sorption experiments were conducted at background electrolyte concentrations of 0.01, 0.1, and 1.0 M NaNO₃ in order to investigate the sorption behavior of Pb(II) as a function of ionic strength. Sodium nitrate (NaNO₃) was chosen to provide the background electrolyte concentration for all of the batch equilibrium sorption experiments because Na⁺ is the highest concentration cation present in the groundwater at the NTS. Overall, the batch equilibrium sorption experiments indicate that the fractional uptake of Pb(II) increases as the ionic strength decreases for the two lowest background electrolyte concentrations investigated (0.1 and 0.01 M NaNO₃). This can be observed in Figure 10, showing the fractional uptake of 1.0x10⁻⁴ M Pb(II) on 2.5 g/L zeolitized tuff as a function of ionic strength. The figure also shows that the fractional uptake of Pb(II) is essentially independent of the pH of the solution for the two lowest background electrolyte concentrations (0.1 and 0.01 M NaNO₃). It has been documented that the cation-exchange capacity derived from isomorphous substitutions within the structures of aluminosilicate minerals is permanent charge and independent of the pH (Goodman, 1986).

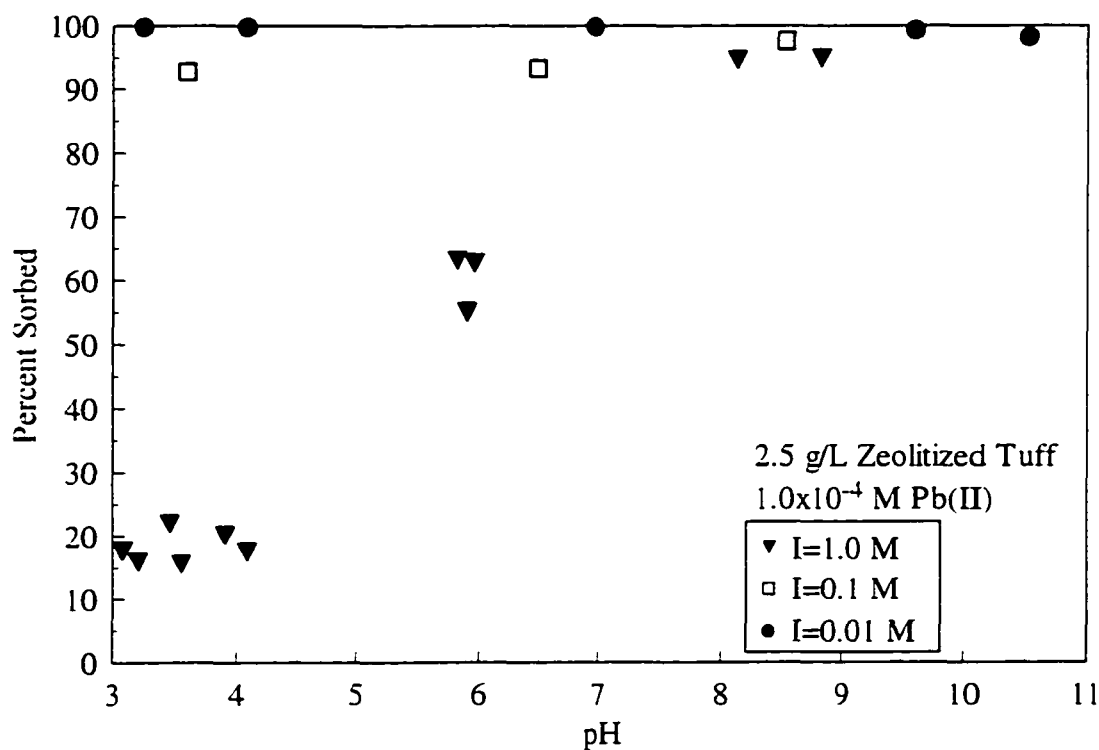


Figure 10. Sorption of 1.0×10^{-4} M Pb(II) on 2.5 g/L zeolitized tuff as a function of ionic strength.

This pH-independent sorption behavior, therefore, suggests that the Pb(II) cation can successfully compete with the Na^+ cation at the lower background electrolyte concentrations, and preferentially replace the cations located within the internal cation-exchange sites of the zeolitized tuff. At these two lower background electrolyte concentrations, the fractional uptake of Pb(II) is nearly complete (>90%) and can be attributed to the high cation-exchange capacity of the zeolitized tuff. For example, Table 7 showed that the zeolitized tuff had the ability to readily accept a divalent metal cation concentration up to 1.79×10^{-3} M for a solid concentration of 2.5 g/L. The fractional uptake of Pb(II) at the lower background electrolyte concentrations increases as the ionic strength decreases because there is less competition with the Na^+ cation for the available

cation-exchange sites of the zeolitized tuff.

It can be seen in Figure 10, however, that the fractional uptake of Pb(II) on the zeolitized tuff is largely dependent on the pH of the solution for the 1.0 M NaNO₃ background electrolyte concentration. For example, the figure clearly shows the fractional uptake of Pb(II) increasing from approximately 20% at a low pH of 3 to a fractional uptake of essentially 95% at a pH of approximately 8. This pH-dependent sorption behavior may suggest that the Pb(II) cation cannot successfully compete with the Na⁺ cation, which is 4 orders of magnitude greater, for the internal cation-exchange sites of the zeolitized tuff at the highest background electrolyte concentration (1.0 M NaNO₃). As a result of being excluded from the internal cation-exchange sites, Pb(II) sorption on the zeolitized tuff is likely controlled either by sorption on external pH-dependent surface sites, or possibly by the formation of surface polymers or precipitates, which are also dependent on the pH of the solution. For example, the Pb(II) cation could be binding to the zeolitized tuff on amphoteric surface sites, possibly as an inner-sphere coordination complex on hydrous oxide surfaces.

According to Stumm and Morgan (1996), a cation can associate with a solid surface as either an inner-sphere or outer-sphere surface complex depending on whether a chemical bond between the metal and the electron-donating oxygen ions is formed (as in an inner-sphere type solute complex), or if a cation of opposite charge approaches the surface groups to a critical distance (as in an outer-sphere type solute complex). Unfortunately, it has been pointed out that macroscopic sorption experiments alone cannot be used to distinguish between different types of sorption complexes (Sposito, 1986). A simple method of possibly distinguishing between inner-sphere and outer-

sphere complexes, however, is to assess the effect of ionic strength on the surface complex formation equilibria (Stumm and Morgan, 1996). Evidently, a strong dependence on the fractional uptake of solutes as a function of ionic strength is typical for the formation of outer-sphere complexes. The formation of inner-sphere coordination complexes, however, is not dependent on ionic strength of the solution because the formation of these type of bonds occurs through the loss of waters of hydration and direct short-range bonding of the complex to surface oxygens. These types of short-range electrostatic or covalent bonds are extremely strong compared to the long-range coulombic or hydrogen bonds of outer-sphere complexes. For example, Figure 11 reveals that there does not appear to be much variation in the fractional uptake of Pb(II) as a

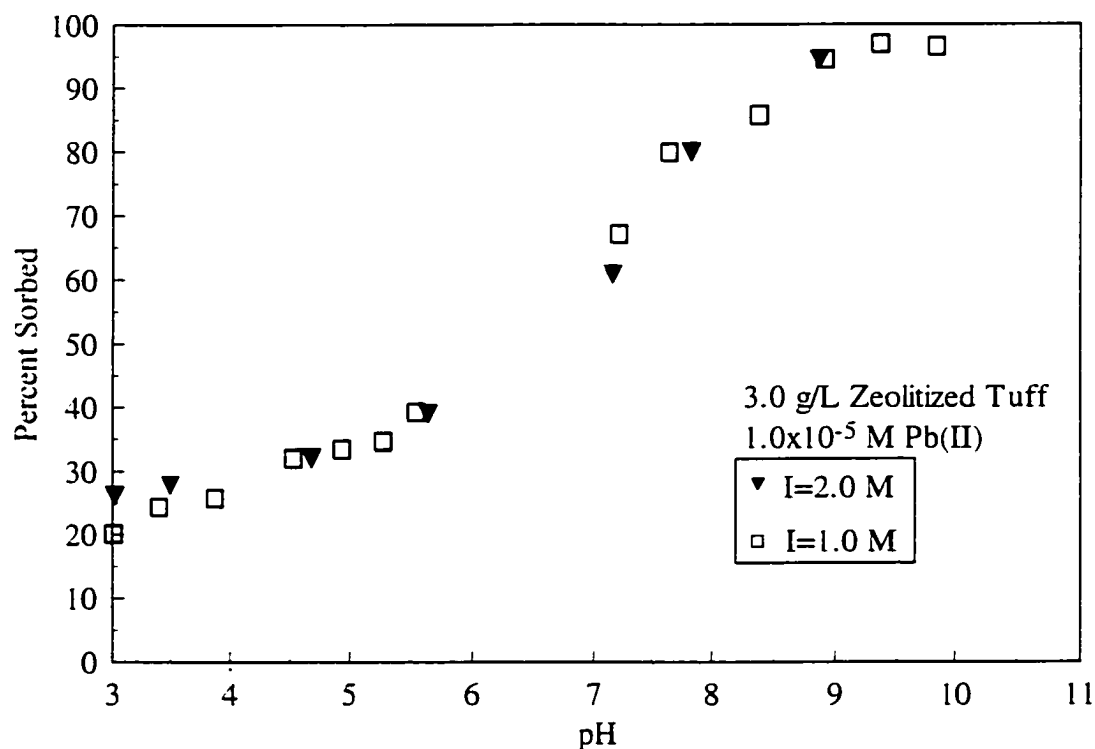


Figure 11. Sorption of 1.0×10^{-5} M Pb(II) on 3.0 g/L zeolitized tuff in 2.0 and 1.0 M NaNO_3 .

function of the ionic strength at background electrolyte concentrations high enough to exclude Pb(II) from the internal cation-exchange sites of the zeolitized tuff (2.0 M and 1.0 M NaNO₃). This suggests that Pb(II) is chemically binding to the zeolitized tuff as an inner-sphere coordination complex. The pH-dependent sorption behavior of Pb(II) at the highest background electrolyte concentrations, however, could also be caused by the formation of surface precipitates or polymers. Unfortunately, there is no way to conclusively distinguish between adsorption and surface precipitation by macroscopic sorption experiments alone.

Sorption behavior as a function of ionic strength can be again demonstrated by Figure 12, showing experiments at a higher solid concentration (3.0 g/L vs. 2.5 g/L) and a

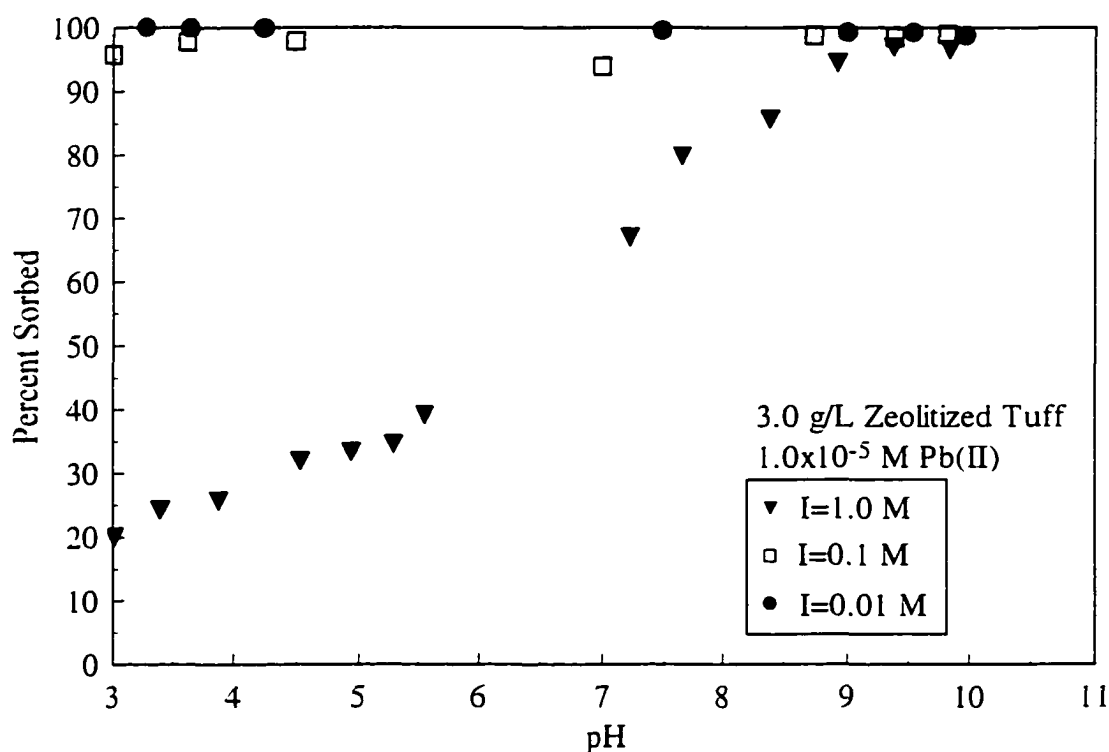


Figure 12. Sorption of 1.0×10^{-5} M Pb(II) on 3.0 g/L zeolitized tuff as a function of ionic strength.

lower metal cation concentration (1.0×10^{-5} vs. 1.0×10^{-4} M) than the previous figure. It can be seen in the figure that the fractional uptake of Pb(II) on the zeolitized tuff for the two lower background electrolyte concentrations is again independent of the pH of the solution and greater than 95% for both ionic strengths due to the large cation-exchange capacity of the zeolitized tuff. It is still possible to distinguish from the experimental data, however, that the lowest background electrolyte concentration results in the greatest fractional uptake of Pb(II) on the zeolitized tuff. The figure also shows that the fractional uptake of Pb(II) is again dependent on the pH of the solution at a background electrolyte concentration of 1.0 M NaNO₃. The figure clearly shows the fractional uptake of Pb(II) increasing from approximately 20% at low pH of 3 to a fractional uptake of approximately 95% at high pH values of 9 and above.

Special attention needs to be drawn to the fact that in the figures illustrating the fractional uptake of Pb(II) as a function of ionic strength, the fractional uptake of Pb(II) is approximately 20% for low pH values of 3 for the 1.0 M NaNO₃ background electrolyte concentration. This limited fractional uptake at low pH values is somewhat surprising because it has been documented that the fractional uptake of metal cations by the formation of surface complexes, which are pH-dependent, increases from essentially zero to almost 100% over a narrow interval of pH units (Stumm and Morgan, 1996). The fractional uptake of Pb(II) at these low pH values, therefore, must be attributed to some other binding mechanism such as cation exchange because precipitation is not likely to occur at this low pH. It can also be seen in Figure 10 and Figure 12 that the increase of fractional uptake is more abrupt for the higher Pb(II) cation concentration. This type of sorption behavior is likely caused by the formation of precipitates for the higher Pb(II)

cation concentration, because as is seen later in this section of the chapter, decreases in the Pb(II) cation concentration should increase the overall fractional uptake of the cation, which is not seen with these two figures.

The batch equilibrium sorption experiments performed as a function of ionic strength, therefore, indicate that there are at least two possible binding mechanisms responsible for the fractional uptake of Pb(II) on the zeolitized tuff: cation exchange at the lower ionic strengths, or the formation of surface complexes at external sites (or precipitates) at the highest ionic strength. This experimental data corresponds well to other studies because it has been documented that the surface charge of aluminosilicate minerals may arise either from isomorphous cation substitution within the structure, which is pH independent, or by protonation/deprotonation reactions at oxide/hydroxide surface groups which are pH dependent (Goodman, 1986). The fractional uptake of Pb(II) by the formation of surface complexes can be regarded as a competition between the Pb(II) cation and the H⁺ cation for any available surface sites. Consequently, the fractional uptake of Pb(II) at low pH values is minimal due to the higher concentrations of H⁺. As the pH of the solution increases, the fractional uptake of Pb(II) increases due to the decreasing amounts of H⁺ in solution, and because of the increased hydrolysis of Pb(II) with increasing pH.

Batch equilibrium sorption experiments were also performed at solid concentrations of 2.5, 3.0, and 20.0 g/L to provide a range of adsorbent to adsorbate ratios. These three different solid concentrations result in a range of differing total surface areas, which would in turn determine the total concentration of available binding sites. The results show that, overall, the fractional uptake of Pb(II) increases as a function

of increasing solid concentration. For example, Figure 13 illustrates the fractional uptake of 1.0×10^{-5} M Pb(II) in 1.0 M NaNO₃ as a function of the zeolitized tuff concentration. The figure clearly shows that the two lowest solid concentrations result in the lowest fractional uptake of Pb(II). The results are almost indistinguishable, as expected, given the small difference between the two concentrations. The 2.5 and 3.0 g/L solid concentrations result in the fractional uptake of approximately 20-95% of the available Pb(II) in solution for pH values in the range of 3 to 10. The highest solid concentration of 20 g/L, however, results in the greatest fractional uptake of approximately 65-100% for pH values in the range of 3 to 8.5. This type sorption behavior of increasing fractional uptake as the solid concentration increases is expected because higher solid adsorbent

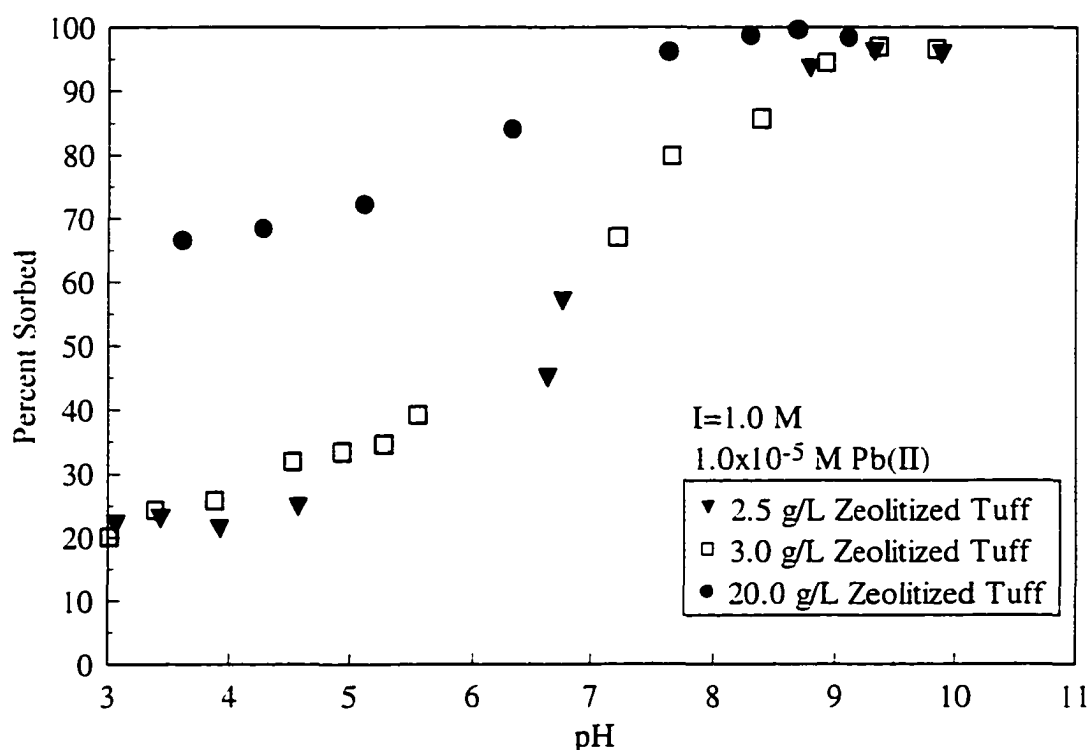


Figure 13. Sorption of 1.0×10^{-5} M Pb(II) in 1.0 M NaNO₃ as a function of zeolitized tuff concentration.

concentrations increase the number of available binding sites for the Pb(II) cation.

Sorption behavior of this type can be seen again in Figure 14. This figure shows the fractional uptake of 1.0×10^{-4} M Pb(II) in 0.1 M NaNO₃ as a function of solid concentration. It is interesting to note that there is not much of a variation in the overall fractional uptake of Pb(II) as a function of solid concentration in this figure compared to the previous figure. This can be explained because at background electrolyte concentrations less than 1.0 M NaNO₃, the fractional uptake of Pb(II) on the zeolitized tuff is extremely favorable because there is less competition for the available cation-exchange sites. It is still visible in this figure, however, that the fractional uptake of Pb(II) increases as the solid adsorbent concentration increases. For example, the figure

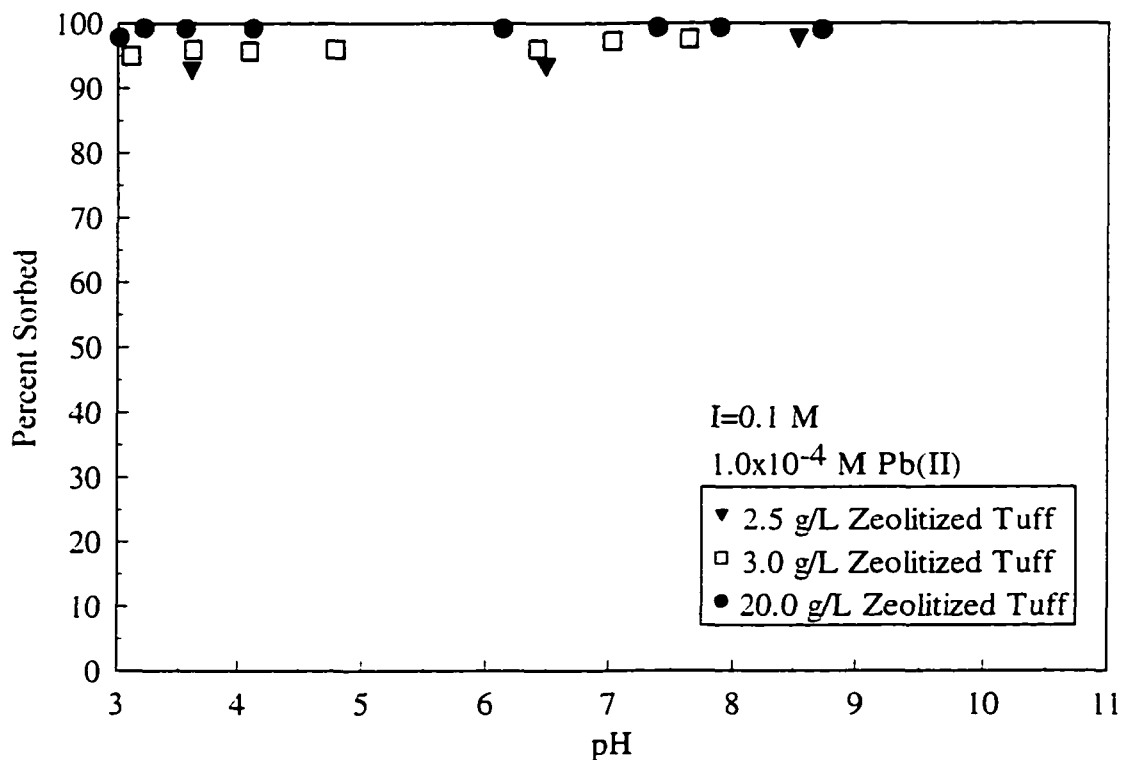


Figure 14. Sorption of 1.0×10^{-4} M Pb(II) in 0.1 M NaNO₃ as a function of zeolitized tuff concentration.

clearly shows that the 20 g/L solid concentration has the highest fractional uptake of Pb(II). This figure also serves to illustrate that the fractional uptake of Pb(II) on the zeolitized tuff is solid-concentration dependent, but qualitatively different depending on the ionic strength. For example, the fractional uptake of Pb(II) in this figure is pH-independent, but in the previous figure, it was pH-dependent.

Batch equilibrium sorption experiments were also performed at 3 different Pb(II) concentrations in an attempt to determine what effect, if any, that changing Pb(II) concentrations have on the fractional uptake of Pb(II) on the zeolitized tuff. Overall, the experimental data show that the fractional uptake of Pb(II) increases as the Pb(II) cation concentration decreases. For example, Figure 15 illustrates the fractional uptake of Pb(II)

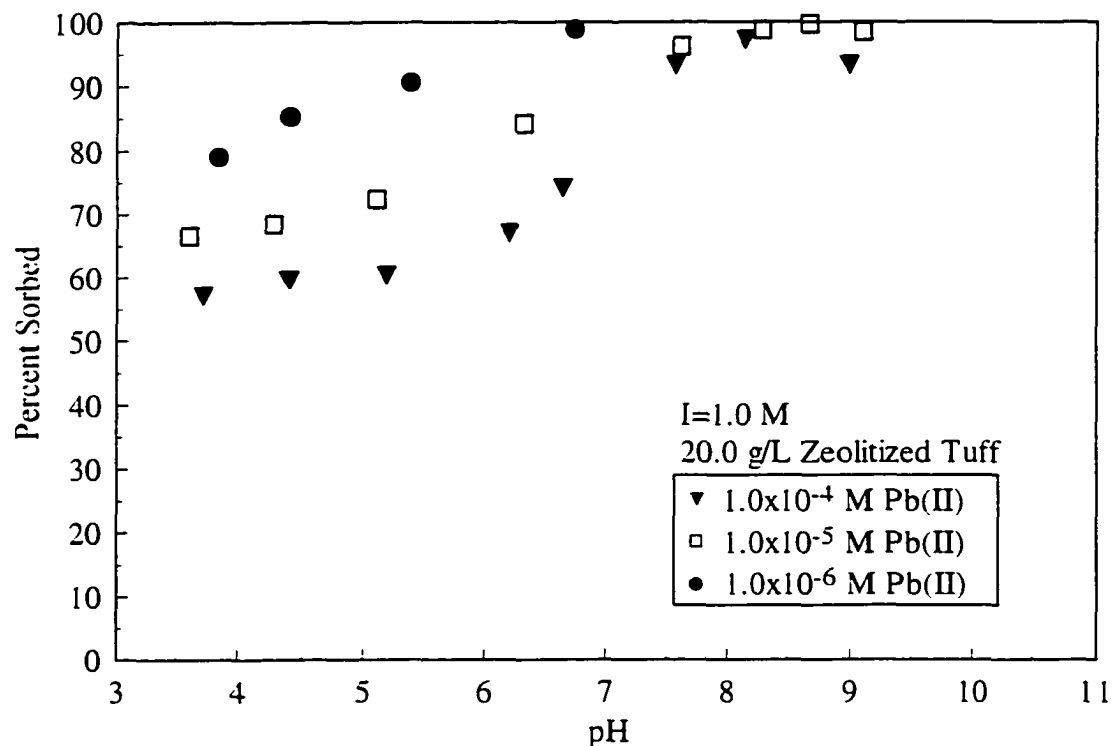


Figure 15. Sorption of Pb(II) on 20 g/L zeolitized tuff in 1.0 M NaNO₃ as a function of Pb(II) concentration.

on 20.0 g/L zeolitized tuff in 1.0 M NaNO₃ as a function of the Pb(II) concentration. The figure shows that the fractional uptake of Pb(II) varies from 57-95% for the 1.0x10⁻⁴ M Pb(II) concentration for pH values in the range of 3.5 to 8, but the 1.0x10⁻⁵ M Pb(II) concentration results in the fractional uptake of approximately 65-99% Pb(II) for pH values in the range 3 to 9. Lastly, the lowest metal cation concentration of 1.0x10⁻⁶ M Pb(II) results in the highest fractional uptake of approximately 80-100% Pb(II) for pH values in the range of 4 to 6.5. This type of sorption behavior where the fractional uptake increases as the Pb(II) cation concentration decreases is also expected because if the total amount of Pb(II) cations in solution available for binding decreases, then proportionately more binding sites will be available for the Pb(II) cations that are remaining in solution.

Pb(II) Sorption Parameter Estimation

The fractional uptake data obtained from the batch equilibrium sorption experiments with Pb(II) were used to estimate parameters for Freundlich and linear sorption isotherms. The equilibrium data points used to construct the isotherms were obtained by hand-fitting a best fit curve to the fractional uptake data for different geochemical conditions (e.g. pH, ionic strength, solid-liquid ratio). Sorption isotherms for Pb(II) contained a minimum of nine points, and were constructed at pH values of 4, 5, 6, 7, 8, and 9. From the experimental data, it was possible to calculate partitioning coefficients for the Pb(II) cation at a background electrolyte concentration of 1.0 M NaNO₃. Sorption isotherms and partitioning coefficients were not constructed for the two lower background electrolyte concentrations (0.1 and 0.01 M NaNO₃) because the fractional uptake of Pb(II) on the zeolitized tuff for these ionic strengths was extremely favorable and approached 100% for more than one set of conditions. Consequently,

Freundlich and linear isotherms could not be calculated because these isotherms do not imply any maximum quantity of adsorption.

To summarize briefly from Chapter 3, the fractional uptake data were first fitted to the logarithmic form of the Freundlich isotherm,

$$\log S = \frac{1}{n} * \log C + \log K_f \quad (6)$$

The parameter $1/n$ is a measure of the linearity of the isotherm. A mathematically valid distribution coefficient (K_d) can be calculated when the $1/n$ term, which is the slope of the logarithmic form of the equation, is equal to 1.0. In such a situation, the Freundlich isotherm reduces to the linear isotherm,

$$S = K_d C \quad (7)$$

If the term $1/n$ is not equal to 1.0, however, the term K_f can be calculated. The term K_f , the Freundlich constant, is equal to the intercept of the isotherm with the y-axis. These two parameters, K_f and $1/n$, can be used as indicators of the sorption capacity of the adsorbent for the specific geochemical conditions at which the equilibrium data points were calculated, whereas the parameter K_d implies a direct linear relationship between the equilibrium concentration of the solute and the sorbed concentration for the geochemical conditions at which the data points were calculated (Weber and DiGiano, 1996). It should be kept in mind that when modeling sorption data by the Freundlich isotherm, the added degree of freedom allows for easy curve fitting, but the isotherms do not guarantee accuracy if the data are extrapolated beyond the experimental points and conditions specified (Travis and Etnier, 1981).

The Freundlich isotherm parameters, K_f and $1/n$, for the Pb(II) cation at a

background electrolyte concentration of 1.0 M NaNO₃ are shown in Table 8. Inspection of the data in the table reveals that the 1/n terms are not equal to 1.0. In fact, the 1/n terms generally deviate more from 1.0 as the pH at which the Freundlich isotherms were constructed increases. The sorption data were therefore fit to the Freundlich isotherm and fits for pH values of 7, 8, and 9 are illustrated in Figure 16. Because of the non-linearity of the isotherms, true distribution coefficients for the Pb(II) cation in contact with the zeolitized tuff from the NTS cannot be defined for this particular background electrolyte concentration. The calculated K_f and 1/n parameters, however, can be used as an indication of the sorption capacity of the adsorbent for the specific geochemical conditions at which the equilibrium data points were calculated. The calculated K_f parameters vary from 1.29x10⁻⁴ to 4.37x10⁻³ (g/g)/(g/m³)^{1/n}, and it can be seen from the table that the K_f parameters increase as the pH of the solution increases. These data

Table 8. Freundlich isotherm parameters for Pb(II) equilibrium sorption isotherms in 1.0 M NaNO₃.

pH	K _f (g/g)/(g/m ³) ^{1/n}	1/n (-)	r ²
4	1.29x10 ⁻⁴	0.800	0.980
5	1.62x10 ⁻⁴	0.786	0.982
6	3.52x10 ⁻⁴	0.899	0.876
7	8.25x10 ⁻⁴	0.616	0.799
8	2.00x10 ⁻³	0.699	0.895
9	4.37x10 ⁻³	0.705	0.925

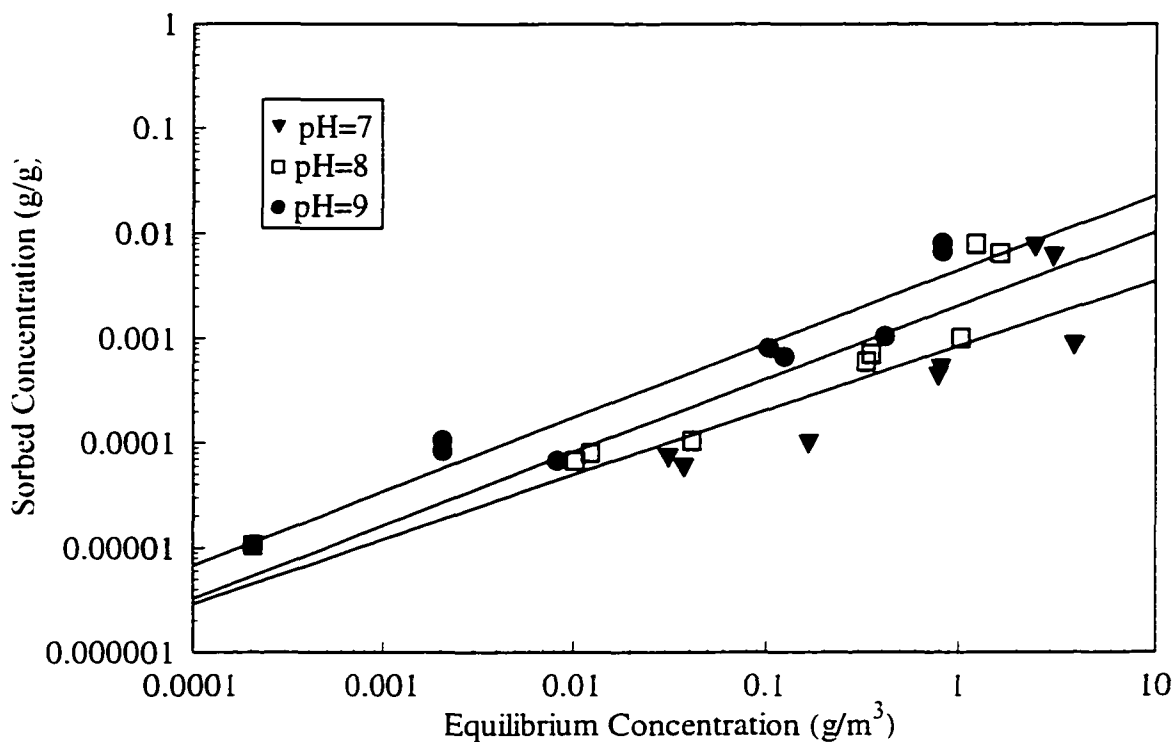


Figure 16. Freundlich isotherms of Pb(II) sorption on zeolitized tuff in 1.0 M NaNO₃ at pH values of 7, 8, and 9.

indicate that the fractional uptake of Pb(II) on the zeolitized tuff increases as the pH of the groundwater increases, as shown from the experiments reported.

Linear isotherms based on fractional uptake data for Pb(II) were also determined even though mathematically valid distribution coefficients can not be calculated for the Pb(II) cation at this background electrolyte concentration. Fitting of the equilibrium sorption data by linear isotherms was performed because distribution coefficients are, most frequently, utilized by mathematical modelers to estimate the transport of contaminants in the subsurface environment. These distribution coefficients, while not mathematically valid, would at least provide a starting point to begin calculations for estimating the migration rate of Pb(II) in the subsurface environment. The K_d values, and

the correlation coefficients, r^2 , obtained from the Pb(II) sorption isotherms are shown in Table 9. The K_d estimates were obtained from a least squares fit. It must be kept in mind, however, that the data in the table cannot be considered completely valid because the Freundlich isotherms for these data were non-linear. In addition, the distribution coefficients shown in Table 9 were obtained by forcing the linear isotherms at each pH through zero. This was done because one of the assumptions for the linear isotherm equation is that the isotherm must go through zero. Figure 17 shows examples of the linear isotherms for pH values of 7, 8, and 9 that were forced through zero to calculate the distribution coefficients. The distribution coefficients based on the best fit linear isotherms, however, can be seen in Appendix 1.

Inspection of the data in the table reveals that the distribution coefficients (K_d) also increase as the pH of the solution increases. This behavior was seen with the

Table 9. Distribution coefficients (K_d) for Pb(II) in 1.0 M NaNO₃ at different pH values.

pH	K_d (m ³ /g)	r^2
4	8.31×10^{-5}	0.984
5	1.05×10^{-4}	0.979
6	5.14×10^{-4}	0.535
7	1.24×10^{-3}	0.392
8	3.87×10^{-3}	0.724
9	8.06×10^{-3}	0.910

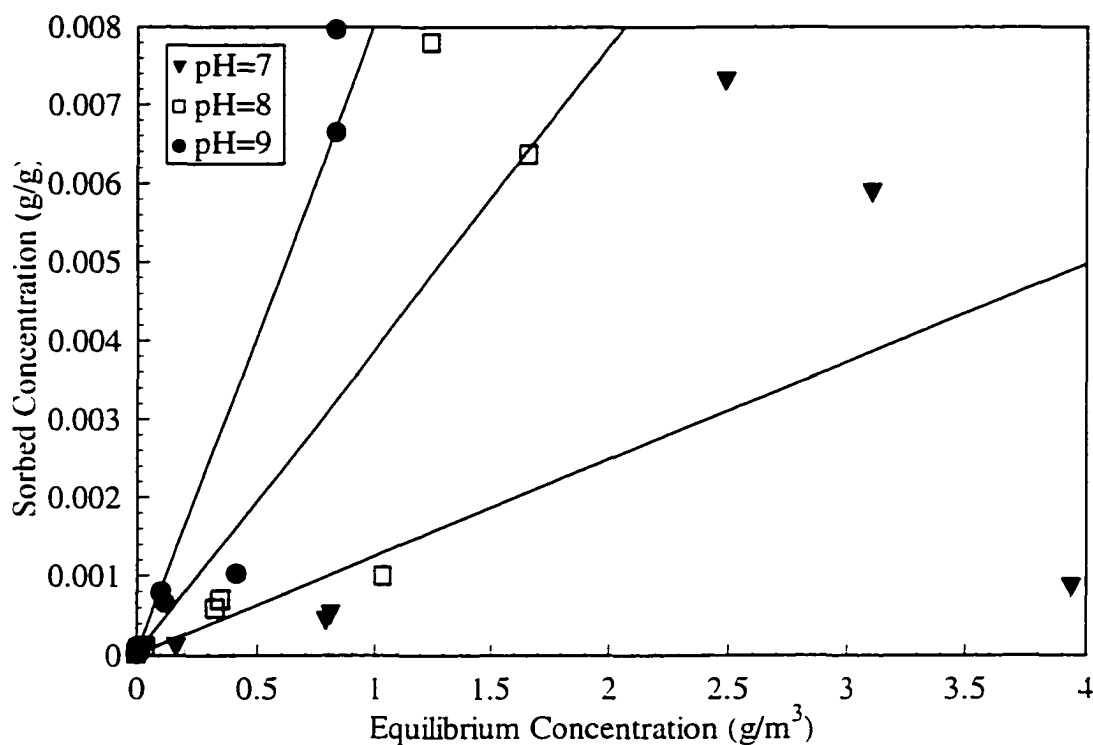


Figure 17. Linear isotherms of Pb(II) sorption on zeolitized tuff in 1.0 M NaNO₃ at pH values of 7, 8, and 9.

calculated K_f parameters, and, of course, indicates that the affinity of the Pb(II) cation for the zeolitized tuff increases as the pH of the solution increases for the reasons mentioned previously. The distribution coefficients vary from a minimum value of $8.31 \times 10^{-5} \text{ m}^3/\text{g}$ to a maximum value of $8.06 \times 10^{-3} \text{ m}^3/\text{g}$. It is interesting to note from both tables that the calculated K_f parameters varied by only 1 order of magnitude for all pH values investigated, but the calculated K_d parameters varied by almost two orders of magnitude for the pH values investigated. The K_d parameters had to vary by two orders of magnitude to account for the exponent of the linear isotherm being held constant at 1.0. This serves to illustrate that the experimental data for Pb(II) are best described by the non-linear Freundlich isotherm.

Chemical Speciation Modeling of Pb(II)

The particular chemical form in which an element exists in water is termed its speciation. The speciation of elements in aqueous environments is extremely important to be aware of because information on the types of species encountered under different chemical conditions is a prerequisite to a better understanding of the distribution and functions of elements in natural waters (Stumm and Morgan, 1996). It has also been suggested that the speciation of metal ions in a multi-component system influences the specific sorption process that may be occurring, and that the speciation of ions can vary during the transport of the pollutant in the groundwater (Stumm and Morgan, 1996). The geochemical modeling program Mineql⁺ (Schecher and McAvoy, 1994), therefore, was used to determine the theoretical speciation of Pb(II) in the groundwater at the NTS, as well as in the solutions used for the equilibrium experiments. Carbon dioxide gas (CO₂ (g)) was excluded from all calculations. These theoretical speciation calculations were performed because it was thought that it would be beneficial to investigate whether precipitates of Pb(II) would be likely to form in the groundwater at the NTS, or in the batch equilibrium sorption reactors. These speciation calculations might make it possible, qualitatively at least, to distinguish between different types of sorption processes occurring at different pHs. For example, these speciation calculations might make it possible to determine whether surface complexes or precipitates would be more likely to form for different geochemical conditions. It has been pointed out, however, that the formation of a precipitate at concentrations not exceeding the solubility of a given phase is thermodynamically feasible because of the presence of the adsorbent which acts as a nucleation site (Sposito, 1986). It must be remembered, therefore, that these speciation

calculations are only theoretical because the addition of a solid adsorbent phase may cause the formation of precipitates not indicated by the geochemical modeling program.

In order to model the speciation of Pb(II) in the groundwater at the NTS, a groundwater analysis from water well U-20 at the NTS was obtained. The results of the chemical analysis of the groundwater are provided in Table 10. Additionally, the pH of the volcanic groundwater was measured as 8.33, and the temperature of the well water was measured as 37.0 °C. Based on the molar concentrations of the elements in the groundwater, the ionic strength of the groundwater was calculated as 3.244×10^{-3} M.

Using this groundwater composition and a Pb(II) concentration of 1.0×10^{-4} M, the speciation of Pb(II) in the groundwater was modeled assuming that the system was closed

Table 10. Chemical analysis of the groundwater from well U-20 on the NTS.

Element	Concentration (mg/L)	Concentration (M)
Na ⁺	57	2.4×10^{-3}
K ⁺	1.74	4.45×10^{-5}
Ca ²⁺	6.15	1.53×10^{-4}
Mg ²⁺	0.44	1.81×10^{-5}
Cl ⁻	11.4	3.21×10^{-4}
HCO ₃ ⁻	107	1.7×10^{-3}
SO ₄ ²⁻	30.7	3.19×10^{-4}
NO ₃ ⁻	2	3.22×10^{-5}

to the atmosphere (no CO_2 (g) exchange). Inspection of Figure 18 reveals that under these particular set of conditions there would be four predominant Pb(II) aqueous species: Pb^{2+} , PbHCO_3^+ , PbCO_3^0 , and PbSO_4^0 . At all pH values less than approximately 6.4, the predominant Pb(II) aqueous species is Pb^{2+} . As the pH of the groundwater exceeds 6.4, the predominant Pb(II) species becomes PbCO_3 (aq). The thermodynamically stable precipitate at pH values above approximately 5 is cerrusite (PbCO_3 (s)). Cerrusite remains the predominant precipitate of Pb(II) until a pH of approximately 8.5, where $\text{Pb}(\text{OH})_2$ (s) becomes the predominant Pb(II) solid phase accounting for almost 100% of the total Pb(II). The formation of these precipitates results in the decrease of the total Pb(II) concentration with increasing pH, as also indicated in Figure 18.

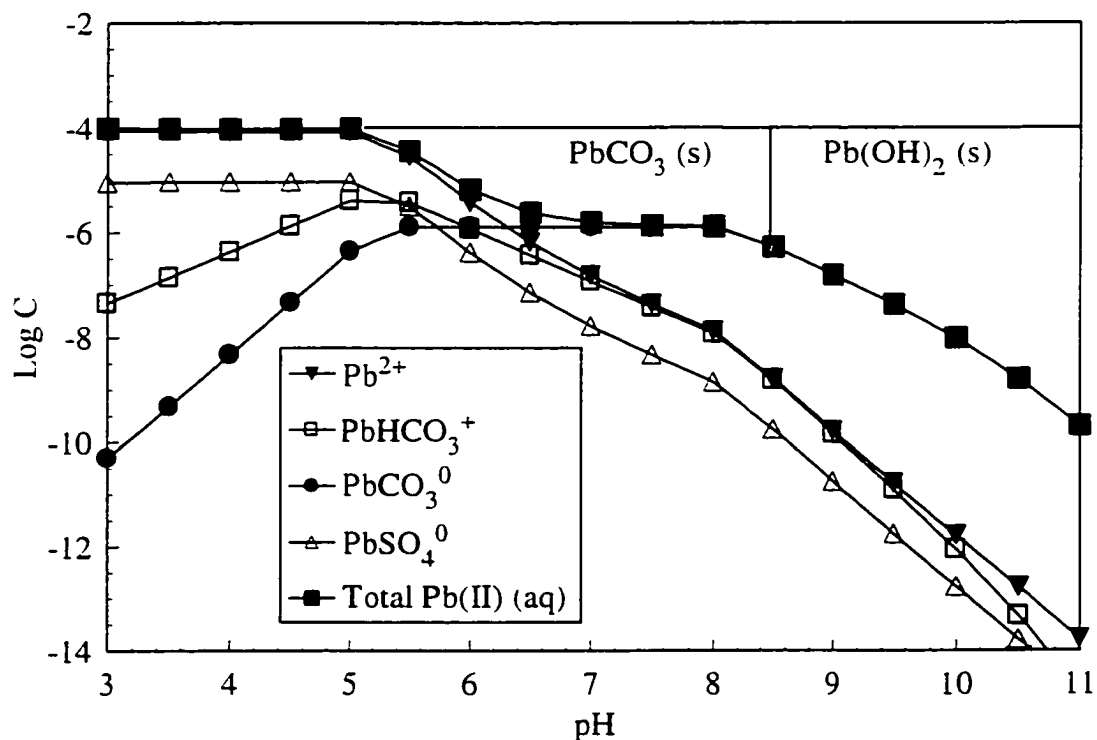


Figure 18. Speciation modeling of 1.0×10^{-4} M Pb(II) in groundwater from well U-20 at the NTS.

The speciation of Pb(II) was also modeled using a total metal cation concentration of 1.0×10^{-6} M Pb(II), the lowest metal concentration used in these studies. Inspection of Figure 19 reveals a slightly different situation than was found with the 1.0×10^{-4} M Pb(II) concentration. At this lower Pb(II) concentration, there would be six predominant aqueous Pb(II) species present in the groundwater rather than four, namely Pb^{2+} , PbOH^+ , PbHCO_3^- , PbCO_3^0 , $\text{Pb}(\text{CO}_3)_2^{2-}$, and PbSO_4^0 . Inspection of the diagram reveals that, again, at low pH values up to approximately a pH of 6, Pb^{2+} would be the predominant Pb(II) aqueous species. PbCO_3^0 (aq) again becomes the predominant Pb(II) aqueous species from a pH of 6 to approximately 9.6. At pH values above 9.6, $\text{Pb}(\text{CO}_3)_2^{2-}$ becomes the predominant Pb(II) aqueous species. The precipitate formed at pH values above 8.4 is

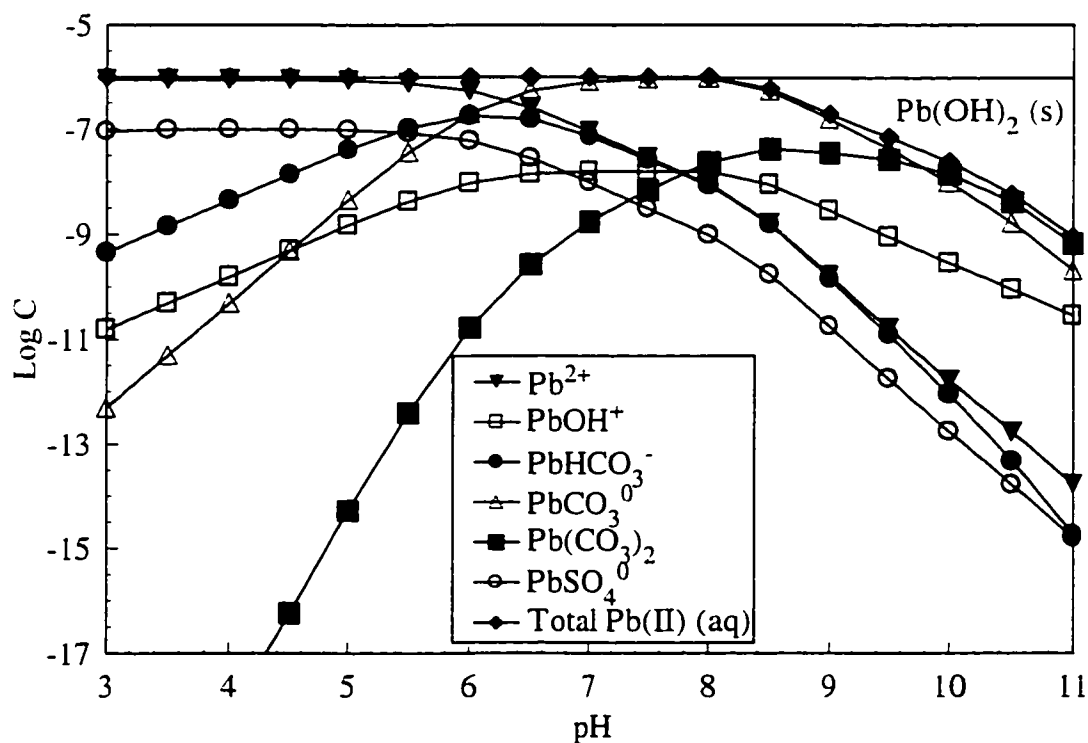


Figure 19. Speciation modeling of 1.0×10^{-6} M Pb(II) in groundwater from well U-20 at the NTS.

Pb(OH)_2 (s).

The theoretical chemical speciation of Pb(II) at two different metal cation concentrations within the batch equilibrium sorption reactors was also modeled. The system was assumed to be closed to the atmosphere with only the background electrolyte present. This is, obviously, a simplification because no special precautions to exclude CO_2 (g) were taken during the experiments. Speciation modeling of Pb(II) was performed at all three background electrolyte concentrations, but the geochemical modeling program Mineql⁺ is not accurate at ionic strengths above 0.1 M. Speciation calculations, therefore, will only be shown for the lowest background electrolyte concentration investigated because it is relatively close to the actual ionic strength of the groundwater obtained from water well U-20. Inspection of Figure 20 reveals that only three aqueous Pb(II) species would be present in the batch equilibrium sorption reactors using a high 1.0×10^{-4} M Pb(II) concentration. Aqueous Pb(II) in the batch equilibrium reactors would be present as either Pb^{2+} , PbOH^+ , or PbNO_3^+ . It can also be seen from the figure that Pb^{2+} would be the predominate Pb(II) species at low pH values until a pH of approximately 7.8. At pH values greater than 7.8, PbOH^+ would become the predominate Pb(II) species. The solid phase Pb(OH)_2 (s) is the thermodynamically stable phase above pH values 5.8. Precipitation at lower pH values in the groundwater at the NTS would be caused by the interactions of the Pb(II) cation with carbonate species present in the groundwater at the NTS that are not present in the batch equilibrium reactors.

The theoretical interaction of 1.0×10^{-6} M Pb(II) with a background electrolyte concentration of 0.01 M NaNO_3 in the batch equilibrium sorption reactors was the last scenario investigated. Inspection of Figure 21 reveals a situation almost identical to the

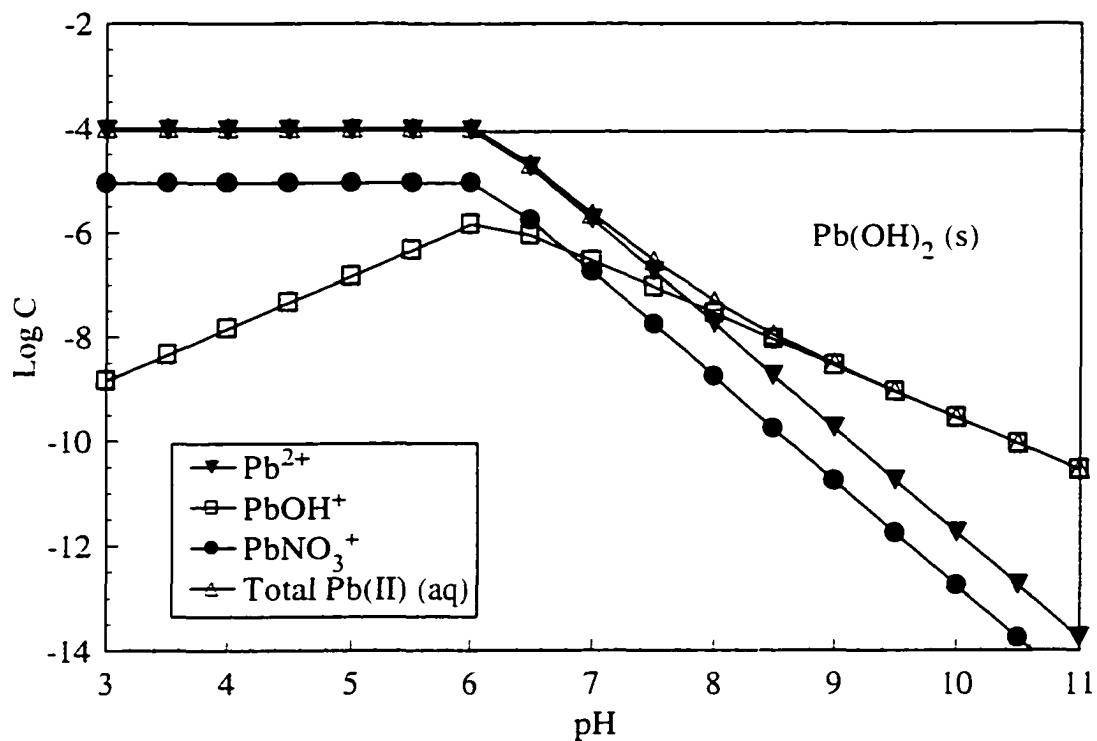


Figure 20. Speciation modeling of 1.0×10^{-4} M Pb(II) in 0.01 M NaNO₃ closed to the atmosphere.

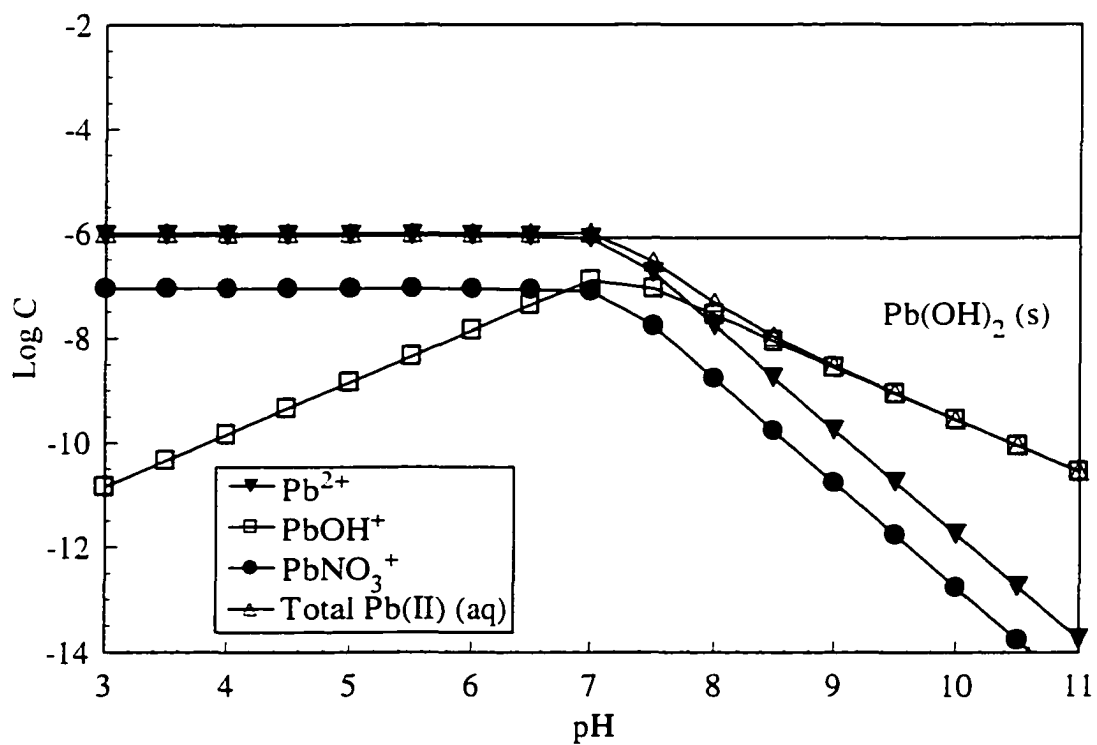


Figure 21. Speciation modeling of 1.0×10^{-6} M Pb(II) in 0.01 M NaNO₃ closed to the atmosphere.

speciation of a 1.0×10^{-4} M Pb(II) concentration. In this figure, however, the precipitation of Pb(II) would not occur until a pH of approximately 7.0, whereas the precipitation of 1.0×10^{-4} M Pb(II) occurred at a pH of approximately 5.8. At this metal cation concentration, Pb^{2+} is the predominate aqueous species until a pH of approximately 7.8. At pH values above 7.8, PbOH^+ becomes the predominate aqueous species.

In conclusion, the speciation of Pb(II) was modeled at two different metal cation concentrations and using two different groundwater compositions. The results of the modeling indicate that precipitation of Pb(II) would occur at both metal cation concentrations studied, and in both the groundwater at the NTS and in the batch equilibrium sorption reactors. The pH at which precipitation of Pb(II) would occur is dependent on the metal cation concentration, and on the composition of the water used. To what extent this precipitation would effect the sorption behavior of Pb(II) is impossible to determine by macroscopic sorption experiments alone. Macroscopic sorption experiments cannot distinguish between adsorption of the cation and precipitation of a solid phase. These types of batch equilibrium sorption experiments would only be able to show that the cation had indeed been removed from solution, but not by what means it had been removed. These speciation calculations, however, have shown that it is at least thermodynamically feasible at pH values above 5 for the precipitation Pb(II) without the presence of any solid adsorbent phase. It must be remembered, however, that precipitates of Pb(II) could form at even lower pH values than suggested by the speciation calculations because precipitates can form in the aqueous solutions at concentrations not exceeding the solubility of a given phase because of the presence of solid mineral phases which act as a nucleation sites (Sposito, 1986). On the

other hand, removal of Pb(II) from solution by sorption reactions would tend to decrease the potential for precipitation of the remaining metal.

Sorption Behavior of Sr(II)

The sorption behavior of Sr(II) was also investigated at background electrolyte concentrations of 0.01, 0.1, and 1.0 M NaNO₃ in order provide clues about the type of adsorption complex being formed (outer-sphere vs. inner-sphere). Overall, the batch equilibrium sorption experiments indicate that the fractional uptake of Sr(II) on the zeolitized tuff increases with decreasing ionic strength. This ionic strength dependence suggests Sr(II) is forming outer-sphere adsorption complexes. Figure 22 shows the fractional uptake of 1.0×10^{-4} M Sr(II) on 2.5 g/L zeolitized tuff as a function of ionic

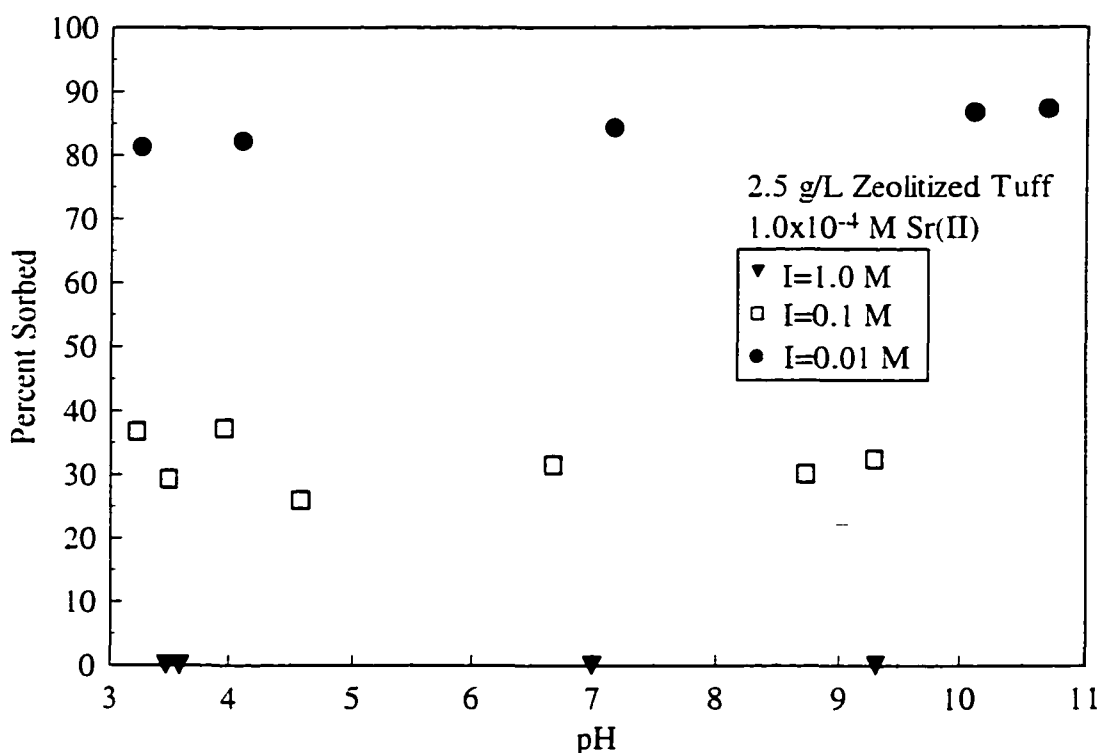


Figure 22. Sorption of 1.0×10^{-4} M Sr(II) on 2.5 g/L zeolitized tuff as a function of ionic strength.

strength. The 0.1 M NaNO_3 concentration results in the fractional uptake of approximately 30% for all pH values investigated, but the 0.01 M NaNO_3 concentration results in a fractional uptake of approximately 80% for all pH values investigated. This behavior of increasing fractional uptake as the ionic strength decreases can be explained because there is less competition with the Na^+ cation for the available cation-exchange sites of the zeolitized tuff at the lower ionic strength. The figure also shows that the fractional uptake of $\text{Sr}(\text{II})$ on the zeolitized tuff is independent of the pH for all background electrolyte concentrations investigated. This type of sorption behavior is consistent with the sorption behavior of the $\text{Pb}(\text{II})$ cation at the two lower background electrolyte concentrations investigated. The pH-independent sorption behavior indicates that the fractional uptake of $\text{Sr}(\text{II})$ is being controlled by cation exchange on the pH-independent permanent-charge sites.

The experiments also show that, like the $\text{Pb}(\text{II})$ cation, the $\text{Sr}(\text{II})$ cation cannot compete successfully with the background electrolyte for the internal cation-exchange sites of the zeolitized tuff at the highest background electrolyte concentration (1.0 M NaNO_3). This type of sorption behavior suggests that $\text{Sr}(\text{II})$ is only able to bind to the zeolitized tuff at cation-exchange sites, unlike the $\text{Pb}(\text{II})$ cation, which was able to bind to amphoteric surface sites, or form surface polymers and precipitates as a function of pH at the highest background electrolyte concentration. The fact that there is no fractional uptake of $\text{Sr}(\text{II})$ at the highest background electrolyte concentration is somewhat expected because $\text{Sr}(\text{II})$ does not form inner-sphere coordination complexes like $\text{Pb}(\text{II})$ with pH dependent surface sites. In addition, the $\text{Sr}(\text{II})$ cation does not hydrolyze significantly like the $\text{Pb}(\text{II})$ cation, and consequently there are no analogous $\text{Sr}(\text{II})$ precipitates.

This type of sorption behavior is again illustrated in Figure 23. The figure shows the fractional uptake of 1.0×10^{-6} M Sr(II) on 2.5 g/L zeolitized tuff as a function of ionic strength. The fractional uptake of Sr(II) is again negligible for the 1.0 M NaNO_3 concentration, which indicates that Sr(II) is completely excluded from the internal cation-exchange sites of the zeolitized tuff. The fractional uptake of Sr(II), however, increases to approximately 40% for the 0.1 M NaNO_3 concentration, and approaches nearly 96% for the 0.01 M NaNO_3 concentration. In addition, it can be seen from the figure that the fractional uptake of Sr(II) on the zeolitized tuff is again pH-independent at all ionic strengths, and that the fractional uptake of Sr(II) increases as the overall ionic strength of the solution decreases.

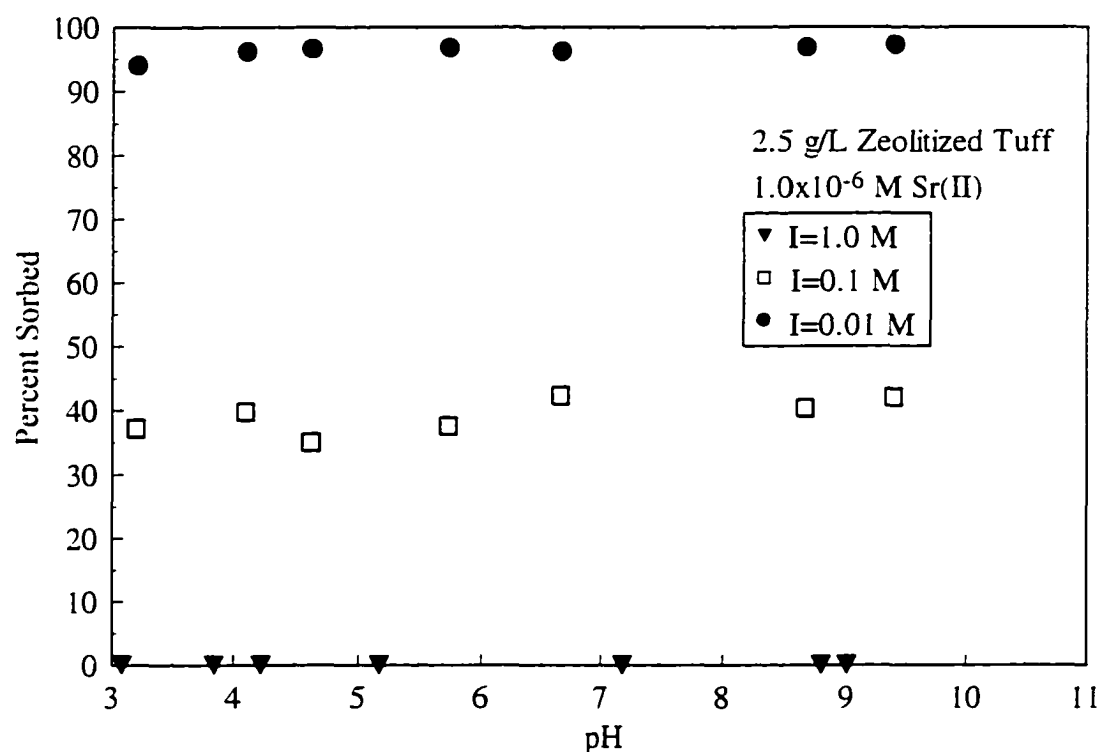


Figure 23. Sorption 1.0×10^{-6} M Sr(II) on 2.5 g/L zeolitized tuff as a function of ionic strength.

The equilibrium sorption behavior of Sr(II) was also studied as a function of the zeolitized tuff solid concentration. Batch equilibrium sorption experiments were performed at solid concentrations of 2.5, 3.0, and 20.0 g/L. The experiments indicate that the fractional uptake of Sr(II) increases as the solid concentration of the adsorbent increases. For example, Figure 24 illustrates the fractional uptake of 1.0×10^{-4} M Sr(II) in 0.1 M NaNO₃ as a function of the zeolitized tuff concentration. It can be seen from the figure that the fractional uptake of Sr(II) is the highest, approximately 70%, for the highest solid concentration of 20 g/L, and decreases to approximately 30% for the 2.5 g/L solid concentration. Again this behavior of increasing fractional uptake of Sr(II) as the solid concentration increases is expected, because as the solid concentration of the

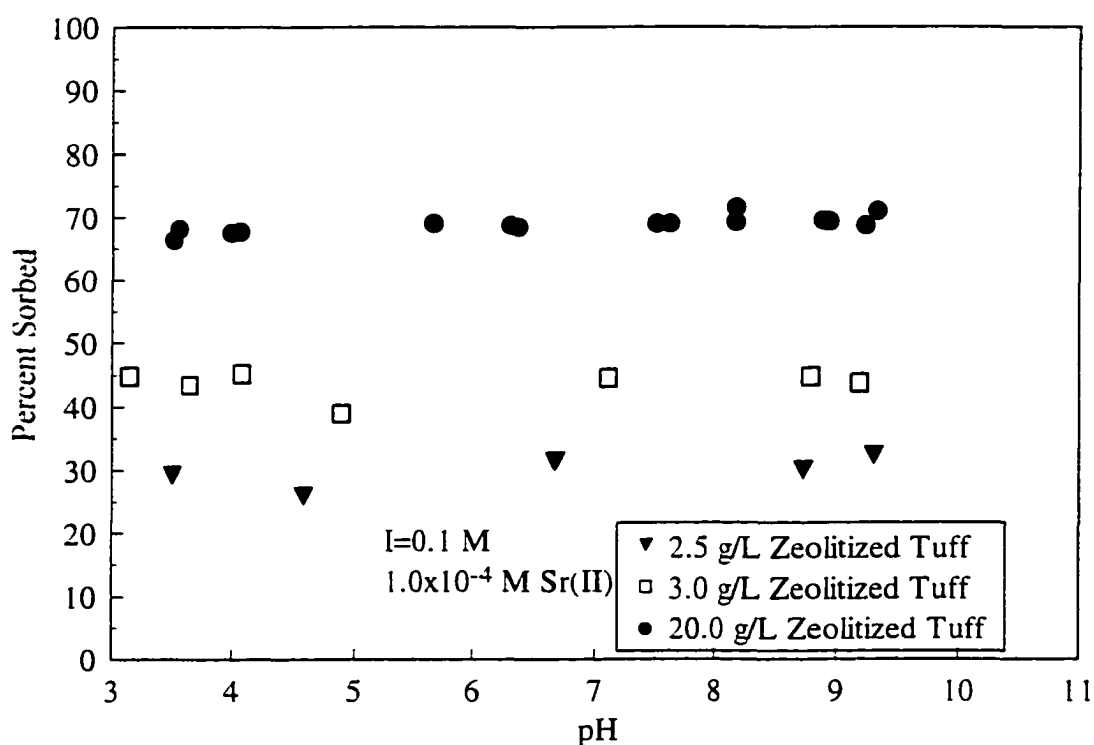


Figure 24. Sorption of 1.0×10^{-4} M Sr(II) in 0.1 M NaNO₃ as a function of zeolitized tuff concentration.

zeolitized tuff increases, relatively more binding sites become available for the Sr(II) cation because increasing solid adsorbent concentrations increase the available surface area of the adsorbent.

The last geochemical parameter investigated was the overall Sr(II) cation concentration. As one would expect from the discussions with the Pb(II) cation, decreases in the Sr(II) cation concentration should increase the fractional uptake of Sr(II) on the zeolitized tuff. In fact, inspection of Figure 25, showing experiments at a background electrolyte concentration of 0.01 M NaNO₃ and a solid concentration of 2.5 g/L, verifies that as the Sr(II) cation concentration decreases the fractional uptake of Sr(II) on the zeolitized tuff increases. In the figure, the 1.0×10^{-4} M Sr(II) cation

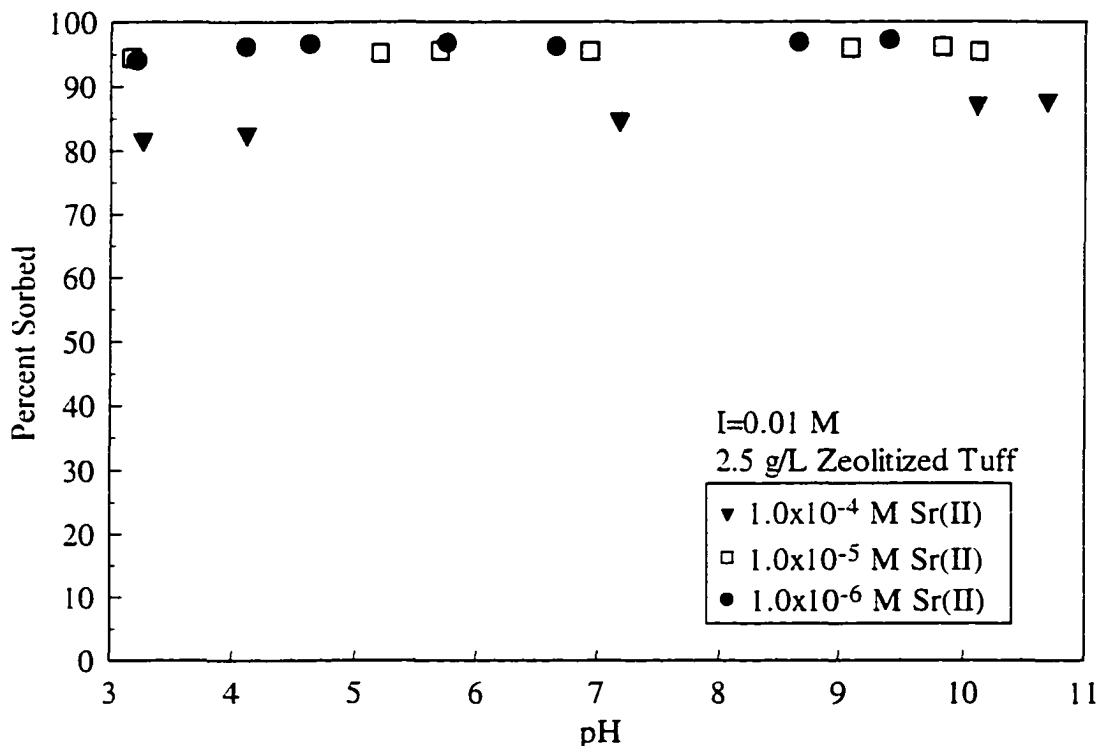


Figure 25. Sorption of Sr(II) on 2.5 g/L zeolitized tuff in 0.01 M NaNO₃ as a function of Sr(II) concentration.

concentration displays a fractional uptake of approximately 85%. and the 1.0×10^{-5} M and 1.0×10^{-6} M Sr(II) concentrations both exhibit fractional uptakes in excess of 95%. It is still somewhat apparent from the figure, however, that the lowest Sr(II) concentration results in the highest fractional uptake of Sr(II) on the zeolitized tuff from the NTS. This equilibrium sorption behavior is again expected, because as the Sr(II) concentration decreases, there are proportionately more available binding sites for the Sr(II) cations that are remaining in solution.

In conclusion, the equilibrium sorption behavior of Sr(II) was investigated as a function of numerous geochemical parameters. Overall, the experiments revealed that the fractional uptake of Sr(II) increased as the ionic strength of the background electrolyte decreased. The experiments also indicated that the fractional uptake of Sr(II) increased as the solid concentration of the adsorbent increased, and that the fractional uptake of Sr(II) increased as the overall Sr(II) cation concentration decreased.

Sr(II) Sorption Parameter Estimation

The fractional uptake data for Sr(II) were used to derive Freundlich and linear isotherm parameters. The isotherms constructed were based on a minimum of 8 different points for the 0.1 M NaNO₃ concentration and 6 different points for the 0.01 M NaNO₃ concentration. Isotherms were constructed at pH values of 4, 5, 6, 7, 8 and 9 by hand fitting a best-fit curve to the fractional uptake data. Partitioning coefficients for Sr(II) in contact with the zeolitized tuff from the NTS were calculated for background electrolyte concentrations of 0.1 M and 0.01 M NaNO₃. No partitioning coefficients were calculated for the highest background electrolyte concentration (1.0 M NaNO₃) because there was no fractional uptake of Sr(II) at that background electrolyte concentration.

The Freundlich isotherm parameters, K_f and $1/n$, calculated for the Sr(II) cation at a background electrolyte concentration of 0.1 M NaNO₃ are displayed in Table 11. The table summarizes the fitting of the equilibrium data points by the logarithmic form of the Freundlich isotherm (See Chapter 3 for a discussion of the Freundlich isotherm). The fitting of the Sr(II) equilibrium data by the Freundlich isotherm can also be seen in Figure 26, and since the fractional uptake of Sr(II) on the zeolitized tuff is the same at each pH value only one isotherm is necessary. Inspection of the data in the table reveals that the $1/n$ term is approximately 1.0 (0.97), and that the K_f parameter is equal to 1.89×10^{-4} (g/g)/(g/m³)^{1/n}. There is only one set of parameters (K_f and $1/n$) since the fractional uptake of Sr(II) on the zeolitized tuff was independent of the pH. In addition, this $1/n$ value suggests that the distribution coefficient calculated for the Sr(II) cation with the linear isotherm is mathematically valid for the 0.1 M NaNO₃ background electrolyte concentration. These two parameters (K_f and $1/n$), however, can also be used as indicators of the sorption capacity of the adsorbent for the specific geochemical conditions at which the equilibrium data points were calculated.

The fractional uptake data for Sr(II) at a background electrolyte concentration of 0.1 M NaNO₃ were also fitted by the linear isotherm. Because of the linearity of the

Table 11. Freundlich isotherm parameters for Sr(II) equilibrium sorption isotherms in 0.1 M NaNO₃.

pH	K_f (g/g)/(g/m ³) ^{1/n}	$1/n$ (-)	r^2
4, 5, 6, 7, 8, 9	1.89×10^{-4}	0.967	0.960

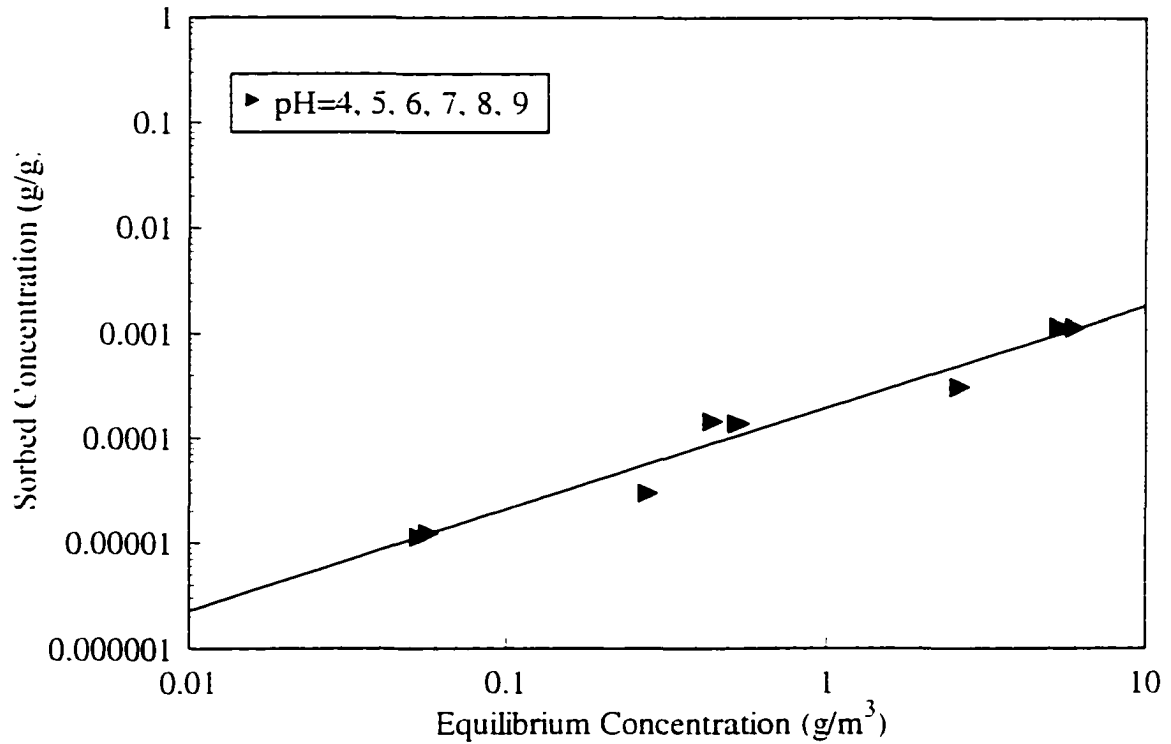
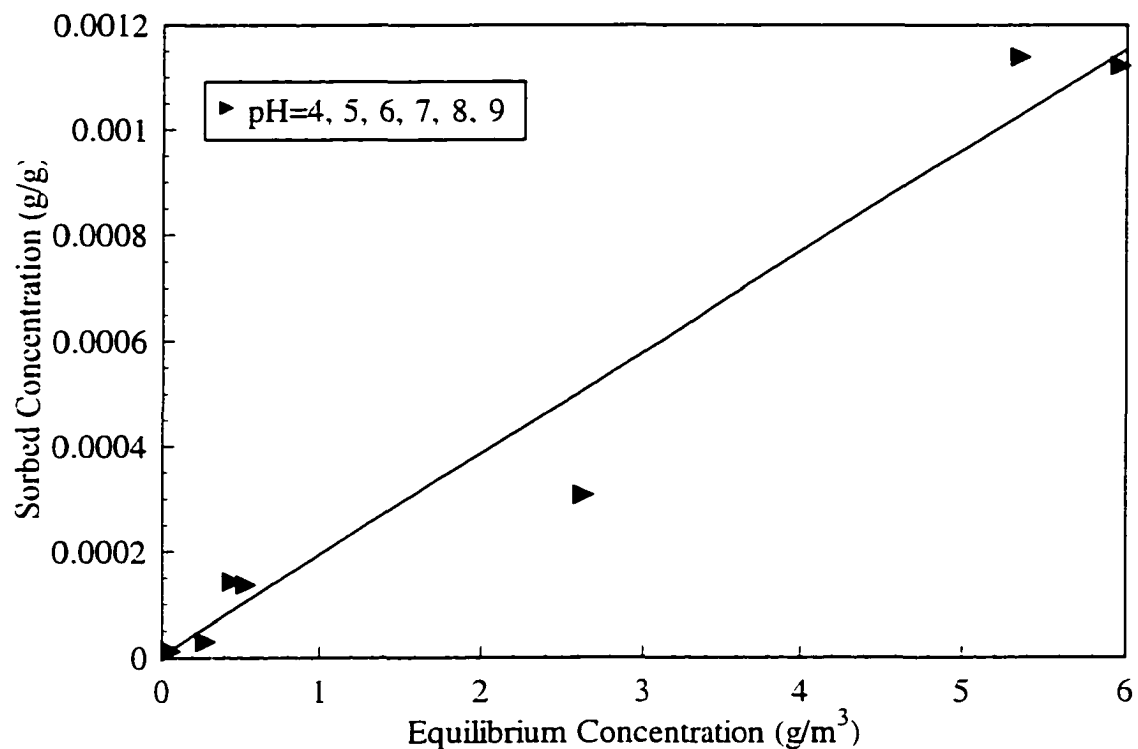


Figure 26. Freundlich isotherm of Sr(II) sorption on zeolitized tuff in 0.1 M NaNO₃.

Freundlich isotherm, the calculated distribution coefficient can be considered mathematically valid. The K_d estimate was obtained from a least squares fit of the data, and the isotherm was forced through zero because that is one of the assumptions of the equation. The K_d value, and the correlation coefficient, r^2 , obtained from the Sr(II) isotherm is shown in Table 12. The best fit partitioning coefficient, however, can be seen in Appendix 1. Inspection of Figure 27 shows the fitting of the equilibrium data by the linear isotherm for pH values of 4, 5, 6, 7, 8, and 9. Only one isotherm is required, however, because the fractional uptake of Sr(II) on the zeolitized tuff was independent of the pH. It can be seen from the table that the distribution coefficient for Sr(II) is equal to $1.92 \times 10^{-4} \text{ m}^3/\text{g}$.

Table 12. Distribution coefficients (K_d) for Sr(II) in 0.1 M NaNO₃ at different pH values.

pH	K_d (m ³ /g)	r^2
4, 5, 6, 7, 8, 9	1.92×10^{-4}	0.965

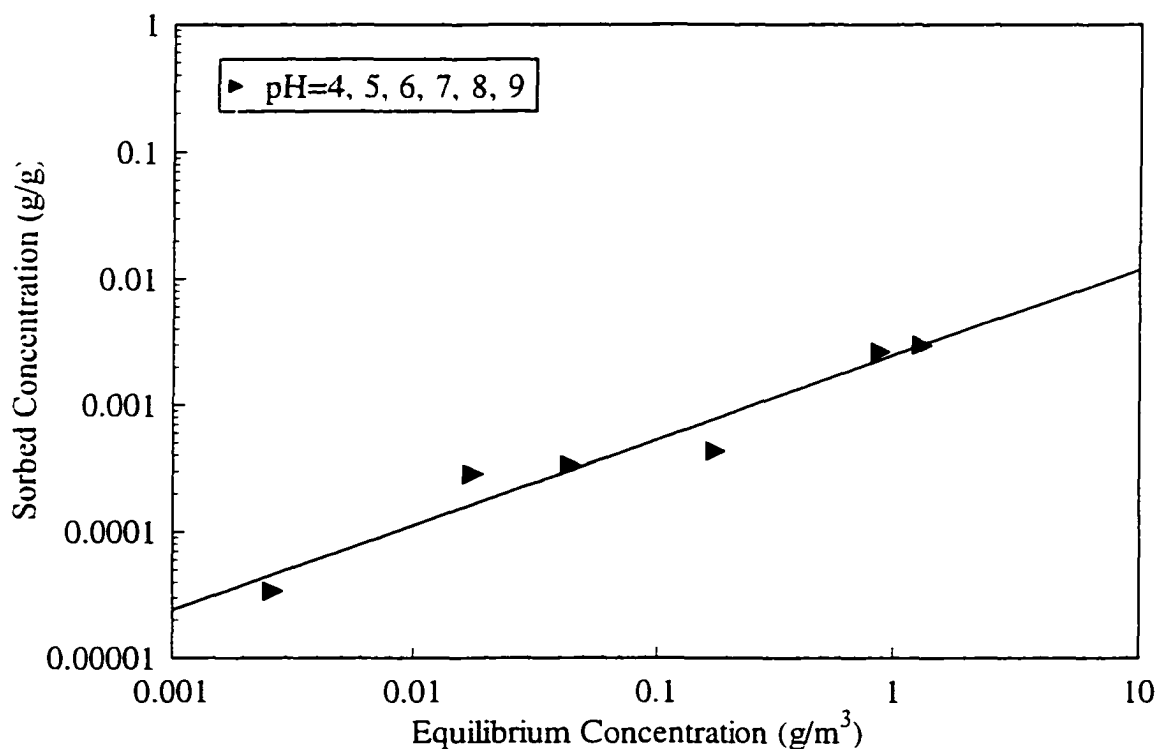
Figure 27. Linear isotherm of Sr(II) sorption on zeolitized tuff in 0.1 M NaNO₃.

It must be remembered, however, that the distribution coefficient is only valid for a background electrolyte concentration of 0.1 M NaNO₃. For example, it can be seen in Table 13 that as the background electrolyte concentration is decreased to 0.01 M NaNO₃, the distribution coefficient calculated from the linear isotherm can no longer be considered to be completely valid because the $1/n$ term of the logarithmic form of the Freundlich isotherm equation deviates more from 1.0 (0.672). The fitting of the

Table 13. Freundlich isotherm equation parameters for Sr(II) in 0.01 M NaNO₃.

pH	K_f (g/g)/(g/m ³) ^{1/n}	1/n (-)	r ²
4, 5, 6, 7, 8, 9	2.45x10 ⁻³	0.672	0.971

equilibrium sorption data at this lower background electrolyte concentration by the Freundlich isotherm can be seen in Figure 28. It is interesting to note, however, that the K_f parameters for the two different background electrolyte concentrations are almost an order of magnitude different with the 0.01 M ionic strength having the larger K_f value. The larger K_f parameter for the 0.01 M NaNO₃ background electrolyte concentration

Figure 28. Freundlich isotherm of Sr(II) sorption on zeolitized tuff in 0.01 M NaNO₃.

indicates that the Sr(II) cation has a greater affinity for the zeolitized tuff at this lower background electrolyte concentration. The dissimilarity in the $1/n$ terms can be explained because at the lower background electrolyte concentration there is less competition with the Na^+ cation for the internal cation-exchange sites of the zeolitized tuff. The fractional uptake of Sr(II) on the zeolitized tuff, therefore, is extremely favorable and approaches 100% for more than one set of geochemical conditions. As previously stated, a limitation of the Freundlich isotherm equation is that it does not imply a maximum quantity of adsorption, and as the fractional uptake of Sr(II) approaches 100% for a number of different geochemical conditions, the isotherm becomes increasingly nonlinear.

The fractional uptake data for Sr(II) at the 0.01 M NaNO_3 background electrolyte concentration, however, were also used to derive parameters from the linear isotherm (Figure 29). It must be remembered that the calculated distribution coefficient cannot be considered completely valid because the $1/n$ term of the Freundlich equation is not equal to 1.0. The calculated distribution coefficient for Sr(II) at the 0.01 M NaNO_3 ionic strength is shown in Table 14. It is interesting to note that the calculated distribution coefficient, while not technically valid at this ionic strength, is somewhat similar to the corresponding K_f parameter that was calculated for this background electrolyte

Table 14. Distribution coefficients (K_d) for Sr(II) sorption isotherms 0.01 M NaNO_3 at different pH values.

pH	K_d (m^3/g)	r^2
4, 5, 6, 7, 8, 9	2.50×10^{-3}	0.967

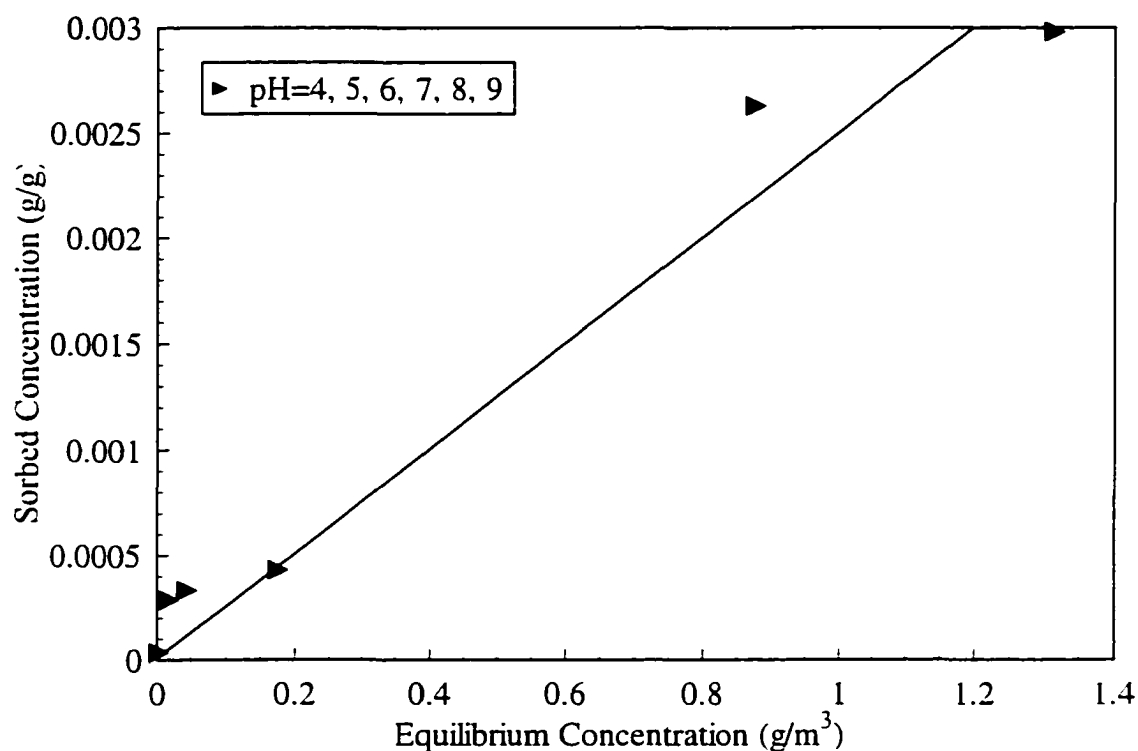


Figure 29. Linear isotherm of Sr(II) sorption on zeolitized tuff in 0.01 M NaNO₃.

concentration. The calculated K_f parameter for all pH values was 2.40×10^{-3} (g/g)/(g/m³)^{1/n}, and the calculated K_d parameter for all pH values was 2.50×10^{-3} m³/g.

Chemical Speciation Modeling of Sr(II)

The theoretical speciation of Sr(II) in groundwater from water well U-20 at the NTS, and in the batch equilibrium sorption reactors was also investigated to gain additional understanding of the possible sorption processes occurring in the system of interest. Investigations into the speciation of Sr(II) might provide clues as to the actual mechanism of sorption occurring at a particular pH. For example, it might be possible, thermodynamically at least, to determine whether precipitation or surface complexation would be more likely at particular pH values. Speciation calculations with Sr(II) were performed using the groundwater composition from well U-20, and using a solution

composition representative of the conditions in the batch equilibrium reactors. In addition, the speciation calculations for both solution compositions were performed assuming the systems were closed to the atmosphere. The results of the calculations with the groundwater composition from the NTS will be discussed first, followed by a discussion of the results in the batch equilibrium reactors.

The first condition investigated for Sr(II) used the groundwater composition from the NTS and 1.0×10^{-4} M Sr(II) concentration. Figure 30 shows that there would be only two aqueous Sr(II) species, Sr^{2+} and SrOH^+ , under these conditions. In addition, Sr^{2+} is the predominant aqueous species under all pH conditions investigated. SrOH^+ would never become the predominant aqueous Sr(II) species in the groundwater at the NTS at

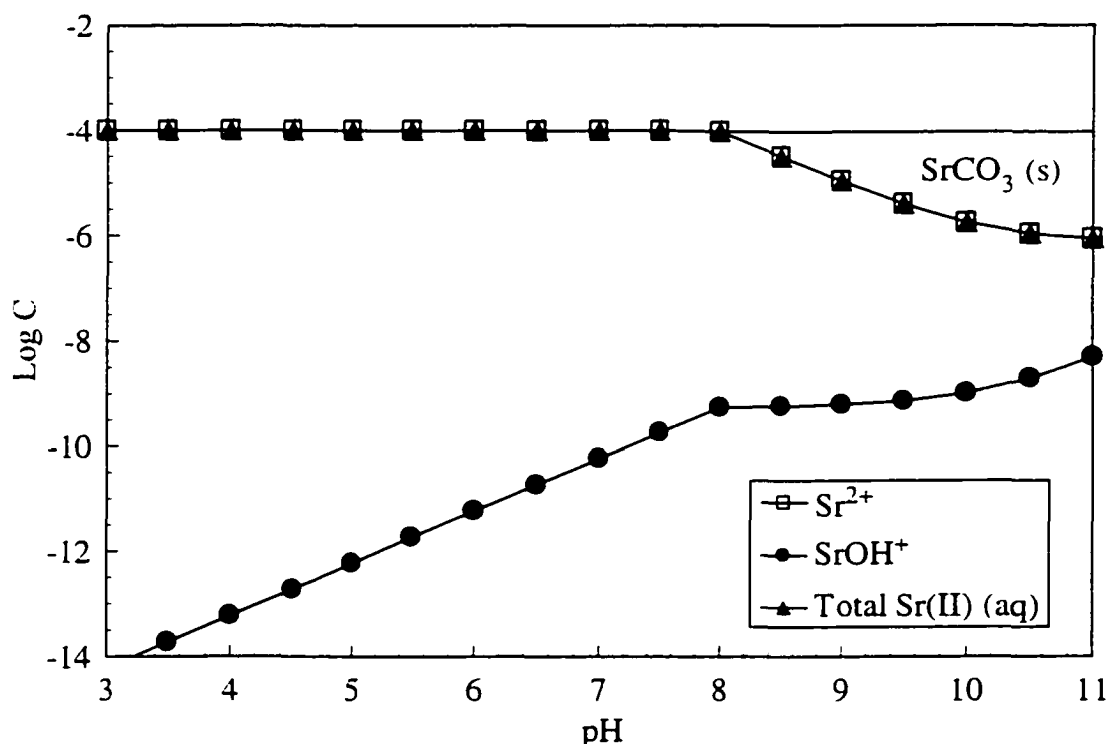


Figure 30. Speciation modeling of 1.0×10^{-4} M Sr(II) in groundwater from well U-20 at the NTS.

any value close to the actual pH of the groundwater. Strontianite (SrCO_3) is expected to precipitate at pH values above 8.0, under equilibrium conditions.

The theoretical interaction of 1.0×10^{-6} M Sr(II) with the groundwater composition obtained from the NTS was also investigated. Inspection of Figure 31 reveals very similar conditions as to those found in the 1.0×10^{-4} M Sr(II) concentration. Sr^{2+} and SrOH^+ would be the only aqueous Sr(II) species in solution. Sr^{2+} would be the predominant aqueous Sr(II) species for all pH values investigated using this groundwater composition. In contrast to the 1.0×10^{-4} M Sr(II) concentration that was modeled, however, there are no thermodynamically stable solid precipitates of Sr(II) at this metal cation concentration. It can be seen from the figure that the entire 1.0×10^{-6} M Sr(II)

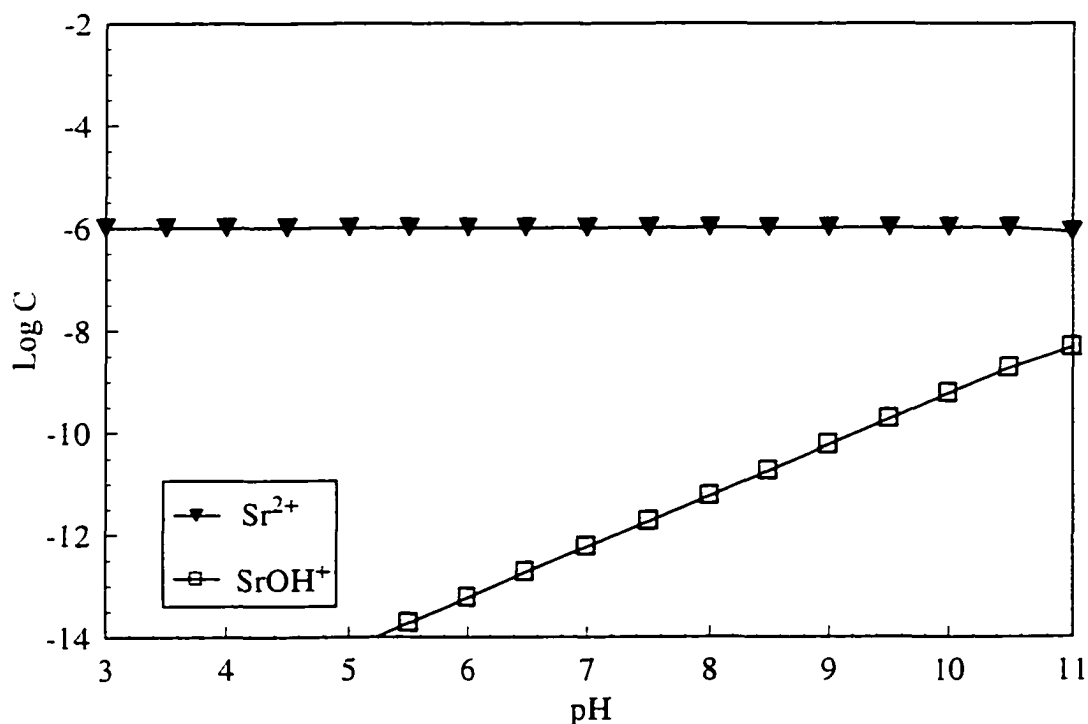


Figure 31. Speciation modeling of 1.0×10^{-6} M Sr(II) in groundwater from well U-20 at the NTS.

concentration can be accounted for by the aqueous species Sr^{2+} . This has important implications for the transport of Sr(II) in the subsurface environment at the NTS. For example, it suggests that the sorption of Sr(II) on the zeolitized tuff can be solely attributed to adsorption, and not by a combination of adsorption and surface precipitation.

The theoretical speciation of Sr(II) in the batch equilibrium sorption reactors was also investigated. The batch equilibrium sorption experiments were performed with high-purity water, therefore, for the speciation calculations only Sr(II) and the background electrolyte were assumed to be present. The speciation of Sr(II) was investigated at metal cation concentrations of 1.0×10^{-4} M and 1.0×10^{-6} M, and at all three background electrolyte concentrations (0.01, 0.1, and 1.0 M NaNO_3). The ionic strength corrections used by the geochemical modeling program are only valid up to an ionic strength of 0.1 M, therefore, speciation calculations will only be presented for the 0.01 M NaNO_3 background electrolyte concentration. In addition, the modeling showed that the speciation of Sr(II) was the same for the different metal cation concentrations with only the total Sr(II) line being adjusted for the actual Sr(II) concentration. Therefore, only one figure will be shown illustrating the speciation of Sr(II) in the batch equilibrium sorption reactors. The results from the speciation modeling indicated that again Sr^{2+} and SrOH^+ would be the only aqueous species present in the batch equilibrium sorption reactors. For example, inspection of Figure 32 shows that Sr^{2+} would be the predominate aqueous species under all pH conditions. Unlike the speciation of Pb(II), however, no precipitates of Sr(II) would form in the batch equilibrium sorption reactors at either the highest or lowest metal cation concentrations investigated. The entire 1.0×10^{-4} and 1.0×10^{-6} M Sr(II) concentrations would be accounted for by the aqueous species assuming that no

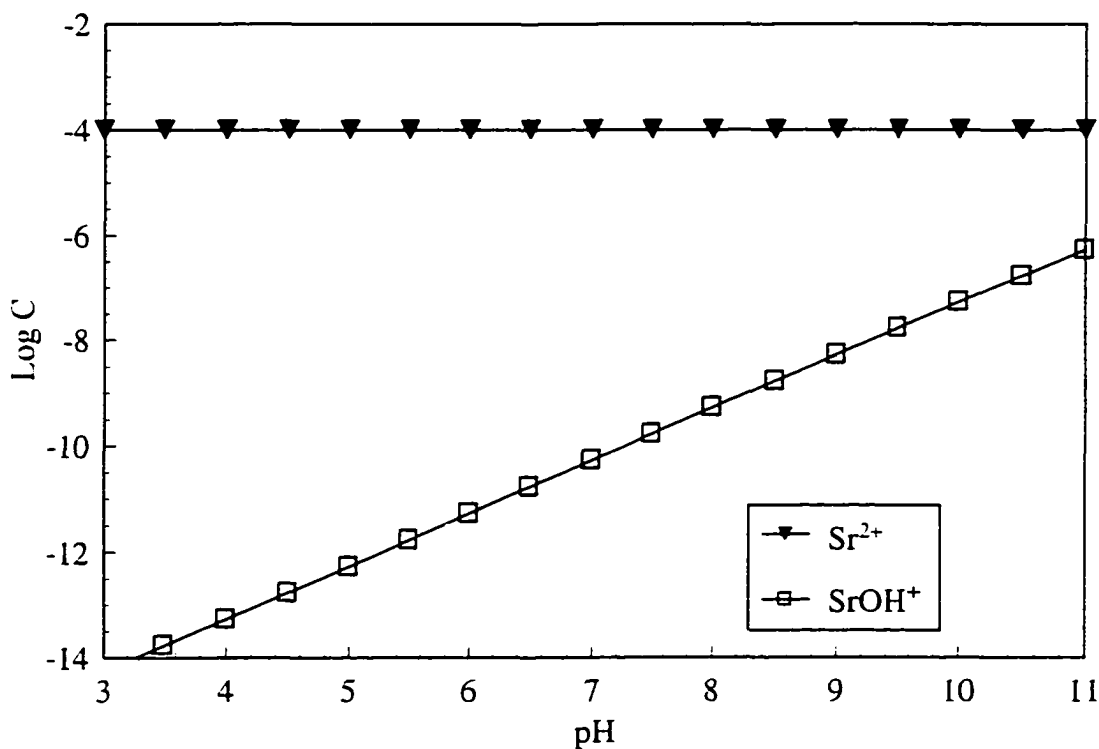


Figure 32. Speciation modeling of 1.0×10^{-4} M Sr(II) in 0.01 M NaNO₃ closed to the atmosphere.

CO₂ (g) is present.

In conclusion, the speciation calculations with Sr(II) have shown that it is at least thermodynamically feasible for precipitates of Sr(II) to form in the groundwater at the NTS at the highest Sr(II) concentration investigated. In addition, the speciation calculations have shown that precipitates of Sr(II) would not be likely to form at the lowest metal cation concentration investigated in the groundwater at the NTS, or in any of the batch equilibrium reactors. It must be remembered, however, that surface precipitates of Sr(II) could form in the system investigated at concentrations not exceeding the solubility of a given phase because of the presence of a solid phase which acts as a nucleation site. The results from these calculations are extremely different from the

results obtained with the Pb(II) cation. Those results showed that, thermodynamically at least, precipitates of Pb(II) would be more likely to form under all the different geochemical conditions. This differing speciation behavior can most likely be attributed to the fact that the Sr(II) cation does not significantly hydrolyze like the Pb(II) cation, and that it is generally less chemically reactive.

A Comparison of the Sorption Behavior of Pb(II) and Sr(II) on the Zeolitized Tuff

The fractional uptake data obtained from the batch equilibrium sorption experiments indicate that the Pb(II) cation has a greater affinity for the zeolitized tuff from Rainier Mesa than the Sr(II) cation regardless of the geochemical parameter investigated. Inspection of Figure 33 displays the typical response of the two cations at a 0.1 M NaNO₃ background electrolyte concentration, a 2.5 g/L zeolitized tuff concentration, and metal concentrations of 1.0×10^{-4} M. As can be seen from the figure, the fractional uptake of Pb(II) is substantially greater than the fractional uptake of Sr(II) for similar geochemical conditions. This type of sorption behavior can be seen again in Figure 34, which is at a higher solid concentration than the previous figure. The figure shows that the fractional uptake of Pb(II) is again greater than the fractional uptake of Sr(II) for similar geochemical conditions.

Although the fractional uptake of Pb(II) is always greater than the fractional uptake of Sr(II) on the zeolitized tuff, both cations show, qualitatively at least, similar behavior to changes in the geochemical parameters of interest. For example, the fractional uptake of both cations increases as the background electrolyte concentration decreases for the two lowest background electrolyte concentrations. In addition, the fractional uptake of both cations increases as the solid concentration of the adsorbent

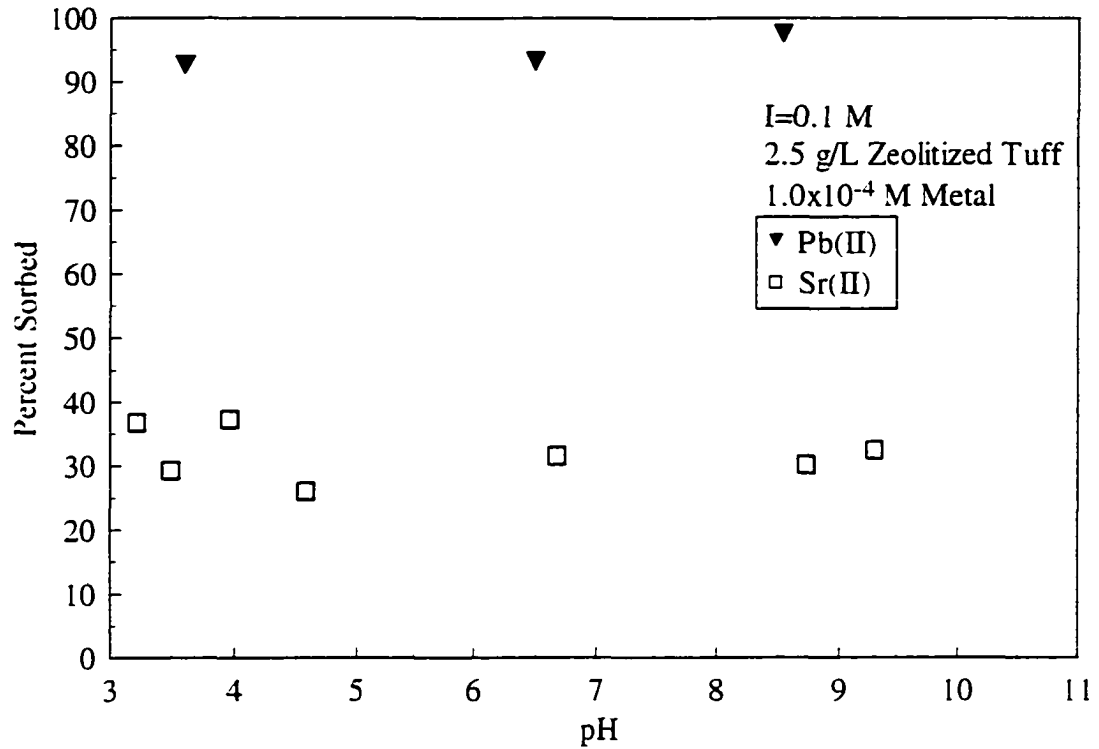


Figure 33. Comparison of the sorption behavior of 1.0×10^{-4} M Pb(II) and Sr(II) on 2.5 g/L zeolitized tuff in 0.1 M NaNO₃.

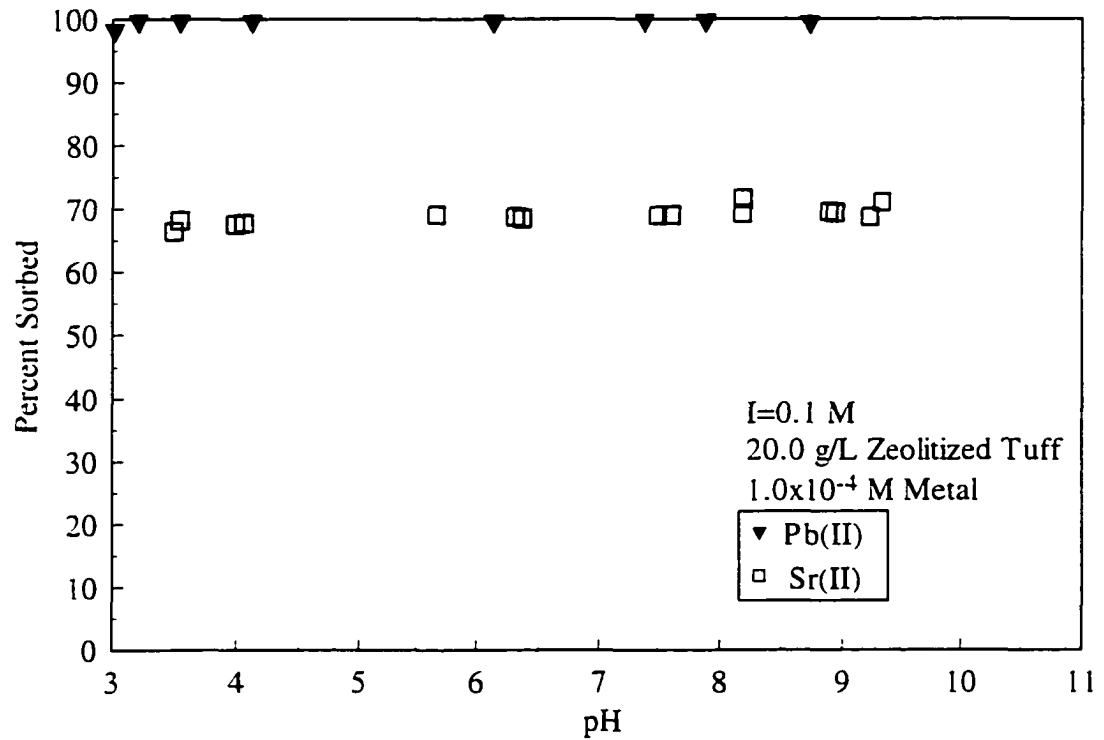


Figure 34. Comparison of the sorption behavior of 1.0×10^{-4} M Pb(II) and Sr(II) on 20 g/L zeolitized tuff in 0.1 M NaNO₃.

increases, and lastly, the fractional uptake of both cations increases as the metal cation concentration decreases.

The two metal cations differ in their sorption behavior, however, when the ionic strength of the background electrolyte is increased to the point where the metal cations are excluded from the internal cation-exchange sites of the zeolitized tuff. For example, the fractional uptake of Sr(II) decreases to 0% as the ionic strength of the background electrolyte is increased to at least 1.0 M NaNO₃. This behavior can be seen in Figure 35, which illustrates the fractional uptake of the cations on 2.5 g/L zeolitized tuff in 1.0 M NaNO₃. The figure reveals that the Sr(II) cation cannot compete with the background electrolyte, which is 6 orders of magnitude greater in concentration, for the internal

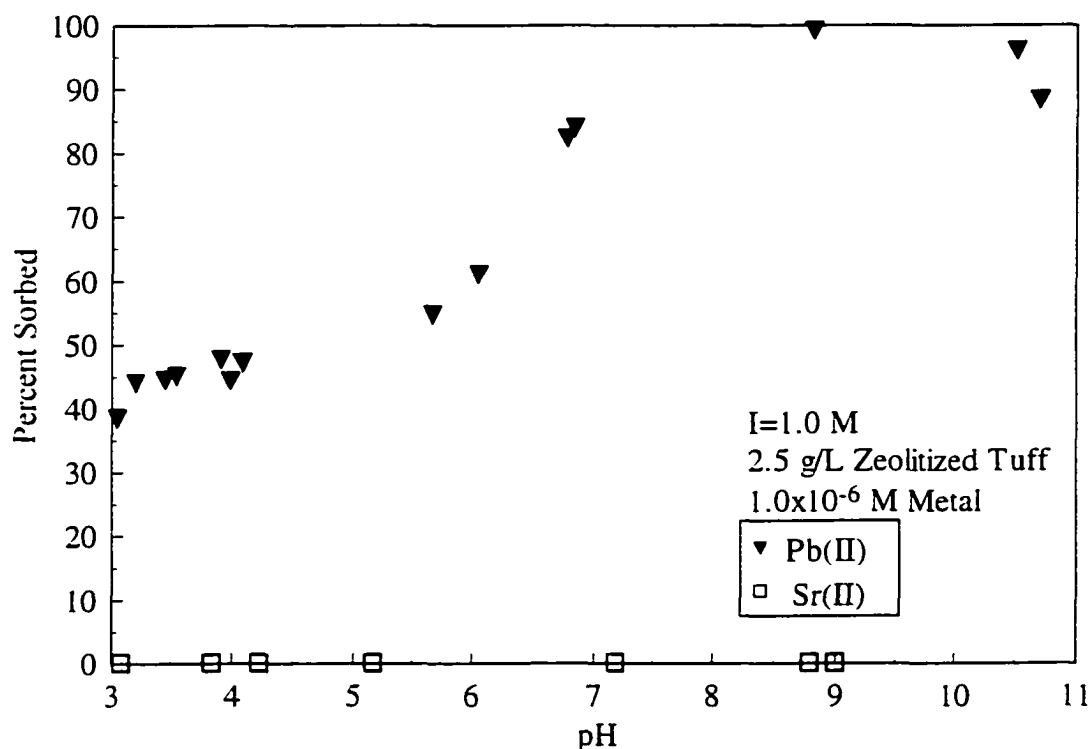


Figure 35. Comparison of the sorption behavior of 1.0×10^{-6} M Pb(II) and Sr(II) on 2.5 g/L zeolitized tuff in 1.0 M NaNO₃.

cation-exchange sites of the zeolitized tuff. There is no fractional uptake of Sr(II) because it, apparently, does not form inner-sphere coordination complexes with pH dependent surface sites, or surface precipitates. The fractional uptake of Pb(II), however, is quite different from that of Sr(II). The Pb(II) cation displays pH-dependent fractional uptake and varies from 40-100% for pH values in the range of 3-11. This pH-dependent sorption behavior suggests that the fractional uptake of Pb(II) is not solely controlled by cation exchange. It suggests that a different type of binding mechanism is responsible for the fractional uptake of Pb(II) as it becomes progressively excluded from the internal cation-exchange sites of the zeolitized tuff. Possible alternatives to cation-exchange at the highest background electrolyte concentration include the formation of inner-sphere coordination complexes with pH dependent surface sites, or the formation of surface precipitates or polymers.

In conclusion, the partitioning characteristics of Pb(II) and Sr(II) were investigated as a function of numerous geochemical parameters. The many experiments indicated that the cations have similar sorption behavior at background electrolyte concentrations of less than 1.0 M NaNO₃. The two cations differ in their sorption behavior, however, when the background electrolyte concentration is increased to 1.0 M NaNO₃. Comparisons of the two cations sorption behavior also showed that the fractional uptake of Pb(II) is always greater than the fractional uptake of Sr(II) when the geochemical conditions for the two cations are similar, which can likely be attributed to the different chemical characteristics of each cation. For example, the Pb(II) cation is a transition metal and the Sr(II) cation is an alkali earth metal.

Sorption of Pb(II) and Sr(II) on Clinoptilolite

Batch equilibrium sorption experiments with Pb(II) and Sr(II) were conducted using the clinoptilolite obtained from Jordan Valley, Oregon. These additional batch equilibrium sorption experiments were performed in order to investigate the sorption behavior of Pb(II) and Sr(II) using the mineralogically pure clinoptilolite. This was done in an attempt to test the hypothesis that the clinoptilolite contained within the zeolitized tuff is mainly responsible for the sorption behavior of the ions, so that extrapolations could be made regarding fractional uptake of the ions by other zeolitized rocks assuming that they contain a significant percentage of similar zeolite minerals. These additional batch equilibrium sorption experiments were also conducted as a function of pH, ionic strength, solid adsorbent concentration, and total metal cation concentration. The fractional uptake of Pb(II) on the clinoptilolite will be discussed first followed by the fractional uptake of Sr(II) on the clinoptilolite. The final section of this chapter will investigate similarities and differences between the sorption behavior of Pb(II) and Sr(II) as a function of adsorbent type, in order to determine whether the zeolite mineral clinoptilolite contained within the zeolitized tuff is controlling the sorption behavior of the cations.

Sorption Behavior of Pb(II)

The batch equilibrium sorption experiments performed as a function of pH, ionic strength, solid adsorbent concentration, and total metal cation concentration of interest have shown that, overall, the sorption of Pb(II) on the clinoptilolite is, at least qualitatively, the same as the sorption of Pb(II) on the zeolitized tuff. This observation has significant implications for the sorption of Pb(II) on the zeolitized tuff, namely that

the sorption of Pb(II) is controlled by the same types of binding sites found in the pure mineral clinoptilolite.

Ionic strength experiments were conducted at background electrolyte concentrations of 0.01, 0.1, and 1.0 M NaNO₃. A solid concentration of 1 g/L clinoptilolite was used because it is equivalent in terms of the surface area to a solid concentration of 3.0 g/L zeolitized tuff. These two solid adsorbent concentrations will be used later in the chapter to illustrate similarities and differences in the sorption behavior of the cations as a function of adsorbent type. Overall, the data show that the fractional uptake of Pb(II) increases as the ionic strength decreases for the two lowest background electrolyte concentrations. For example, Figure 36 shows the fractional uptake of 1.0×10^{-5} M Pb(II) on 1 g/L clinoptilolite as a function of ionic strength. It can be clearly seen from the figure that the fractional uptake of Pb(II) on the clinoptilolite is approximately 95% for the 0.1 M NaNO₃ concentration, and increases to essentially 100% for the 0.01 M NaNO₃ concentration. In addition, it can be seen that at these ionic strengths the fractional uptake of Pb(II) is independent of the pH. The fractional uptake of Pb(II) on the clinoptilolite at a 1.0 M NaNO₃ background electrolyte concentration, however, varies from approximately 20% at low pH values to fractional uptake of approximately 100% at pH values above 8.5. This type of sorption behavior can again be seen in Figure 37 showing experiments at a lower metal cation concentration than the previous diagram. The fractional uptake of Pb(II) on the clinoptilolite at the 1.0 M NaNO₃ concentration exhibits pH-dependent sorption behavior, and varies from approximately 25% at low pH values to 100% at pH values above approximately 8.5 or so. The fractional uptake of Pb(II) at the 0.1 M NaNO₃ background electrolyte concentration, however, is

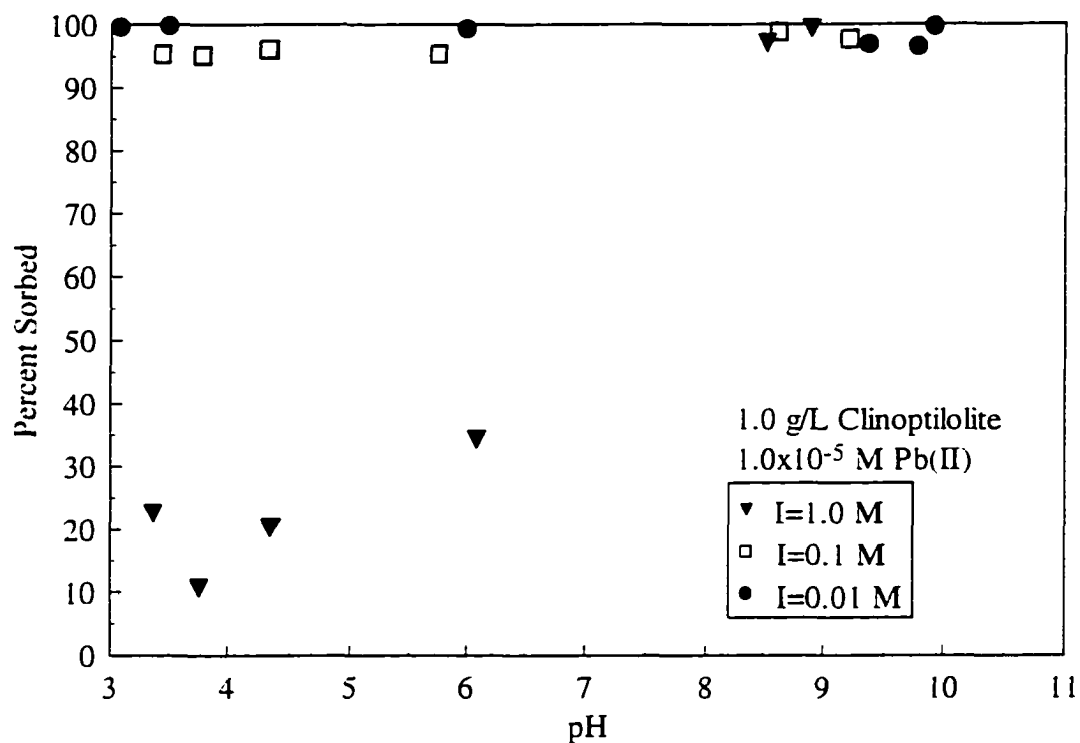


Figure 36. Sorption of 1.0×10^{-5} M Pb(II) on 1.0 g/L clinoptilolite as a function of ionic strength.

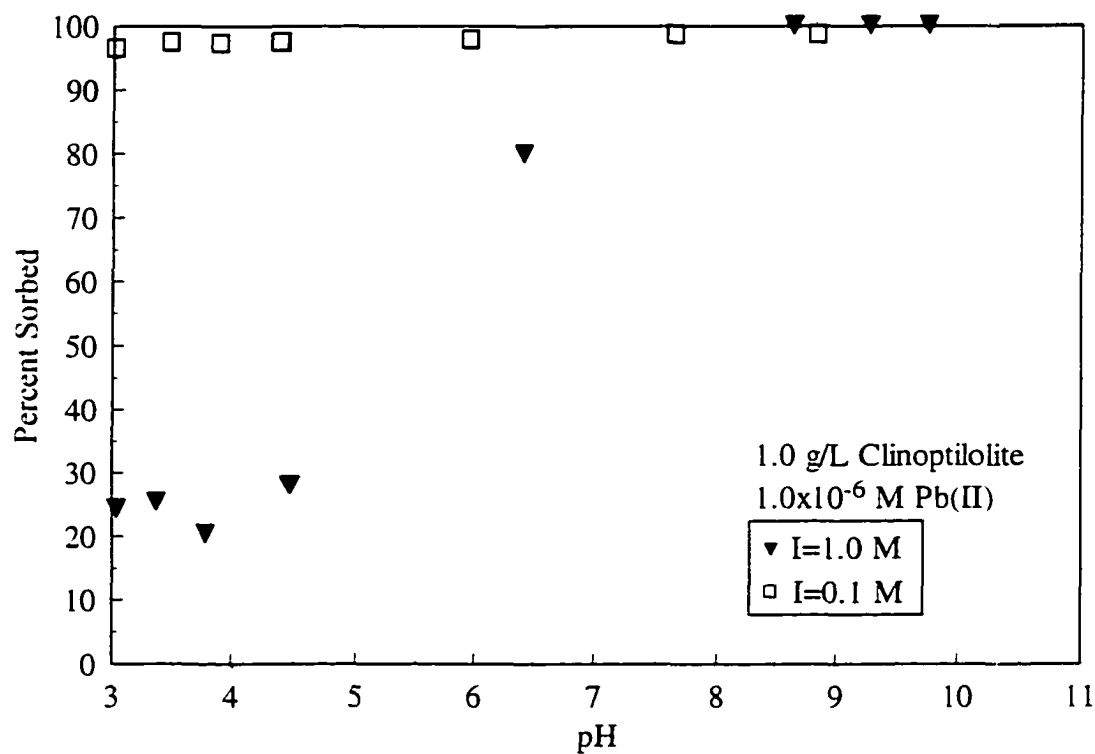


Figure 37. Sorption of 1.0×10^{-6} M Pb(II) on 1.0 g/L clinoptilolite as a function of ionic strength.

approximately 95% for all pH values investigated. This type of sorption behavior as a function of ionic strength appears to be similar to the behavior found with the zeolitized tuff, and can be similarly explained.

To illustrate any similarity in the sorption behavior of Pb(II) as a function of the solid concentration, batch equilibrium sorption experiments were performed at 1 g/L and 20 g/L solid concentrations. The results from these experiments indicate that, again, the fractional uptake of Pb(II) increases as the solid concentration of the adsorbent increases. This type of sorption behavior is consistent with all of the previous sorption experiments performed during this research, and can be similarly explained. Figure 38 shows the fractional uptake of 1.0×10^{-5} M Pb(II) in 1.0 M NaNO₃ as a function of the

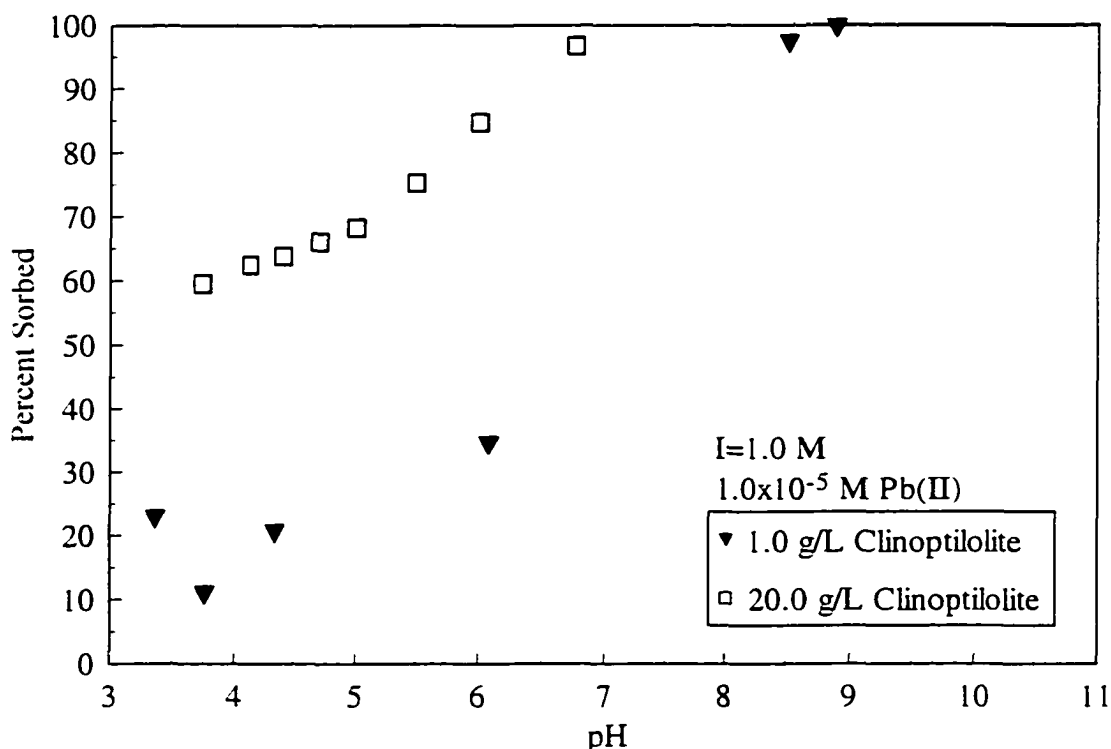


Figure 38. Sorption of 1.0×10^{-5} M Pb(II) in 0.01 M NaNO₃ as a function of clinoptilolite concentration.

clinoptilolite concentration. The 1 g/L solid adsorbent concentration has a fractional uptake of 20% at low pH values that increases to approximately 100% at pH values above approximately 8. The 20 g/L solid adsorbent concentration on the other hand has a fractional uptake of approximately 60% at low pH values that increases to greater than 95% at approximately a pH of 6.5.

Sorption behavior of this type can be seen again in Figure 39, showing the fractional uptake of 1.0×10^{-4} M Pb(II) in 0.1 M NaNO₃ as a function of the clinoptilolite concentration. This figure reveals that at the 1 g/L clinoptilolite concentration results in a fractional uptake of approximately 90% Pb(II) for all pH values investigated, and that the 20 g/L clinoptilolite concentration results in a fractional uptake of 100% Pb(II). These

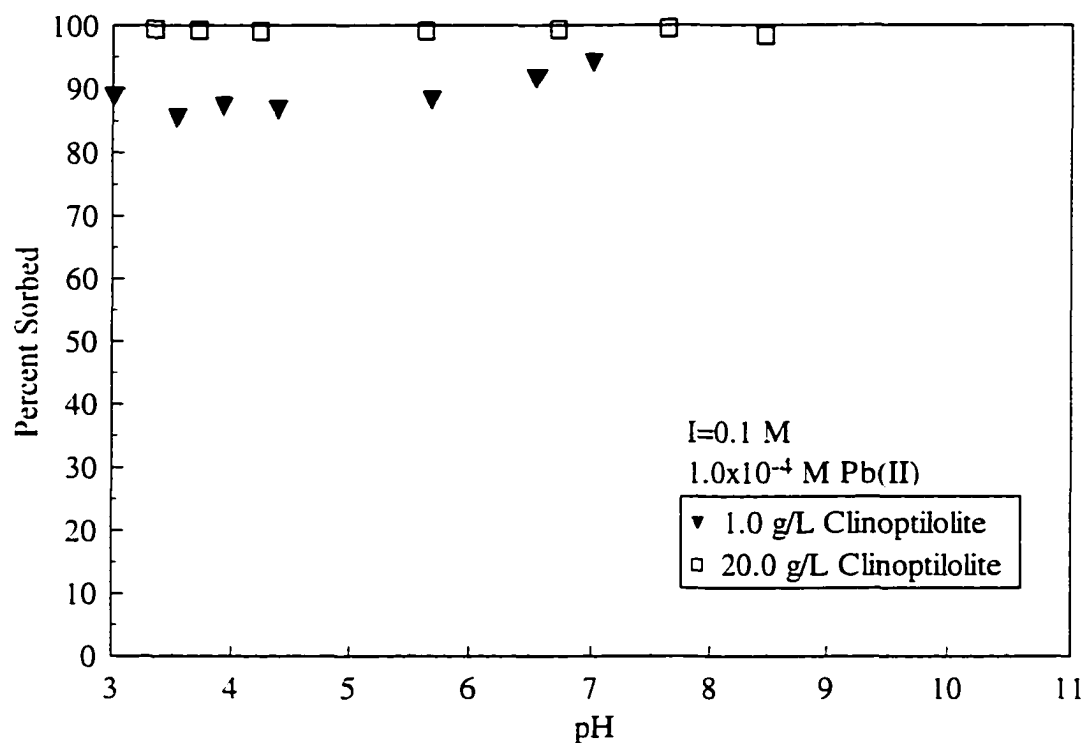


Figure 39. Sorption of 1.0×10^{-4} M Pb(II) in 0.1 M NaNO₃ as a function of clinoptilolite concentration.

two figures as a function of solid concentration serve to illustrate, once again, that the fractional uptake of Pb(II) is solid-concentration dependent, but qualitatively different depending on the ionic strength. Both figures show, however, that as the solid concentration increases, the fractional uptake of Pb(II) on the clinoptilolite also increases.

In order to investigate the partitioning behavior of Pb(II) on the clinoptilolite as a function of the Pb(II) cation concentration, batch equilibrium sorption experiments were conducted at numerous Pb(II) concentrations. Overall, the results show that the sorption of Pb(II) on the clinoptilolite as a function of Pb(II) concentration is similar to the experiments with the zeolitized tuff, namely that the fractional uptake of Pb(II) on the clinoptilolite increases as the Pb(II) concentration decreases. This type of behavior can be seen in Figure 40. It shows the fractional uptake of Pb(II) on 20 g/L clinoptilolite in 1.0 M NaNO₃ as a function of cation concentration. The figure reveals that the fractional uptake of Pb(II) increases as the metal cation concentration decreases from 1.0×10^{-4} M to 1.0×10^{-6} M. Additionally, it can be seen in the figure that the fractional uptake of Pb(II) on the clinoptilolite is dependent on the pH for this particular ionic strength.

Sorption behavior that is also metal-concentration dependent, but qualitatively different because of the ionic strength can be seen in Figure 41. This figure shows the fractional uptake of Pb(II) on 1 g/L clinoptilolite in 0.1 M NaNO₃ as a function of the Pb(II) concentration. This figure also shows that the fractional uptake of Pb(II) increases as the Pb(II) concentration decreases. For example, the 1.0×10^{-4} M Pb(II) concentration results in a fractional uptake on the clinoptilolite of approximately 90% for all pH values investigated, and the 1.0×10^{-5} M Pb(II) concentration results in the fractional uptake of approximately 95% Pb(II) from solution. Lastly, the lowest metal cation concentration of

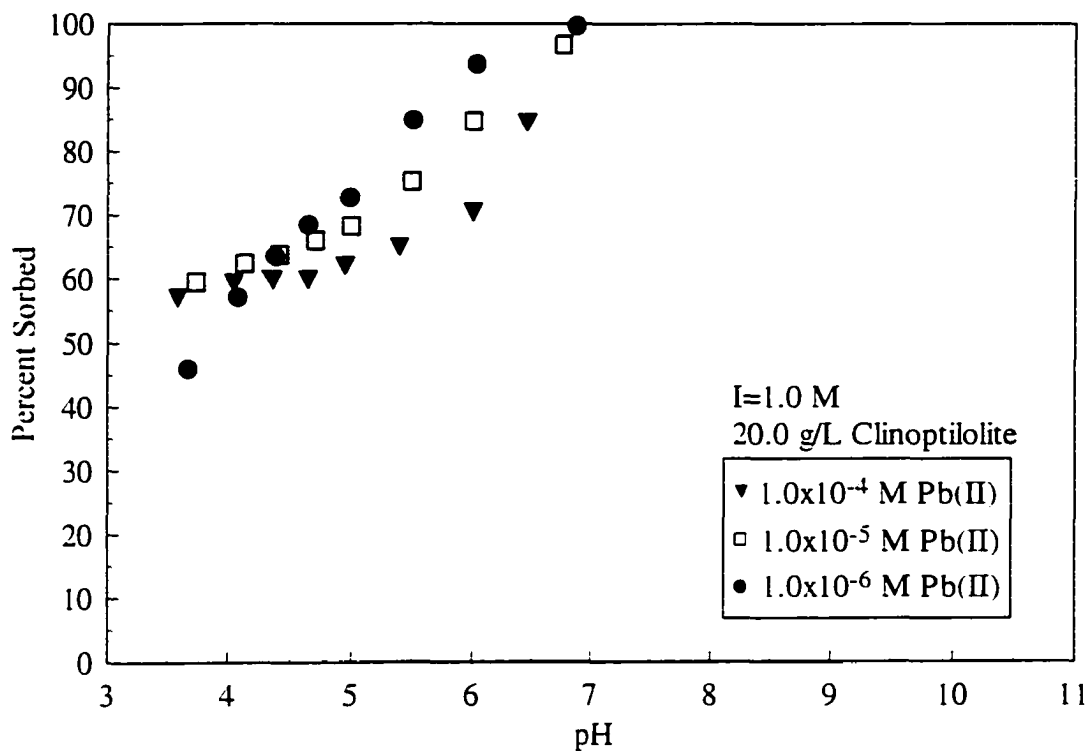


Figure 40. Sorption of Pb(II) on 20 g/L clinoptilolite in 1.0 M NaNO₃ as a function of Pb(II) concentration.

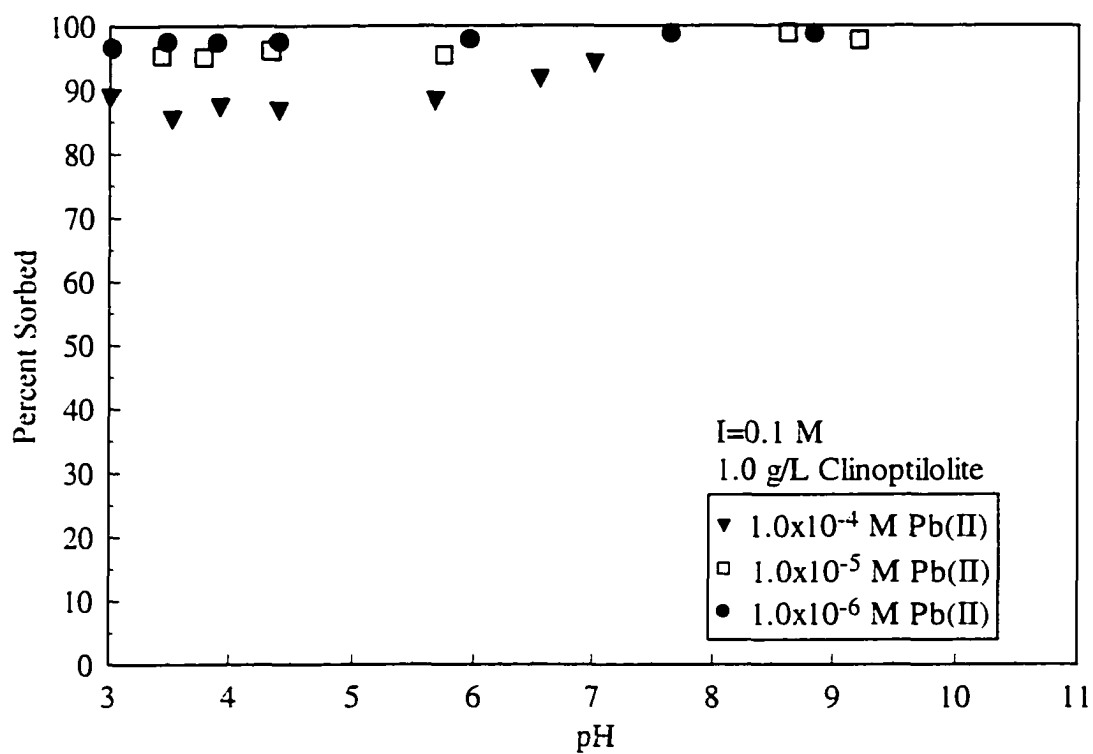


Figure 41. Sorption of Pb(II) on 1.0 g/L clinoptilolite in 0.1 M NaNO₃ as a function of Pb(II) concentration.

1.0×10^{-6} M Pb(II) results in the greatest fractional uptake of approximately 98%.

Although the differences between the fractional uptakes are small, the figure shows that as the Pb(II) concentration decreases the fractional uptake of Pb(II) on the clinoptilolite increases. This type of behavior is similar to the behavior found with the zeolitized tuff, and can be similarly explained.

Sorption Behavior of Sr(II)

The batch equilibrium sorption experiments performed as a function of pH, ionic strength, solid adsorbent concentration, and total metal cation concentration have shown that, overall, the sorption of Sr(II) on the clinoptilolite is also, at least qualitatively, the same as the sorption of Sr(II) on the zeolitized tuff. This behavior would tend to indicate that the fractional uptake of Sr(II) on the zeolitized tuff is also controlled by the same types of binding sites present in the clinoptilolite.

In order to investigate the equilibrium sorption behavior of Sr(II) as a function of ionic strength, batch equilibrium sorption experiments were performed at ionic strengths of 0.01, and 0.1 M NaNO₃. Previous investigations of the ionic strength dependence of Sr(II) with the zeolitized tuff revealed that no fractional uptake of Sr(II) could be observed at the 1.0 M NaNO₃ concentration. Therefore, only one experiment was performed with Sr(II) at the 1.0 M NaNO₃ concentration with the clinoptilolite, and the results of that experiment were identical to the experiments using the zeolitized tuff. The fractional uptake of Sr(II) on the clinoptilolite at the 1.0 M NaNO₃ concentration is negligible. Therefore, batch equilibrium sorption experiments performed as a function of the ionic strength with the clinoptilolite were only performed at background electrolyte concentrations of 0.1 and 0.01 M NaNO₃.

The batch equilibrium experiments confirmed that the fractional uptake of Sr(II) on the clinoptilolite increases, once again, as the background electrolyte decreases for the same reasons stated earlier in the discussion with the zeolitized tuff. This can be seen in Figure 42 showing the fractional uptake of 1.0×10^{-4} and 1.0×10^{-5} M Sr(II) on 1 g/L clinoptilolite as a function of the ionic strength. It can be seen from the figure that at the 0.1 M NaNO_3 concentrations, the fractional uptake of Sr(II) is approximately 25% for the 1.0×10^{-4} M Sr(II) and approximately 35% for the 1.0×10^{-5} M Sr(II) regardless of pH. Furthermore, as the background electrolyte concentration decreases to 0.01 M NaNO_3 , the fractional uptake of Sr(II) on the clinoptilolite increases to approximately 80% for the 1.0×10^{-4} M Sr(II) concentration and approximately 90% for the 1.0×10^{-5} M Sr(II)

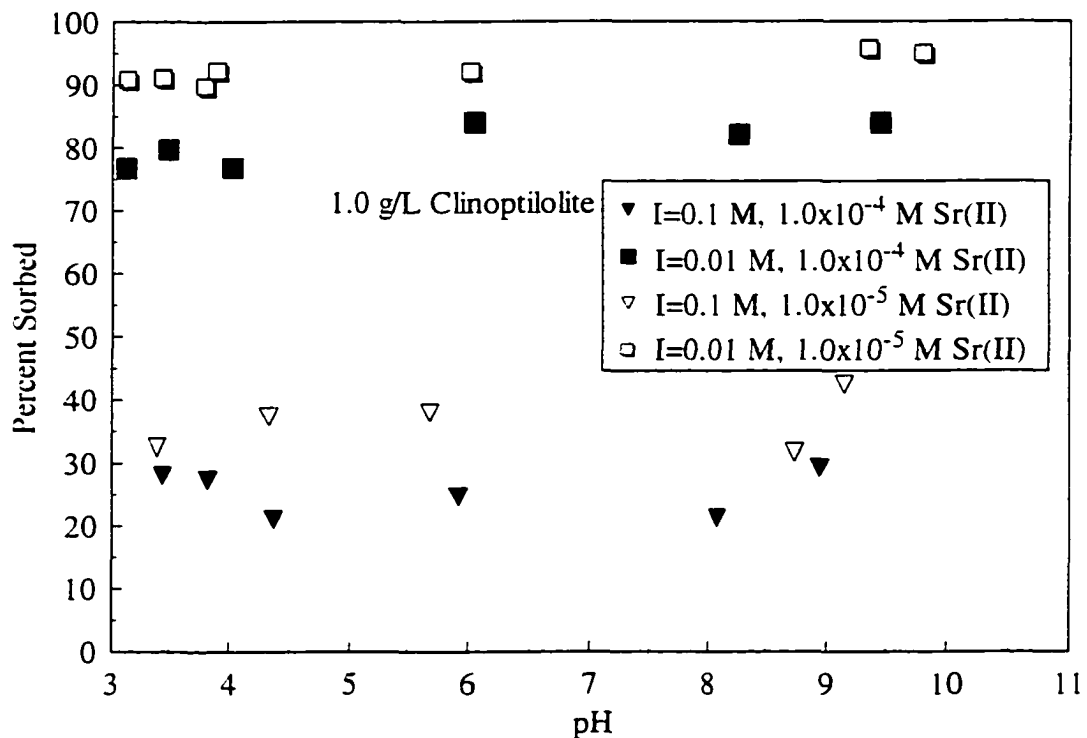


Figure 42. Sorption of 1.0×10^{-4} M and 1.0×10^{-5} M Sr(II) on 1.0 g/L clinoptilolite as a function of ionic strength.

concentration regardless of pH.

Batch equilibrium sorption experiments were also performed as a function of the clinoptilolite concentration. Experiments were performed at solid concentrations of 1.0 and 20.0 g/L. The experiments indicate that, as was found with the zeolitized tuff, increasing solid concentrations result in an increase in the fractional uptake of Sr(II) on the clinoptilolite for the reasons explained earlier. Figure 43 illustrates the fractional uptake of 1.0×10^{-4} M Sr(II) in 0.1 M NaNO₃ as a function of clinoptilolite concentration. The figure shows the fractional uptake of approximately 25% for the 1.0 g/L solid adsorbent concentration for all pH values investigated, and a fractional uptake of approximately 75% for the 20 g/L solid adsorbent concentration for all pH values

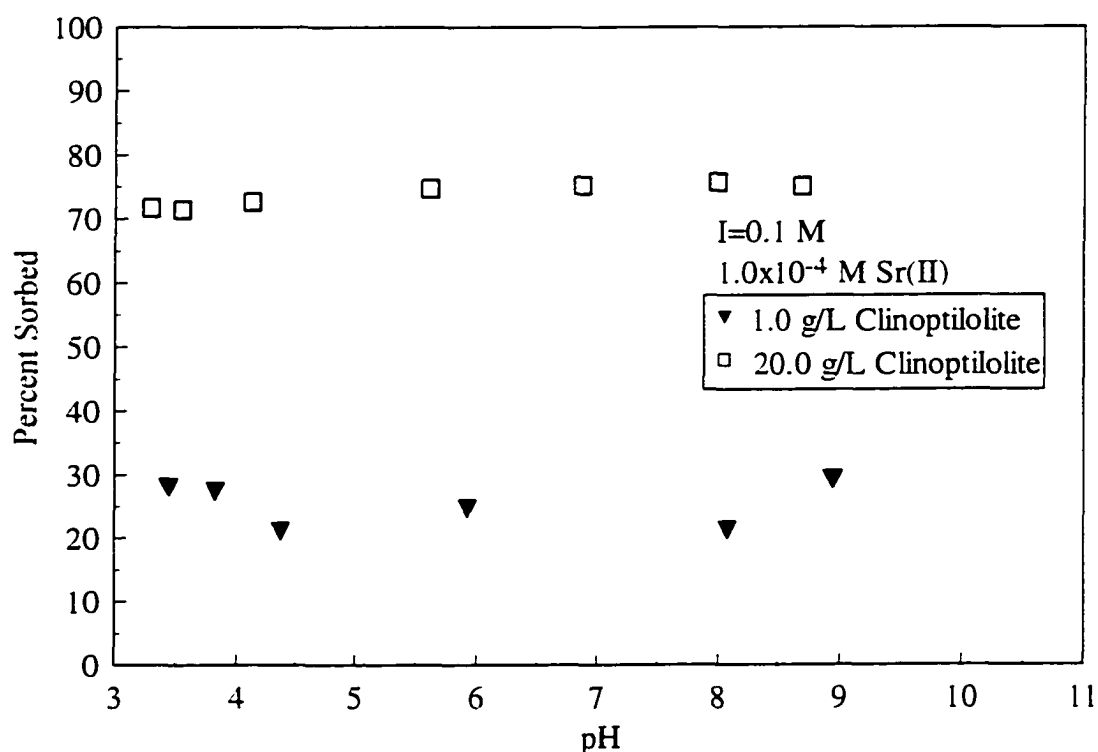


Figure 43. Sorption of 1.0×10^{-4} M Sr(II) in 0.1 M NaNO₃ as a function of solid concentration.

investigated. It is apparent from the figure that at this background electrolyte concentration the fractional uptake of Sr(II) on the clinoptilolite is pH-independent, and that an increase in the solid adsorbent concentration results in an increase in the fractional uptake of Sr(II).

The last geochemical parameter investigated using the clinoptilolite and the Sr(II) cation was concerned with changes in the overall Sr(II) concentration. Not surprisingly, the experiments indicate that the fractional uptake of Sr(II) increases as the Sr(II) concentration decreases. This behavior can be seen in Figure 44, showing the fractional uptake of Sr(II) on 1.0 g/L clinoptilolite in 0.1 M NaNO₃. The figure clearly shows that the 1.0x10⁻⁴ M Sr(II) concentration results in a fractional uptake of approximately 25%.

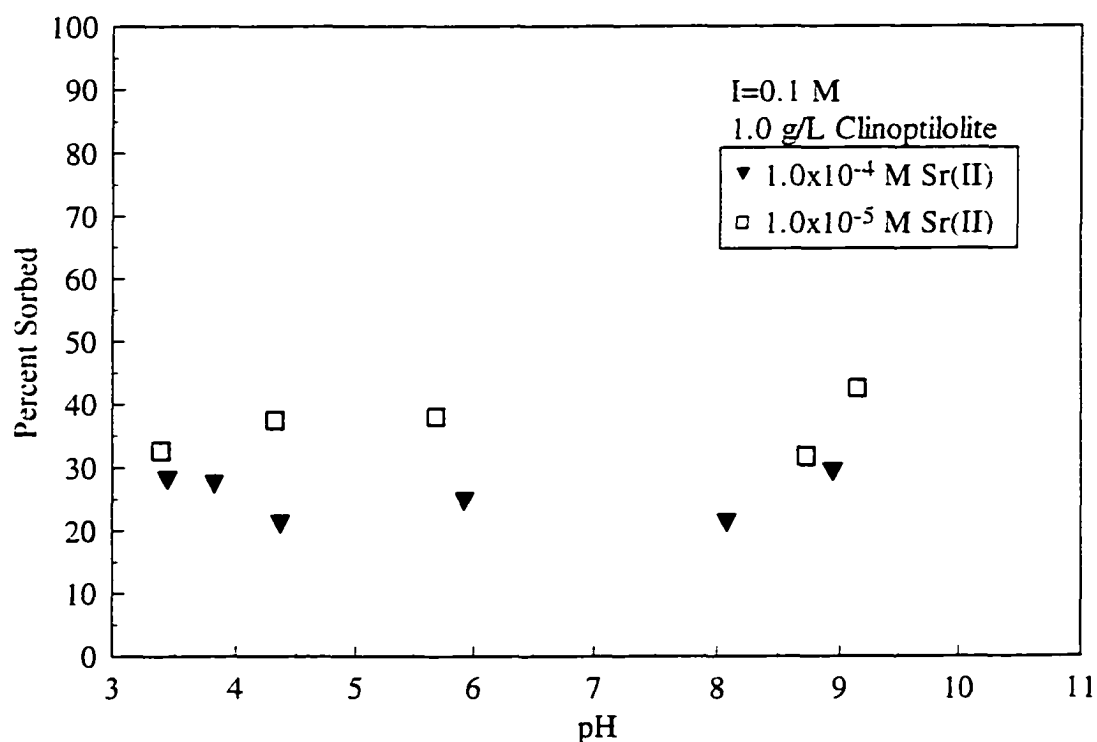


Figure 44. Sorption of Sr(II) on 1.0 g/L clinoptilolite in 0.1 M NaNO₃ as a function of Sr(II) concentration.

while the 1.0×10^{-5} M Sr(II) concentration results in a fractional uptake of approximately 35%. This behavior is again expected since a decrease in the Sr(II) cation concentration results in an increase in the number of available binding sites for the cations remaining in solution.

A Comparison of the Sorption Behavior of Pb(II) and Sr(II) on the Clinoptilolite

Comparing the equilibrium sorption behavior of Pb(II) and Sr(II) on the clinoptilolite reveals behavior that is, qualitatively, similar to the behavior observed with the zeolitized tuff from the NTS. For example, the fractional uptake of Pb(II) is always greater than the fractional uptake of Sr(II) on the clinoptilolite for all of the experiments in which the conditions for the two cations were identical. This indicates that Pb(II) has a greater affinity for the clinoptilolite than Sr(II). An example of this type of sorption behavior can be seen in Figure 45 showing the fractional uptake of 1.0×10^{-4} M Pb(II) and Sr(II) on 1.0 g/L clinoptilolite in 0.1 M NaNO₃. The figure clearly shows that the Pb(II) cation has a fractional uptake of approximately 90%, and that the Sr(II) cation has a fractional uptake of approximately 25% for all pH values investigated. The figure also reveals that at a background electrolyte concentration of 0.1 M NaNO₃, both cations show pH-independent sorption behavior.

A comparison of the equilibrium sorption behavior of the two cations at identical conditions also revealed that the two cations behave similarly to changes in the geochemical parameters investigated. For example, the experiments showed that fractional uptake of both cations on the clinoptilolite increased as the background electrolyte decreased. In addition, the experiments showed that fractional uptake of both cations on the clinoptilolite increased as the clinoptilolite concentration increases. Lastly,

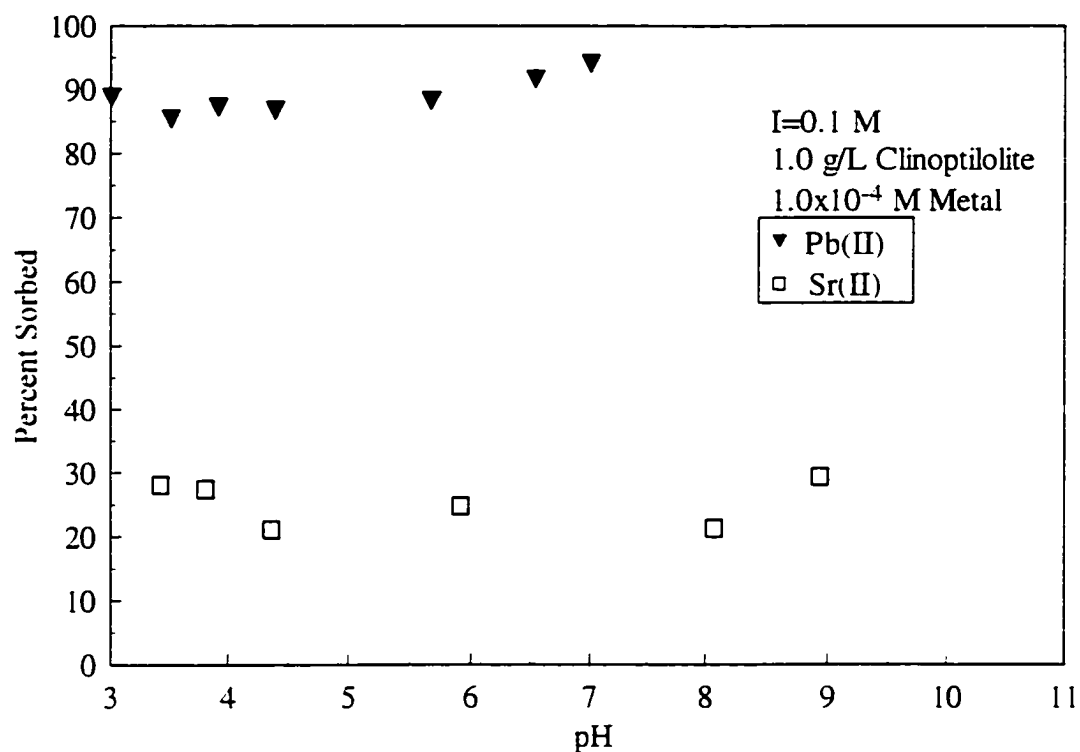


Figure 45. Comparison of the sorption behavior of 1.0×10^{-4} M Pb(II) and Sr(II) on 1.0 g/L clinoptilolite in 0.1 M NaNO₃.

the fractional uptake of both cations on the clinoptilolite increased as the total metal cation concentration decreased.

The sorption behavior of the two cations differ, however, when the background electrolyte concentration increases to 1.0 M NaNO₃. At that high of an ionic strength, the fractional uptake of Sr(II) on the clinoptilolite is negligible. The fractional uptake of Pb(II), however, becomes controlled by the pH of the solution. This pH-dependent sorption behavior of the Pb(II) cation at the 1.0 M NaNO₃ concentration suggests even though Pb(II) is excluded from the internal cation-exchange sites of the zeolitized tuff, it still binds to the external amphoteric surface sites of the adsorbent or it forms surface precipitates.

Comparison of Pb(II) and Sr(II) Sorption as a Function of Adsorbent Type

The reason to perform the additional batch equilibrium sorption experiments with the clinoptilolite was to compare a simple case (mineralogically pure clinoptilolite) and a complex case (naturally occurring zeolitized tuff). A comparison of the sorption behavior of the two cations on both adsorbents is important to understanding the overall sorption behavior of the cations on the zeolitized tuff. For example, if the partitioning behavior of the cations is found to be the same for both adsorbents then one would expect that most of the fractional uptake of the cations is being controlled by the clinoptilolite or by an analogous mineral or suite of minerals. If the fractional uptake of the cations is not the same, however, then one could conclude that some other mineralogical phase is at least partly responsible for the fractional uptake of the cations. For comparisons of the sorption behavior of the cations as a function of the adsorbent type to be meaningful, it must be remembered that the surface area of the clinoptilolite is approximately 3 times greater than the surface area of the zeolitized tuff (see Chapter 3). The solid concentrations of the adsorbents, therefore, were normalized with respect to the overall surface area. For example, batch equilibrium sorption experiments performed with the zeolitized tuff were conducted at solid concentrations of 3.0 g/L, and the experiments with the clinoptilolite were conducted at solid concentrations 1.0 g/L.

Pb(II) Sorption as a Function of Adsorbent Type

Figure 46 shows the fractional uptake of 1.0×10^{-6} M Pb(II) on both adsorbents in 1.0 M NaNO₃. As can be seen from the figure, the fractional uptake of Pb(II) on both adsorbents is pH-dependent for experiments performed at this background electrolyte concentration of 1.0 M NaNO₃. The qualitatively similar fractional uptake suggests that

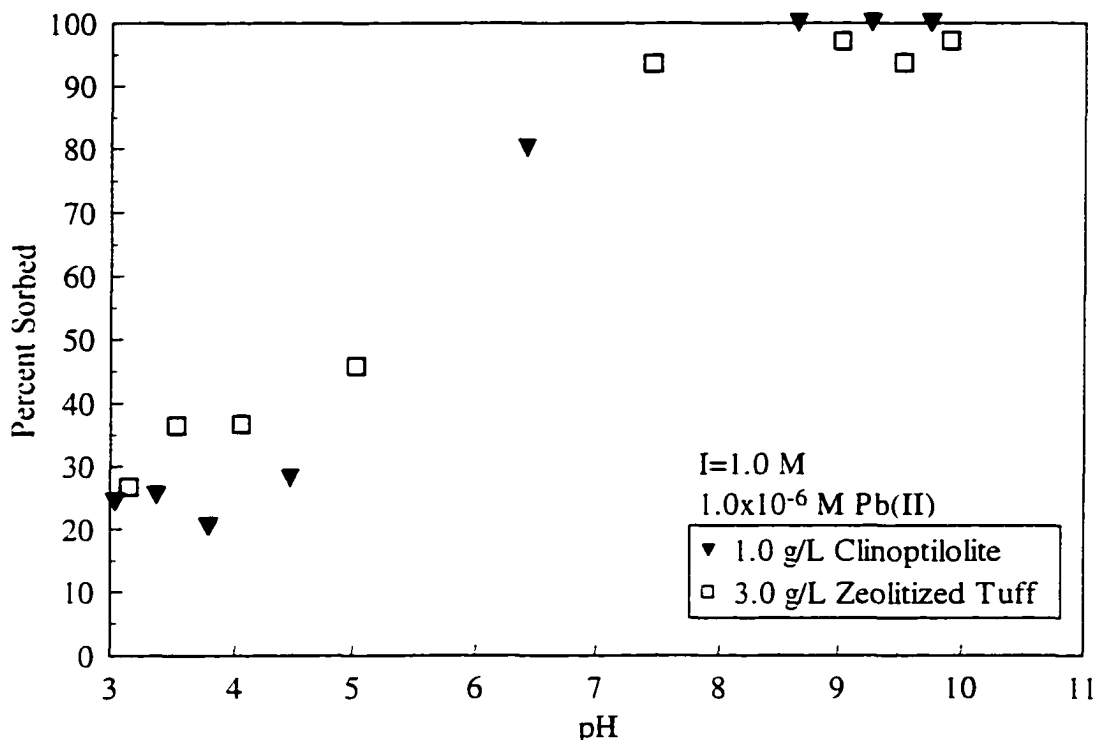


Figure 46. Sorption of 1.0×10^{-6} M Pb(II) in 1.0 M NaNO₃ as a function of adsorbent type.

the same sorts of mechanisms must be controlling the sorption behavior of Pb(II) in both materials. The fractional uptake of Pb(II) on both adsorbents varies as a function of pH from approximately 25% at a pH of 3 to a fractional uptake of approximately 100% at pH values above approximately 8.5. It should be noted, however, that the two fractional uptake curves, while qualitatively similar, are not identical. For example, the zeolitized tuff results in the greater fractional uptake than the clinoptilolite at low pH, while the clinoptilolite results in the greater fractional uptake at high pH. From previous discussions concerning the sorption of Pb(II) at background electrolyte concentrations of 1.0 M NaNO₃, it is assumed that the fractional uptake of Pb(II) on both adsorbents is controlled by the formation of inner-sphere coordination complexes on pH dependent surface sites, or by the formation of surface precipitates which are also pH-dependent.

Another comparison of the fractional uptake of Pb(II) as a function of adsorbent type behavior can be seen in Figure 47. This figure shows the fractional uptake of 1.0×10^{-6} M Pb(II) in 0.1 M NaNO₃ as a function of adsorbent type. The figure shows that, once again, the fractional uptake of Pb(II) on both adsorbents is qualitatively similar, however, in this figure it is easily seen that the fractional uptake of Pb(II) on the clinoptilolite is lower than on the zeolitized tuff. The fractional uptake of Pb(II) in this figure varies from approximately 90 to 95% for all pH values investigated depending on the adsorbent type. It must be remembered that for ionic strengths less than 1.0 M NaNO₃ the fractional uptake of Pb(II) is assumed to be controlled by cation-exchange sites. Both of these adsorbents have extremely large cation-exchange capacities, and the

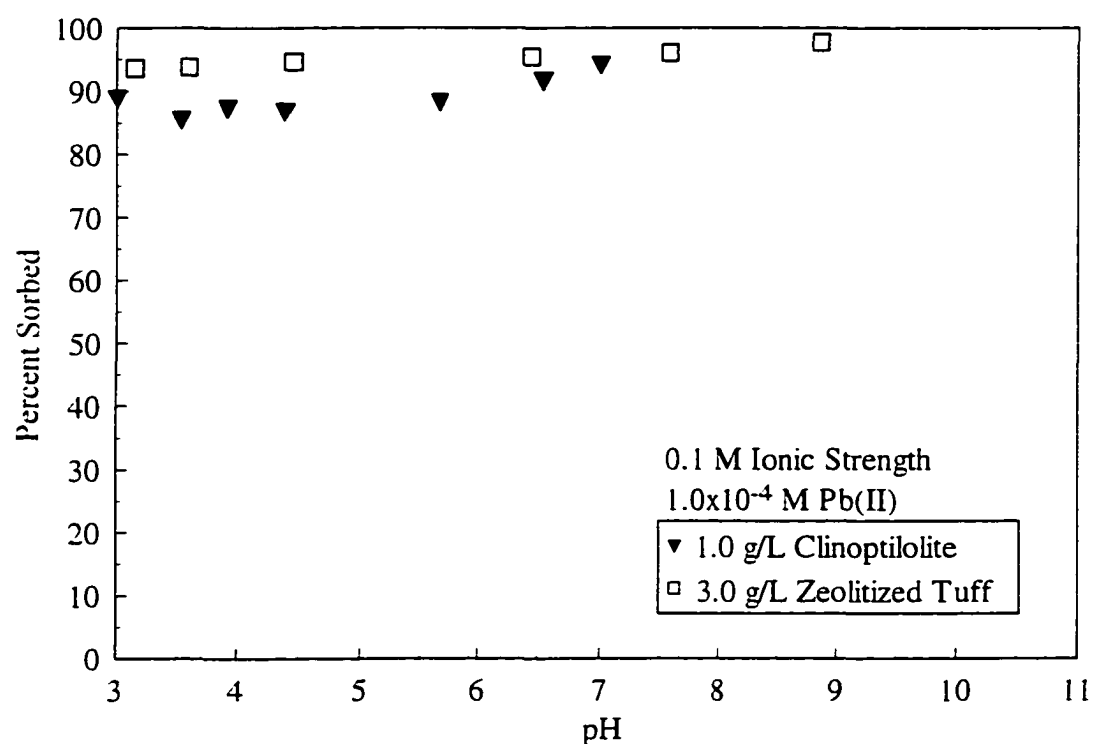


Figure 47. Sorption of 1.0×10^{-4} M Pb(II) in 0.1 M NaNO₃ as a function of adsorbent type.

almost complete removal of the Pb(II) cation from solution would be expected if the solid concentration of the adsorbents is large enough, which appears to be the case. The fact that the clinoptilolite results in a little less fractional uptake than the zeolitized tuff can likely be explained because the adsorbents were normalized with respect to the surface area and not the cation-exchange capacity. Normalization of the surface area of both adsorbents would not necessarily result in the same number of internal cation-exchange sites. The 3 g/L zeolitized tuff concentration would actually have more cation-exchange sites than the 1 g/L clinoptilolite concentration (Table 7). Consequently, the zeolitized tuff has a somewhat greater fractional uptake of Pb(II) than the clinoptilolite for the solid concentrations that were used.

It appears from the comparisons of the sorption behavior of Pb(II) as a function of adsorbent type that the following conclusions can be made as to the mineral phase or phases responsible for the sorption of Pb(II) on the zeolitized tuff. For example, it can be concluded that the clinoptilolite present in the zeolitized tuff from Rainier Mesa is in fact responsible for most, if not all, of the removal of the Pb(II) cation from solution at the lower background electrolyte concentrations investigated. This conclusion can be reached because the fractional uptake of Pb(II) on both adsorbents is almost quantitatively the same in Figure 47. At the lower background electrolyte concentrations, there would be less competition for the internal cation-exchange sites of either adsorbent. The result would be that the Pb(II) cation would not be forced into binding to either adsorbent in some other manner. Most, if not all, of the cations in solution could be completely removed by cation exchange at this lower background electrolyte concentration. This type of sorption behavior would be indicated by the pH-independent fractional uptake of

Pb(II), which was seen at the two lower background electrolyte concentrations. It must be remembered that the high cation-exchange capacity of the zeolitized tuff is attributed to the presence of the zeolite clinoptilolite. Consequently, the similar quantitative removal of Pb(II) on both adsorbents suggests that the fractional uptake of Pb(II) on the zeolitized tuff is controlled by the clinoptilolite present in the zeolitized tuff.

It is somewhat surprising to note, however, that the fractional uptake of Pb(II) on both adsorbents is so similar for the highest background electrolyte concentration investigated. In those situations in which the Pb(II) cation would be forced into binding on pH-dependent surface sites, the fractional uptake of Pb(II) is likely not controlled by the zeolite mineral phases. As a result, one would expect the fractional uptake of Pb(II) on both adsorbents to be somewhat dissimilar for identical geochemical conditions because the fractional uptake would be likely to be controlled by other constituent minerals present in volcanic tuff. The similarity in the fractional uptakes of Pb(II) on both adsorbents at the highest background electrolyte concentration, however, can most likely be attributed to either surface precipitation of Pb(II), or the similar aluminol site (Al_2O_3) concentrations of both adsorbents. For example, if the surface sites responsible for the fractional uptake of Pb(II) can be attributed to aluminol groups, then the fractional uptake of Pb(II) on both adsorbents would be similar due to the similar Al_2O_3 concentrations of both adsorbents. It cannot be conclusively determined, however, that the clinoptilolite contained within the zeolitized tuff is solely responsible for the Al_2O_3 concentration of the zeolitized tuff. The only conclusion that can be drawn at the highest background electrolyte concentration is that the same sorts of sorption processes are responsible for the uptake of Pb(II) because of the similar qualitative fractional uptake

behavior. It cannot be determined, however, whether the sorption process is precipitation or surface complexation.

Sr(II) Sorption as a Function of Adsorbent Type

The sorption behavior of Sr(II) as a function of the adsorbent type was also investigated. Batch equilibrium sorption experiments were again conducted at solid concentrations of 3.0 g/L zeolitized tuff and 1.0 g/L clinoptilolite. Inspection of Figure 48 reveals the affinity of the Sr(II) cation for both adsorbents. The figure shows the fractional uptake of 1.0×10^{-4} M Sr(II) on both adsorbents at background electrolyte concentrations of 0.01 and 0.1 M NaNO₃. As can be seen from the figure at the 0.1 M NaNO₃ concentration, a 3.0 g/L zeolitized tuff concentration results in the fractional

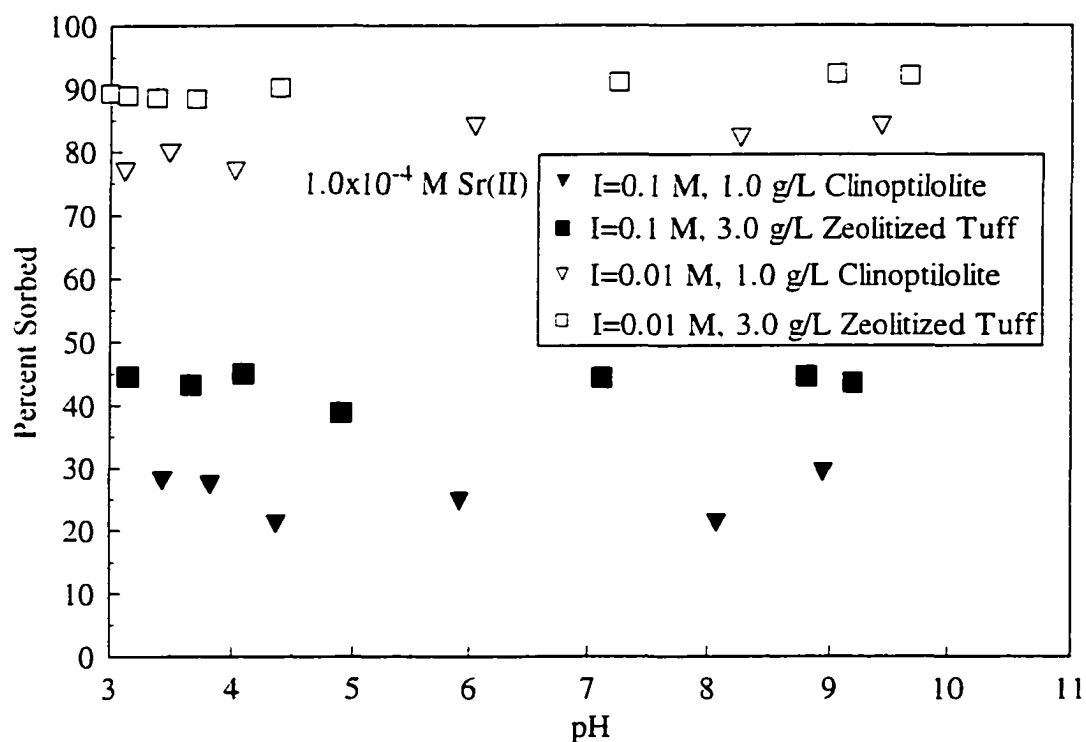


Figure 48. Sorption of 1.0×10^{-4} M Sr(II) in 0.1 and 0.01 M NaNO₃ as a function of adsorbent type.

uptake of approximately 45% of the available Sr(II) in solution. A 1.0 g/L clinoptilolite concentration at the 0.1 M NaNO₃ concentration, however, results in the fractional uptake of approximately 25% of the available Sr(II). It can also be seen that the clinoptilolite adsorbent results in, once again, the least amount of cation sorption. This type of sorption behavior can be seen again in Figure 48 at the lower background electrolyte concentration of 0.01 M NaNO₃. The 3 g/L zeolitized tuff concentration results in the fractional uptake of approximately 90%, and the 1 g/L clinoptilolite concentration results in the fractional uptake of approximately 80-85%. The differences between the two fractional uptakes at this lower background electrolyte concentration are not as pronounced as at the 0.1 M NaNO₃ concentration because the fractional uptakes are approaching 100%, but it can still be seen that the clinoptilolite results in the least amount of fractional uptake.

These comparisons of the sorption behavior of Sr(II) as a function of the adsorbent type were made so that a determination could be made as to the mineral phase or phases responsible for the fractional uptake of Sr(II) on the zeolitized tuff. Overall, the comparisons reveal that the fractional uptake of Sr(II) on the zeolitized tuff is also controlled by the zeolite mineral clinoptilolite contained within the altered vitric tuffs. This can be concluded because the fractional uptake of Sr(II) on both adsorbents is qualitatively the same (Figure 48). In addition, the fractional uptake of Sr(II) on both adsorbents was shown to be controlled by cation-exchange, and the cation-exchange capacity of the zeolitized tuff is due to the presence of the zeolite mineral. The behavior of clinoptilolite resulting in the least fractional uptake can be explained because the adsorbents were normalized with respect to the surface area and not the cation-exchange capacity. Normalization of the surface area of the adsorbents would result in roughly the

same number of available surface sites, but not necessarily internal cation-exchange sites, as explained with the Pb(II) cation. It can be easily postulated, however, that if the adsorbent concentrations were normalized with respect to the cation-exchange capacity and not the surface area, the clinoptilolite would most likely have a greater capacity to bind Sr(II) than the zeolitized tuff because of its larger cation-exchange capacity.

Conclusions

Experiments with the clinoptilolite were performed so that a comparison of the sorption behavior of the cations as a function of adsorbent type could be made. These comparisons revealed that the zeolite mineral clinoptilolite contained within the zeolitized tuff is mainly responsible for the fractional uptake of both cations, at least for the low background electrolyte concentrations. This can be concluded because of the similar qualitative fractional uptakes of both cations. This conclusion suggests that the partitioning parameters calculated describing the affinity of the cations for the zeolitized tuff from Rainier Mesa could be potentially extrapolated to other zeolitized rocks at the NTS. Zeolitized rocks at the NTS cover several thousand square miles, and underlie most of the volcanic formations and alluvial basins in the area. It would be impossible to perform batch equilibrium sorption experiments for all of the different zeolitized rocks. If a good estimation of the percentage of clinoptilolite contained within a particular sample can be made, however, then the partitioning parameters calculated for the zeolitized tuff from Rainier Mesa would be more relevant to the new sample (at least by an order of magnitude), assuming that the sample had a significant percentage of the zeolite mineral clinoptilolite.

CHAPTER 5

SORPTION OF CrO_4^{2-} AND SeO_3^{2-} ON ZEOLITIZED TUFF AND CLINOPTILOLITE: EQUILIBRIUM EXPERIMENTS, SORPTION PARAMETER ESTIMATION, AND SPECIATION

The transport of potentially harmful anions in the subsurface environment can pose a serious health risk to humans. As a result, batch equilibrium sorption experiments with CrO_4^{2-} and SeO_3^{2-} were conducted in order to determine whether these anions would be retarded in the subsurface environment by interactions with the zeolitized tuff or clinoptilolite, which have large cation-exchange capacities. These particular anions were selected for study because of their potentially harmful effects to humans (Chapter 1), and because the CrO_4^{2-} anion can occur in the subsurface environment at the NTS. Specifically, batch equilibrium sorption experiments were conducted with SeO_3^{2-} , which is known to be a strongly binding anion on hydrous oxide surfaces, and CrO_4^{2-} , which is assumed to be a weakly binding anion (Hayes et al., 1988). As stated in Chapter 4, it has been documented by other studies that in natural systems the fractional uptake of cations and anions by oxides and other minerals in the subsurface environment can be pH dependent, and influenced by ionic strength effects depending on the nature of the anion or cation (Hayes and Leckie, 1987; Hayes et. al., 1988). In addition, the total

concentration of the ion of interest and the total solid concentration of the mineral phase in natural aqueous systems determine the ratio of sorbate ions to the total number of sorbent sites, thereby affecting the relative fractional uptake of the ions. Therefore, in order to determine the sorption behavior of CrO_4^{2-} and SeO_3^{2-} , batch equilibrium sorption experiments were conducted using both adsorbents, again, as a function of pH, ionic strength, solid adsorbent concentration, and total anion concentration. It is worth repeating, however, that both adsorbents have large cation-exchange-capacities and not anion-exchange-capacities, therefore, substantially higher solid adsorbent concentrations were required for any meaningful fractional uptake of the anions. Preliminary batch equilibrium sorption experiments revealed that a zeolitized tuff concentration of at least 100 g/L was required to produce any meaningful fractional uptake of CrO_4^{2-} .

This chapter is also divided into three sections. The first section contains the results of the batch equilibrium sorption experiments performed with the zeolitized tuff, the sorption parameter estimations, and the speciation calculations for each anion. The second section of this chapter discusses the experiments performed with the anions of interest and the clinoptilolite, and the final section of the chapter contains a comparison of the sorption behavior of the two anions as a function of adsorbent type .

Sorption of CrO_4^{2-} and SeO_3^{2-} on Zeolitized Tuff

Sorption Behavior of CrO_4^{2-}

The batch equilibrium sorption experiments revealed that, overall, the CrO_4^{2-} anion has little or no affinity for the zeolitized tuff from Rainier Mesa. These findings have significant implications for the transport of CrO_4^{2-} in the subsurface environment at

the NTS, namely that CrO_4^{2-} would not be retarded significantly with respect to groundwater flow due to sorption on zeolitized tuff. The lack of affinity for the zeolitized tuff can be explained because most zeolites, like smectite clays, possess a net negative structural charge resulting from isomorphic substitution of cations in the crystal lattice (Haggerty and Bowman, 1994). It is this isomorphic substitution that imparts such a high cation-exchange capacity to zeolites, but due to the overall negative charge, natural zeolites have little or no affinity for anionic species. The experiments also showed that the fractional uptake of CrO_4^{2-} is a mirror image of the fractional uptake of Pb(II) at a background electrolyte concentration of 1.0 M NaNO_3 . Specifically, experiments showed that the fractional uptake of CrO_4^{2-} is favored at low pH values and decreases with increasing pH. The fractional uptake of CrO_4^{2-} can be thought of as essentially a competition with OH^- anions for sorption sites, so the fractional uptake of CrO_4^{2-} is a mirror image of cation sorption on external pH-dependent surface sites. For example, sorption of anions decreases from 100% at low pH values to essentially zero at high pH values. The sorption of anions, however, is often complicated by a change in speciation of the solute as a function of the pH (Drever, 1997), which is later seen with the CrO_4^{2-} anion and the clinoptilolite adsorbent.

In order to investigate the ionic strength dependence of CrO_4^{2-} , batch equilibrium sorption experiments were performed at background electrolyte concentrations of 0.01, 0.1, and 1.0 M NaNO_3 . Figure 49 shows the fractional uptake of 5.0×10^{-7} M CrO_4^{2-} on 100 g/L zeolitized tuff as a function of ionic strength. From the figure, it can be seen that a decrease in the background electrolyte concentration results in an increase in the fractional uptake of CrO_4^{2-} on the zeolitized tuff. This type of sorption behavior where

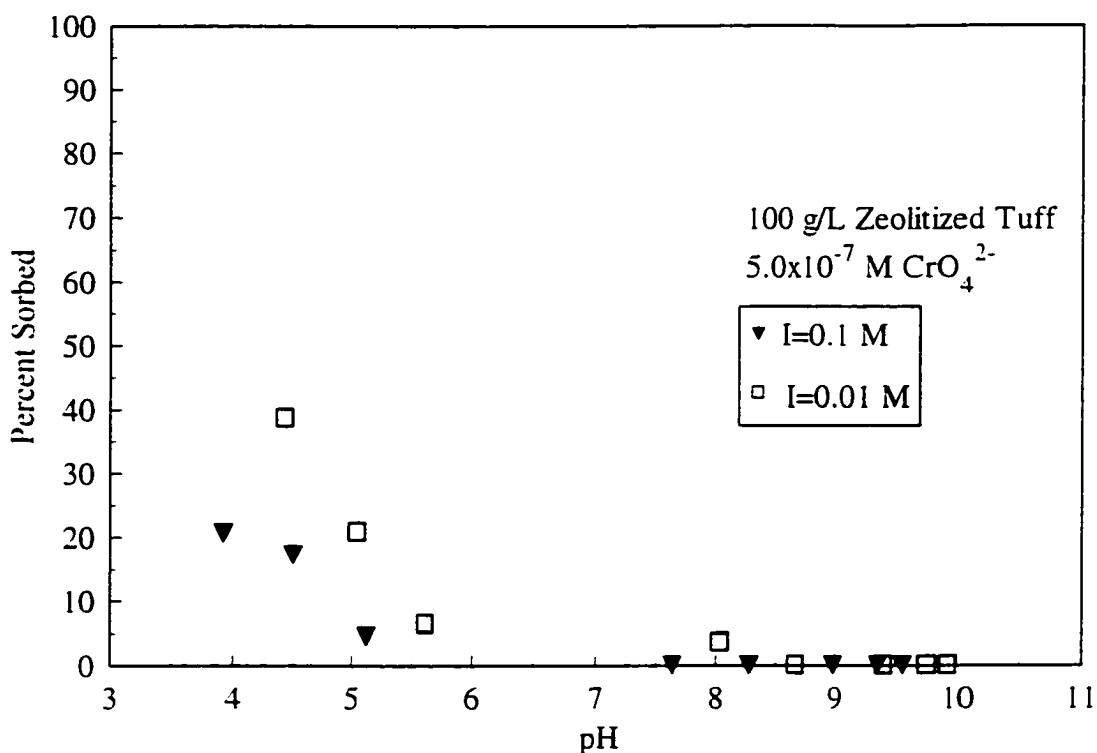


Figure 49. Sorption of 5.0×10^{-7} M CrO_4^{2-} on 100 g/L zeolitized tuff as a function of ionic strength.

the fractional uptake of the anion increases as the background electrolyte concentration decreases is identical to the sorption behavior that was found with cation sorption discussed in Chapter 4. Increases in the fractional uptake of CrO_4^{2-} as the background electrolyte concentration decreases can be attributed to the decreasing amounts of the NO_3^- anions in solution, however, and not because of decreases in the Na^+ cation concentration. Decreasing background electrolyte concentrations decrease the amount of NO_3^- anions in solution, which would compete with CrO_4^{2-} for surface sites. In addition, it can be seen from the figure that the fractional uptake of CrO_4^{2-} is, qualitatively, a mirror image to the fractional uptake of Pb(II) at a background electrolyte concentration of 1.0 M NaNO_3 . For example, it can be seen in the figure that the 0.1 M NaNO_3 background

electrolyte concentration results in the fractional uptake of approximately 20% at a pH of 4 that decreases to approximately 0% at a pH 5.5, whereas the 0.01 M NaNO_3 background electrolyte concentration results in the greatest fraction uptake of approximately 40% at a pH of 4.5 that decreases to approximately 0% at a pH of 5.5. The fractional uptake of Pb(II) , however, increased to 100% as a function of increasing pH. The ionic strength dependence shown in the figure also suggests that the CrO_4^{2-} anion is forming, at best, outer-sphere complexes with pH-dependent surface sites. It must be remembered, however, that macroscopic sorption experiments alone cannot be used to distinguish between inner and outer-sphere complexes.

Batch equilibrium sorption experiments were also performed at a number of solid adsorbent concentrations to illustrate the fractional uptake of CrO_4^{2-} as a function of solid concentration. Not all of the solid adsorbent concentrations investigated, however, resulted in significant fractional uptake of CrO_4^{2-} . For example, a number of experiments were performed at a solid adsorbent concentration of 20 g/L with various anion concentrations and ionic strengths, but none of these experiments produced any meaningful fractional uptake of the CrO_4^{2-} anion. In fact, the zeolitized tuff concentration had to be increased to 100 g/L before any noticeable fractional uptake was obtained. Therefore, one can conclude that as the solid concentration of the zeolitized tuff increases, the fractional uptake of CrO_4^{2-} also increases, as expected.

In order to illustrate the sorption behavior of CrO_4^{2-} as a function of the CrO_4^{2-} concentration, batch equilibrium sorption experiments were performed at CrO_4^{2-} concentrations of 1.0×10^{-5} M, 1.0×10^{-6} , and 5.0×10^{-7} M. Figure 50 illustrates the sorption behavior of CrO_4^{2-} on 100 g/L zeolitized tuff in 1.0 M NaNO_3 as a function of the CrO_4^{2-}

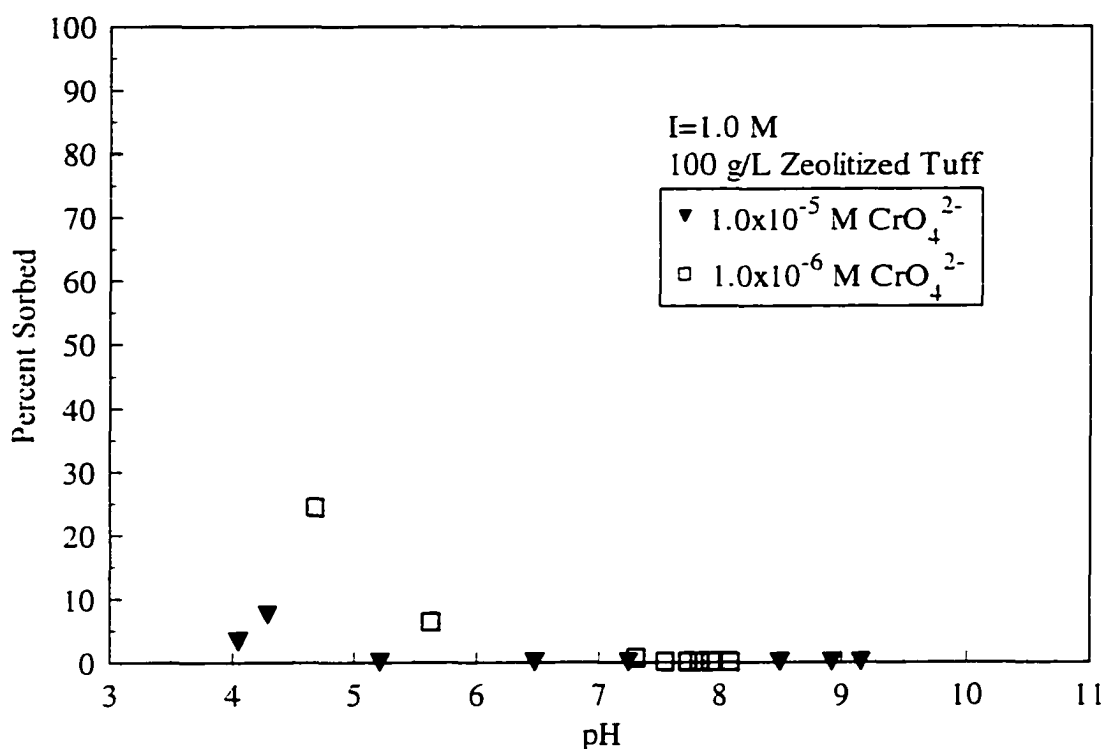


Figure 50. Sorption of CrO_4^{2-} on 100 g/L zeolitized tuff in 1.0 M NaNO_3 as a function of CrO_4^{2-} concentration.

concentration. As one would expect from the experiments with the cations in this study, decreases in the overall CrO_4^{2-} concentration should result in an increase in the fractional uptake of CrO_4^{2-} , and that is exactly what is observed with the CrO_4^{2-} anion. Inspection of the figure shows that the 1.0×10^{-5} M CrO_4^{2-} concentration results in essentially negligible uptake at all pH values, whereas the 1.0×10^{-6} M CrO_4^{2-} concentration results in the fractional uptake of approximately 25% at a pH of 4.5 that decreases to approximately 0% around pH of approximately 6.0. This behavior can be explained, once again, because as the CrO_4^{2-} concentration decreases there are proportionally more binding sites available for the CrO_4^{2-} anions remaining in solution.

CrO₄²⁻ Sorption Parameter Estimation

The fractional uptake data for CrO₄²⁻ were used to derive linear isotherm parameters. It must be remembered, however, that the CrO₄²⁻ anion did not have a significant affinity for the zeolitized tuff from Rainier Mesa. Consequently, the distribution coefficients were calculated from a single equilibrium data point and presented for that particular pH value and ionic strength. The distribution coefficients (K_d) for the sorption of CrO₄²⁻ on the zeolitized tuff at all three ionic strengths are presented in Table 15. No correlation coefficients, r^2 , could be calculated for the sorption of CrO₄²⁻ on the zeolitized tuff because the partitioning coefficients were based on only one equilibrium data point. In addition, no distribution coefficients could be calculated at any pH higher than approximately 7.0 because the fractional uptake of CrO₄²⁻ decreased to 0%.

It can be seen from the data in the table that the distribution coefficients for CrO₄²⁻ at each ionic strength decrease as the pH increases, as expected. This can be explained because the fractional uptake of CrO₄²⁻ on the zeolitized tuff decreased as the pH increased. For example, the distribution coefficients vary from 3.22×10^{-6} to 6.24×10^{-8} m³/g as the pH increases for the 1.0 M NaNO₃ concentration. In addition, it can be seen in the table that the distribution coefficients for approximately the same pH increase as the ionic strength decreases, which is also expected. For example, the 1.0 M NaNO₃ concentration has a distribution coefficient of 6.69×10^{-7} m³/g at a pH of 5.64, but the 0.01 M NaNO₃ concentration has a distribution coefficient of 6.83×10^{-7} m³/g at a pH 5.62. In addition, the 0.1 M NaNO₃ concentration has a distribution coefficient of 4.7×10^{-7} m³/g at a pH of 5.12, but the 0.01 M NaNO₃ concentration has a distribution coefficient of

Table 15. Distribution coefficients (K_d) for CrO_4^{2-} in 1.0, 0.1, and 0.01 M NaNO_3 for different pH values.

Ionic Strength (M)	pH	K_d (m^3/g)
1.0	4.68	3.22×10^{-6}
1.0	5.64	6.69×10^{-7}
1.0	7.33	6.24×10^{-8}
0.1	3.93	2.60×10^{-6}
0.1	4.50	2.08×10^{-6}
0.1	5.12	4.70×10^{-7}
0.01	4.43	6.30×10^{-6}
0.01	5.05	2.62×10^{-6}
0.01	5.62	6.83×10^{-7}

$2.6 \times 10^{-6} \text{ m}^3/\text{g}$ at a pH of approximately 5.1. This type of behavior is also expected because the ionic strength dependence experiments showed that the fractional uptake of CrO_4^{2-} increased for decreasing ionic strengths.

Chemical Speciation Modeling of CrO_4^{2-}

The theoretical speciation of CrO_4^{2-} in the groundwater from water well U-20, and in the batch equilibrium reactors was also investigated in an attempt to gain additional understanding of the possible sorption processes that might be occurring. For example, it might be possible, thermodynamically at least, to determine whether precipitation or surface complexation would be more likely at a particular pH value. The geochemical modeling program Mineql⁺ was used to investigate the speciation of CrO_4^{2-} in both the

groundwater composition from water well U-20 at the NTS, and in a solution composition made to be representative of the conditions found in the batch equilibrium reactors. In addition, the speciation modeling for CrO_4^{2-} was done in such a way as to exclude CO_2 (g) from the calculations, which effectively removes the possibility of equilibration of CrO_4^{2-} with the atmosphere. The theoretical chemical speciation of CrO_4^{2-} in both solution compositions was investigated at the lowest and highest anion concentrations used for the batch equilibrium sorption experiments, and for all three different background electrolyte concentrations. It must be remembered, however, that Mineql⁺ calculations cannot account for changes in the activity coefficient at high background electrolyte concentrations. Therefore, only modeling results for the lowest background electrolyte concentration in the batch equilibrium reactors will be shown, which is relatively close to the actual ionic strength of the groundwater from water well U-20 at the NTS.

The theoretical speciation of 1.0×10^{-4} M CrO_4^{2-} in the groundwater composition from the NTS was the first scenario investigated. Inspection of Figure 51 reveals that HCrO_4^- and CrO_4^{2-} would be the predominant Cr(VI) aqueous species for these particular groundwater conditions. It can be seen from the figure that at pH values less than 6.4 HCrO_4^- would be the predominate aqueous species, while the predominate aqueous species would become CrO_4^{2-} at all pH values above 6.4. The figure also shows that there would be two other aqueous CrO_4^{2-} species present in the groundwater at the NTS. These other two aqueous species, however, are at least two orders of magnitude lower in concentration than the predominate aqueous species, and they do not really contribute much to the total CrO_4^{2-} concentration. Inspection of the figure also reveals that

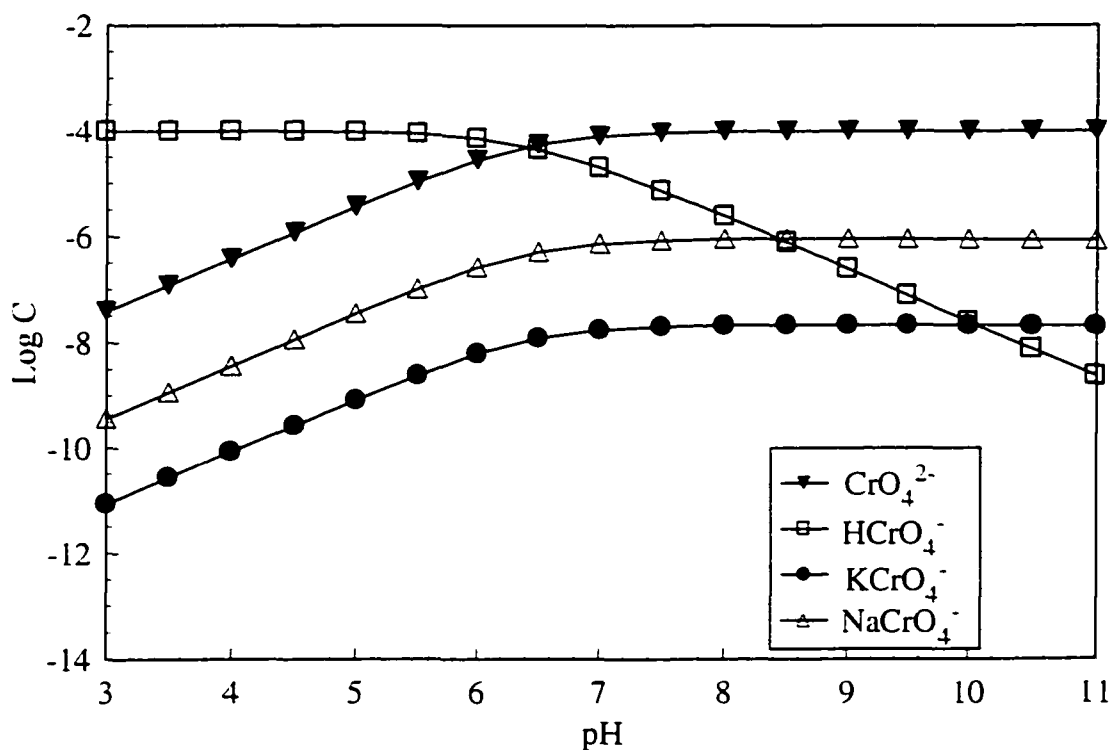


Figure 51. Speciation modeling of 1.0×10^{-4} M CrO_4^{2-} in groundwater from well U-20 at the NTS.

thermodynamically, at least, no precipitates of CrO_4^{2-} would be likely to form in the groundwater at the NTS using the composition of the groundwater from water well U-20.

The theoretical chemical speciation of CrO_4^{2-} in the groundwater at the NTS was also investigated at the lowest anion concentration used during the batch equilibrium sorption experiments. The distribution of CrO_4^{2-} species, however, at this 5.0×10^{-7} M concentration is identical to the results obtained with the 1.0×10^{-4} M CrO_4^{2-} concentration and, therefore, the corresponding diagram is not shown.

The speciation of CrO_4^{2-} in the batch equilibrium sorption reactors was investigated at CrO_4^{2-} concentrations of 1.0×10^{-4} M and 5.0×10^{-7} M. In addition, modeling was also performed at all three background electrolyte concentrations, but

speciation results will only be presented for the lowest background electrolyte concentration for the reasons stated earlier. Overall, the modeling indicated that the distribution of CrO_4^{2-} species in the batch equilibrium sorption reactors is independent of anion concentration. Therefore, only one figure will be shown illustrating the speciation of CrO_4^{2-} in the batch equilibrium reactors. If one will recall, the batch equilibrium experiments were performed with water that had a resistivity of at least $18.1 \text{ M}\Omega\text{-cm}$. This resistivity indicates that the water was essentially pure. Therefore, the CrO_4^{2-} speciation modeling did not include other ions except for the background electrolyte. Figure 52 illustrates the theoretical speciation of $1.0 \times 10^{-4} \text{ M}$ CrO_4^{2-} in the batch equilibrium reactors with a background electrolyte concentration of 0.01 M NaNO_3 .

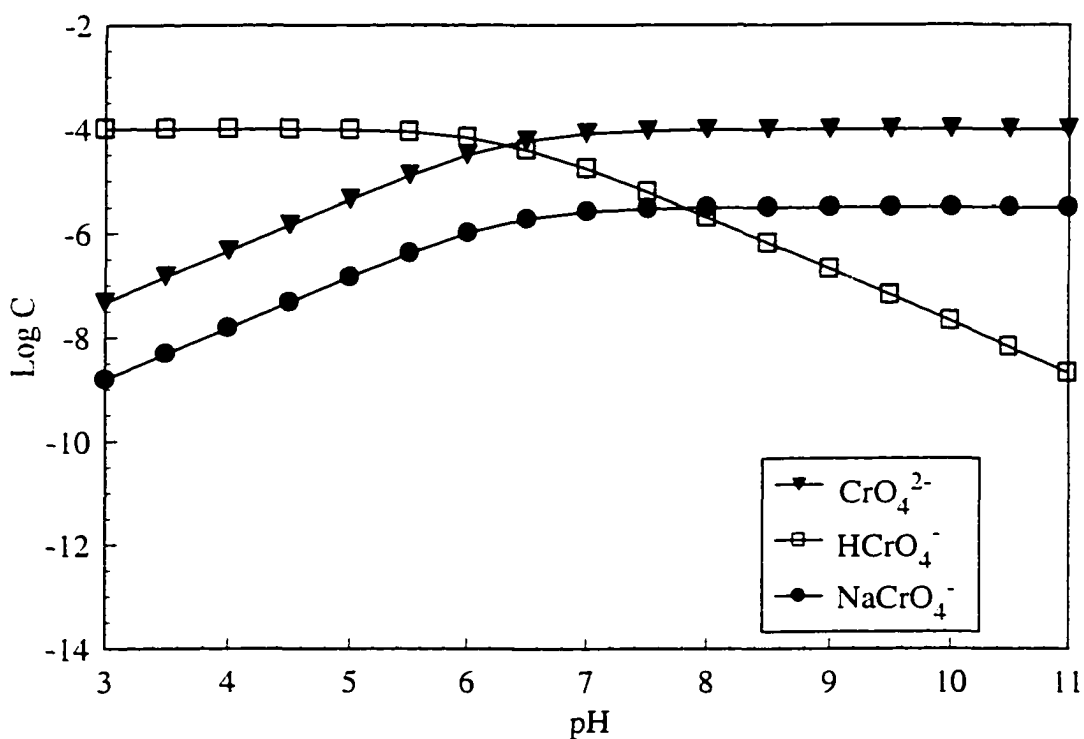


Figure 52. Speciation modeling of $1.0 \times 10^{-4} \text{ M}$ CrO_4^{2-} in 0.01 M NaNO_3 closed to the atmosphere.

From the figure, it can be clearly seen that HCrO_4^- and CrO_4^{2-} are again the predominate aqueous species for this particular set of geochemical conditions. The figure shows, like the modeling conducted with the groundwater composition from the NTS, that HCrO_4^- is the predominate aqueous species at pH values less than 6.4. It also shows that the CrO_4^{2-} anion becomes the predominate aqueous species as the pH exceeds 6.4. In addition, it can also be seen from the figure that there are no precipitates of CrO_4^{2-} in the batch equilibrium sorption reactors either. It should be noted that the speciation of 1.0×10^{-4} M CrO_4^{2-} in the batch equilibrium reactors is almost identical to the speciation that was observed using the groundwater composition from the NTS. Both groundwater compositions resulted in HCrO_4^- and CrO_4^{2-} being the predominate aqueous species for certain pH ranges, and both groundwater compositions showed that precipitates of CrO_4^{2-} are not likely to form at any of the anion concentrations that were investigated for this research.

In conclusion, the speciation of CrO_4^{2-} in the groundwater from the NTS and in the batch equilibrium reactors was investigated at numerous geochemical conditions. Overall, the speciation modeling showed that, thermodynamically at least, no precipitates of CrO_4^{2-} are likely to form in either groundwater composition. The speciation modeling showed that only two aqueous species would be responsible for the entire total concentration of CrO_4^{2-} in both groundwater compositions. This information coupled with the knowledge that the CrO_4^{2-} anion has little affinity for the zeolitized tuff has significant implications for the fate and transport of CrO_4^{2-} in the groundwater at the NTS. For instance, the CrO_4^{2-} anion would be extremely mobile in the subsurface environment at the NTS. For example, any CrO_4^{2-} contamination in the groundwater

would most likely flow downgradient at the same rate as the groundwater.

Sorption Behavior of SeO_3^{2-}

Batch equilibrium sorption experiments were performed as a function of the geochemical parameters of interest including pH, ionic strength, total adsorbent concentration, and total anion concentration in order to investigate the sorption behavior of SeO_3^{2-} on the zeolitized tuff. These experiments were performed so that a comparison between the apparently weakly binding anion CrO_4^{2-} , and the strongly binding anion SeO_3^{2-} could be made. Overall, the experiments indicate that the fractional uptake of SeO_3^{2-} is qualitatively similar to the fractional uptake of CrO_4^{2-} . For example, the fractional uptake of SeO_3^{2-} is greatest at low pH values and decreases as the pH increases. This fractional uptake behavior is consistent with the fractional uptake behavior of CrO_4^{2-} on the zeolitized tuff, and other studies of anion sorption by hydrous oxide surfaces. The fractional uptake of SeO_3^{2-} can be thought of as a competition between the SeO_3^{2-} anion and the OH^- anion for any available surface sites. At low pH values, the fractional uptake of SeO_3^{2-} is greatest because there are few OH^- anions present, but as the pH increases the fractional uptake of SeO_3^{2-} decreases because of the increased amounts of OH^- anions.

Batch equilibrium sorption experiments were performed at background electrolyte concentrations of 0.01, 0.1, and 1.0 NaNO_3 in order to illustrate the sorption behavior of SeO_3^{2-} as a function of ionic strength. Figure 53 illustrates the fractional uptake of 1.0×10^{-5} M SeO_3^{2-} on 100 g/L zeolitized tuff as a function of ionic strength. The figure shows that there is no change in the fractional uptake of SeO_3^{2-} as a function of ionic strength. It can be seen from the figure that each of the ionic strengths investigated result in roughly the same 40% fractional uptake of SeO_3^{2-} at a pH of 3.5 that decreases to a

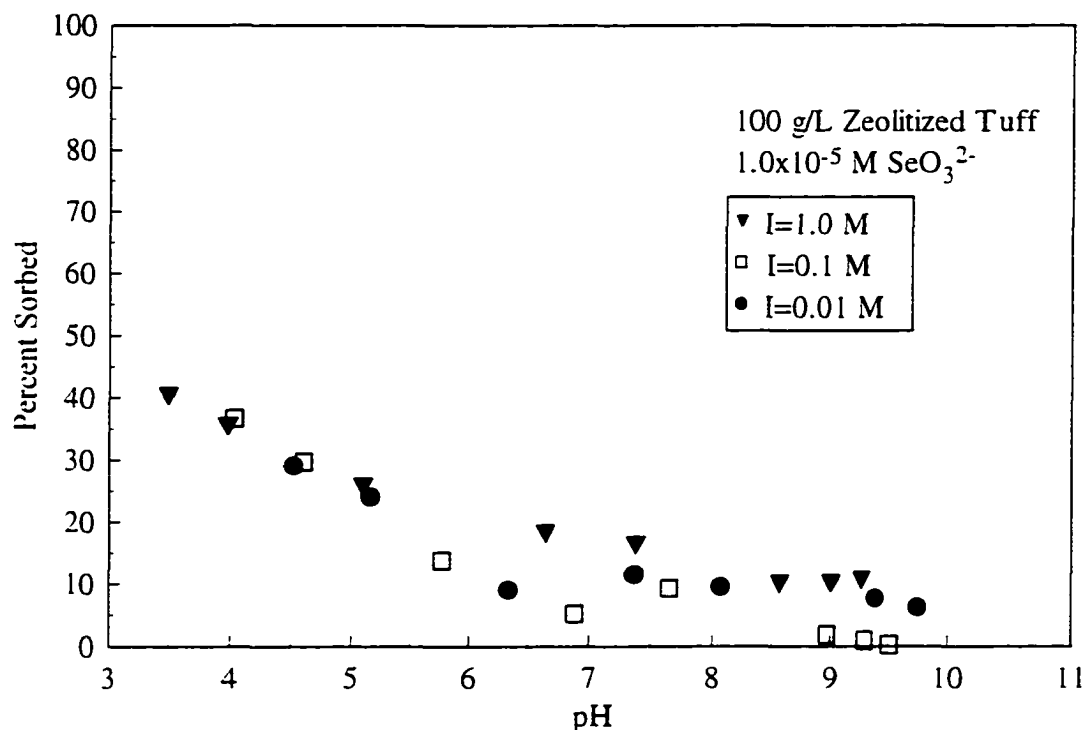


Figure 53. Sorption of 1.0×10^{-5} M SeO_3^{2-} on 100 g/L zeolitized tuff as a function of ionic strength.

fractional uptake of approximately 10% at pH values around 7-10. This ionic strength independence is indicative of strong binding and consistent with SeO_3^{2-} forming inner-sphere coordination complexes with amphoteric surface sites. These type of bonds are little affected by the presence of the background electrolyte because the two different anions would be binding to the available surface sites in two totally different ways. For example, the NO_3^- anion would be most likely forming ion-pairs with oppositely charged surface sites because it is the conjugate base of a strong acid, and as a result it has little tendency to chemically react with anything. The SeO_3^{2-} anion would be likely forming chemical bonds with pH-dependent surface hydroxyl sites because it is the conjugate base of a weak acid, and as a result it is more likely to form chemical bonds with pH-

dependent surface sites. It must be remembered, however, that ionic strength independence is not a direct confirmation for the formation of inner-sphere coordination complexes. The formation of inner-sphere coordination complexes can only be verified by spectroscopic techniques. The formation of SeO_3^{2-} inner-sphere complexes on transition aluminas and on goethite, however, has been documented by spectroscopic techniques (Papelis et al. 1995a; Hayes et al., 1987). The ionic strength independence of SeO_3^{2-} can be again seen in Figure 54, showing the fractional uptake of 1.0×10^{-6} M SeO_3^{2-} on 100 g/L zeolitized tuff. The fractional uptake of SeO_3^{2-} in this figure varies from approximately 70% at a pH of 4 to approximately 20% at a pH from 7.5 to 10. Additionally, it can be seen from the figure that all three ionic strengths (1.0, 0.1, and

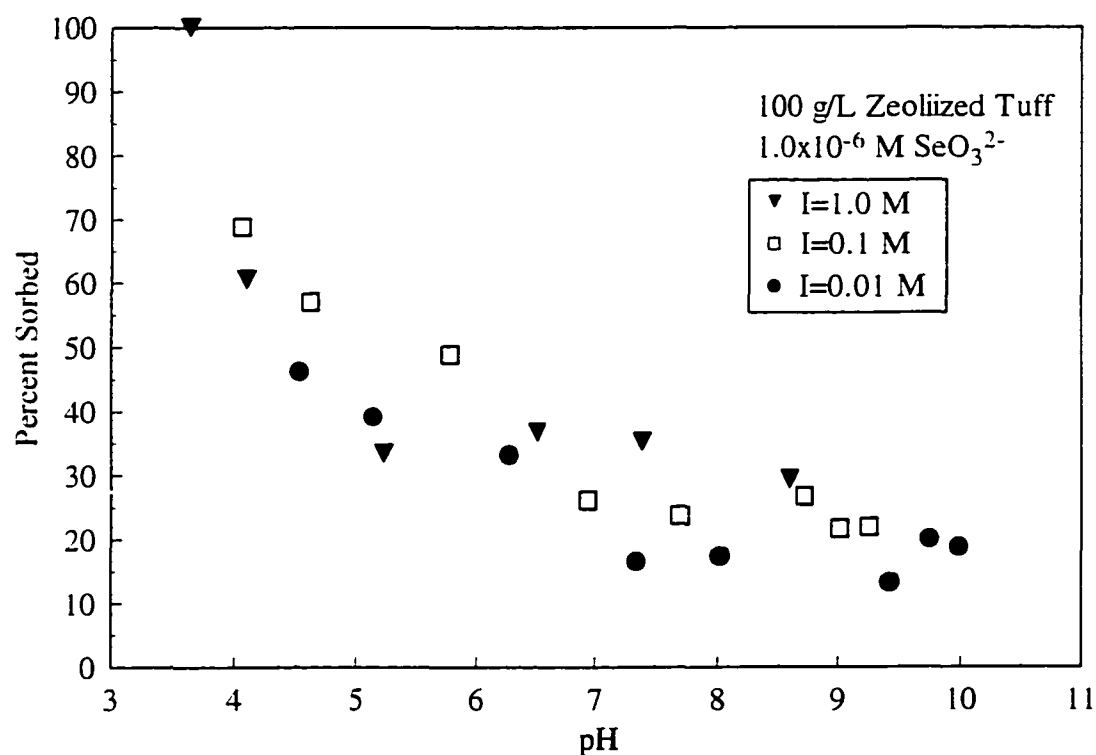


Figure 54. Sorption of 1.0×10^{-6} M SeO_3^{2-} on 100 g/L zeolitized tuff as a function of ionic strength.

0.01 M NaNO₃) result in essentially the same fractional uptake of SeO₃²⁻ even though there is scatter associated with the fractional uptake curves.

Batch equilibrium sorption experiments using SeO₃²⁻ anions and the zeolitized tuff adsorbent were only performed at one solid adsorbent concentration. Therefore, no data are available to provide direct confirmation that increasing zeolitized tuff concentrations result in an increase in the fractional uptake of SeO₃²⁻.

The last geochemical parameter investigated attempted to determine the sorption behavior of SeO₃²⁻ on the zeolitized tuff as a function of the SeO₃²⁻ concentration. Therefore, batch equilibrium sorption experiments were performed at SeO₃²⁻ concentrations of 1.0x10⁻⁴, 1.0x10⁻⁵, and 1.0x10⁻⁶ M. Overall, the results show that the fractional uptake of SeO₃²⁻ increases as the SeO₃²⁻ concentration decreases, as expected. For example, Figure 55 shows the sorption behavior of SeO₃²⁻ on 100 g/L in 1.0 M NaNO₃ as a function of the SeO₃²⁻ concentration. It can be seen in the figure that a 1.0x10⁻⁴ M SeO₃²⁻ concentration results in a fractional uptake of approximately 20% at a pH of 4 that decreases to approximately 0% at a pH of 6.5. As the anion concentration decreases to 1.0x10⁻⁵ M SeO₃²⁻, it can be seen that the fractional uptake increases. For example, the 1.0x10⁻⁵ M SeO₃²⁻ concentration results in a fractional uptake of approximately 35% at a pH of 4 that decreases to a fractional uptake of approximately 0% at a pH of 9. The lowest anion concentration of 1.0x10⁻⁶ M, as one would expect, results in the highest fractional uptake because, once again as the anion concentration decreases there are proportionally more binding sites available for the remaining anions in solution.

In conclusion, several geochemical parameters were investigated in order to achieve a better understanding of the sorption behavior of SeO₃²⁻ on the zeolitized tuff.

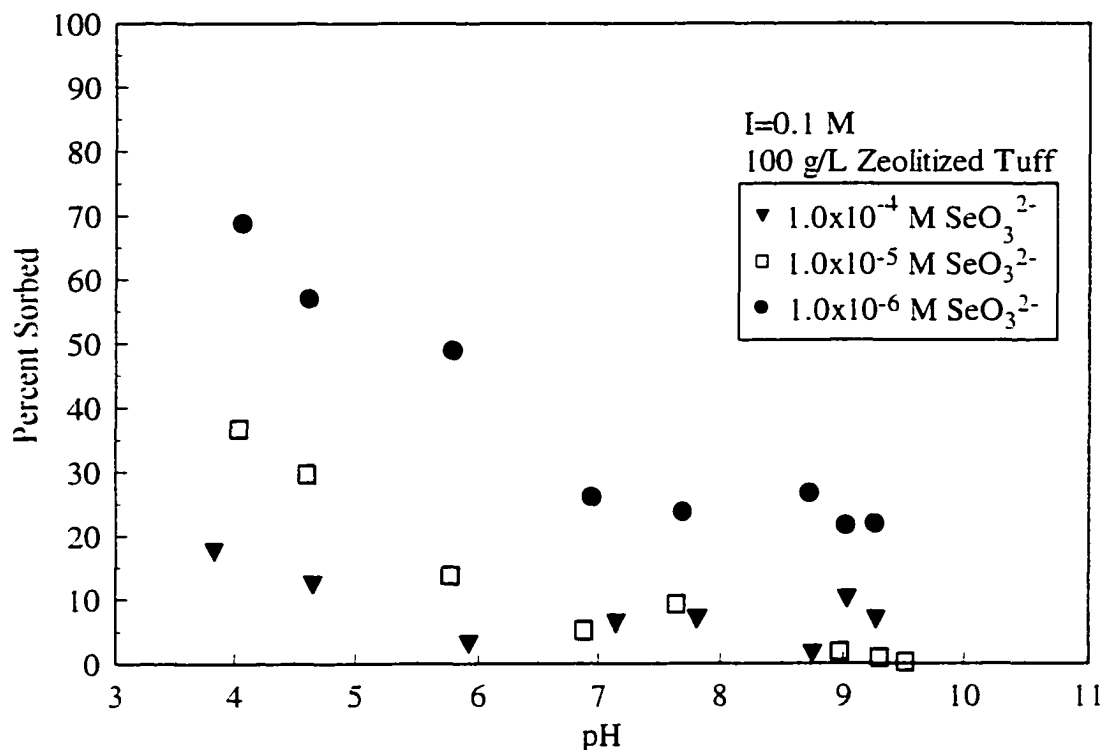


Figure 55. Sorption of SeO_3^{2-} on 100 g/L zeolitized tuff in 0.1 M NaNO_3 as a function of SeO_3^{2-} concentration.

Batch equilibrium sorption experiments were performed as a function of pH, ionic strength, total adsorbent concentration, and total anion concentration. The results from the experiments indicated that the fractional uptake of SeO_3^{2-} is not affected by any variations in the ionic strength. This suggests that SeO_3^{2-} is forming inner-sphere coordination complexes on amphoteric surface sites. Consequently, the fractional uptake of SeO_3^{2-} decreased as a function of pH from a maximum at low pH values. In addition, the experiments also indicated that the fractional uptake of SeO_3^{2-} on the zeolitized tuff increased as the overall SeO_3^{2-} concentration decreased.

SeO_3^{2-} Sorption Parameter Estimation

The fractional uptake data for SeO_3^{2-} were used to derive Freundlich and linear isotherms. The batch equilibrium sorption experiments conducted with SeO_3^{2-} were only

performed at one solid adsorbent concentration, therefore, only three different equilibrium concentrations as a function of ionic strength and pH were available for the construction of the sorption isotherms. Sorption isotherms were constructed at pH values of 4, 5, 6, and 7 for the 1.0 M NaNO₃ concentration, and at pH values of 4, 5, and 6 for the 0.1 M NaNO₃ concentration. Isotherms were not constructed at higher pH values because the fractional uptake of SeO₃²⁻ on the zeolitized tuff was approaching 0%.

The fractional uptake data were first used to derive Freundlich isotherms, in order to determine whether true distribution coefficients can be calculated for SeO₃²⁻. The Freundlich isotherm parameters, K_f and $1/n$, for both background electrolyte concentrations are shown in Table 16. The data in the table reveal that the $1/n$ exponents for both isotherms are strongly nonlinear. Therefore, mathematically valid distribution coefficients for SeO₃²⁻ cannot be calculated at either ionic strength. These two parameters, K_f and $1/n$, can be used as indicators of the sorption capacity of the adsorbent for the specific geochemical conditions at which the equilibrium data points were calculated. The Freundlich sorption isotherms for pH values of 4, 5, and 6 for both the 1.0 M and 0.1 M NaNO₃ background electrolyte concentrations can be seen in Figure 56 and Figure 57, respectively. Inspection of the data in the table also reveals that the K_f parameters decrease as the pH increases, which is consistent with the experimental observations. Inspection of data, however, reveals that the calculated Freundlich parameters for the two different background electrolyte concentrations are somewhat dissimilar for corresponding pH values. This is somewhat counterintuitive since the fractional uptake curves for SeO₃²⁻ showed no variation as a function of the ionic strength. This variability in the calculated Freundlich parameters as a function of ionic

Table 16. Freundlich isotherm parameters for SeO_3^{2-} in 1.0 and 0.1 M NaNO_3 for different pH values.

Ionic Strength (M)	pH	K_f $(\text{g/g})/(\text{g/m}^3)^{1/n}$	$1/n$ (-)	r^2
1.0	4	4.62×10^{-6}	0.642	0.998
1.0	5	3.51×10^{-6}	0.726	0.991
1.0	6	2.72×10^{-6}	0.730	0.995
1.0	7	1.93×10^{-6}	0.722	0.999
0.1	4	4.55×10^{-6}	0.589	0.999
0.1	5	2.94×10^{-6}	0.630	0.999
0.1	6	1.35×10^{-6}	0.511	0.997

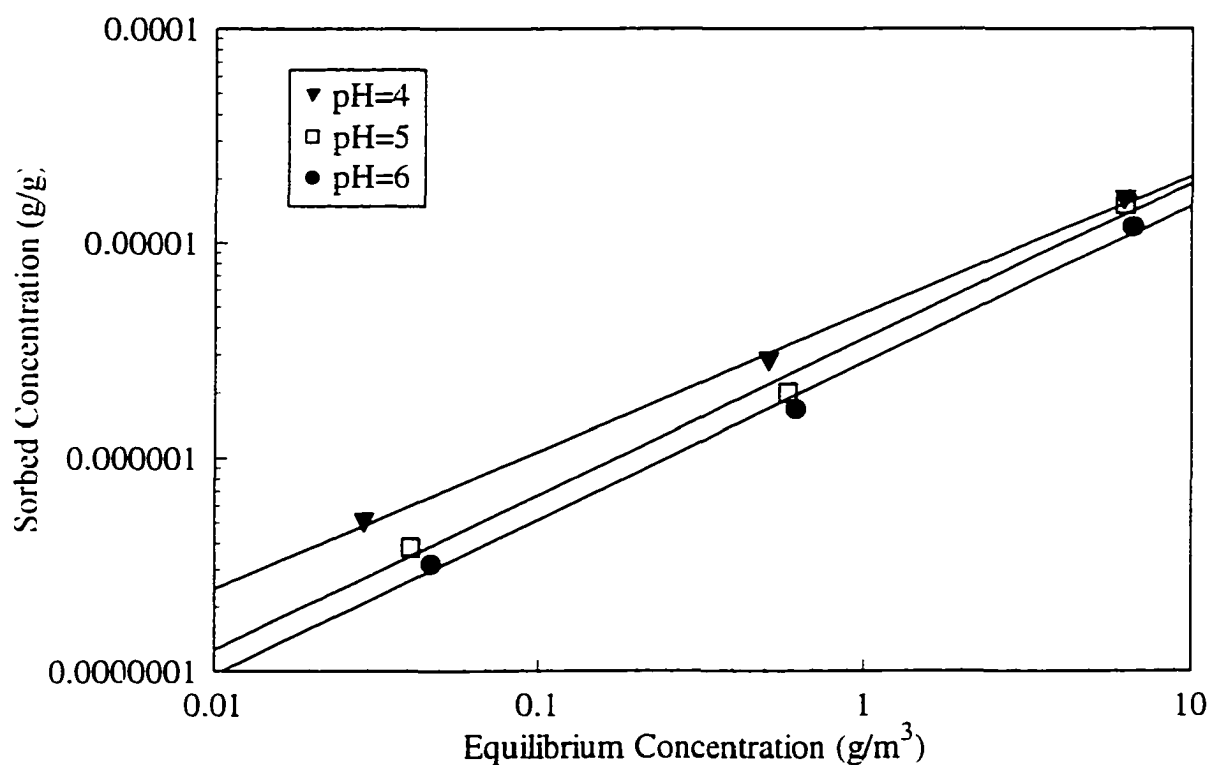


Figure 56. Freundlich isotherms of SeO_3^{2-} sorption on zeolitized tuff in 1.0 M NaNO_3 at pH values of 4, 5, and 6.

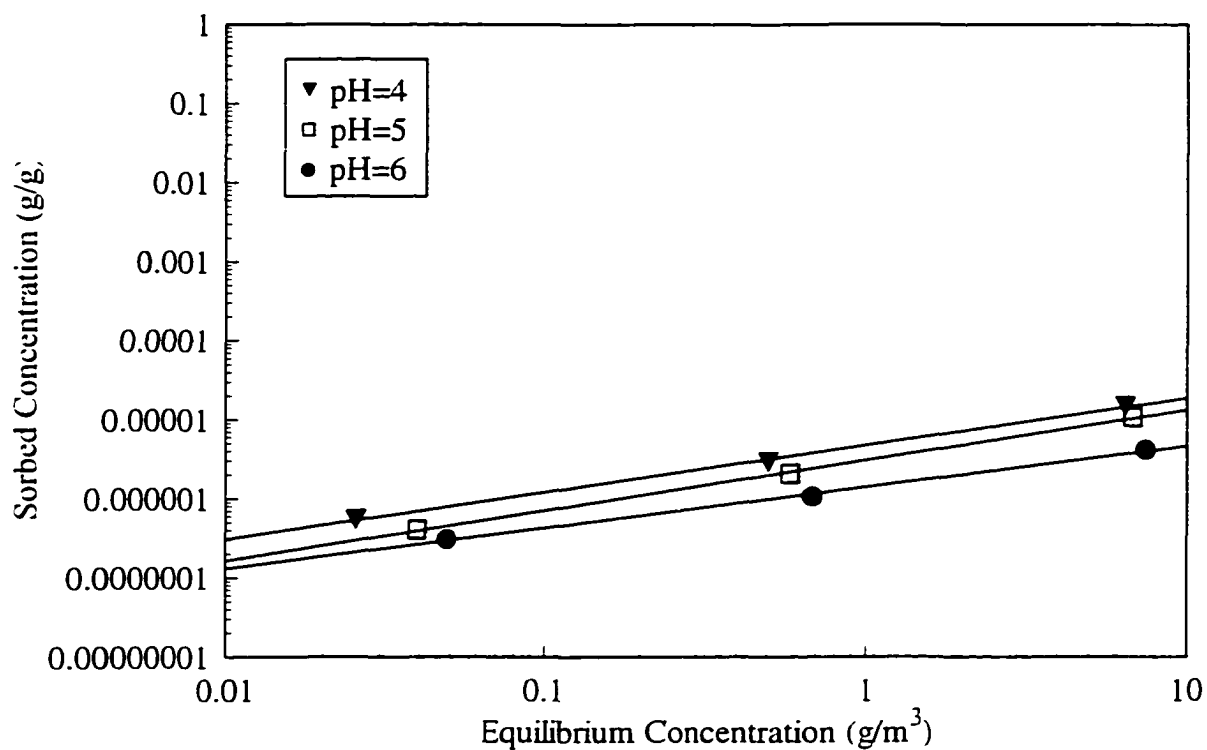


Figure 57. Freundlich isotherms of SeO_3^{2-} sorption on zeolitized tuff in 0.1 M NaNO_3 at pH values of 4, 5, and 6.

strength can be explained because the fractional uptake curves did have some scatter associated with them. If one will recall, the equilibrium data points used to construct the isotherms were obtained by hand-fitting a best-fit curve to the fractional uptake data, and evaluating the fractional uptake of SeO_3^{2-} based on this curve. Because of the best-fit selection, variability in the fractional uptake of SeO_3^{2-} is introduced into the partitioning coefficient calculations as a function of ionic strength. The K_f parameters for the two different background electrolyte concentrations, however, do not differ by more than a factor of 2, in the worst case, a reasonably good agreement. In addition, it can be seen from the table that the K_f parameters deviate more from each other at the high pH values

where the fractional uptake curves begin to approach 0%. The low uptake can introduce additional variability into the sorption parameter calculations.

Although the Freundlich isotherms were highly nonlinear, distribution coefficients for SeO_3^{2-} were calculated for comparative purposes. It must be remembered that such distribution coefficients are not strictly valid for transport codes because the sorption isotherms are not truly linear. The K_d values, and the correlation coefficients, r^2 , obtained from SeO_3^{2-} sorption isotherms at background electrolyte concentrations of 1.0 and 0.1 M NaNO_3 are shown in Table 17. The calculated distribution coefficients (K_d) were obtained from a least squares fit. In addition, the K_d values were obtained by forcing the linear isotherm through zero because that is one of the assumptions of the linear isotherm. Linear isotherms for pH values of 4, 5, and 6 for both the 1.0 and the 0.1 M NaNO_3 background electrolyte concentrations can be seen in Figure 58 and Figure 59, respectively. It can be seen from the data in the table that the distribution coefficients also decrease as the pH of the solution increases. For example, the distribution coefficients for the 1.0 M NaNO_3 concentration vary from a maximum value of $2.52 \times 10^{-6} \text{ m}^3/\text{g}$ at a pH of 4 to a minimum value of $1.12 \times 10^{-6} \text{ m}^3/\text{g}$ at a pH of 7. The distribution coefficients for the 0.1 M NaNO_3 concentration vary from a maximum value of $2.22 \times 10^{-6} \text{ m}^3/\text{g}$ at a pH of 4 to minimum value of $5.36 \times 10^{-7} \text{ m}^3/\text{g}$ at a pH of 6. This behavior is also expected because the affinity of the SeO_3^{2-} anion for the zeolitized tuff decreases as the pH of the solution increases. The table also shows that the distribution coefficients at similar pH values but different background electrolyte concentrations differ by up to approximately a factor of 2. The variability seen in the distribution coefficients can be explained because of the scatter of the data points in the fractional uptake curves, and

Table 17. Distribution coefficients (K_d) for SeO_3^{2-} in 1.0 and 0.1 M NaNO_3 for different pH values.

Ionic Strength (M)	pH	K_d (m^3/g)	r^2
1.0	4	2.52×10^{-6}	0.995
1.0	5	2.35×10^{-6}	0.999
1.0	6	1.77×10^{-6}	0.999
1.0	7	1.12×10^{-6}	0.995
0.1	4	2.22×10^{-6}	0.992
0.1	5	1.51×10^{-6}	0.994
0.1	6	5.35×10^{-7}	0.988

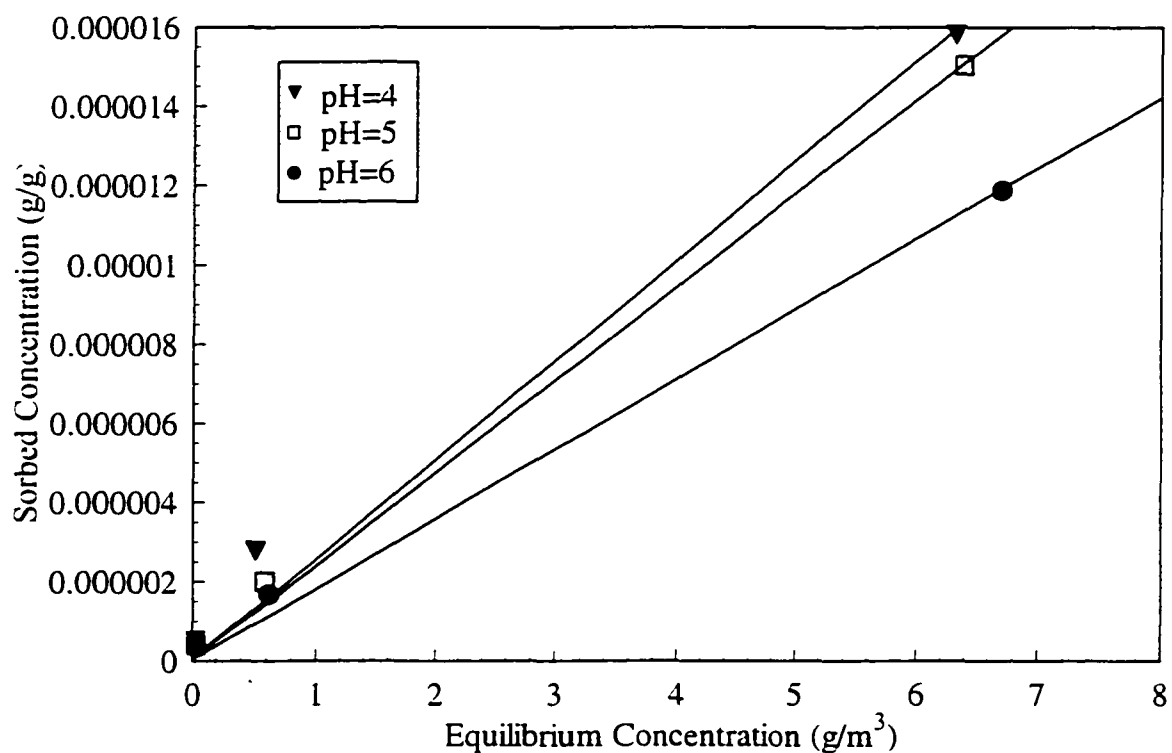


Figure 58. Linear isotherms of SeO_3^{2-} sorption on zeolitized tuff in 1.0 M NaNO_3 at pH values of 4, 5, and 6.

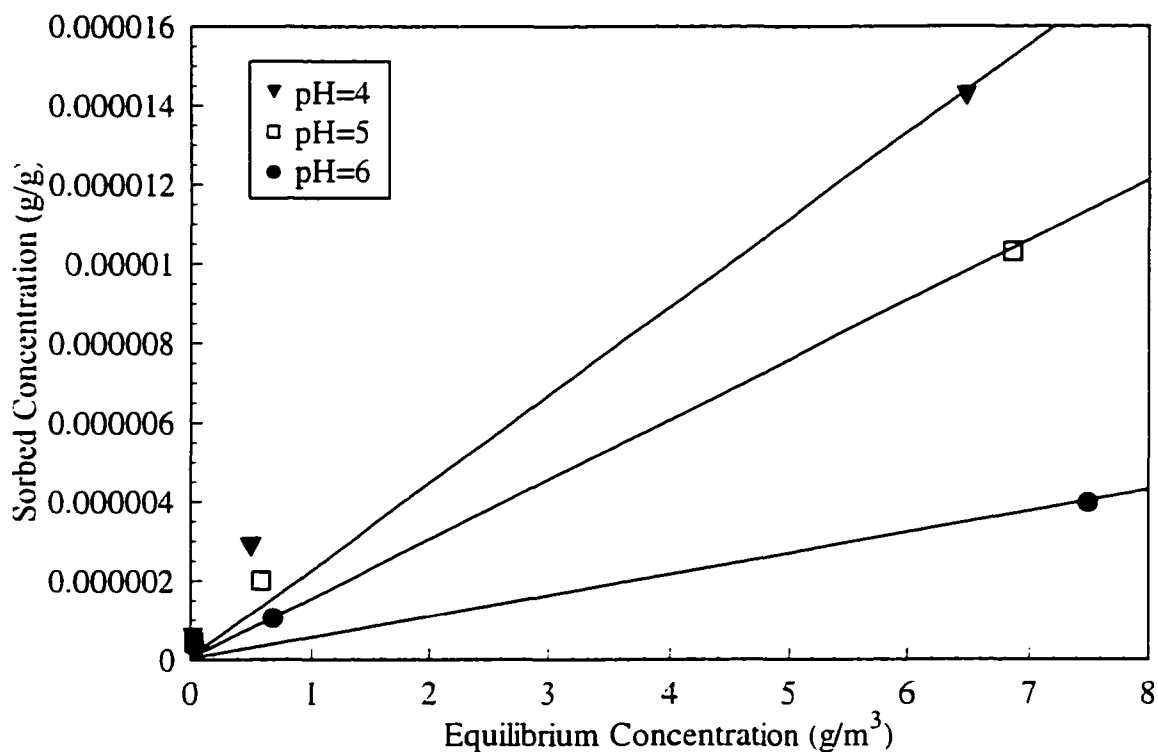


Figure 59. Linear isotherms of SeO_3^{2-} sorption on zeolitized tuff in 0.1 M NaNO_3 at pH values of 4, 5, and 6.

because of the method used to derive the isotherms. It can be seen from the data, however, that the incorporation of sorption parameters for SeO_3^{2-} into transport codes would be definitely dependent on the pH of the solution, and well as slightly affected by the background electrolyte concentration.

Chemical Speciation Modeling of SeO_3^{2-}

The theoretical speciation of SeO_3^{2-} in the groundwater from well U-20 at the NTS, and in the batch equilibrium sorption reactors was also investigated. The modeling assumed a system closed to the atmosphere. Speciation calculations for SeO_3^{2-} were performed at both the highest and lowest anion concentrations used for the batch equilibrium sorption experiments, and at all three background electrolyte concentrations.

The objective of the modeling was to gain additional understanding of possible processes that might occur in the groundwater at the NTS, and in the batch equilibrium sorption reactors. These investigations into the speciation of SeO_3^{2-} might provide clues as to the mechanism of sorption at particular pH values. For example, it might be possible, thermodynamically at least, to determine whether precipitation or surface complexation would be more likely at specific pH values.

The speciation modeling revealed, however, that the speciation of SeO_3^{2-} is the same using either groundwater composition, therefore, only one figure will be presented to illustrate the theoretical speciation of SeO_3^{2-} . Inspection of Figure 60 reveals that there are three predominate aqueous SeO_3^{2-} species. The figure shows that the aqueous species

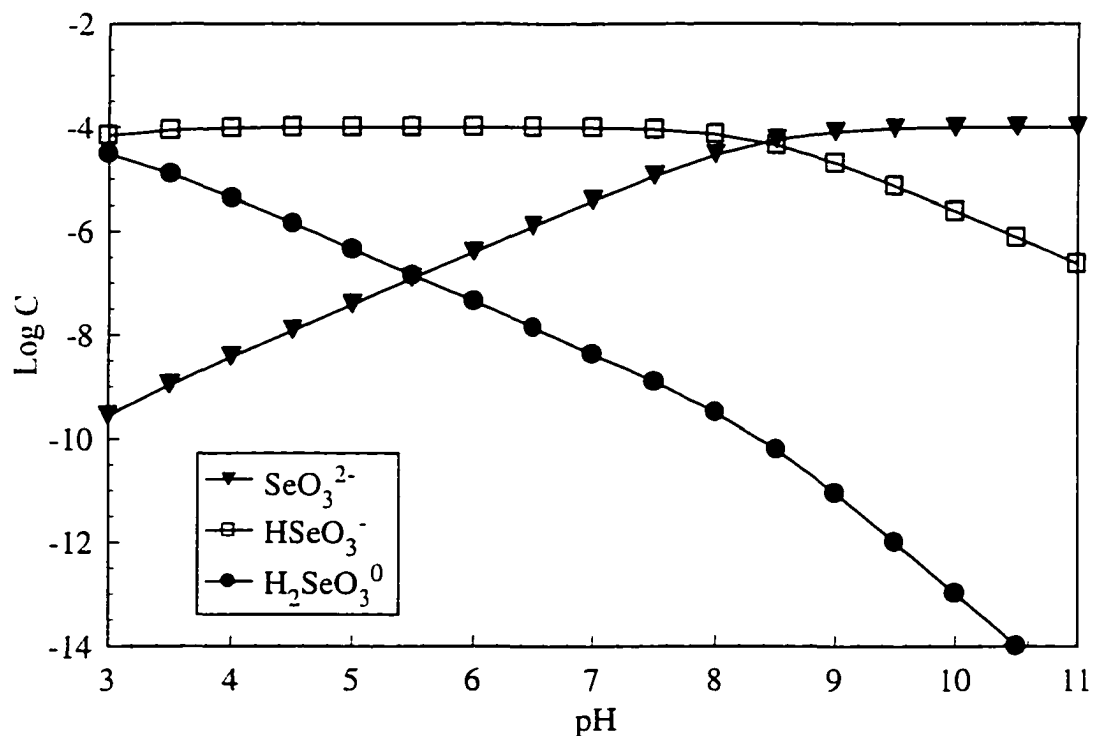


Figure 60. Speciation modeling of 1.0×10^{-4} M SeO_3^{2-} in the groundwater from well U-20 at the NTS and in the batch equilibrium reactors.

SeO_3^{2-} , HSeO_3^- , and H_2SeO_3^0 would be present regardless of the concentration of additional species present in the solution. Inspection of the figure also reveals that the predominate aqueous species is HSeO_3^- at all pH values less than 8.2. As the pH exceeds 8.2, the predominate aqueous species becomes SeO_3^{2-} . No precipitates of SeO_3^{2-} would form in the groundwater at the NTS or in the batch equilibrium reactors under any conditions. Consequently, the fractional uptake of SeO_3^{2-} has to be attributed to either adsorption or absorption. The speciation modeling was also conducted at numerous anion concentrations, however, the results were identical to the results at the 1.0×10^{-4} M SeO_3^{2-} concentration.

This speciation modeling has significant implications for the transport of SeO_3^{2-} in the subsurface environment at the NTS. For example, the SeO_3^{2-} anion, while it has a greater affinity for the zeolitized tuff than the CrO_4^{2-} anion, is still extremely mobile in this geochemical environment especially at pH values that are likely to be encountered at the NTS. Therefore, SeO_3^{2-} contamination in the groundwater would not be retarded to a great extent due to interactions with the zeolitized tuff.

A Comparison of the Sorption Behavior of CrO_4^{2-} and SeO_3^{2-} on the Zeolitized Tuff

A comparison of the anions' sorption behavior on the zeolitized tuff was made to investigate the differences in the partitioning behavior between a strongly binding anion versus a weakly binding anion. This comparison serves to illustrate the large differences in binding strength between an anion assumed to be forming inner-sphere coordination complexes, and an anion assumed to be forming outer-sphere complexes on several mineral surfaces. Overall, the experiments indicate that the fractional uptake of SeO_3^{2-} is always greater than the fractional uptake of CrO_4^{2-} on the zeolitized tuff regardless of the

geochemical parameters varied. Figure 61 illustrates the differences in the binding strength between the two anions. The CrO_4^{2-} anion for these particular geochemical conditions shows very little, if any, fractional uptake by the zeolitized tuff. The fractional uptake of SeO_3^{2-} , however, is approximately 40% at low pH of 3.5 and decreases as a function of pH to approximately 10% at pH values above 8.5. This sorption behavior can again be seen in Figure 62, which shows the fractional uptake of the two anions on 100 g/L zeolitized tuff in 1.0 M NaNO_3 . The fractional uptake of CrO_4^{2-} decreases as a function of the pH from a maximum value of approximately 30% at a pH of 4.5 to a fractional uptake of 0% at a pH of approximately 6. The SeO_3^{2-} anion, however, has a much greater fractional uptake than the CrO_4^{2-} anion with a fractional uptake that decreases from a maximum value of approximately 100% at a pH of 3.5 to a minimum fractional uptake of approximately 30% at pH values greater than 5.

The two previous diagrams, showing experiments at different ionic strengths and anion concentrations, have shown that the fractional uptake of SeO_3^{2-} on the zeolitized tuff from the NTS is always greater than the fractional uptake of CrO_4^{2-} for similar geochemical conditions. The differences in the fractional uptakes can likely be explained because the SeO_3^{2-} anion is the conjugate base of a weak acid, which means it would be more likely to form chemical bonds with pH-dependent surface sites. The CrO_4^{2-} anion is the conjugate base of a stronger acid, and consequently it is less likely to form chemical bonds with surface sites. This type of fractional uptake behavior is consistent with selenite inner-sphere coordination complex formation and chromate outer-sphere complex formation. In addition, the formation of inner-sphere coordination complexes by SeO_3^{2-} would also explain why the fractional uptake of SeO_3^{2-} does not vary as a function

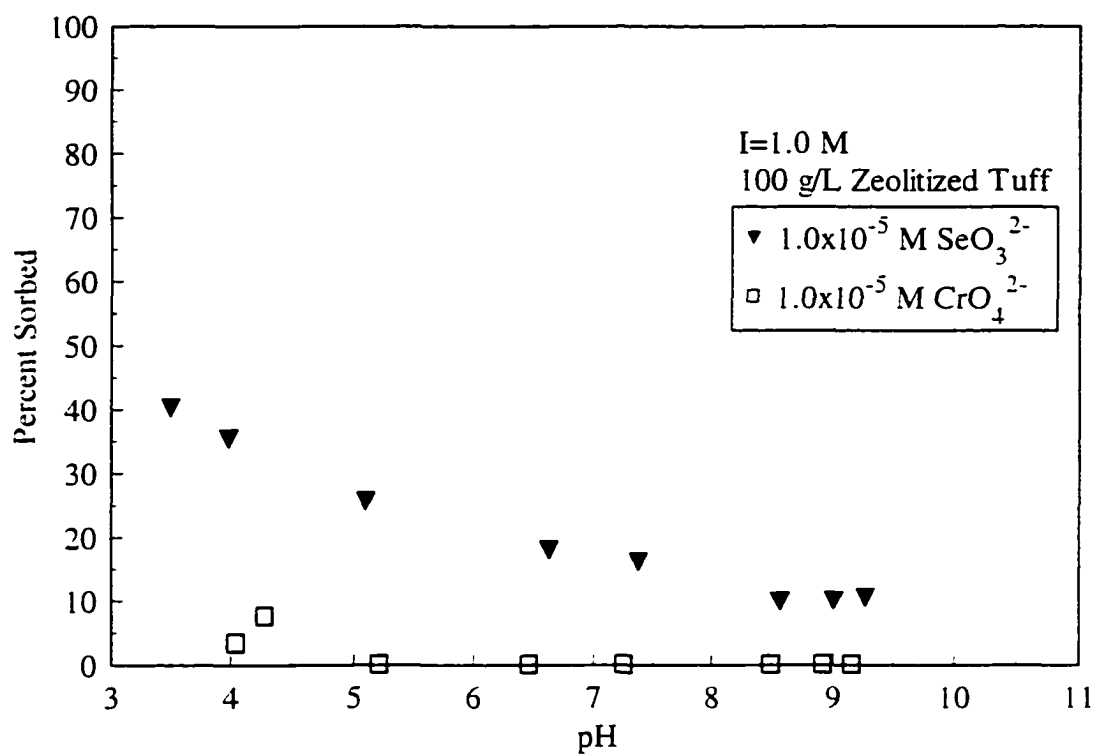


Figure 61. Comparison of the sorption behavior of $1.0 \times 10^{-5} \text{ M CrO}_4^{2-}$ and SeO_3^{2-} on 100 g/L zeolitized tuff in 1.0 M NaNO_3 .

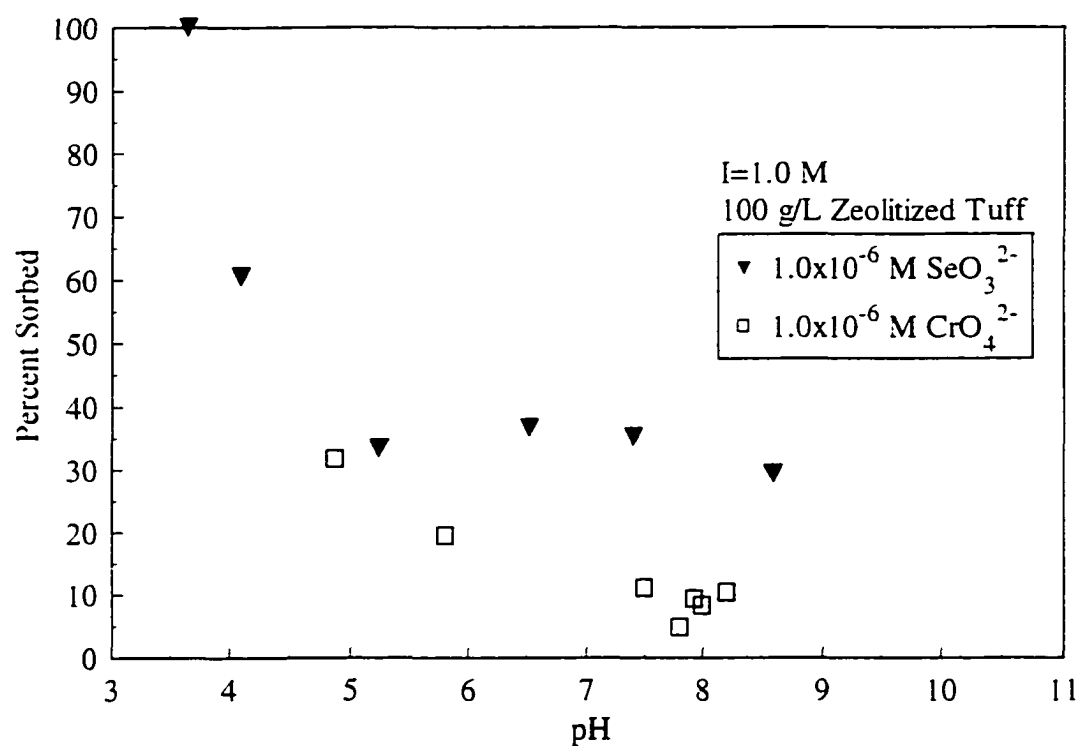


Figure 62. Comparison of the sorption behavior of $1.0 \times 10^{-6} \text{ M CrO}_4^{2-}$ and SeO_3^{2-} on 100 g/L zeolitized tuff in 1.0 M NaNO_3 .

of ionic strength. The CrO_4^{2-} anion, however, is affected by changes in the background electrolyte concentration, and this tends to indicate the formation outer-sphere complexes.

Sorption of CrO_4^{2-} and SeO_3^{2-} on Clinoptilolite

Batch equilibrium sorption experiments with the two anions were also performed using the pure clinoptilolite. These additional experiments were conducted so that a comparison between the natural zeolitized tuff, which contains a significant percentage of clinoptilolite, and the pure clinoptilolite could be made. The fractional uptake of the two anions on the pure zeolite (clinoptilolite) is important to the overall understanding of the sorption behavior of the anions on the zeolitized tuff from the NTS. It was thought that by comparing the sorption behavior of the anions as a function of the adsorbent type, a determination could be made whether the mineral phase clinoptilolite or some other mineral phase is primarily responsible for the sorption of the anions. Therefore, batch equilibrium sorption experiments with the two anions were also performed using the clinoptilolite as a function of pH, ionic strength, anion concentration, and solid adsorbent concentration.

Sorption Behavior of CrO_4^{2-}

Figure 63 shows the fractional uptake of 1.0×10^{-7} M CrO_4^{2-} on 33 g/L clinoptilolite as a function of ionic strength. It must be remembered that a solid concentration of 33 g/L clinoptilolite is equivalent in terms of the surface area of the adsorbent to a solid concentration of 100 g/L zeolitized tuff. Overall, the results indicate that the fractional uptake of CrO_4^{2-} increases as the background electrolyte concentration decreases. The figure, however, also demonstrates some unusual fractional uptake

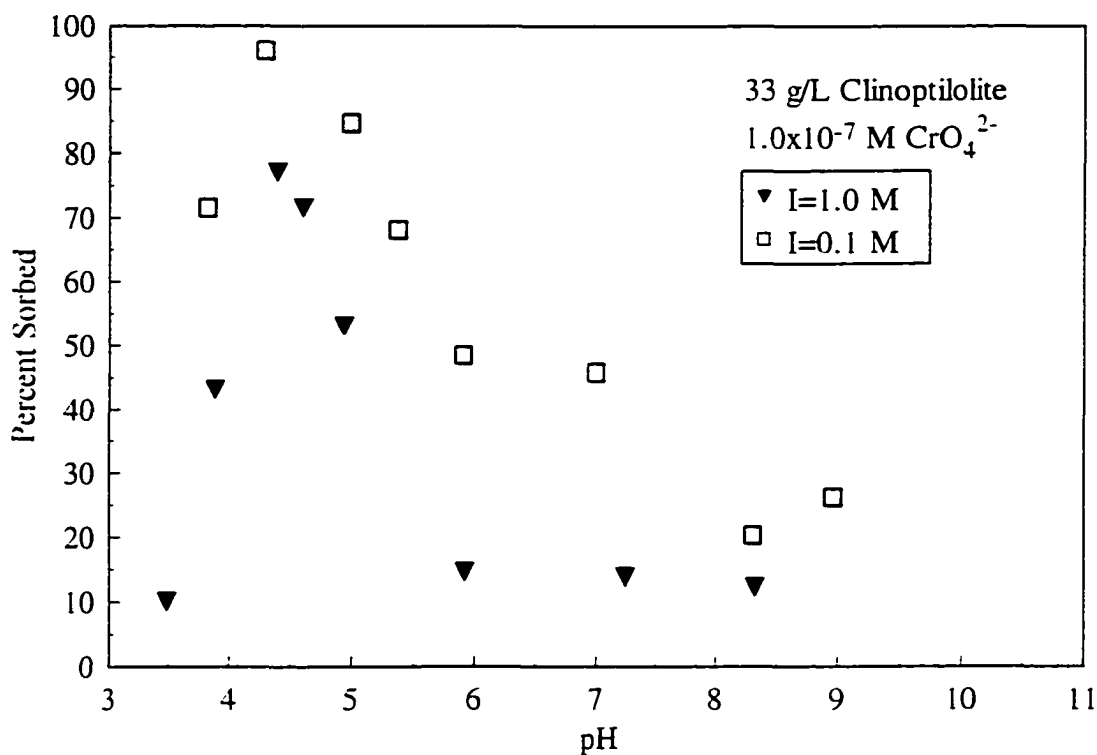


Figure 63. Sorption of 1.0×10^{-7} M CrO_4^{2-} on 33 g/L clinoptilolite as a function of ionic strength.

behavior that has not been seen with any of the other ions of interest. As expected, the fractional uptake of CrO_4^{2-} on the clinoptilolite varies as a function of pH, but a maximum value of fractional uptake of approximately 75% is achieved at a pH of approximately 4.25 for the 1.0 M NaNO_3 background electrolyte concentration. The fractional uptake of CrO_4^{2-} then decreases from this maximum value as a function of increasing pH to approximately 10% at pH 8.5. The fractional uptake of CrO_4^{2-} , however, also decreases from the maximum value as a function of decreasing pH to approximately 10% at a low pH of 3.5. Experiments performed at the lower background electrolyte concentration show similar behavior. The fractional uptake of CrO_4^{2-} at the 0.1 M NaNO_3 background electrolyte concentration has a maximum value of

approximately 95% at a pH of 4.5. The fractional uptake decreases as a function of increasing pH to approximately 20% at a pH 9. In addition, the fractional uptake of CrO_4^{2-} also decreases as a function of decreasing pH to approximately 70% at a pH of 3.5. It is obvious from the figure, however, that the fractional uptake of CrO_4^{2-} on the clinoptilolite increases as the background electrolyte concentration decreases. This type of sorption behavior where the maximum fractional uptake of CrO_4^{2-} occurs at pH value of approximately 4.5 or so that decreases both as the pH increases and decreases can be explained because the CrO_4^{2-} anion is most likely undergoing a speciation change at the lower pH values, or a change in the oxidation state. For example, the CrO_4^{2-} anion is most likely being protonated to HCrO_4^- , or H_2CrO_4 at the low pH values. This change in the speciation of CrO_4^{2-} would affect the overall fractional uptake curve because the protonated species would be less likely to bind to surface sites which have an overall positive charge at the lower pH values than the negatively charged CrO_4^{2-} anion. As a result of the differing electrical charges of the protonated CrO_4^{2-} anion, the fractional uptake curves would deviate from their normal sorption behavior where the maximum fractional uptake occurs at low pH and decreases only as a function of increasing pH. Another explanation for this type of sorption behavior, however, could be attributed to the dissolution of the adsorbent. At low pH values, the adsorbent may undergo dissolution, which would decrease the ability of the CrO_4^{2-} anion to sorb to the mineral surface.

Batch equilibrium sorption experiments with the clinoptilolite were also performed as a function of changing CrO_4^{2-} concentration in order to investigate the effects, if any, on the fractional uptake of CrO_4^{2-} . Sorption experiments were performed

at CrO_4^{2-} concentrations of 1.0×10^{-6} and 1.0×10^{-7} M. Inspection of Figure 64 reveals that the fractional uptake of CrO_4^{2-} on the clinoptilolite increases as the CrO_4^{2-} concentration decreases. The figure clearly shows that the 1.0×10^{-6} M CrO_4^{2-} concentration increases as a function of the pH from approximately 70% at a pH of 4.0 to a maximum fractional uptake of approximately 85% at a pH of 4.25. The fractional uptake of 1.0×10^{-6} M CrO_4^{2-} then decreases as a function of pH to approximately 0% at a pH of 7.5 or so. It is obvious from the figure that the overall fractional uptake increases as the anion concentration decreases to 1.0×10^{-7} M CrO_4^{2-} . As can be seen from the figure, the 1.0×10^{-7} M concentration results in the fractional uptake of approximately 70% at a pH of around 3.8 that increases like the higher anion concentration to a maximum fractional uptake of 95%

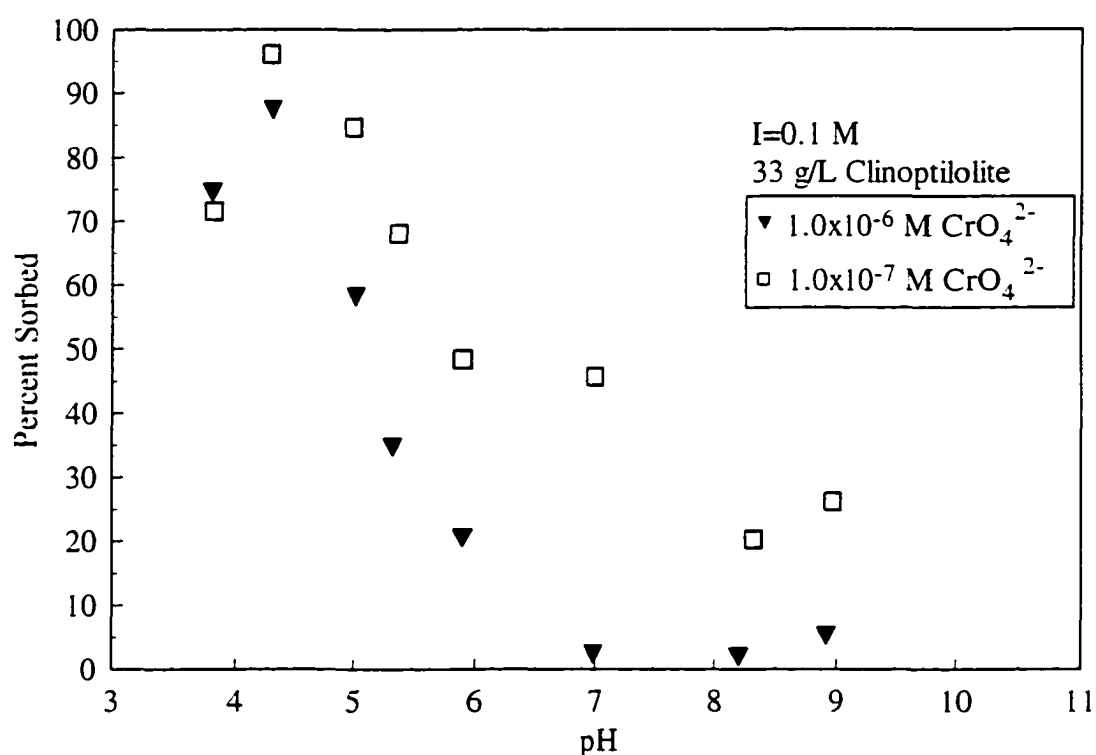


Figure 64. Sorption of CrO_4^{2-} on 33 g/L clinoptilolite in 0.1 M NaNO_3 as a function of CrO_4^{2-} concentration.

at a pH of 4.3. The fractional uptake of CrO_4^{2-} then decreases as a function of pH to a fractional uptake of approximately 20% at a pH above 8.5 or so. This type of sorption behavior is expected because as the CrO_4^{2-} concentration in solution decreases, there are proportionally more binding sites available at the lower anion concentration for the CrO_4^{2-} anions remaining in solution. This type of behavior has been seen with all other ions investigated during this project.

Batch equilibrium sorption experiments investigating the sorption behavior of CrO_4^{2-} on the clinoptilolite were only performed at one solid concentration in order to normalize the surface area of the clinoptilolite to that of the zeolitized tuff from the NTS. This normalization of the surface area allows for a comparison of the sorption behavior of CrO_4^{2-} as a function of the adsorbent type in the final section of the thesis. Therefore, no figures will be presented illustrating the fractional uptake of CrO_4^{2-} on the clinoptilolite as a function of the clinoptilolite concentration.

Sorption Behavior of SeO_3^{2-}

Batch equilibrium sorption experiments with the SeO_3^{2-} anion and the clinoptilolite were conducted so that a comparison of the anion's sorption behavior on the pure mineralogical phase could be made. Experiments were only performed at one solid adsorbent concentration (33 g/L clinoptilolite). These experiments were performed to illustrate any similarities and differences in the fractional uptake of SeO_3^{2-} between the two different adsorbents types.

Ionic strength dependence experiments indicated that the fractional uptake of SeO_3^{2-} on the clinoptilolite does not vary as a function of the ionic strength of the solution. Figure 65 shows the fractional uptake of 1.0×10^{-5} M SeO_3^{2-} on 33 g/L

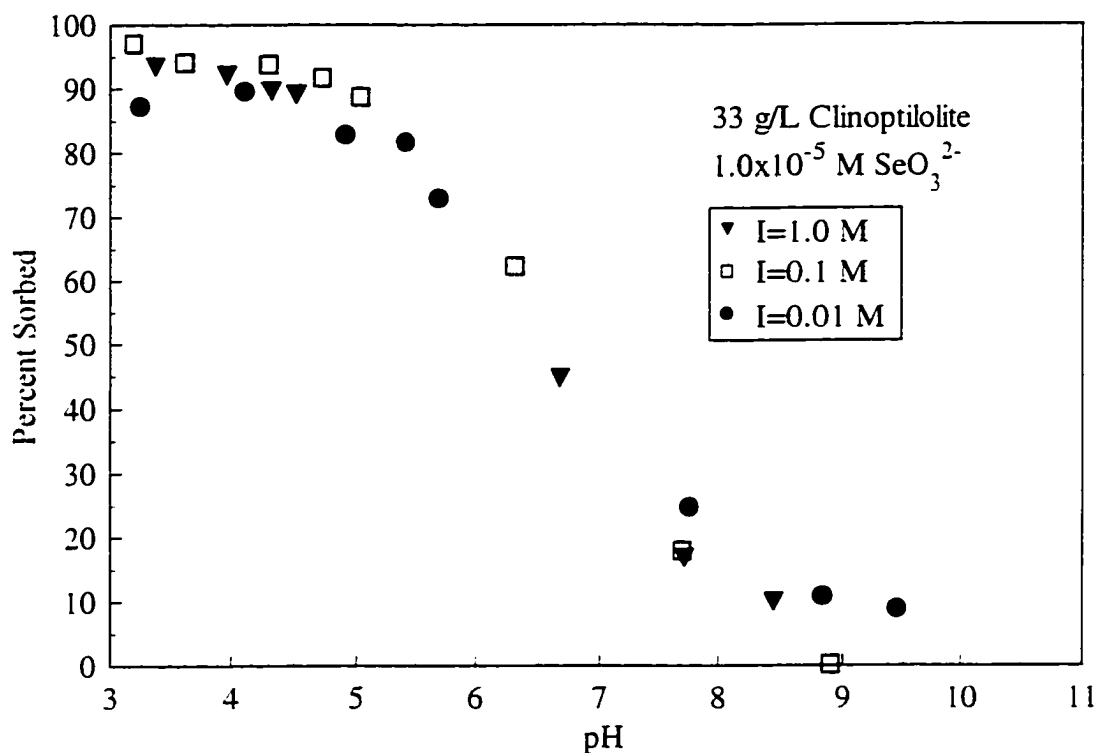


Figure 65. Sorption of 1.0×10^{-5} M SeO_3^{2-} on 33 g/L clinoptilolite as a function of ionic strength.

clinoptilolite as a function of ionic strength. It can be seen from the figure that all three background electrolyte concentrations investigated result in the fractional uptake of approximately 95% at low pH values of 3 to 4 that decrease as a function of pH to a fractional uptake of less than 10% above pH 9.0. This type of sorption behavior is similar to the fractional uptake behavior of SeO_3^{2-} on the zeolitized tuff, and it can be similarly explained.

Batch equilibrium sorption experiments were also performed with the clinoptilolite to investigate the effects, if any, that changing SeO_3^{2-} concentrations have on the fractional uptake of SeO_3^{2-} . The fractional uptake curves showed that, once again, the fractional uptake of SeO_3^{2-} increases as the SeO_3^{2-} concentration in solution decreases,

as shown in Figure 66. The figure shows the fractional uptake of SeO_3^{2-} on 33 g/L clinoptilolite in 1.0 M NaNO_3 . The figure clearly illustrates that the 1.0×10^{-4} M SeO_3^{2-} concentration shows the lowest fractional uptake. As the anion concentration decreases to 1.0×10^{-5} and 1.0×10^{-6} M SeO_3^{2-} , the fractional uptake increases accordingly.

In conclusion, several batch equilibrium sorption experiments were performed with the SeO_3^{2-} anion and the clinoptilolite adsorbent. The experiments showed that the fractional uptake of SeO_3^{2-} on the clinoptilolite is not affected by changes in the ionic strength of the solution, which suggests the formation of inner-sphere coordination complexes. The experiments also showed that increasing SeO_3^{2-} concentrations result in a decrease in the fractional uptake of SeO_3^{2-} on the clinoptilolite adsorbent. Experiments

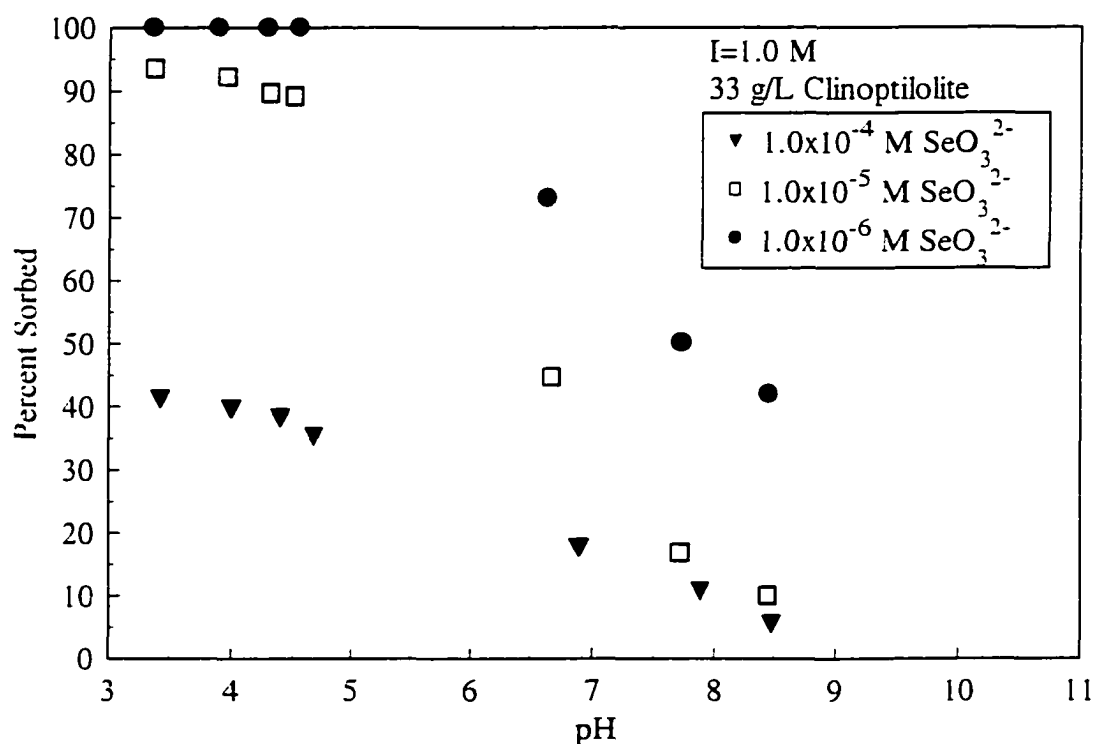


Figure 66. Sorption of SeO_3^{2-} on 33 g/L clinoptilolite in 1.0 M NaNO_3 as a function of SeO_3^{2-} concentration.

were not performed as a function of the solid adsorbent concentration, however, experiments with the other ions of interest in this thesis have shown that increasing solid concentrations result in increase in fractional uptake of the ion of interest, and there is no reason to believe that SeO_3^{2-} would behave differently.

A Comparison of the Sorption Behavior of CrO_4^{2-} and SeO_3^{2-} on the Clinoptilolite

A comparison of the anions' sorption on the clinoptilolite was made to illustrate the similarities and differences in the fractional uptake between a strongly binding anion (SeO_3^{2-}) and a weakly binding anion (CrO_4^{2-}). The experiments performed indicate that both anions show pH-dependent behavior. For example, the experiments show that the fractional uptake of the anions is at its greatest at low pH values and decreases as the pH of the solution increases. The pH-dependent sorption behavior that both anions exhibit can be thought of as a competition for the available surface sites between the anions of interest and the OH^- anion. The experiments have also shown that the fractional uptake of SeO_3^{2-} is always greater than the fractional uptake of CrO_4^{2-} for similar geochemical conditions. This is consistent with SeO_3^{2-} forming inner-sphere coordination complexes with pH-dependent surface sites. These types of chemical bonds are much stronger than the outer-sphere complexes that CrO_4^{2-} is assumed to be forming. For example, Figure 67 shows the fractional uptake of 1.0×10^{-6} M CrO_4^{2-} and SeO_3^{2-} at a background electrolyte concentration of 1.0 M NaNO_3 , and a solid concentration of 33 g/L clinoptilolite. The figure reveals that the fractional uptake of SeO_3^{2-} is greater at all pH values than the fractional uptake of CrO_4^{2-} . This behavior can be seen again in Figure 68, which is at a lower background electrolyte concentration of 0.1 M NaNO_3 .

The two anions differ in their sorption behavior, however, to changes in the

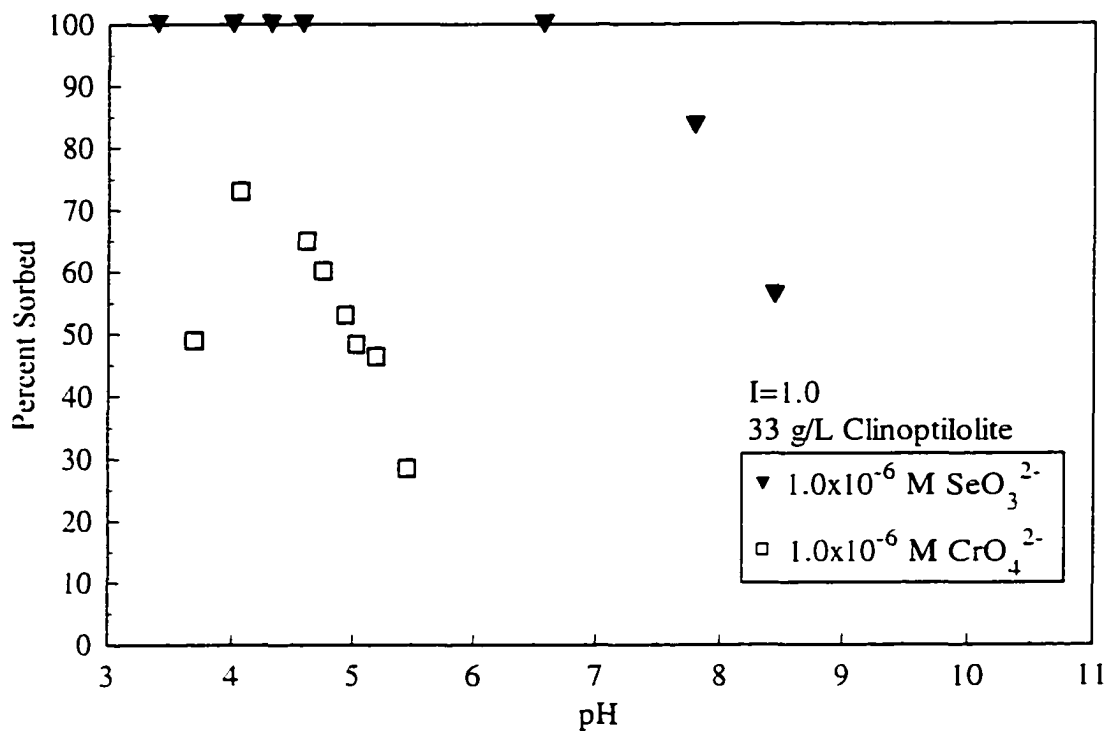


Figure 67. Comparison of the sorption behavior of CrO_4^{2-} and SeO_3^{2-} on 33 g/L clinoptilolite in 1.0 M NaNO_3 .

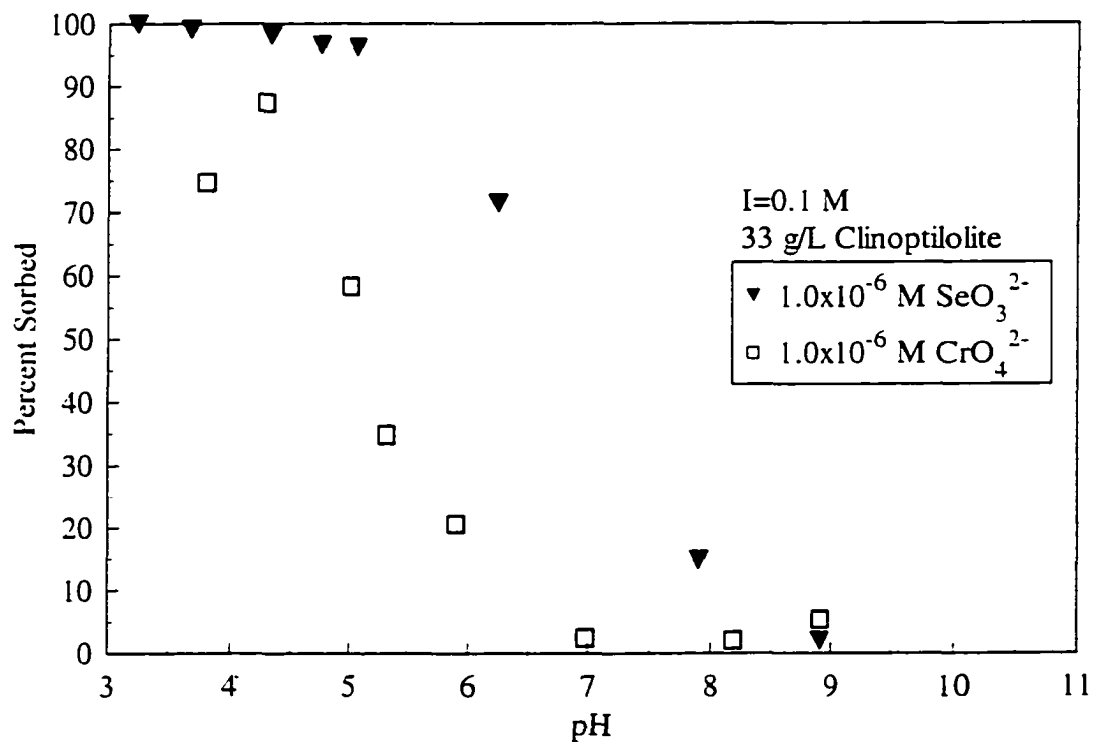


Figure 68. Comparison of the sorption behavior of 1.0×10^{-6} M CrO_4^{2-} and SeO_4^{2-} on 33 g/L clinoptilolite in 0.1 M NaNO_3 .

background electrolyte concentration. For example, the SeO_3^{2-} anion is not affected by changes in the background electrolyte concentration (Figure 65). This behavior is consistent with strong binding of SeO_3^{2-} to surface sites, possibly by the formation of inner-sphere coordination complexes. The fractional uptake of CrO_4^{2-} on the clinoptilolite, however, is affected by changes in the background electrolyte concentration (Figure 63). This behavior indicates that CrO_4^{2-} is binding to weakly binding surface sites, possibly forming outer-sphere complexes.

Comparison of CrO_4^{2-} and SeO_3^{2-} Sorption as a Function of Adsorbent Type

In the final section of this chapter, a comparison of the sorption behavior of CrO_4^{2-} and SeO_3^{2-} as a function of adsorbent type will be made. Such a comparison is important to understanding the overall sorption behavior of the anions on the zeolitized tuff from the NTS. It was hoped that a determination could be made as to the primary mineral phase responsible for the fractional uptake of the anions by comparing the fractional of the anions on the zeolitized tuff to the fractional uptake of the anions on the clinoptilolite. For example, it was shown in Chapter 4 that the clinoptilolite present in the volcanic tuff was controlling the fractional uptake of the cations for the lower background electrolyte concentrations. It was obvious from the figures that the fractional uptake of the cations was, qualitatively at least, the same as a function of the adsorbent type, once the solid concentrations of both adsorbents were normalized with respect to specific surface area. Therefore, a comparison of the anions fractional uptake as a function of adsorbent type was also made in an attempt to determine what mineral phase is controlling the sorption behavior of the anions. Solid concentrations of 33 g/L and 100

g/L were used for the clinoptilolite and the zeolitized tuff from the NTS, respectively. These solid adsorbent concentrations were chosen to normalize the surface areas of the adsorbents, and because at least that high of a solid concentration was needed to result in any sorption of the CrO_4^{2-} anion on the zeolitized tuff. The results of the experiments with the CrO_4^{2-} anion will be discussed first, followed by a discussion of the fractional uptake of the SeO_3^{2-} anion as a function of the adsorbent type.

CrO_4^{2-} Sorption as a Function of Adsorbent Type

In order to compare the sorption behavior of CrO_4^{2-} as a function of adsorbent type, batch equilibrium sorption experiments were performed with both adsorbents at similar geochemical conditions. Overall, the experiments indicate that the fractional uptake of CrO_4^{2-} is, qualitatively at least, the same for both adsorbents. For example, the fractional uptake of CrO_4^{2-} on both adsorbents is favored at low pH values and decreases as the pH of the solution increases. This suggests that the same types of surface sites are responsible for the fractional uptake of the CrO_4^{2-} anion on both adsorbents. In addition, the experiments showed that the fractional uptake of CrO_4^{2-} on the clinoptilolite is greater than on the zeolitized tuff for all of the pH ranges and geochemical conditions investigated. It was stated earlier that the fractional uptake of CrO_4^{2-} on the zeolitized tuff was not very favorable at high anion concentrations, therefore, experimental data will only be presented for the 1.0×10^{-6} M anion concentration. Figure 69 shows the fractional uptake of 1.0×10^{-6} M CrO_4^{2-} in 0.1 M NaNO_3 as a function of adsorbent type. The figure clearly shows that the fractional uptake of CrO_4^{2-} on the clinoptilolite is greater than on the zeolitized tuff. The greater fractional uptake of CrO_4^{2-} on the clinoptilolite can be likely attributed to the clinoptilolite's higher Al_2O_3 concentration. If one will recall from

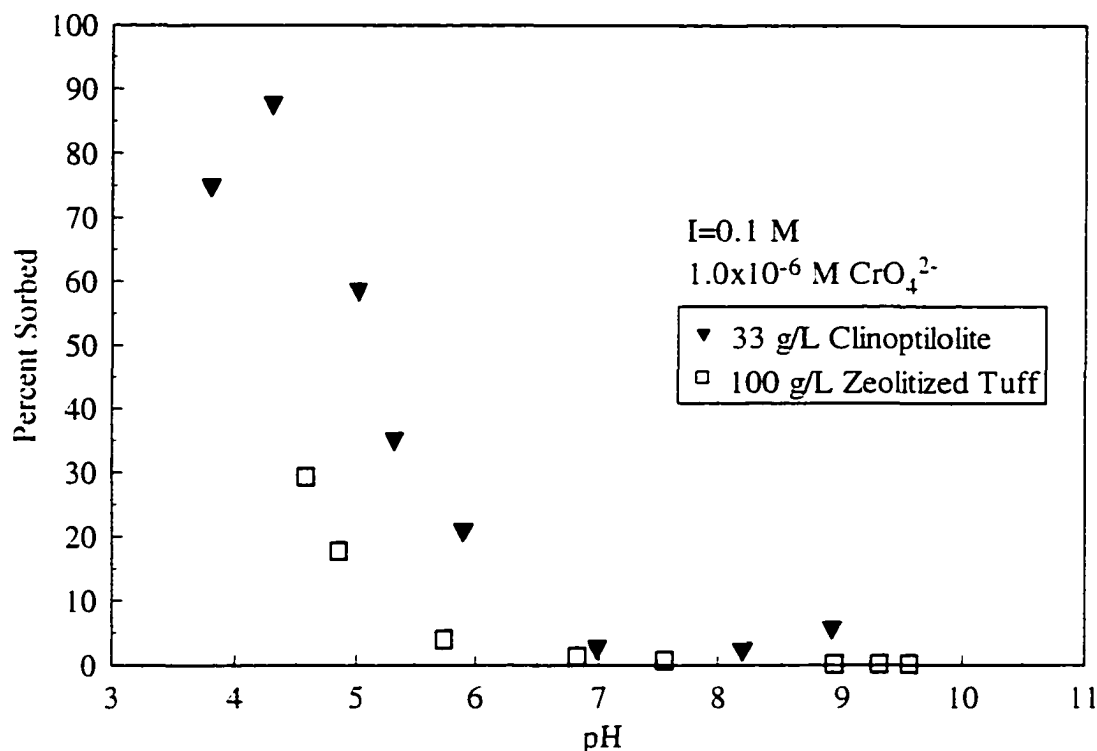


Figure 69. Comparison of the sorption behavior of 1.0×10^{-6} M CrO_4^{2-} in 0.1 M NaNO_3 as a function of adsorbent type.

the XRF data in Chapter 3, the clinoptilolite has a 15% greater Al_2O_3 concentration than the zeolitized tuff. A greater Al_2O_3 concentration would provide more surface aluminol groups for anion sorption. These type of sites are much more conducive to anion sorption than silanol surface sites. Consequently, the fractional uptake of CrO_4^{2-} on the clinoptilolite is greater than on the zeolitized tuff.

The fractional uptake of CrO_4^{2-} on the zeolitized tuff, however, must be controlled by the same types of binding sites, namely surface aluminol groups. This can be concluded because the fractional uptake of CrO_4^{2-} on both adsorbents is, qualitatively at least, the same. It seems unlikely, however, that the surface aluminol groups available for binding within the zeolitized tuff are solely a result of the clinoptilolite contained within

the zeolitized tuff. For example, it was stated in Chapter 2 that the zeolitized tuff found at Rainier Mesa contains 5-30% non-zeolitic constituents. These constituents included feldspar and biotite, which are also aluminosilicate minerals. Consequently, these types of minerals would also provide surface aluminol groups for binding. Therefore, it cannot be conclusively determined that the clinoptilolite contained within the zeolitized tuff is solely responsible for the sorption behavior of CrO_4^{2-} .

SeO_3^{2-} Sorption as a Function of Adsorbent Type

Comparisons of the sorption behavior of SeO_3^{2-} as a function of adsorbent type indicate that the fractional uptake of SeO_3^{2-} on both adsorbents is also, qualitatively at least, the same. For example, the fractional uptake of SeO_3^{2-} is favored at low pH values and decreases as the pH increases. The experiments also show that, like the CrO_4^{2-} anion, the fractional uptake of SeO_3^{2-} on the clinoptilolite is always greater than on the zeolitized tuff regardless of the geochemical parameters used. The explanation for this type of fractional uptake behavior can be considered the same as the explanation provided for the CrO_4^{2-} anion. The greater Al_2O_3 concentration of the clinoptilolite results in more aluminol surface sites being available for anion binding. For example, Figure 70 illustrates the affinity of the SeO_3^{2-} anion for both adsorbents at similar geochemical conditions. As can be seen from the figure, the fractional uptake of SeO_3^{2-} on the clinoptilolite is greater than on the zeolitized tuff. The figure clearly displays the typical pH-dependent sorption behavior of the anions where the fractional uptake decreases from a maximum value at low pH to almost 0% at high pH. In addition, it can be seen from the figure that the zeolitized tuff results in substantially less fractional uptake than the clinoptilolite. The fractional uptake of SeO_3^{2-} on the zeolitized tuff varies from a

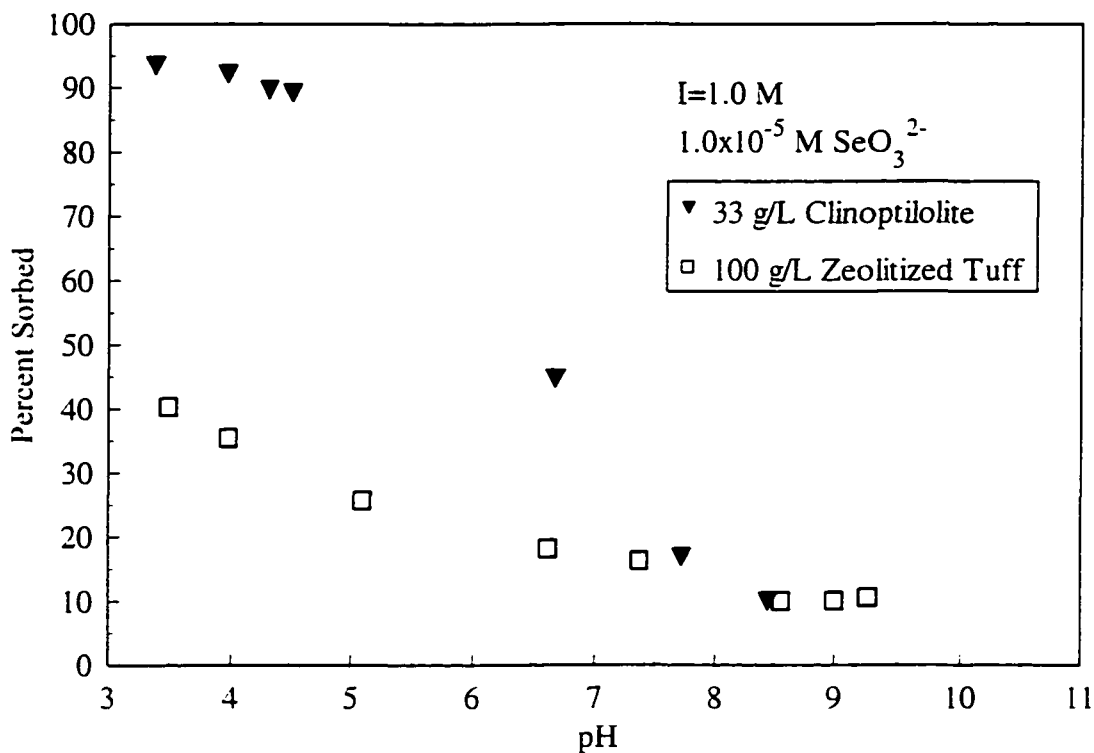


Figure 70. Comparison of the sorption behavior of 1.0×10^{-5} M SeO_3^{2-} in 1.0 M NaNO_3 as a function of adsorbent type.

maximum value at approximately 40% at a low pH of 3.5 that then decreases as a function of the pH to a minimum value of approximately 10% at pH above 8.5. This relative binding affinity can be seen again in Figure 71, which illustrates the fractional uptake of 1.0×10^{-6} M SeO_3^{2-} in 0.1 M NaNO_3 as a function of adsorbent type. This figure shows that once again the fractional uptake of SeO_3^{2-} on the clinoptilolite is greater than the fractional uptake of SeO_3^{2-} on the zeolitized tuff from the NTS.

In conclusion, comparisons were made illustrating the sorption behavior of SeO_3^{2-} as a function of adsorbent type. These comparisons showed that the fractional uptake of SeO_3^{2-} is greater on the clinoptilolite than on the zeolitized tuff. This type of fractional uptake behavior can be likely attributed to the greater Al_2O_3 concentration of the

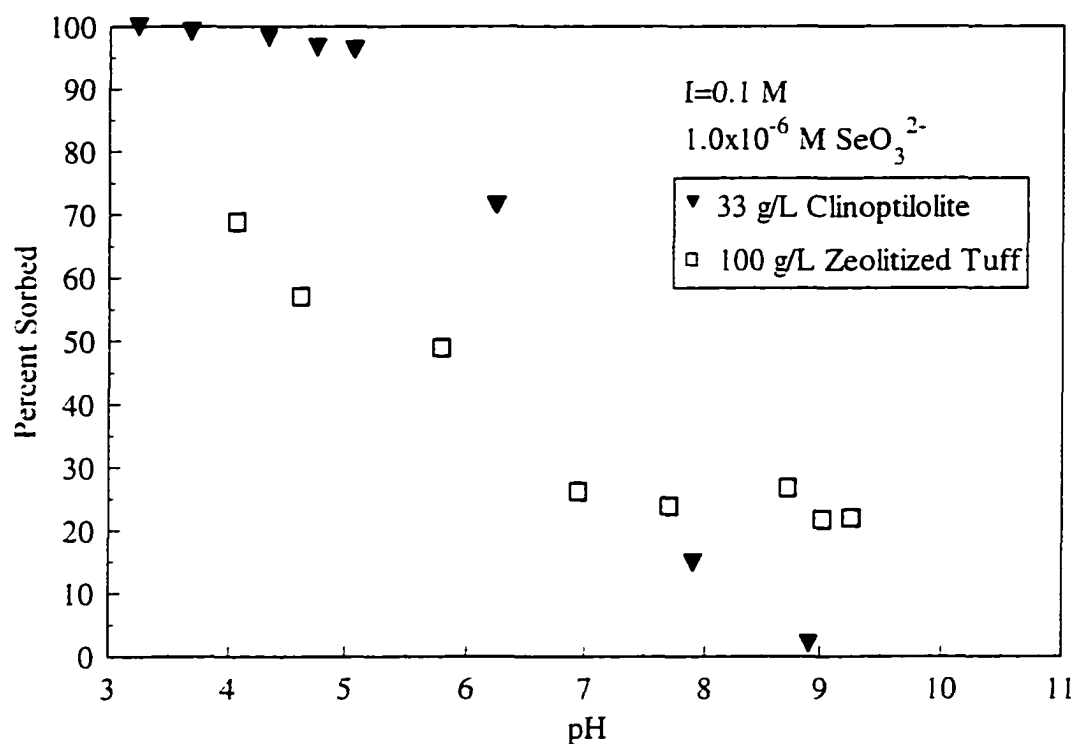


Figure 71. Comparison of the sorption behavior of $1.0 \times 10^{-6} \text{ M SeO}_3^{2-}$ in 0.1 M NaNO_3 as a function of adsorbent type.

clinoptilolite. A greater Al_2O_3 concentration would provide more surface aluminol groups for SeO_3^{2-} to bind to. Unfortunately, the exact proportion of zeolite minerals to non-zeolite minerals contained within the zeolitized tuff was never determined.

Therefore, it cannot be conclusively determined which mineral phase is contributing the most surface aluminol groups for anion binding.

Conclusions

Comparisons of the anion sorption behavior as a function of adsorbent type were made so that a determination could be made as to whether the clinoptilolite contained within the zeolitized tuff from Rainier Mesa is responsible for the fractional uptake of the anions. The comparisons have shown that the fractional uptake of the anions on both

adsorbents is qualitatively, at least, the same. This suggests that the same sorts of binding sites are controlling the fractional uptake of the anions. For example, the fractional uptake of the anions is most likely related to the Al_2O_3 concentration of the adsorbent. Unfortunately, the zeolitized tuff from Rainier Mesa contains a number of aluminosilicate minerals. Therefore, it cannot be conclusively proven that the clinoptilolite contained within the zeolitized tuff controls the sorption behavior of the anions.

CHAPTER 6

CONCLUSIONS AND RECOMMENDATIONS

FOR FUTURE RESEARCH

Numerous batch equilibrium sorption experiments, sorption parameter estimations, and speciation calculations were performed for this research project in order to address the proposed hypotheses. It had been proposed that the movement of any Pb(II), Sr(II), CrO₄²⁻, and SeO₃²⁻ ions in the groundwater at the NTS would be retarded due to sorption of the ions on zeolitized tuff. In addition, it was hypothesized that the cations would be retarded more than the anions, and that lastly, the zeolite mineral clinoptilolite contained within the zeolitized tuff is responsible for the sorption behavior of the ions. The batch equilibrium experiments were conducted as a function of pH, ionic strength, total solid concentration, and total ion concentration. From these experiments, partitioning coefficients of the cations and anions of interest for the zeolitized tuff from Rainier Mesa were calculated. These geochemical parameters can then be used in transport codes to help estimate the fate and transport of these contaminants in the subsurface environment at the NTS, and to help increase our overall understanding of these interactions. In this chapter, the conclusions of the research project and recommendations for future research are presented.

Conclusions

The batch equilibrium experiments revealed that the fractional uptake of the cations on the zeolitized tuff and clinoptilolite was controlled by cation exchange at background electrolyte concentrations of 0.1 M and 0.01 M NaNO_3 . This type of sorption is pH-independent and varies only as a function of the adsorbent concentration, metal cation concentration, or the overall background electrolyte concentration. The batch equilibrium experiments also indicated that the cations of interest were, most likely, excluded from the internal cation-exchange sites of both adsorbents for background electrolyte concentrations of at least 1.0 M NaNO_3 . This could be concluded because there was no fractional uptake of Sr(II) under these conditions, and the Pb(II) cation began to display pH-dependent fractional uptake behavior. There was no fractional uptake of Sr(II) at this high background electrolyte concentration because it, presumably, cannot form any other type of bond with either adsorbent. The Pb(II) cation, however, was able to form either surface complexes with pH-dependent surface sites or precipitates of Pb at this high background electrolyte concentration. This would tend to indicate that the Pb(II) cation is binding to both adsorbents in a completely different manner than was seen at the lower background electrolyte concentrations. The ionic strength dependence experiments performed at background electrolyte concentrations above 1.0 M NaNO_3 revealed that there is no variation in the fractional uptake of Pb(II) as a function of the ionic strength. This fractional uptake indicates, but is not direct evidence for the fact, that Pb(II) is most likely forming inner-sphere coordination complexes with pH-dependent surface groups, or forming surface precipitates.

The experiments with the cations of interest also revealed that regardless of the

geochemical parameters, the Pb(II) cation had a greater affinity for the adsorbents than the Sr(II) cation. The complete removal of these cations from the groundwater at the NTS would most likely occur, however, because of the ionic strength of the groundwater at the NTS. This can be based on the fact that the ionic strength of the groundwater from water well U-20 was calculated as 3.2×10^{-3} M. It should be recalled that the fractional uptake of both cations on both adsorbents was essentially 100% for the lowest ionic strength investigated (1.0×10^{-2} M). If the ionic strength of the solution were decreased to an even lower value, there would be even less competition for the cation-exchange sites, and the complete removal of Pb(II) and Sr(II) from solution would be expected. This has significant implications for the mobility of these metal cations in the subsurface environment at the NTS. Specifically, the numerous batch equilibrium sorption experiments have shown that the Pb(II) and Sr(II) cations would be significantly retarded in the aqueous environment at the NTS due to sorption on zeolitized tuff.

The results from the batch equilibrium sorption experiments revealed that the fractional uptake of the anions is controlled by sorption on external pH-dependent surface sites. Based on ionic strength dependence experiments, it appears that the SeO_3^{2-} anion is forming inner-sphere coordination complexes with amphoteric surface sites. The fractional uptake of SeO_3^{2-} on both adsorbents is only affected by changes in pH, solid concentration, and anion concentration. The fractional uptake of CrO_4^{2-} on both adsorbents, however, is affected by changes in the ionic strength, as well as the other geochemical parameters studied. This tends to indicate that CrO_4^{2-} is forming weakly binding, possibly outer-sphere complexes with pH dependent surface sites. In fact, the fractional uptake data revealed that the sorption of CrO_4^{2-} on the zeolitized tuff adsorbent

is so weak for all of the geochemical parameters investigated that anion concentrations had to be decreased to 5.0×10^{-7} M to result in any meaningful uptake.

The results of the experiments also showed that regardless of the geochemical parameters investigated, the SeO_3^{2-} anion had a greater affinity for both adsorbents than the CrO_4^{2-} anion. The fractional uptake of the anions, however, does not approach the fractional uptake of the cations as can be seen by the solid adsorbent concentration needed to produce any fractional uptake of the anions. This is in no way surprising since both adsorbents have high cation-exchange capacities, and no appreciable anion-exchange capacities. The observed fractional uptake of the anions has significant implications for their mobility in the aqueous environment at the NTS, namely that the anions would not be retarded with respect to groundwater flow due to sorption on zeolitized tuff. Specifically, the experiments showed that the CrO_4^{2-} anion would not be retarded to any great extent by the zeolitized tuff at the NTS. The SeO_3^{2-} anion, however, would be retarded more than the chromate anion, but it would still be significantly more mobile in the subsurface environment than either of the cations especially at the pH values likely to be encountered at the NTS.

From the previous discussions concerning the mobility of the ions in the groundwater at the NTS, it can be concluded that the cations would, in fact, be retarded to a greater extent than the anions. This can be attributed to the large cation-exchange capacity of the zeolitized tuff, and the fact that most zeolites tend to possess a net negative structural charge resulting from isomorphic substitution of cations in the crystal lattice. Specifically, the following selectivity series for the zeolitized tuff and the ions studied can be established for groundwater conditions likely to be found at the NTS:



The batch equilibrium experiments using the clinoptilolite were performed so that a comparison with the zeolitized tuff could be made. These comparisons as a function of adsorbent type were made in order to determine whether the most common zeolite present in the zeolitized tuff from Rainier Mesa was responsible for the fractional uptake of the ions. The comparisons revealed that the clinoptilolite contained within the zeolitized tuff is responsible for the fractional uptake of the cations at background electrolyte concentrations of 0.1 and 0.01 M NaNO₃. This can be attributed to the large cation-exchange capacity of the clinoptilolite. For example, it was shown that even at relatively low solid adsorbent concentrations, the metal cations could be almost completely removed from solution by cation-exchange. The comparisons as a function of adsorbent type, however, could not conclusively prove that the clinoptilolite contained within the zeolitized tuff is mainly responsible for the sorption of Pb(II) at a background electrolyte concentration of 1.0 M NaNO₃. At that background electrolyte concentration, it was assumed that the Pb(II) cation was most likely binding as an inner-sphere coordination complex to surface aluminol sites, or forming surface precipitates. It would be extremely difficult to prove, however, that the surface aluminol sites of the zeolitized tuff are solely provided by the clinoptilolite, because there are other aluminosilicate minerals present in the altered vitric tuffs.

The comparisons of anion sorption behavior as a function of adsorbent type were also unable to conclusively show that the clinoptilolite contained within the zeolitized tuff is responsible for the sorption behavior of the anions. For example, based on the experimental data, the fractional uptake of the anions was assumed to be controlled by

surface aluminol groups. As with the case of the Pb(II) cation at the highest ionic strength, it cannot be conclusively proven that the Al₂O₃ concentration of the zeolitized tuff is solely related to the presence of clinoptilolite, because there are other aluminosilicate minerals present in the zeolitized tuff.

Recommendations for Future Research

Future work based on the results of the batch equilibrium sorption experiments presented in this thesis can be divided into the two following categories: kinetic investigations, and spectroscopic investigations. A number of other equilibrium sorption experiments, however, that were not conducted for this thesis due to time and budgetary constraints could be easily completed and help to increase the overall understanding of the sorption properties of the zeolitized tuff from the NTS. For example, it would be extremely beneficial to perform similar types of batch equilibrium sorption experiments with the ions of interest using either a water made to be representative of the groundwater from the NTS, or using actual groundwater obtained from a well at the NTS. These types of equilibrium experiments would have the advantage of simulating the actual groundwater conditions found in the subsurface environment at the NTS. It has been pointed out, however, that sample disturbance, and the lack of representation of field flow conditions in batch equilibrium studies can detract from the validity of the equilibrium sorption data if they have been applied to field situations (Patterson and Spoel, 1981).

In addition to performing additional batch equilibrium sorption experiments with groundwaters from the NTS, it would be beneficial to conduct column experiments with the zeolitized tuff adsorbent. In these types of experiments, a natural groundwater with

the contaminant of interest already added is passed through columns containing the zeolitized tuff. Using this type of approach, distribution coefficients can be calculated from the shape of the breakthrough curve (Patterson and Spoel, 1981). These types of experiments would be more similar to conditions found in an aquifer, but it must be remembered that a natural flow system can never be completely reproduced in a laboratory setting. In addition, it would be useful to compare the partitioning coefficients calculated with the column studies to the calculated sorption parameters from the batch studies. It would also be beneficial to perform more batch equilibrium experiments with other ions supplying the background electrolyte concentration. For example, it would be interesting to see how background electrolyte concentrations supplied by say Mg^{2+} or Ca^{2+} would effect the overall sorption behavior of the ions of interest.

Further studies into the suitability of the zeolitized tuff from the NTS to retard the transport of potentially dangerous ions must include investigations into the kinetics of sorption. Kinetic studies would provide information on the rate of uptake of the ions of interest by the zeolitized tuffs. These types of experiments would be able to determine whether the rate of uptake is a function of the particle size or the pore structure of the adsorbent, and whether the rate of ion exchange is controlled by internal diffusion, or external liquid film resistance. These types of studies are important because it has been pointed out by Stumm and Morgan (1996) that various steps are involved in the transfer of an ion to the adsorption layer, including the transport to the surface by convection or molecular fusion. In addition, it has been pointed out by Papelis et al. (1995b) that in the majority of studies of inorganic ion rate of uptake by oxides, a distinct two-step behavior is reported, including a fast initial uptake followed by much slower gradual uptake that

may continue for a period of days to months. These types of studies would help to clarify the mechanisms responsible for ion sorption on the zeolitized tuffs from the NTS.

It has been pointed out numerous times that macroscopic sorption experiments alone cannot be used to distinguish between different types of sorption complexes. Therefore, it is also recommended that spectroscopic methods be employed to provide specific structural information about the possible sorbed complexes that are formed by the interactions of the ions with the zeolitized tuff. These types of experiments can help to distinguish between inner-sphere and outer-sphere complexes. For example, Papelis et al. (1995a) state that structural information obtained from X-ray absorption fine structure experiments can be used to determine the closeness of the approach of an ion to a surface, which indicates the type of coordination complex being formed. It is important to distinguish between the type of complex being formed because it has been shown that ions behave as different chemical entities when the complex being formed is different. It is extremely important, therefore, to know the type of coordination complex being formed. In addition, these types of studies would help to clarify whether surface precipitates are being formed.

APPENDIX I

CALCULATED BEST-FIT DISTRIBUTION COEFFICIENTS

The distribution coefficients reported in the body of the text were obtained by forcing the linear isotherm through the origin because that is one of the assumptions of a linear isotherm. Consequently, the reported slope of the isotherms does not represent the best-fit to the data. The best-fit to the slopes, K_d , the intercepts, and correlation coefficients, r^2 , for each ion are reported in Table I- 1, Table I- 2, and Table I- 3,

Table I- 1. Best-fit calculated slopes and intercepts for Pb(II) in 1.0 M NaNO₃ at different pH values.

pH	K_d (m ³ /g)	Intercept (g/g)	r^2
4	8.21×10^{-5}	1.37×10^{-5}	0.984
5	1.05×10^{-4}	8.74×10^{-6}	0.980
6	5.15×10^{-4}	-7.02×10^{-6}	0.535
7	1.16×10^{-3}	2.16×10^{-4}	0.392
8	4.11×10^{-3}	-2.90×10^{-4}	0.742
9	8.42×10^{-3}	-2.40×10^{-4}	0.910

respectively. No results are reported for the CrO_4^{2-} anion because the calculated sorption parameters for this anion were based on only one equilibrium data point for each pH value investigated.

Table I- 2. Best-fit calculated slopes and intercepts for Sr(II) in 0.1 and 0.01 M NaNO_3 at different pH values.

Ionic Strength (M)	pH	K_d (m^3/g)	Intercept (g/g)	r^2
0.1	4, 5, 6, 7, 8, 9	1.93×10^{-4}	-7.37×10^{-6}	0.965
0.01	4, 5, 6, 7, 8, 9	2.33×10^{-3}	1.70×10^{-4}	0.966

Table I- 3. Best-fit calculated slopes and intercepts for SeO_3^{2-} in 1.0 and 0.1 M NaNO_3 at different pH values.

Ionic Strength (M)	pH	K_d (m^3/g)	Intercept (g/g)	r^2
1.0	4	2.35×10^{-6}	9.70×10^{-7}	0.995
1.0	5	2.28×10^{-6}	4.48×10^{-7}	0.999
1.0	6	1.71×10^{-6}	4.06×10^{-7}	0.999
1.0	7	1.05×10^{-6}	4.47×10^{-7}	0.995
0.1	4	2.03×10^{-6}	1.13×10^{-6}	0.992
0.1	5	1.39×10^{-6}	7.27×10^{-7}	0.994
0.1	6	4.65×10^{-7}	4.83×10^{-7}	0.988

APPENDIX II

CALCULATED RETARDATION FACTORS BASED ON THE DISTRIBUTION COEFFICIENTS

The distribution coefficients (K_d) reported in the body of the text and in Appendix I can be used to estimate retardation factors (R) for the $Pb(II)$, $Sr(II)$, CrO_4^{2-} , and SeO_3^{2-} ions as they travel in the groundwater while in contact with the zeolitized tuff from Rainier Mesa using the following equation:

$$R = 1 + (\rho_b/\theta)(K_d) \quad (8)$$

where

ρ_b = bulk density of the material

θ = porosity of the material

K_d = distribution coefficient of the solute for the material

According to Patterson and Spoel (1981), if a solute is reactive, it will travel at a slower rate than the groundwater owing to sorption processes. The rate of the solute movement can be determined by the retardation equation:

$$V_c = V_{gw} / R \quad (9)$$

where

V_{gw} = average groundwater velocity

V_c = average velocity of the contaminant

Employing this equation, predictions concerning the mobility of radionuclides and other inorganic contaminants in a groundwater flow system may be made if the distribution coefficient and the other hydrogeological parameters are known (Patterson and Spoel, 1981). Using the porosity and bulk density values calculated by Micromeritics, retardation factors were estimated for both the linear distribution coefficients and for the best-fit linear distribution coefficients. The retardation factors for each ion are listed in Table II- 1, Table II- 2, Table II- 3, and Table II- 4, respectively. No retardation factors based on the best-fit distribution coefficients could be calculated for the CrO_4^{2-} anion because the distribution coefficients for CrO_4^{2-} were based on only one equilibrium data point. It needs to be emphasized, however, that these calculated retardation factors can only be considered to be estimates because the bulk density and

Table II- 1. Retardation factors for the Pb(II) cation in 1.0 M NaNO_3 at different pH values.

pH	K_d (m^3/g)	R (K_d)	Best-fit K_d (m^3/g)	R (Best-fit K_d)
4	8.31×10^{-5}	318	8.21×10^{-5}	314
5	1.05×10^{-4}	402	1.05×10^{-4}	402
6	5.14×10^{-4}	1967	5.15×10^{-4}	1971
7	1.24×10^{-3}	4745	1.16×10^{-3}	4439
8	3.87×10^{-3}	14810	4.11×10^{-3}	15729
9	8.06×10^{-3}	30846	8.42×10^{-3}	32223

porosity values that were used in the retardation equation were obtained from the ground zeolitized tuff. Values for the bulk density and porosity of the natural zeolitized tuff in the field would be very different than the values for the bulk density and porosity that were used to calculate these retardation factors. For example, differences in these values would arise because the bulk density of a material is highly dependent on the degree of compaction, and to calculate true retardation factors the effective porosity of the material needs to be used. The effective porosity takes into account pore spaces that are actually interconnected for groundwater flow, whereas porosity does not. In addition, the K_d values that were used are highly dependent on the specific geochemical conditions at which the fractional uptake data were obtained (e.g. the solid concentration and the ion concentration), and there is some debate as whether these K_d values would be applicable to the subsurface environment. Consequently, the true retardation factors for the ions of interest in the actual subsurface environment would be different from the values reported in this appendix. These retardation factors, however, do at least provide a starting point to begin calculations estimating the migration of these contaminants in the subsurface environment at the NTS.

Table II- 2. Retardation factors for the Sr(II) cation in 0.1 and 0.01 M NaNO₃.

Ionic Strength	K_d (m ³ /g)	R (K_d)	Best-fit K_d (m ³ /g)	R (Best-fit K_d)
0.1 M	1.92x10 ⁻⁴	735	1.93x10 ⁻⁴	739
0.01 M	2.50x10 ⁻³	9565	2.33x10 ⁻³	8917

Table II- 3. Retardation factors for the CrO_4^{2-} anion in 1.0, 0.1, and 0.01 M NaNO_3 at different pH values.

Ionic Strength (M)	pH	K_d (m^3/g)	R (K_d)
1.0	4.68	3.22×10^{-6}	12.3
1.0	5.64	6.69×10^{-7}	2.56
1.0	7.33	6.24×10^{-8}	0.24
0.1	3.93	2.60×10^{-6}	10.0
0.1	4.50	2.08×10^{-6}	7.96
0.1	5.12	4.70×10^{-7}	1.80
0.01	4.43	6.30×10^{-6}	24.1
0.01	5.05	2.62×10^{-6}	10.0
0.01	5.62	6.83×10^{-7}	2.61

Table II- 4. Retardation factors for the SeO_3^{2-} anion in 1.0 and 0.1 M NaNO_3 at different pH values.

Ionic Strength (M)	pH	K_d (m^3/g)	R (K_d)	Best-fit K_d (m^3/g)	R (Best-fit K_d)
1.0	4	2.52×10^{-6}	9.6	2.35×10^{-6}	9.0
1.0	5	2.35×10^{-6}	9.0	2.28×10^{-6}	8.7
1.0	6	1.77×10^{-6}	6.8	1.71×10^{-6}	6.5
1.0	7	1.12×10^{-6}	4.3	1.05×10^{-6}	4.0
0.1	4	2.22×10^{-6}	8.5	2.03×10^{-6}	7.8
0.1	5	1.51×10^{-6}	5.8	1.39×10^{-6}	5.3
0.1	6	5.35×10^{-7}	2.0	4.65×10^{-7}	1.8

REFERENCES

- Barrett, E.P., Joyner, L.G., and P.P Halenda. "The Determination of Pore Volume and Area Distributions in Porous Substances." *Journal American Chemical Society* 73, (1951) : 373-380.
- Bedient, P.B., Hanadi R.S., and C. J. Newell. *Ground Water Contamination: Transport and Remediation*. Englewood Cliffs, NJ : Prentice Hall, 1994, 542 pp.
- Blankennagel, R.K. "Geophysical Logging and Hydraulic Testing, Pahute Mesa, Nevada Test Site." *Groundwater* 6, (1968) : 24-31.
- Blankennagel, R.K., and J.E. Weir. "Geohydrology of the Eastern Part of Pahute Mesa, Nevada Test Site, Nye County, Nevada." *U.S. Geological Survey Professional Paper 712-B* (1973) : 35 pp.
- Brunauer, S., Emmett P.H., and E. Teller. "Adsorption of Gases in Multimolecular Layers." *J. Am. Chem. Soc.* 60 (1938) : 309-319.
- Brown, G.E. "Spectroscopic Studies of Chemisorption Reaction Mechanisms at Oxide-Water Interfaces." In *Mineral-Water Interface Geochemistry* (Edited by M.F. Hochella Jr. and A.F. White). Reviews in Mineralogy, no. 23, Washington, DC : Mineralogical Society of America, (1990) : 309-363.
- Busenberg, E., and C. V. Clemency. "Determination of the Cation Exchange Capacity of Clays and Soils Using an Ammonia Electrode." *Clays and Clay Minerals* 21 (1973) : 213-217.
- Chang, R. *Chemistry*, 3rd ed. New York : McGraw-Hill Publishing Company, 1988, 1046 pp.
- Davis, J.A., and D.B. Kent. "Surface Complexation Modeling in Aqueous Geochemistry." In *Mineral-Water Interface Geochemistry* (Edited by M.F. Hochella Jr. and A.F. White). Reviews in Mineralogy, no. 23, Washington, D.C. : Mineralogical Society of America, (1990) : 177-260.

- Deer, W.A., Howie R.A., and J. Zussman. *An Introduction to the Rock-Forming Minerals*. Hong Kong : Longman, 1992, 696 pp.
- Drever, J.I. *The Geochemistry of Natural Waters: Surface and Groundwater Environments*, 3rd ed. Upper Saddle River, NJ : Prentice Hall, 1997, 436 pp.
- Ekren, E.B. "Geologic Setting of Nevada Test Site and Nellis Air Force Range." In *Nevada Test Site* (Edited by E.B. Eckel). *Geologic Society of America Memoir* 110 (1968) : 11-20.
- Goldstein, F.I., Newbury D.E., Echlin P., Joy D.C., Fiori C., and E. Lifshin. *Scanning Electron Microscopy and X-ray Microanalysis*. New York : Plenum Press, 1981. 673 pp.
- Goodman, B.A. "Adsorption of Metal Ions and Complexes on Aluminosilicate Minerals." In *Geochemical Processes at Mineral Surfaces* (Edited by J.A. Davis, and K.F. Hayes). Washington, DC : American Chemical Society (1986) : 342-361.
- Gottardi, G., and E. Galli. *Natural Zeolites*. New York : Springer-Verlag, 1985, 409 pp.
- Gregg, S.J., and K.S.W. Sing. *Adsorption, Surface Area, and Porosity*, 2nd ed. Orlando, Florida : Academic Press, Inc., 1982, 303 pp.
- Haggerty, G.M., and R.S. Bowman. "Sorption of Chromate and Other Inorganic Anions by Organo-Zeolite." *Environmental Science and Technology* 28, no. 3 (1994) : 52-458.
- Hay, R.L. "Zeolites and Zeolitic Reactions in Sedimentary Rocks." *Geologic Society of America Special Papers* 85 (1966) : 130 pp.
- Hay, R.L. "Geology of Zeolites in Sedimentary Rocks." In *Mineralogy and Geology of Natural Zeolites 2nd Printing* (Edited by F.A. Mumpton). *Reviews in Mineralogy* 4. Chelsea, Michigan : Mineralogical Society of America (1981) : 53-63.
- Hayes, K.F., and J.O. Leckie. "Modeling Ionic Strength Effects on Cation Adsorption at Hydrous Oxide / Solution Interfaces." *J. Colloid Interface Sci.* 115 (1987) : 564.
- Hayes, K.F., Papelis C., and J.O. Leckie. "Modeling Ionic Strength Effects on Anion Adsorption at Hydrous Oxide / Solution Interfaces." *J. Colloid Interface Sci.* 125 (1988) : 717-726.
- Hochella, M.F. Jr., "Atomic Structure, Microtopography, Composition, and Reactivity of Mineral Surfaces." In *Mineral-Water Interface Geochemistry* (Edited by M.F. Hochella Jr. and A.F. White). *Reviews in Mineralogy* 23. Washington, DC :

- Mineralogical Society of America (1990) : 309-363.
- Hochella, M.F. Jr., and Art F. White, eds. *Mineral-Water Interface Geochemistry*. Washington, DC : The Mineralogical Society of America, 1990.
- Hogan, R.G. "Selenium." In *Handbook of Hazardous Materials*, (Edited by M. Corn). San Diego, California: Academic Press Inc. (1993) : 649-660.
- Hoover, D.L. "Genesis of Zeolites, Nevada Test Site." In *Nevada Test Site* (Edited by E.B. Eckel) *Geologic Society of America Memoir* 110 (1968) : 275-284.
- Ming, D.W., and F.A. Mumpton. "Zeolites in Soils." In *Minerals in Soil Environments*. 2nd ed. (Edited by J.B. Dixon and S.B. Weed). Madison, WI : Soil Science Society of America (1989) : 873-911.
- Moncure, G.K., Surdam R.C., and H.L McKague. "Zeolite diagenesis Below Pahute Mesa, Nevada Test Site." *Clays and Clay Minerals* 29, no. 5 (1981) : 385-396.
- Mumpton, F.A. "Natural Zeolites." In *Mineralogy and Geology of Natural Zeolites* (Edited by F.A. Mumpton). *Reviews in Mineralogy* 4. Chelsea, Michigan : Mineralogical Society of America (1981) : 1-17.
- Mumpton, F.A., and W.C. Ormsby. "Morphology of zeolites in sedimentary rocks by scanning electron microscopy." *Clays and Clay Minerals* 24 (1976) : 1-23.
- Newbury, D.E., Joy D.C., Echlin P., Fiori C.E., and J.I Goldstrin. *Advanced Scanning Electron Microscopy and X-ray Microanalysis*. New York : Plenum Press. 1985. 454 pp.
- Papelis, C., Brown G.E., Parks G.A., and J.O. Leckie. "X-Ray Absorption Spectroscopic Studies of Cadmium and Selenite Adsorption on Aluminum Oxides." *Langmuir* 11, no.6 (1995a) : 2041-2048.
- _____, Roberts P., and J.O. Leckie. "Modeling the Rate of Cadmium and Selenite Adsorption on Micro- and Mesoporous Transition Aluminas." *Environmental Science & Technology* 29, no. 4 (1995b) : 1099-1108.
- _____. "Cadmium and Selenite Adsorption on Porous Aluminum Oxides : Equilibrium, Rate of Uptake, and Spectroscopic Studies." Ph.D. dissertation, Stanford University, Stanford, CA, 1992.
- Patterson, R.J., and T. Spoel. "Laboratory Measurements of the Strontium Distribution Coefficient K_d^{Sr} for Sediments from a Shallow Sand Aquifer." *Water Resources Research* 17, no. 3 (1981) : 513-520.

- Percival, J.B., and P.J. Lindsay. "Measurement of Physical Properties of Sediments." In *Manual of Physico-Chemical Analysis of Aquatic Sediments* (Edited by A. Mudroch, J. M. Azcue, and P. Mudroch). New York : Lewis (1997) : 7-45.
- Piwoni, M.D., and J.W. Keeley. "Basic Concepts of Contaminant Sorption at Hazardous Waste Sites." *EPA Ground Water Issue* (1991) : 7 pp.
- Schecher, W.D., and D.C. McAvoy. *MINEQL⁺: A Chemical Equilibrium Program For Personal Computers*. Hallowell, Maine : Environmental Research Software, 1994.
- Sposito, G. "Distinguishing Adsorption from Surface Precipitation." In *Geochemical Processes at Mineral Surfaces* (Edited by J.A. Davis, and K.F. Hayes). Washington, DC : American Chemical Society (1986) : 217-228.
- Squibb, K.S., and E.T. Snow. "Chromium." In *Handbook of Hazardous Materials* (Edited by Morton Corn). San Diego, California : Academic Press (1993) : 127-144.
- Stockham, J.D. "What is Particle Size: The Relationship Among Statistical Diameters." In *Particle Size Analysis* (Edited by J.D. Stockham and E.G. Fochtman). Ann Arbor, Michigan : Science Publishers, 1979, 140 pp.
- Stumm, W., and J.J. Morgan. *Aquatic Chemistry: Chemical Equilibria and Rates In Natural Waters*. New York : John Wiley & Sons, 1996, 1022pp.
- Thordarson, W. "Perched Ground Water in Zeolitized-Bedded Tuff, Rainier Mesa and Vicinity, Nevada Test Site, Nevada." *Desert Research Institute Report TEI-862* (1965) : 89 pp.
- Travis, C.C., and E.L. Etnier. "A Survey of Sorption Relationships for Reactive Solutes in Soil." *J. Environ. Qual.* 10, no. 1 (1981) : 8-17.
- U.S. Department of Energy, Nevada Operations Office, Office of External Affairs. *Announced United States Nuclear Tests, July 1945 Through December 1994*. DOE/NV-209, Washington, D.C. (1994): 124 pp.
- Weber, W.J., and F.A. DiGianno. *Process Dynamics in Environmental Systems*. John Wiley & Sons, New York, 1996, 943 pp.
- Winograd, I.J., and W. Thordarson. "Hydrogeologic and Hydrochemical Framework, South-Central Great Basin, Nevada-California, with Special Reference to the Nevada Test Site." *U.S. Geological Survey Professional Paper 712-C* (1975) : 126 pp.

Winograd, I.J., Thordarson W., and R.A. Young. "Hydrology of the Nevada Test Site and Vicinity, Southeastern Nevada." *U.S. Geologic Survey Open-File Report* (1971) : 429 pp.

VITA
Graduate College
University of Nevada, Las Vegas

Derek A. Sloop

Local Address:

6930 S. Paradise #1064
Las Vegas, NV 89119

Home Address:

6930 S. Paradise #1064
Las Vegas, NV 89119

Degrees:

Bachelor of Science, Geology, 1993
University of New Mexico

Special Honors and Awards:

Recipient of 1997 Maxey Award in Water Resources

Publications:

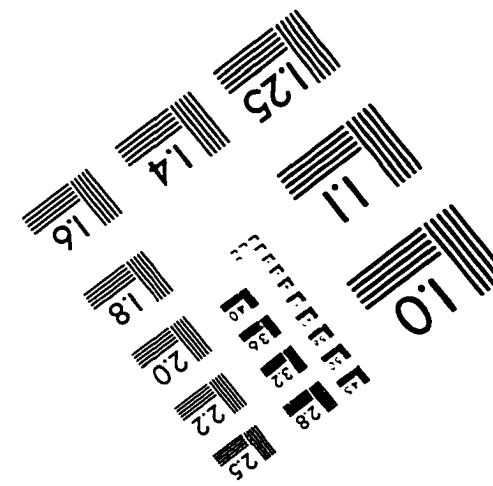
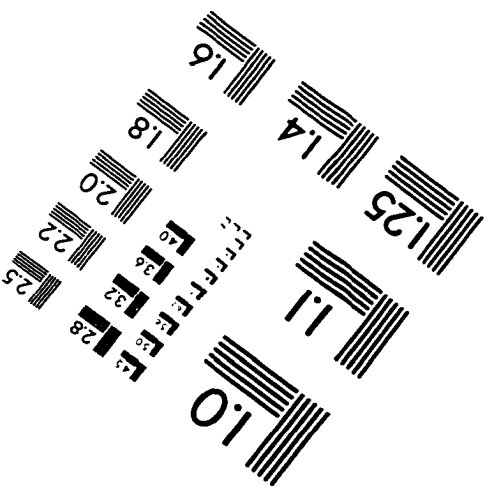
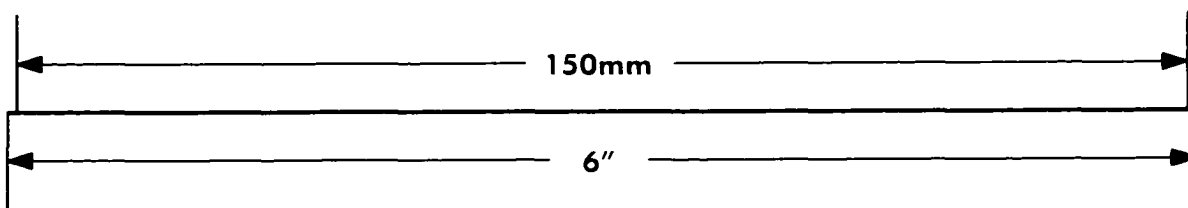
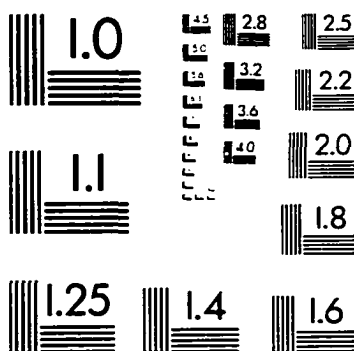
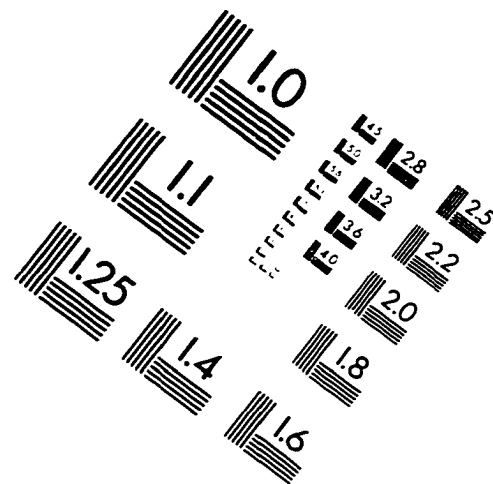
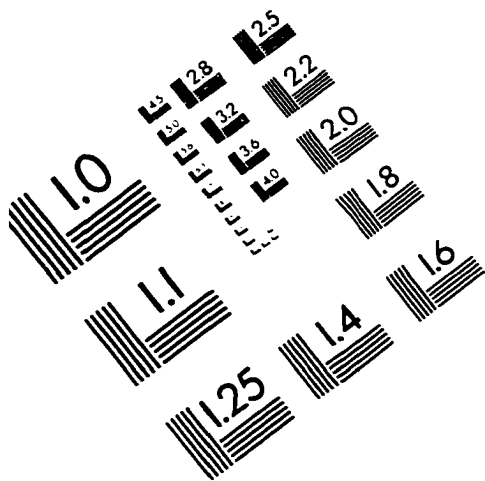
Bernot, P.A., D.A. Sloop, and C. Papelis. Rates of lead and strontium cation uptake by zeolitized tuffs from the Nevada Test Site, Nevada: Effects of cation type, ionic strength, and pH. Presented at the AGU 1997 Fall meeting, San Francisco, December 1997 (EOS, Transactions, American Geophysical Union, 78, No. 46, November 18, 1997/Supplement).

Papelis, C. and D.A. Sloop (1997). Comparison of cation and ionic strength effects on metal ion sorption on clinoptilolite and zeolitized tuffs. Presented at the 213th ACS National Meeting, San Francisco, CA, April 13-17, 1997.

Thesis Title: Equilibrium Studies of Ion Sorption on Zeolitized Tuff from Rainier Mesa, Nye County, Nevada

Thesis Examination Committee:**Chairperson, Dr. Charalambos Papelis, Ph.D.****Committee Member, Dr. Vernon Hodge, Ph.D.****Committee Member, Dr. Spencer Steinberg, Ph.D.****Graduate Faculty Representative, Dr. William H. Johnson, Ph.D.**

IMAGE EVALUATION TEST TARGET (QA-3)



APPLIED IMAGE, Inc
1653 East Main Street
Rochester, NY 14609 USA
Phone: 716/482-0300
Fax: 716/288-5989

© 1993, Applied Image, Inc., All Rights Reserved